# A Multi-Model Study of Extracellular Vesicles in Bowel Cancer Invasion and Metastasis

Sonia Guarnerio

A thesis submitted in partial fulfilment of the requirements of
Sheffield Hallam University
for the degree of Doctor of Philosophy

August 2023

# Candidate Declaration

I hereby declare that:

I have not been enrolled for another award of the University, or other academic or professional organisation, whilst undertaking my research degree.

None of the material contained in the thesis has been used in any other submission for an academic award.

I am aware of and understand the University's policy on plagiarism and certify that this thesis is my own work. The use of all published or other sources of material consulted have been properly and fully acknowledged.

Some of the data from chapter 4 were performed in collaboration with Dr. Luca Urbani and his lab (King's College, Institute of Hepatology, the Foundation for Liver Research, London). I played a major role in the obtainment of the data, data processing and interpretation. The contributions from colleagues in the collaboration are explicitly referenced in the text.

The work undertaken towards the thesis has been conducted in accordance with the SHU Principles of Integrity in Research and the SHU Research Ethics Policy.

The word count of the thesis is 46,739

| | |
|---|---|
| Name | Sonia Guarnerio |
| Award | PhD |
| Date of Submission | 6th August 2023 |
| Faculty | Health and Wellbeing |
| Director(s) of Studies | Dr Nicholas Peake |

# Acknowledgements

*"I wanna thank me for believing in me, I wanna thank me for doing all this hard work"*

Snoop Dogg

I wouldn't have learnt the meaning of resilience if it wasn't for:

My DoS, Dr Nick Peake, who bet on me in 2019 and then taught me everything he knew, like how to be a good researcher, but also to appreciate some in-house electronic music.

The rest of my supervisory team, Prof Christine Le Maitre and Dr Laura Cole, who supported me during the dark times of crying every other meeting, giving me precious advice when research was confusing.

The PeakEV group, the old and the new, for the enlightening conversations about EVs in front of a beer… well, at least 20% of the time was about EVs. Rob, thank you for teaching me the subtle science and exact art of isolating EVs.

All the people in the BMRC, which really made the working time shining. When I moved to UK for this PhD, Cristina and Filipe you were the first people to make me feel I could call Sheffield "home". During the pandemic, the concerns for family at home and the desire to reach them was relieved by the silly times with Paula, Oana, Lucy, and then, later, also by the drunky hugs of my Katie. Thankful that the PhD gifted me with your friendship, especially since you love to go to Italy for a girls' trip. A special thanks to who has shared (and overshared) the office with me, in particularly Muna – I feel we have always been the mirror of each other during the PhD and your help was essential. And then, a person that popped up during the last year of this adventure, who gave me a sudden strength and a model to follow, thank you Celine.

Mami e Papi, che non avete mai giudicato le mie scelte, anche quando sembravo aver perso un po' la testa e ho ribaltato la mia vita. Grazie per aspettarmi sempre con gioia a casa e per tutto il bene, lo spirito e la saggezza che mi avete trasmesso. Grazie anche per avermi regalato la mia gattina e averla amata cosi tanto che, nonostante i 20 anni, ho ancora la fortuna di tornare a casa e coccolare.

My Lilu, old grey lad who never wore the embroidered t-shirt I gifted you the first Secret Santa in uni, when I was already falling in love with you. However, thank you for never leaving my side (literally never..), you saw the worst period of me, but you have never left. You pushed me, you encouraged me, and you showed me that there is always a positive side in everything.

It is true, this PhD was challenging for many reasons. But I am here now and whatever happens in the future I don't regret any of it. It allowed me to know myself and the person I can and want to be. This thesis is dedicated to my late nonna Linda and nonno Learco, which I lost last winter. I wish I could show you that all your teachings and your strength have brought to this great goal.

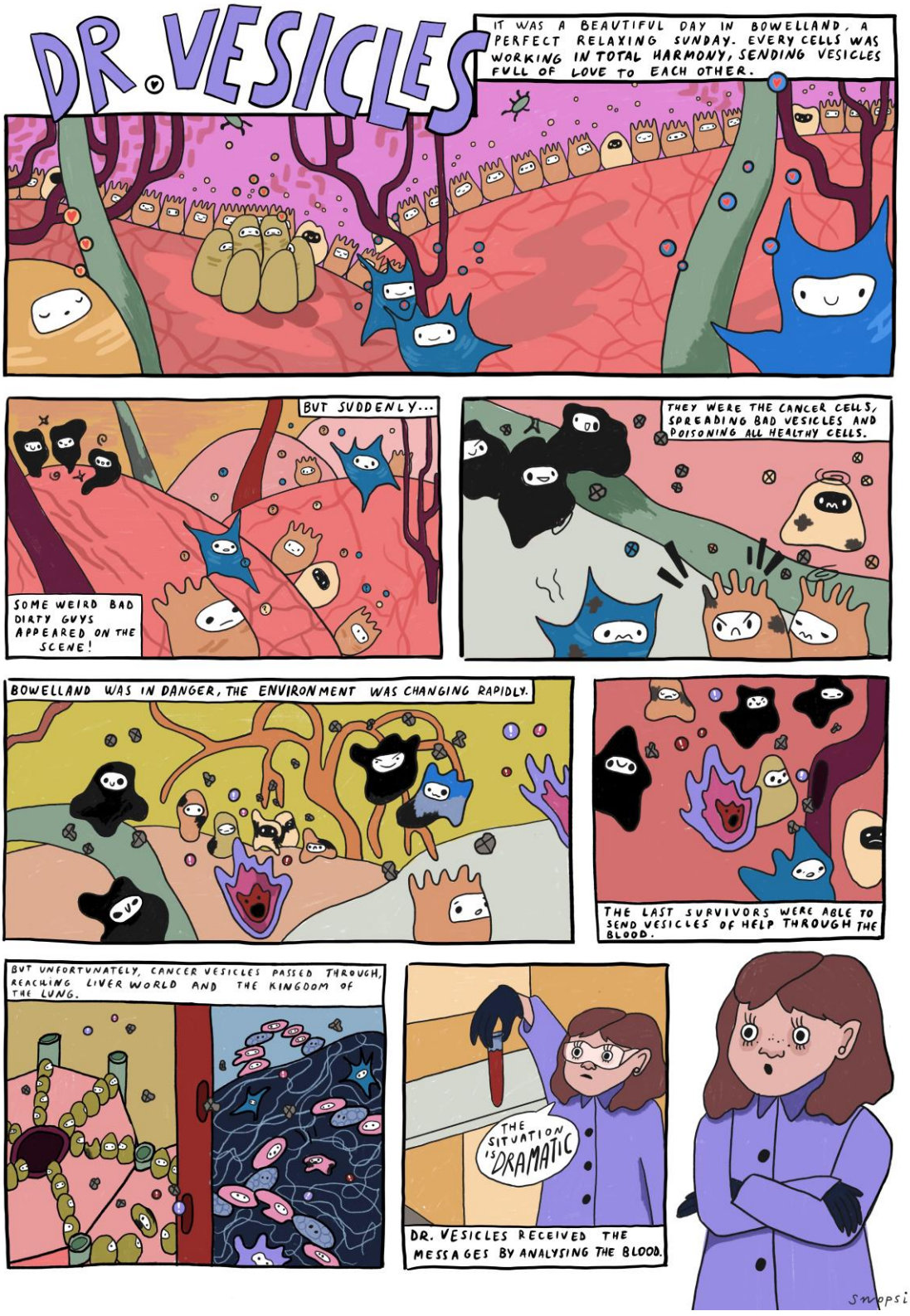
DR. VESICLES
IT WAS A BEAUTIFUL DAY IN BOWELLAND, A PERFECT RELAXING SUNDAY. EVERY CELLS WAS WORKING IN TOTAL HARMONY, SENDING VESICLES FULL OF LOVE TO EACH OTHER.
BUT SUDDENLY...
SOME WEIRD BAD DIRTY GUYS APPEARED ON THE SCENE!
THEY WERE THE CANCER CELLS, SPREADING BAD VESICLES AND POISONING ALL HEALTHY CELLS.
BOWELLAND WAS IN DANGER, THE ENVIRONMENT WAS CHANGING RAPIDLY.
THE LAST SURVIVORS WERE ABLE TO SEND VESICLES OF HELP THROUGH THE BLOOD.
BUT UNFORTUNATELY, CANCER VESICLES PASSED THROUGH, REACHING LIVER WORLD AND THE KINGDOM OF THE LUNG.
THE SITUATION IS DRAMATIC
DR. VESICLES RECEIVED THE MESSAGES BY ANALYSING THE BLOOD.
snopsi

# Abstract

Colorectal cancer (CRC) has one of the highest rates of cancer mortality worldwide. Despite progress in improving screening rates, approximately 35% of CRC patients are diagnosed with stage IV (metastatic) disease which has poor prognosis. *In vitro* 3D models have been developed which provide useful platforms to explore biomolecular processes in pre-clinical studies of cancer and metastasis, enabling the characterisation of mechanisms which can then be applied to the improvement of diagnosis, prognosis and disease treatment. Extracellular vesicles (EVs) are now known to play a critical role in cancer progression. Not only do they support cancer progression towards metastasis, but as carriers of bioactive cargo, they also show promise as potential cancer biomarkers. In this study, organotypic 3D models mimicking cancer invasion and pre-metastatic niche (PMN) in lung were developed to explore the role of EVs in advanced CRC stages and to evaluate their potential as prognostic markers.

After validating a transwell system as an effective 3D model, this work establishes that CRC EVs induce the invasion of cancer cells in a stage-dependent manner, with metastatic SW620 EVs driving a more aggressive phenotype than SW480 EVs. Proteomic profiling of the PMN showed differences in protein content upon treatment and a list of potential *m/z* signals able to distinguish between SW480 and SW620 EV treatment was obtained by multivariate analysis. CRC EVs also induced α-smooth muscle actin (α-SMA) expression in fibroblasts, demonstrating activation of fibroblasts in the 3D model. Expression and activity of TG2, a multifunctional enzyme involved in cancer progression, was increased after CRC EVs treatment in the 3D model of invasion. This led to the exploration of the cell-specific expression of TG2 in a cancer cells/fibroblasts co-culture, which showed an EV-mediated increase of TG2 on the surface of cancer cells and a non-EV mediated decrease of TG2 expression in the fibroblast surface. TG2 activity was further explored in hepatic stellate cells, crucial cellular components of liver metastasis. Finally, a pilot biomarker study on a small cohort of patients was performed, using multivariate analysis of cell responses to plasma-derived EVs and was able to separate patients according to disease stage.

The 3D models established and validated provided biomolecular information about the complex milieu of factors involved in CRC progression, including EVs, thus confirming the importance of 3D culture modelling in pre-clinical research. Moreover, this study was able to demonstrate key roles of cancer EVs on cellular activities which could then be translated for the development of alternative screening and prognostic approaches which may have application in improving the early diagnosis of patients with CRC.

# Table of contents

# List of Tables

# List of Figures

# Abbreviations

2D = two dimensional

3D = three dimensional

Ab = antibody

ABC = avidin-biotin complex

ABTS = 2,2’-azino-bis (3-ethylbenz-thiazoline-6-sulfonic acid) disodium salt

ACTA-2 = α-smooth muscle actin gene

ADAM = a disintegrin and metalloproteinase

ADAMT = a metalloproteinase with thrombospondin motifs

ALIX = ALG-2-interacting protein X

ANOVA = analysis of variance

APC = adenomatous polyposis coli gene

BCA = bicinchoninic acid

BRAF = mitogen-activated protein kinase (MAPK) pathway

BSA = bovine serum albumin

CAF = cancer-associated fibroblasts

CDM = cell derived matrix

CIMP-H = genome hypermethylation

CM = conditioning media

CO1A1 = collagen I gene

$CO_2$ = carbon dioxide

CO3A1 = collagen III gene

CO6A1 = collagen VI gene

CO7A1 = collagen VII gene

COBA1 = collagen XI gene

COL1 = collagen I

COLase III = bacterial collagenase III

CRC = colorectal cancer

CSC = cancer stem cell

CTLA-4 = cytotoxic T-lymphocyte-associated protein-4

DAB = 3,3-diaminobenzidine tetrahydrochloride

DAPI = 4′,6-diamidino-2-phenylindole

DC = dendritic cell

DELFIA = dissociation-enhanced lanthanide fluorescence immunoassay

DMA = dimethyl amiloride

DMEM = Dulbecco’s Modified Eagle Medium

ECACC = European Collection of Authenticated Cell Cultures

E-cad = E-cadherin

ECM = extracellular matrix

EGF = epithelial growth factor

EGFR = epithelial growth factor receptor

ELISA = enzyme-linked immunosorbent assay

EMT = epithelial to mesenchymal transition

ESCRT = endosomal sorting complex required for transport

EtOH = ethanol

EV = extracellular vesicle

FBS = foetal bovine serum

FFPE = formalin-fixed paraffin embedded

FIT = faecal immunochemical test

FN = fibronectin

FOBT = faecal detected occult blood

GDF-15 = growth/differentiation factor 15

GM130 = Golgi matrix protein 130

H&E = Haematoxylin/Eosin

H2O = water

HC = healthy control

HCl = hydrochloric acid

HGF = hepatic growth factor

HIAR = heat-induced antigen retrieval

HPLC = high-performance liquid chromatography

HRP = horseradish peroxidase

HSC = hepatic stellate cell

HUVEC = human umbilical vein endothelial cells

IBD = immune bowel disease

IEC = intestinal epithelial cell

IF = immunofluorescence

IgG = immunoglobulin

IHC = immunohistochemistry

IL = interleukin

ILV = intraluminal vesicles

IMS = industrial methylated spirit

IQR = interquartile range

ISC = intestinal stem cell

ISEV = International society for extracellular vesicles

KRAS = Kirsten rat sarcoma virus

KW = Kruskal-Wallis

LGR5+ = leucine-rich repeat-containing G-protein coupled receptor

LOH = loss of heterozygosity

LOX = lysyl oxidase

LRG1 = leucine rich alpha-2-glycoprotein 1

MALDI = matrix-assisted/laser desorption ionisation

MAPK = mitogen-activated protein kinase

MCP-1 = monocyte chemoattractant protein-1

MCTS = multicellular tumour spheroids

MDC = monodansylcadaverine

MET = mesenchymal to epithelial transition

MISEV = Minimal Information for Studies of EV

MLH1 = MutL homolog 1

MMP = matrix metalloproteinase

MS = mass spectrometry

MSI = mass spectrometry imaging

MV = microvesicle

MVB = multivesicular body

MW = Mann-Whitney

NaCl = sodium chloride

NAFLD = non-alcoholic fatty liver disease

nanoFCM = nanoflow cytometry

NASH = non-alcoholic steatohepatitis

N-cad = N-cadherin

Nd:YAG = neodymium/yttrium aluminium garnet

NK = natural killer

NTA = nanoparticle tracking analysis

OD = optical density

ON = overnight

P/S = penicillin/streptomycin

P120 = catenin delta-1

PBS = phosphate buffered saline

PC = principal component

PCA = principal component analysis

PD-1 = programmed cell death protein 1

PDC = poorly differentiated cluster

PFA = paraformaldehyde

PLS-DA = partial least squares discriminant analysis

PMA = phorbol 12-myristate 13-acetate

PMN = pre-metastatic niche

ppm = part per million

PS = phosphatidylserine

qTOF = quadrupole time of flight

RM-ANOVA = repeated measures ANOVA

ROI = region of interest

RT = room temperature

SDS = sodium dodecyl sulphate

SEC = size-exclusion chromatography

SEM = standard error of the mean

SM = sphingomyelin

Sub-x = xylene substitute

TAM = tumour-associated macrophage

TB = tumour budding

TBS = tris buffered saline

TEM = transmission electron microscopy

TFA = trifluoroacetic acid

TG = transglutaminase

TG2 = transglutaminase-2

TGF-β = transforming growth factor

TGM2 = transglutaminase-2 gene

TIMP = tissue inhibitor of matrix metalloproteinases

TMB = tetramethylbenzidine

TME = tumour microenvironment

TOF = time of flight

TSG101 = tumour susceptibility gene 101

VEGF = vascular endothelial growth factor

VEGFR = vascular endothelial growth factor receptor

VIP = variable importance in projection

vWF = Von Willebrand factor

WNT = wingless-related integration site

YAP/TAZ = Yes-associated protein/PDZ binding motif

α-CHCA = alpha-cyano-hydroxy-aminic acid

α-SMA = alpha-smooth muscle actin

µg = microgram

µl = microlitre

mg = milligram

ml = millilitre

ng = nanogram

nm = nanometre

pg = picogram

# 1 Introduction

## 1.1 Colorectal cancer background and progression

### 1.1.1 Clinical background and epidemiology

Colorectal cancer (CRC) or bowel cancer is the third most common cancer worldwide, being responsible for 10% of cancer-related deaths in developed countries (Li *et al*., 2021; Siegel *et al*., 2023). Incidence and mortality greatly vary depending on sex, with 25% less diagnosis in women compared to men. Being associated with increased wealth and progress in developing countries, it is predicted that there will be 2.5 million new cases for 2035 (Dekker *et al*., 2019). Whilst hereditary cases are limited to 6-10%, a large proportion of patients develop CRC sporadically, with the risk increasing when present with other pathologies (e.g. inflammatory bowel diseases, diabetes mellitus and ulcerative colitis) and environmental causes, such as smoking, alcohol and increased body weight. Although CRC mainly affects individuals over 50, in the last few years there has been an alarming increase in the incidence of young patients (7.9% in 20-29 years old) (Kanth & Inadomi, 2021; Vuik *et al*., 2019). Approximately 35% of CRC patients reach stage IV - in which the tumour becomes metastatic and invades different organs - and the five-year survival rate of these patients is less than 10% (Siegel *et al*., 2023). Generally, the most common sites of metastasis are liver, lungs and peritoneum, whilst cerebral metastasis is uncommon (Field, 2007).

The multifactorial origin of CRC leads to high phenotypic and molecular heterogeneity that can be distinct for each patient. For this reason, the molecular processes involved in the pathogenesis of CRC are not completely understood. This makes it difficult to detect reliable biomarkers for an early diagnosis and to correctly predict the prognosis of the patients (Martini *et al*., 2017). Currently, colonoscopy is the gold standard for the diagnosis of CRC with complementary CT scans (Kuipers *et al*., 2015). However, the discovery of biomarkers is crucial for all the steps of patient care, including early diagnosis, prognosis and therapy monitoring. Alongside the invasive strategies to obtain tissue biopsies during colonoscopy, liquid biopsies have been sought after to improve screening uptake and outcomes (Zygulska & Pierzchalski, 2022). In the UK there are currently two screening programs based on biomarker discovery; the first is the faecal detected occult blood (FOBT) and the second is the faecal immunochemical test (FIT). Both screening programs are utilised before invasive colonoscopy and have

contributed to the decrease of the overall mortality rate. These tests are however not always effective in early-stage CRC, which are mostly asymptomatic, making early diagnosis challenging.

If the patient presents in the early stages of the disease, endoscopic based resections and surgery resections are the main choices to manage the primary tumour (Jayaram *et al*., 2019), whilst adjuvant chemotherapy with fluoropyrimidines in combination with leucovorin or oxaliplatin is recommended for grades III-IV CRC (Field, 2007). According to the type of cancer, biologic treatments, such as monoclonal antibodies, may be prescribed to support the chemotherapy (Mahipal & Grothey, 2016). In CRC, the first validated and currently most prescribed monoclonal antibody is Bevacizumab, which targets vascular endothelial growth factor (VEGF), and is mainly used to support chemotherapy in advanced and metastatic CRC (Kazazi-Hyseni *et al*., 2010).

### 1.1.2 Pathogenesis of colorectal cancer

In terms of phenotype, early-stage CRC is characterised by malignant polyps in the affected epithelial areas of the colon called colonic glands. Polyps are sporadic protrusions occurring in the epithelium of the intestine. Although most are benign, they can progress to malignant when genetic and epigenetic instabilities occur. Despite the molecular heterogeneity complicating CRC cases, many cases present the adenoma-carcinoma sequence, in which chromosomal instabilities (CIN) are accompanied by a specific series of mutations responsible for the transformation from a healthy bowel to an adenoma neoplasia and progressively to carcinoma (Malki *et al*., 2020).

The first genetic event in the canonical pathway (70% cases) is the disruption of the adenomatous polyposis coli gene (APC) and activation of the essential wingless-related integration site (WNT) signalling cascade, that regulates the self-renewal of the epithelial stem cells, amongst other roles (Schneikert & Behrens, 2007). In the physiological context, the WNT cascade ending with the translocation of the transcription factor β-catenin to the nucleus, is highly regulated since it works as a pro-survival signal for the colonic stem cells (CSCs) present at the base of the glands (Mah *et al*., 2016). APC encodes for a protein that inhibits the pathway, leading eventually to the degradation of β-catenin. Alteration in the APC gene results in the production of a truncated protein, that

loses its ability to bind to β-catenin, thus sustaining a prolonged activation of the pathway (Zhao *et al*., 2022). This earliest mutation is then followed by the activation of the proto-oncogene Kirsten rat sarcoma virus (KRAS), loss of function of tumour suppressor gene TP53 and loss of heterozygosity (LOH) in the short arm of chromosome 18. The cell of origin in which all these events take place is still debated, whether intestinal epithelial cells (IECs), stem cells or both (Huels & Sansom, 2015). There is a strict relationship between the two cell types, since ISCs are responsible for the renewal of IECs, which reside above them in the glands of the colon. Both cell-types have shown potential for adenoma formation through a depletion of APC; however, IECs induce adenoma only if additional conditions, such as inflammation combined with multiple mutations, are present (Huels & Sansom, 2015).The serrated pathway (10-20% of cases) follows the adenoma-carcinoma sequence, but it is generally accompanied by a cancer in the proximal region with good prognosis (De Palma *et al*., 2019). Mutations in the mitogen-activated protein kinase (MAPK) pathway (BRAF) and genome hypermethylation (CIMP-H) are responsible for inducing serrated adenomas, followed by MutL homolog 1 (MLH1) promoter methylation and microsatellite instability-high (MSI-H). Alternative pathways have been recently observed (30% of cases), characterised by higher molecular heterogeneity and poorer prognosis, therefore increasing the unpredictability of the disease. Details on their mechanism of action have been extensively reviewed previously (Kasi *et al*., 2020; Yamagishi *et al*., 2016).

### 1.1.3 Metastatic colorectal cancer

At late stages of CRC (III - IV), patients present with metastasis in different organs. Approximately 35% of patients are diagnosed with spread to lymph nodes and close organs, while 20% of patients are diagnosed with ongoing distant metastasis (Siegel *et al*., 2023). Of the patients with metastasis, around 70% have metastasis in the liver, 48% in the lungs, 16% in distant lymph nodes, and 15 % peritoneum (Holch *et al*., 2017).

The progression of the understanding of biological processes has contributed to new therapeutic strategies, meaning that metastatic CRC is no longer considered incurable (Morris *et al*., 2023). However, with the survival rate lower than 10% in metastatic patients, the need for understanding of biomolecular processes and

identification of potential targets to be translated into clinical phase is of high demand.

## 1.2 Cancer cell plasticity and metastasis

The establishment of metastasis in all cancers is characterised by a series of events that are recognised as cancer hallmarks (Hanahan, 2022; Hanahan & Weinberg, 2011) and have been extensively reviewed (Fares *et al*., 2020; Majidpoor & Mortezaee, 2021; Zhuyan *et al*., 2020). Previously, the metastatic process was thought as a linear sequence of steps. The first step was the detachment of cells from the primary mass that migrate towards the closest capillaries, cross the basement membrane and intravasate to the blood. Circulating cancer cells adapt to the physical flow in the blood to then extravasate and colonise the new site (Fares *et al*., 2020). However, recent evidence suggests the process may be more complex, with metastasis occurring early and disease progression developing simultaneously at the primary and metastatic sites (Figure 1.1) (Majidpoor & Mortezaee, 2021). Plasticity of cancer cells is a crucial feature that allows them to change polarity and adapt cellular pathways to survive in heterogeneous environments throughout the process (Friedl, 2004). Components of the tumour microenvironment (TME) surrounding the tumour are also fundamental in regulating the process and allowing metastatic spreading.

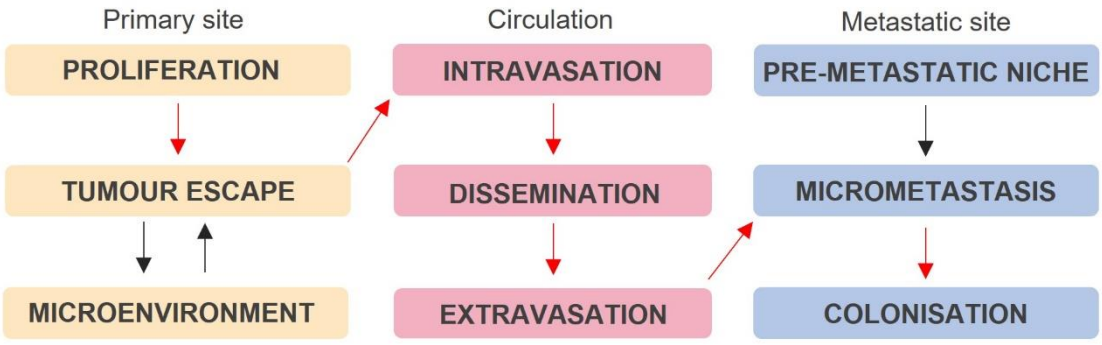


**Figure 1.1. The metastatic process.** Red arrows indicate the linear canonical process which coincides with the cellular steps towards metastasis. TME supports progression and in the migration of cancer cells in the primary sites. In the metastatic site, the establishment of the pre-metastatic niche (PMN) is considered an early event.

### 1.2.1 Tumour escape and invasion modalities

One of the first events in which the extreme plasticity of cancer cells can be observed is tumour escape. Cancer cells need to detach from the primary mass and invade the surrounding tissue to reach the circulation. It was initially thought

that the only way for a cancer cell to invade was to singularly detach and travel through the stroma (Martin & Jiang, 2009). Subsequently, different ways of collective migration have now been discovered (Figure 1.2) (Friedl *et al*., 2012).

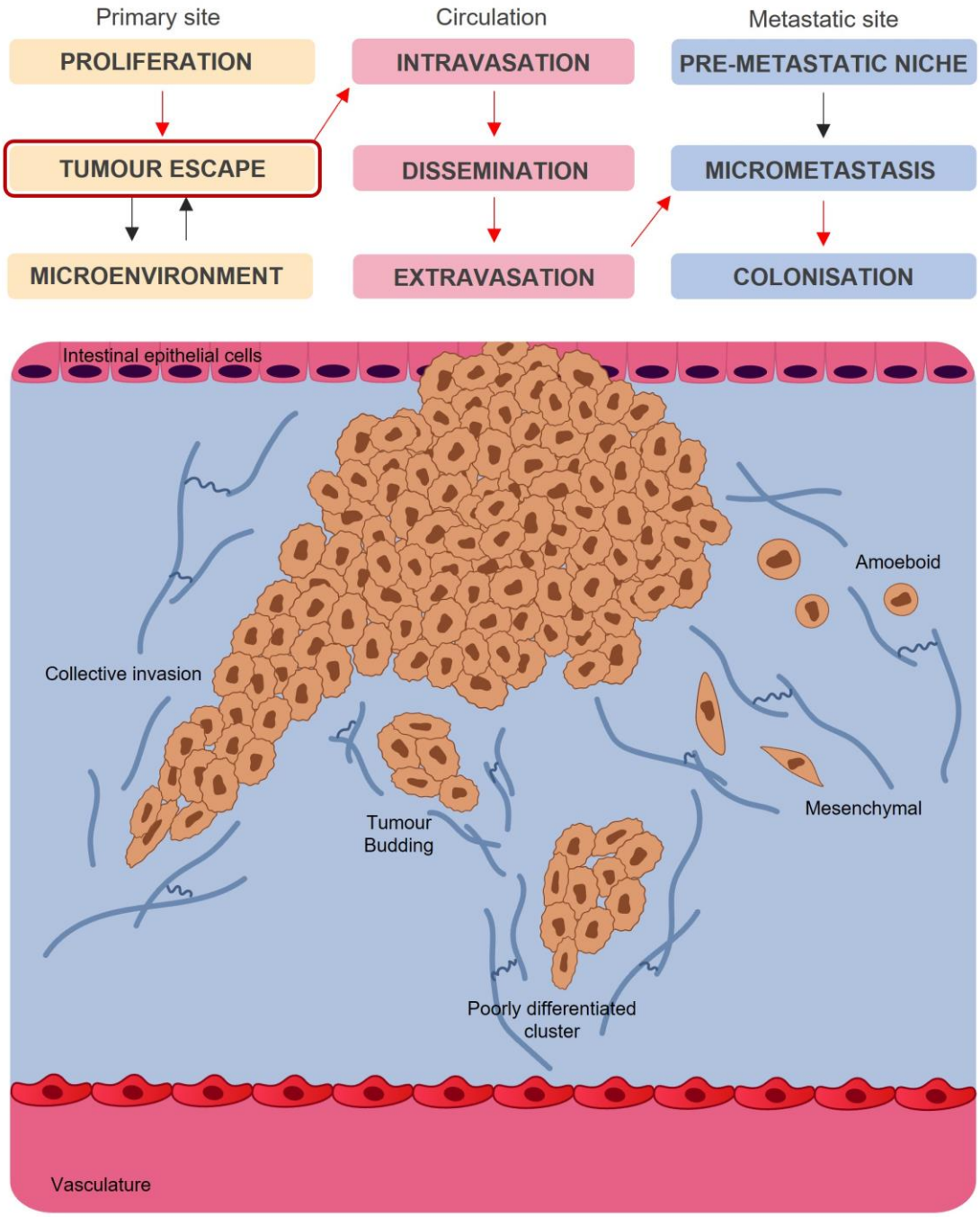


**Figure 1.2. Modalities of invasion in CRC.** Detachment from the primary mass can be collective or individual (Pandya *et al*., 2017).

### *1.2.1.1 EMT and individual migration*

In epithelial cancers such as CRC, the phenotype of cancer cells switching to a mesenchymal phenotype through epithelial-to-mesenchymal transition (EMT) is now well established (Ribatti *et al*., 2020). EMT is a unique cellular process

physiologically active in embryonic epithelial cells that are destined to form the mesoderm. Cancer cells undergo EMT during invasion to acquire a series of advantages, such as resistance to programmed cell death (apoptosis or anoikis) and degradation of extracellular matrix (ECM) (Ribatti *et al*., 2020). Through EMT, cancer cells lose cell-cell adhesions, cell-ECM adhesions and acquire an elongated shape. E-cadherin (E-Cad) is a cell-cell adhesion protein responsible for epithelial junctions and is the most well characterised protein lost during EMT (Bruner & Derksen, 2018). At the same time, molecules associated with mesenchymal feature are expressed by cells undergoing EMT, including N-cadherin (N-cad) and vimentin. The switch between E-cad and N-cad is generally used to identify EMT events and is often the initiating stage for cell detachment from other epithelial cells expressing E-cad (Loh *et al*., 2019). Once the invasive cancer cells have reached their destination and are ready to colonise, EMT can be reverted through mesenchymal-to-epithelial transition (MET) (Thiery *et al*., 2009). Alongside the mesenchymal differentiation, amoeboid migration has also been observed, less frequently in CRC due to the epithelial origin (Paňková *et al*., 2010). Amoeboid movements consist of continuous contraction and expansion monitored by actin and myosin in the cytoskeleton (Sahai *et al*., 2007).

#### *1.2.1.2 Collective invasion and tumour budding*

The EMT/MET exchange is not exclusively binary. EMT can happen partially, allowing cells to maintain some adhesion with each other, whilst acquiring the resistant feature of mesenchymal cells in the stroma (Saitoh, 2018). This partial EMT has been associated with more collective forms of invasion. Tumour budding (TB) consists of small clusters of cells close to the front of invasion, which is the border of between the primary mass and the stroma. TB is extensively found in CRC and is still linked with EMT and downregulation of E-Cad (De Smedt *et al*., 2016). Poorly differentiated clusters (PDCs) have also been defined and are distinguished from TB according to a cut-off in the number of cells, up to five cells for TB and over five for PDCs. Despite the formal distinction between the TB and PDCs, they are similar in their intermediate EMT properties, and also by their unfavourable link to prognosis in CRC (Shivji *et al*., 2022). Whether PDCs are just a further development of TBs or they are two different processes is not fully understood. When invasion is driven by cell-cell adhesions, cells move in large masses, identified as collective invasion (Friedl *et al*., 2012; Ilina *et al*.,

2020). In these clusters, leader cells are identified at the front of the clusters as the only one acquiring partial mesenchymal features. These leader cells determine the invasive pathway by remodelling the surrounding stroma.

Cancer cell plasticity allows for switching between these different mechanisms, resulting in the display of multiple modalities of invasion simultaneously. Initially a spontaneous event, plasticity in invasive behaviour is further driven by biomechanical forces and cellular signalling within the tumour stroma (Friedl, 2004; Ilina *et al*., 2020).

### 1.2.2 Colorectal cancer and the tumour microenvironment

As previously mentioned, high phenotypic and molecular heterogeneity can be observed between CRC patients. This is partly due to the molecular events involved in tumour formation and progression, which do not rely just on a mass of highly proliferating cells, but on interaction of these malignant cells with the environment around them, creating an effective organ-like system defined as the tumour microenvironment (TME) (Balkwill *et al*., 2012). Inside this complex and unique microenvironment, host cellular and non-cellular components interact with the malignant cells, resulting in disrupted homeostasis, with both positive and negative contributions to the disease (Balkwill *et al*., 2012). Despite the mechanisms of TME being common across cancer types, it is possible to isolate specific behaviours and molecular mechanisms in the CRC microenvironment (Figure 1.3). Local elements surrounding the tumour region, such as infiltrating immune cells and stromal components of the tissue, are commonly involved in the TME of all cancer types. Their behaviour is frequently tumour-specific, emphasising the need to understand the TME and its role in CRC.

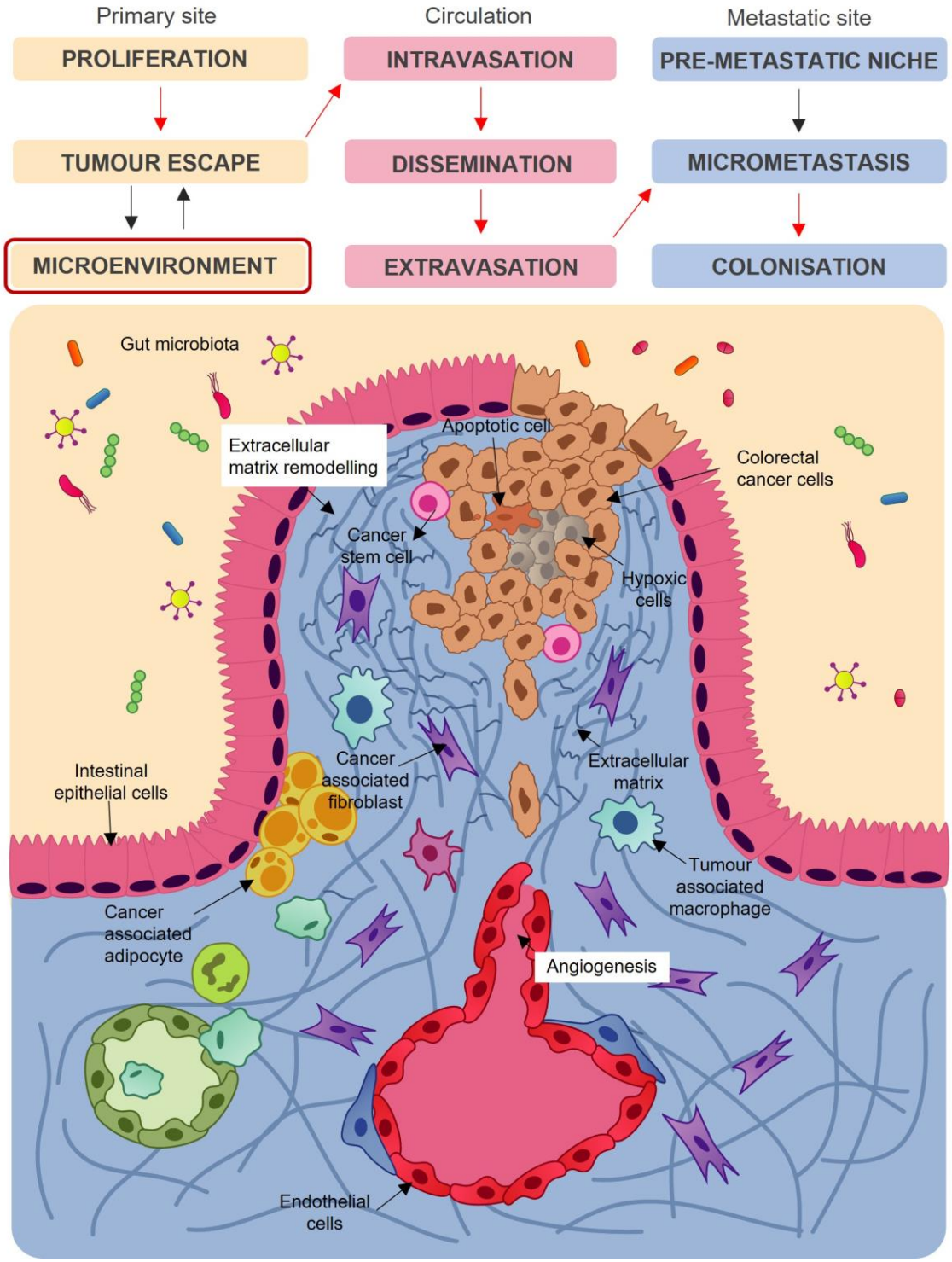


**Figure 1.3. Schematic representation of CRC TME.** Main cellular and extracellular components of the TME. CRC develops from aberration of epithelial cells. The expanded tumoral mass is constituted of cancer cells, hypoxic cancer cells and apoptotic events. Extracellular matrix (ECM) stiffening and cross-linking driven by cancer associated fibroblasts (CAFs) surround the tumoral mass. Immune cells, such as macrophages, infiltrate and play pro and anti-cancer roles. Endothelial cells create new abnormal capillaries for the sustainment of the tumoral mass. EMT processes are the early sign of cancer malignancy.

#### *1.2.2.1 Cellular interactions within the tumour microenvironment*

The stroma encloses the structural tissues of the organs, in which resident cells co-actively function around a dense net of ECM that allows cell migration and exchange of nutrients (Xu *et al*., 2022). In the presence of cancer, the stroma becomes a key source of exchange between the tissues and cancerous cells and can independently contribute to tumour progression. Many normal stromal cells in the presence of cancer can be activated and acquire phenotypes coupled to pro-tumour activities.

##### 1.2.2.1.1 Immune system

The relationship between the immune system and cancer is complex, resulting in pro and anti-tumour functions at the same time (Cui *et al*., 2013; Koido *et al*., 2005; Tachibana *et al*., 2005). From one side, the tumour is recognised by the host physiology as an alteration of the homeostasis. As such, cells from the innate and adaptive responses are recruited into the TME and they can infiltrate or interact with the malignant cells in multiple ways, either through adhesion molecules or paracrine signalling (Zhang *et al*., 2020). In the early stages of cancer, tumour antigens are recognised and processed into peptides by resident dendritic cells (DCs), which are antigen-presenting cells able to stimulate the immune response of CD4+ and CD8+ lymphocytes (Koido *et al*., 2005). CD8+ T cytotoxic cells recruited to and infiltrating the stroma have been shown to generate an anti-tumour response, increasing the overall survival, and are thus considered positive prognostic markers (Makaremi *et al*., 2021). On the other side, immunoediting, which enables the tumour to evade the immune response, and the presence of a strong inflammatory response in the bowel have been clearly associated with disease progression (Hanahan & Weinberg, 2011). In many cancers, immunosurveillance is also led by natural killer cells (NK), lymphocytes acting during the innate immune response, which are however found decreased in CRC (Jobin *et al*., 2017)

Inflammation is commonly observed in the colon, and persistent inflammatory signalling is a hallmark of cancer (Hanahan & Weinberg, 2011). There are high rates of people affected by inflammatory bowel diseases (IBD) (30-50% increase in the last 10-20 years) (Caviglia *et al*., 2023; Freeman *et al*., 2021), a multifactorial disorder, resulting in an inappropriate immune response and chronic inflammation. IBD patients are at increased risk of developing CRC,

associated with molecular changes leading to a inflammation-dysplasia-adenocarcinoma histologic pathway, rather than the sporadic sequence (Axelrad & Shah, 2020; Feagins *et al*., 2009). Resident stromal macrophages also undergo differentiation, constituting the first mechanism of defence against the tumour by actively removing cancer cells by phagocytosis, but they can also become tumour-associated macrophages (TAMs) with contrasting functions (Mehla & Singh, 2019). In normal conditions, macrophages possess significant plasticity to switch between different phenotypes; the two main types being M1, which initiates the response to pathogens and M2, responsible for wound repair. These two phenotypes contrast each other in terms of inflammatory response, since M1 macrophages can be considered to positively contribute to inflammation while M2 resolve it (Shapouri-Moghaddam *et al*., 2018). In cancer, TAMs that infiltrate are considered crucial for the progression of the disease and they mostly assume an M2-like phenotype (Mehla & Singh, 2019). Surprisingly, although the ratio M2/M1 is high even in CRC, studies on TAMs report contrasting actions on the tumour site; several pieces of evidence show pro-tumorigenic activity, with TAMs predicting an increased occurrence of liver metastasis (Cui *et al*., 2013), while other studies correlate TAMs with an improved overall survival (Cavnar *et al*., 2017; Koelzer *et al*., 2016).

Immunotherapy is a recently developed strategy to fight CRC and is based on targeting and reducing immune escape (Golshani & Zhang, 2020). The heterogeneous response of the immune microenvironment in CRC complicates the use of immunotherapy as an alternative treatment of the disease. Cytotoxic T-lymphocyte-associated protein-4 (CTLA-4) and programmed cell death protein 1 (PD-1) are immune checkpoint proteins, that once upregulated, are responsible of downregulation of lymphocytes response and immune escape (Makaremi *et al*., 2021). Currently, only few immune checkpoint inhibitors against CTLA-4 and PD-1 have been approved to be used in CRC as adjuvant therapy. However, side effects (auto-immune responses) and poor response rates (15-30% in most cancers) still limit the use of immune checkpoint inhibitors (Das & Johnson, 2019). Understanding the key roles of the immune compartment is therefore critical to develop the early promise of immunotherapy (Ganesh *et al*., 2019).

#### 1.2.2.1.2 Cancer-associated fibroblasts

Fibroblasts are the major cellular component in the stroma and provide structure and growth factors for sustaining tissue homeostasis. During physical injury, they can transform into myofibroblasts, an active phenotype with enhanced expression of alpha-smooth muscle actin (α-SMA) (Hinz, 2016). As myofibroblasts, they secrete collagen and proteins of the ECM to aid wound healing. A similar event has been found in cancer progression, in which fibroblasts assume an α-SMA positive myofibroblast-like phenotype referred to as cancer-associated fibroblasts (CAFs) (Shiga *et al*., 2015). Among the factors involved in the trans-differentiation of fibroblasts into CAFs, transforming growth factor-β (TGF-β) has been identified as the main mediator (Calon *et al*., 2014). TGF-β activates CAFs to secrete proteinases and other factors, including TGF-β itself, thus creating a feedback loop of enriched TGF-β in the TME (Hawinkels *et al*., 2014).

Although the main origin of CAFs is resident stromal fibroblasts which then hyper proliferate, other mesenchymal cell types, such as pericytes, adipocytes, endothelial cells and mesenchymal stem cells, can become CAF like (Deng *et al*., 2021). This leads to the creation of a variety of CAF subtypes, with diverse behaviours and functions that contribute to cancer progression (LeBleu & Kalluri, 2018). This phenotypic diversity still needs to be fully explored (Liu *et al*., 2019; Shiga *et al*., 2015), but the main role of CAFs is clear – they are promoters of tumorigenesis, cancer progression and invasion. Because of CAFs heterogeneity, a diverse variety of marker proteins have been identified (Deng *et al*., 2021). Using new high-throughput screening and omics technologies, it is possible to obtain information about the heterogeneity of CAF phenotypes. With this type of technique, two main subsets of CAFs were found in CRC, CAF-A with an intermediate phenotype, and fully activated CAF-B (Li *et al*., 2017). Very recently, a database called CAFrgDB has been developed to collect CAFs genetic and functional information (Foster *et al*., 2022; Yuan *et al*., 2023). In breast cancer for example, a wide range of phenotypes has already been defined (Elwakeel & Weigert, 2021). Identifying the CAF subtypes in CRC can help in the discrimination of targeted therapies and adjuvants. There is growing evidence that CAF influence the immune response and dysfunctions in CRC. Also, they have been associated with TAMs due to the shared stromal space (Gunaydin,

2021; Zhang *et al*., 2019) and they are responsible to induce TAM M2 phenotype (Zhang *et al*., 2023).

CAFs are known to be major constituents of the TME that contribute to cancer cell EMT. They do so by different mechanisms according to the type of cancer (Goulet *et al*., 2019; Xuefeng *et al*., 2020; Yang *et al*., 2023). Increased expression of Leucine Rich Alpha-2-Glycoprotein 1(LRG1) in CRC cells was shown to be induced by CAFs and to promote CRC cell EMT (Zhong *et al*., 2021). In CRC, CAFs have been shown to express high amounts of Wnt2, activating the canonical Wnt/β-catenin pathway and promoting cancer cell migration and progression (Aizawa *et al*., 2019).

#### 1.2.2.1.3 Endothelial cells and angiogenesis

Vascularisation is an important step in cancer progression. Not only does it contribute to the delivery of growth factors and nutrients for the sustainment of the tumoral mass, but it also mediates the infiltration of immune cells (Al-Ostoot *et al*., 2021). Under normal conditions, the formation of new vessels is controlled by a balance between pro- and anti-angiogenic factors. In cancer, this balance is disrupted and pro-angiogenic factors prevail to significantly induce angiogenesis (Al-Ostoot *et al*., 2021).

Endothelial cells are elongated cells that constitute the inner monolayer of vessels by the formation of tight junctions, thus being responsible for the barrier between tissues and circulation (Pugsley & Tabrizchi, 2000). To sustain this function, pericytes form tight junctions with the monolayer of endothelial cells, helping in the defence of the barrier as well as in the sustainment of the endothelial cells. In response to metabolic demand of a developing cancer, new tumour endothelial cells and pericytes can derive not only from the normal progenitors, but also from cancer stem cells (CSCs) (Lizárraga-Verdugo *et al*., 2020). CSCs are a population of multipotent and self-renewing cells found in many cancers. (Batlle & Clevers, 2017; Bonnet & Dick, 1997; Hervieu *et al*., 2021). In CRC, endothelial differentiation was found arising from CSCs, as well as poorly differentiated CRC cells (Liu *et al*., 2017; Shangguan *et al*., 2017). The phenotype of tumour associated endothelial cells is different from normal endothelial cells and this is reflected by the structure of the new capillaries, which

are characterised by abnormal morphology, impaired flow, and leaky junctions (Liu *et al*., 2017).

Tumour endothelial cells are also involved in the communication with cancer cells through the release of cytokines and growth factors. VEGF released by cancer cells is the main pro-angiogenic factor and it binds to its receptor (VEGFR) on endothelial cell surfaces (Melincovici *et al*., 2018). In CRC, VEGF levels found in tissue and in plasma correlate with disease advancement (Baker *et al*., 2019). In metastasis, the role of endothelial cells is even more important, as the cancer cells need to adhere to them to undergo extravasation (Zhang *et al*., 2022). After extravasation, circulating cancer cells travel towards new sites of metastasis where they require further adhesion to endothelial cells to infiltrate the new tissue. E-selectin is an adhesion molecule found highly expressed in serum of metastatic cancer patients and endothelial cells close to the metastatic site (McDonald *et al*., 2009). CRC cells adhere to endothelial cells presenting E-selectin, by expressing ligands such as neural cell adhesion molecule L1 (L1CAM) (Deschepper *et al*., 2020). Other factors can contribute to these cell-to-cell interactions and they can derive from early events of the disease progression, such as EMT (Dou *et al*., 2021; Izutsu *et al*., 2022). Von Willebrand factor (vWF) is a glycoprotein secreted by endothelial cells under physiological conditions to recruit platelets where vascular injury is identified (Patmore *et al*., 2020). Its evident increase in many cancers has been observed in recent studies exploring coagulation. In breast cancer, the mechanism of vWF expression was related to endothelial cell activation and secretion of Weibel-Palade bodies, which are endothelial cell storage granules that contain mainly vWF and P-selectin (Dhami *et al*., 2022). In CRC, increased expression of vWF is marker of poor prognosis linked to higher mortality and thrombosis (Garam *et al*., 2018).

Despite a clear understanding of the role of endothelial cells in the advancement of the disease, the factors that allow communication between endothelial cells and cancer cells are still not fully characterised.

#### *1.2.2.2 Extracellular matrix and colorectal cancer*

The ECM surrounding cells in the stroma is a complex dynamic system of macromolecules, essential for the biomechanical and structural properties of the tissue. Within its composition, the ECM consists of fibrous proteins such as collagen and elastin, polysaccharides and liquid space, creating a biological

scaffold which is responsible for tissue organisation and supporting cell migration (Theocharis *et al*., 2016). Cancer cells, which interact with the components of the ECM through different receptors, can alter and deregulate this physiological scaffold facilitating cancer progression. The ECM remodelling is a result of biochemical and biomechanical events which impact on ECM homeostasis and components both at the primary and at metastatic site (Winkler *et al*., 2020). A list of the most recent findings on ECM proteins affected in CRC is summarised in Table 1.1.

Frequently, the TME is characterised by a pronounced desmoplasia, which is defined by excessive deposition of ECM components by cells like CAFs and alterations in the ratio of the types of collagen present (Zeltz *et al*., 2020). The deposited fibrils reorganise in an anisotropic alignment leading to an increase in tumour stiffness frequently observed in primary and solid cancers (Han *et al*., 2016). The mechanotransduction of cells within the stiff environment results in the nuclear relocation of Yes-associated protein/PDZ binding motif (YAP/TAZ) (Ishihara & Haga, 2022), which in turns activates a series of events linked to cancer progression, including EMT (Cheng *et al*., 2020). The increase of matrix stiffness is linked to tumour progression and invasion towards metastasis (Brauchle *et al*., 2018; Levental *et al*., 2009). Alignment of the ECM fibrils supports the change in cell polarity which is essential for migration once detaching from the primary tumour (Ray *et al*., 2017). Enzymes, such as lysyl oxidases (LOXs) and transglutaminases (TGs) catalyse covalent cross-links of ECM collagens and elastin, contributing to matrix stiffness (Baker *et al*., 2011; Yuzhalin *et al*., 2018). LOX activity has been mainly associated with aggression and it is considered a CRC metastatic biomarker (Liu *et al*., 2018; Murdocca *et al*., 2019; Wei *et al*., 2017). On the contrary, TGs and in particularly transglutaminase-2 (TG2) have shown opposing and context-dependent functions, which still requires clarification (Tempest *et al*., 2021).

**Table 1.1. ECM proteins with a function in CRC.** Most recent findings of upregulated ECM proteins in CRC.

| ECM component | Modification | Role | Reference |
|---|---|---|---|
| Collagen I | Increased expression | Induce metastasis and stemness | (Wu *et al*., 2019) |
| Collagen III | Increased expression of turnover fragments | Presence in metastatic patients, potential stage biomarker | (Kehlet *et al*., 2016) |
| Collagen IV | Expression in CAFs | Presence in stroma of CRC liver metastasis | (Lindgren *et al*., 2022) |
| Collagen VI | High in plasma | Prognostic and diagnostic marker | (Qiao *et al*., 2015) |
| Collagen XI | Increased expression in cell lines | Activate CRC cells functions | (Liu & Meng, 2022) |
| Collagen XII | Increased expression | Regulation of focal adhesion, poorer prognosis | (Wu & Xu, 2020) |
| Collagen XVII | Increased expression in CSCs | Tumorigenesis | (Liu *et al*., 2016) |
| Vimentin | Increased expression in cell extensions | Activate ECM degradation | (Ostrowska-Podhorodecka *et al*., 2023) |
| Elastin | Increased expression | Induce CRC progression | (Li, Xu, *et al*., 2020) |
| Laminin | Increased expression in tumour myeloid cells | Induce CRC liver metastasis and angiogenesis | (Gordon-Weeks *et al*., 2019) |

In apparent opposition to ECM desmoplasia, there is the high degradation of ECM promoted by cancer cells. This is generally a localised event necessary when travelling in tissues with small gaps or non-aligned ECM, where cancer cells cannot easily reorganise the cytoskeleton to find a way through (Vasudevan *et al*., 2022). This degradation is also observed in metastatic sites, necessary to facilitate cancer cell invasion (Paolillo & Schinelli, 2019). Thus, cancer cells release a series of proteases such as matrix metalloproteinases (MMPs), a disintegrin and metalloproteinases (ADAMs), a disintegrin and metalloproteinase with thrombospondin motifs (ADAMTs) and cathepsins. Their role has been extensively reviewed (Vasudevan *et al*., 2022). MMPs are a large family of proteinases that collectively can degrade all protein components of the ECM. In

cancer, most of the MMPs found have been linked with poor outcome and for this reason were considered as therapeutic targets but failed in clinical trials due to poor side effects (Fingleton, 2008). It became clear that MMPs had also beneficial roles. In CRC, MMP-12 (metalloelastase), which is expressed by TAMs, has shown protective functions and is found in non-metastatic CRC only (Asano *et al*., 2008; Shi *et al*., 2006; Yang *et al*., 2001). Interestingly, alongside MMPs, tissue inhibitor of matrix metalloproteinases (TIMPs) are released in the TME. Although the name implies an inhibitory action on MMPs, the main TIMPs found (TIMP-1 and TIMP-2) seem to behave in a context dependent manner (Escalona *et al*., 2020; Gong *et al*., 2013; Reis *et al*., 2015; Wang *et al*., 2019). Studies have demonstrated the expression of TIMPs as a balancing action when MMPs are over expressed (Wang *et al*., 2019) and linked a lower expression of TIMPs to poorer outcome and recurrence (Reis *et al*., 2015). However, there has been also evidence on TIMPs in supporting cancer progression (Escalona *et al*., 2020; Gong *et al*., 2013). Despite the opposing roles, the often-high levels of TIMPs in cancer led to their consideration as prognostic biomarkers (Song *et al*., 2016).

**Table 1.2. Recent findings of proteinase activities in CRC.**

| Type | Recent findings in CRC | Recent findings in CRC |
|---|---|---|
| MMPs | MMP-7 associated to KRT15 oncogene increases migration and invasion<br>MMP-1 drives proliferation and EMT | (Chen & Miao, 2022)<br>(Wang *et al*., 2020) |
| ADAMs | ADAM9 cleaves ephrin-B and mediate Akt downstream pathway | (Chandrasekera *et al*., 2022) |
| ADAMTs | ADAMTS4 induces tumour growth via macrophage infiltration<br>ADAMTS8 associated to tumour suppression | (Chen *et al*., 2018)<br>(Li *et al*., 2020) |
| Cathepsins | Cathepsin S enhances antigen cross-presentation in CAFs<br>Cathepsin K induced by gut microbiota promotes M2 macrophage polarisation | (Harryvan *et al*., 2022)<br>(Li *et al*., 2019) |

#### *1.2.2.3 Other TME components*

Other cell subtypes have been discovered infiltrating and acting in the TME. Many reviews have been published with the aim of collecting information of TME in different cancer types (Balkwill *et al*., 2012; Boyle *et al*., 2020). Moreover, the

lumen of the gut contains the largest population of symbiotic microorganisms, falling under the term of gut microbiota, which is composed of a wide variety of bacteria, fungi, protozoa, and viruses (Thursby & Juge, 2017). The balance between beneficial and detrimental microorganisms in symbiosis with the host is delicate and susceptible to external factors. When the balance is broken and pathogenic strains prevail, the gut microbiota is in dysbiosis (Hrncir, 2022). There is a close relationship between CRC and the gut microbiota. In fact, some of the factors are shared with CRC, including smoking, alcohol and high-fat diet (Engen *et al*., 2015; Gui *et al*., 2021; Singh *et al*., 2017). Moreover, some pathogenic species have been confirmed to induce CRC such as *Fusobacterium nucleatum*, which has been linked to CRC carcinogenesis, as well as progression towards metastasis (Casasanta *et al*., 2020; Chen *et al*., 2020; Rubinstein *et al*., 2019). For these reasons, the microbiota is now considered part of the TME.

Increasing the current knowledge of the TME at different stages of CRC progression is essential in stratifying patients and in breaking down CRC heterogeneity.

### 1.2.3 The pre-metastatic niche

Of the CRC metastatic sites, liver is the most common, accounting for about 30% of diagnosed patients. Undoubtedly, the main reason for this incidence is the proximity of the organ to the gastrointestinal system and the direct communication offered by the portal vein (Stewart *et al*., 2018). In the event of cancer cells reaching the circulatory system, the path towards the liver is the shortest. The second most common site of CRC metastasis is the lung. Once again, the connection with the gastrointestinal system is mediated by a direct link via the heart. Whereas the spread of cancer cells towards the liver is facilitated by the portal vein and the hepatic artery, CRC lung metastasis may also arise from lymphatic circulation (de Ridder *et al*., 2016; Stella *et al*., 2019). In 1889, Stephen Paget introduced the theory that metastasis is not a casual event, but they are a result of an affinity between metastatic cells (seed) and certain modified factors in the metastatic site (soil) (Paget, 1889). This theory was supported by further studies, which demonstrated that a large number of circulating metastatic cells did not correspond to an increase in the presence of metastasis in organs proximal to the invaded capillaries (Tarin *et al*., 1984). The direct metastatic mechanisms do not exclude the influence of a targeted seed and soil mechanism,

where the invasion of cancer cells in a new organ is anticipated and supported by biomolecular signalling (Akhtar *et al*., 2019).

Organotropism is defined as the preference of cancer cells to invade specific organs and it varies according to the type of cancer. The traditional thinking that metastasis arises as a late event in cancer and are the result of late somatic changes in cancer cells in the primary site has been recently questioned, as observations of the early presence of aggressive phenotypes have arisen (Friberg & Nystrom, 2015). In the last decade, more findings have discovered that the survival of the invading cancer cells is driven by factors released at earlier stages of cancer in the metastatic site, resulting in the so-called pre-metastatic niche (PMN) (Peinado *et al*., 2017).

The specific mechanisms leading to the PMN and organotropism have been the focus of significant recent interest (Azubuike & Tanner, 2023; Chen *et al*., 2018). It is crucial to improve knowledge about CRC organotropism since patient prognosis is dependent on the site of the metastatic organ. For example, lung metastasis has shown a higher overall survival compared to liver or brain metastases (Prasanna *et al*., 2018).

Among the factors released by the TME that have been found to contribute to the PMN, extracellular vesicles (EVs) have recently been identified as critical mediators of PMN formation and organotropism (Figure 1.4).

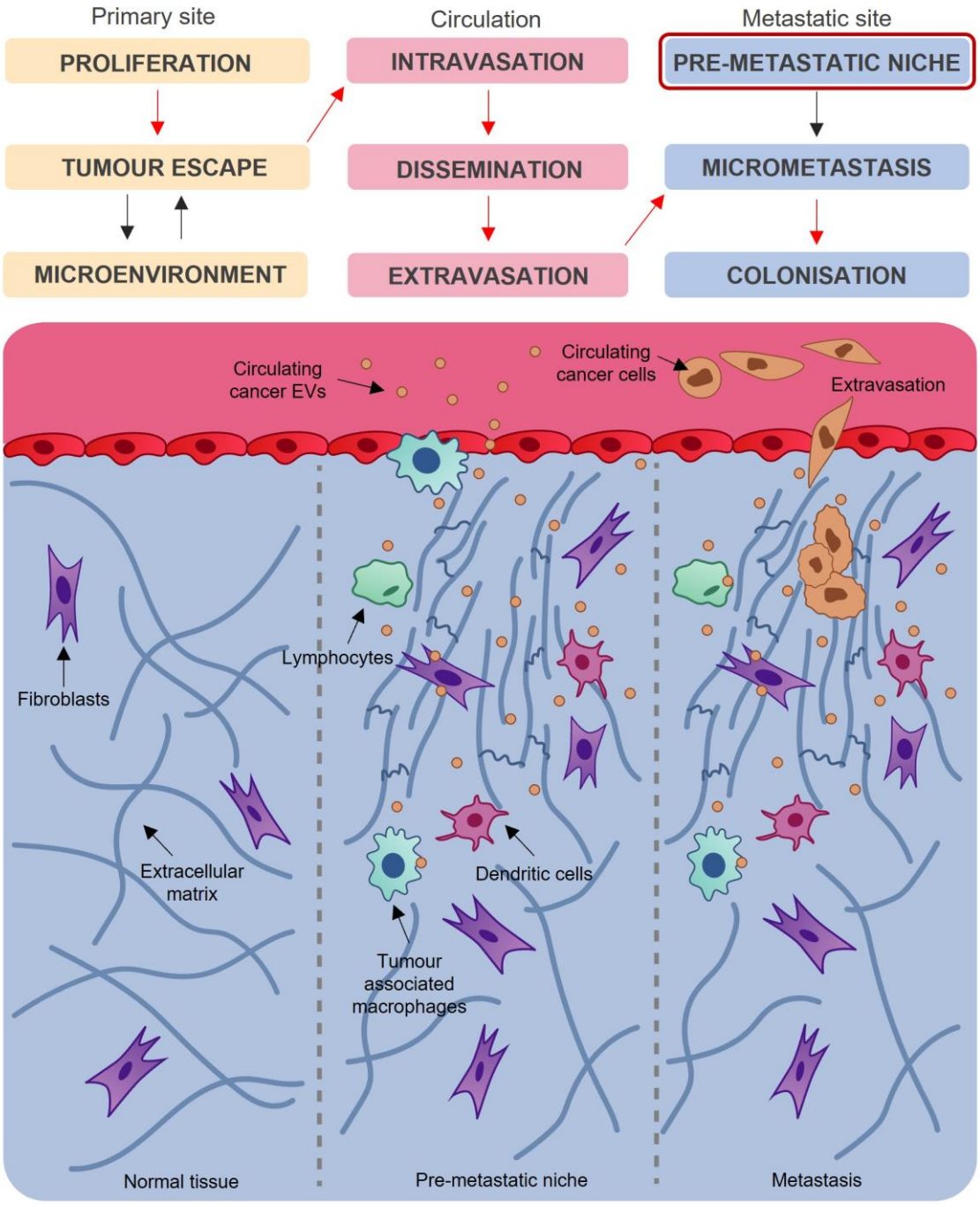


**Figure 1.4. The pre-metastatic niche.** Main players investigated in the PMN. Cancer EVs have been considered the key mediators in the establishment of the PMN. Extravasation and survival of circulating cancer cells depends on successful PMN events.

## 1.3 Extracellular vesicle involvement in colorectal cancer progression

### 1.3.1 Introduction to extracellular vesicles

EVs are lipid bi-layered structures secreted by all cells, including cancer cells. They are secreted through different mechanisms according to the specific type of EVs. Apoptotic bodies derive from the membranes of cells in apoptosis and

microvesicles (MV) bud outward from the cell membrane (Teng & Fussenegger, 2021). Exosome biogenesis is more complicated; they are enclosed in late endosomes and termed intraluminal vesicles (ILVs). The late endosome rich in ILVs is directed towards the cell membrane as multivesicular body (MVB) and secretes the exosomes via exocytosis (Teng & Fussenegger, 2021). In recent years, thanks to new isolation and characterisation methodologies, new sub-classes of EVs have been discovered, which are summarised in Table 1.1. EVs are not empty, their lumen contains DNA, mRNA, miRNA long non-coding RNA and proteins, alongside surface proteins which interact with target cells. This EV cargo is thought to be responsible for the intracellular communication, in particularly miRNAs (Li *et al*., 2022) and proteins (Chang *et al*., 2021). EV cargo can be transferred to other cells, thus implying that the general role of EVs is communication between cells. Due to their bi-layered membrane, EVs can travel through body fluids, acting on cells in both a paracrine and endocrine manner (Chang *et al*., 2021; Liu *et al*., 2021). According to the cell of origin, EVs also vary in size and content, which leads to a diversity of functions.

**Table 1.3. EVs types discovered.** Exosomes are the only vesicles secreted in an endosomal way. All the other vesicles are secreted from the plasma membrane (ectosomes).

| Type | Size | Cell type | First publication |
|---|---|---|---|
| Exosomes | 30-150 nm | All cells | (Harding *et al*., 1983) |
| Microvesicles (MV) | 100-1000 nm | All cells | (Wolf, 1967) |
| Apoptotic bodies | 50-5000 nm | Apoptotic cells | (Ihara *et al*., 1998) |
| Oncosomes/ large oncosomes | 100-400 nm (oncosomes)/ 1000-10000 nm large oncosomes | Tumour cells | (Al-Nedawi *et al*., 2008) |
| Ciliary ectosomes | 50-150 nm | All cells | (Cao *et al*., 2015) |
| T cell microvilli particles | < 200 nm | T cells | (Kim *et al*., 2018) |
| Elongated neutrophil derived structures (END) | ~ 120 nm | Neutrophils | (Marki *et al*., 2021) |
| Secreted midbody remnants | 200-600 nm | Dividing cells | (Rai *et al*., 2021) |
| Beaded apoptopodia | n.d. | Apoptotic cells | (Atkin-Smith *et al*., 2019) |
| Migrasomes | ~ 3000 nm | Migrating cells | (Ma *et al*., 2015) |
| Cytoplasts | n.d. | Leukocytes | (Malawista & Van Blaricom, 1987) |
| *En bloc* MVB-like EV clusters | 600-2000 nm | Tumour cells | (Valcz *et al*., 2019) |
| Exophers | ~ 4000 nm | n.d. | (Melentijevic *et al*., 2017) |

#### *1.3.1.1 Studying extracellular vesicles*

With the rapid recent increase in the research around EVs, the Minimal Information for Studies of EVs (MISEV) was created by the International Society for EVs (ISEV), which are general guidelines on the study and publication in the EV field, updated every few years (Théry *et al*., 2018; Witwer *et al*., 2021). Within the guidelines, different isolation methods have been recommended to obtain EVs from cells and tissues; the most frequently used are sequential ultra-centrifugations (UC) and size-exclusion chromatography (SEC). The choice of the isolation technique needs first to consider that none of the methodologies can give a fully purified EV sample; secondly, high EV yield generally corresponds to a lower specificity and higher contamination (Théry *et al*., 2018). After isolation,

EVs must be characterised to confirm their identity. Despite this diversity, it is possible to distinguish EVs from other secreted particles, as specific markers have been found to be frequently expressed, including tetraspanins CD9, CD63, CD81 as well as other proteins involved in their biogenesis. Tumour susceptibility gene 101 (TSG101) and ALG-2-interacting protein X (ALIX), for example, are specific to exosomes since they participate in the endosomal sorting complex required for transport (ESCRT) pathway, a key mediator of MVB formation from late endosomes. Alongside proteins, lipids such as cholesterol, glycosphingolipids, sphingomyelin (SM) and phosphatidylserine (PS) are enriched in EV membranes. Markers such as tetraspanins have been fundamental in EV characterisation and isolation, but their expression differs according with the cell origin. Marker characterisation is just one of the recommended aspects, along with quantification strategies such as particle count and imaging of the EV structure through electron microscopy (TEM or SEM).

Many findings have demonstrated that EVs, especially small EVs and exosomes, are crucial in the communication between TME components. EVs released by cancer cells, but also by all the cells in the TME exert functions at every step of the disease, from carcinogenesis to late metastasis (Chang *et al*., 2022; Kotelevets & Chastre, 2023). Moreover, they have been found to influence pathways and events associated with drug resistance and chemosensitivity. For these reasons, specific EV-related pathways and molecules are currently under consideration as novel biomarkers and for clinical trials (Sanz-Ros *et al*., 2023).

### 1.3.2 Cancer extracellular vesicles and primary colorectal cancer

Cancer EVs can remain within the mass of primary tumour and mediate cancer cell cross-talk and phenotypes in a paracrine manner. Cancer EVs were found regulating and promoting EMT leading to the acquisition of an invasive phenotype (Greening *et al*., 2015). It was observed that CRC EVs deriving from both primary and metastatic cell lines can induce cancer cell EMT via the transmission of a membrane protein receptor of WNT named Frizzled 10 (Scavo *et al*., 2020).

Alongside potentiating the phenotypic features of cancer cells, CRC EVs can deliver signals to different cells of the TME to achieve features related to the progression of cancer. Crosstalk between cancer cells and CAFs is partly

orchestrated by EVs (Naito *et al*., 2022). Cancer EVs from CRC as well as in other types of cancer were detected in the switch from normal fibroblasts to myofibroblast phenotype, alongside the main activation factor TGF-β (Webber *et al*., 2010). The involvement of EVs in the maintenance of CAFs leads to different impacts, including metabolic changes and synthesis of ECM components (Giusti *et al*., 2022). TIMP-1 found enriched in CRC EVs in turn upregulated TIMP-1 in recipient fibroblasts which induced ECM remodelling found in cancer progression (Rao *et al*., 2022). CAF activation by cancer EVs is correlated with the advanced stage of the cancer cells. Cancer cells that had undergone EMT and showed a mesenchymal phenotype produced EVs with reduced miR-200, a miRNA found in EV cargo, compared to epithelial CRC cells. The loss of miR-200 lead to the aberrant activation of TGF-β pathway for CAF switching, leading to an increase in CAFs in the presence of a more aggressive cancer phenotype (Bhome *et al*., 2022).

Likewise, EVs released by CRC cells promoted immune escape by altering TAM and macrophages phenotype from pro-inflammatory M1 to anti-inflammatory M2 (Shinohara *et al*., 2017; Yin *et al*., 2022). The effect and the polarisation pathways were however dependent on the cell type of origin. EVs from DLD-1 cells induced the M2 phenotype in THP-1 by the expression of miR-145 (Shinohara *et al*., 2017), whereas SW620 EVs enhanced PD-L1 in THP-1 through the expression of miR-21-5p and miR-200a (Yin *et al*., 2022). In another recent study, SW480 EVs polarised macrophages towards an M1 phenotype instead of M2, whereas SW620 EVs induced a mixed M1/M2 phenotype (Popēna *et al*., 2018).

Continuous findings are showing how the impact of cancer EVs spreads throughout the TME, as an extension of direct communication between cells. However, these EVs were rarely found involved in basal communication for the sustainment of the malignant cells; rather, they were mainly observed promoting pathways and activities for the progression of the disease.

### 1.3.3 Cancer extracellular vesicles and chemoresistance

A big challenge in the treatment of cancer is the development of resistance to chemotherapy. Chemotherapy is the front-line approach to treat CRC alongside surgery and despite the continuous development of new chemotherapeutics, the treatment often fails due to an intrinsic resistance of cancer. The cross-talk with

other types of cells, specifically of the immune TME, is also crucial for chemoresistance (Khalaf *et al*., 2021). There are processes promoted by EVs which directly target pro-survival pathways and chemoresistance, decreasing of apoptosis in cancer cells in response to treatment (Akao *et al*., 2014). Furthermore, EVs present in the TME can also shield anticancer drugs, thus limiting their delivery against the target cell (Aung *et al*., 2011). By inducing cancer progression and aggressive phenotypes, cancer EVs also indirectly confer cancer cells with resistance to drugs (Yang *et al*., 2022). This evidence emphasises the need to further investigate the roles of cancer EVs in chemotherapy resistance.

### 1.3.4 Cancer extracellular vesicles and colorectal cancer metastasis

After the seed and soil theory was established, many studies have focussed on investigating the main factors responsible for determining organotropism and preparing the PMN (Dong *et al*., 2023; Patras *et al*., 2023; Peinado *et al*., 2017). It was successfully demonstrated that cancer EVs are involved, alongside other secreted factors, in determining cancer organotropism, by circulating in the body as endocrine factors. EVs do so by recognising cells in the PMN through the expression of tissue-specific integrins, thus biasing the metastatic selection (Hoshino *et al*., 2015).

In order for circulating cancer cells to extravasate, the binding between integrins and adhesion molecules on the endothelial cells is essential (Sökeland & Schumacher, 2019). Importantly, CRC EVs and their cargo can be up taken by endothelial cells and induce reduced vascular permeability (Zeng *et al*., 2018). Once established in the PMN, they induce changes to cell behaviour supporting cancer cell establishment and invasion in the tissue. Many of the TME components previously described are found in the metastatic site interacting with cancer EVs. The most altered feature of the PMN is the immune response (Patras *et al*., 2023). CRC EVs can also contribute to the activation of CAFs and their functions in the metastatic site (Ji *et al*., 2020; Zhang *et al*., 2022). In other cancers, EVs were observed indirectly to induce ECM remodelling (Deep *et al*., 2020; Novo *et al*., 2018), but to date this has not been investigated in CRC.

The lack of *in vitro* models able to represent the complexity of the TME in advanced CRC has limited the exploration of the role of cancer EVs and PMN events to complex animal models. The development of *in vitro* alternatives can facilitate the investigations and unravel CRC heterogeneity.

## *1.4* Modelling colorectal cancer *in vitro*

### 1.4.1 Progress of cancer cell culture systems

The use of *in vitro* culture enables hypotheses on pathogenesis to be tested which aids the understanding of cancer formation, and approaches for diagnosis, prognosis and treatments. New *in vitro* models mimicking cancer are engineered and developed following the availability of new technologies. Traditionally, *in vitro* models are based on cells cultured in monolayer in which biomolecules and cell behaviour upon a specific treatment are investigated. Two dimensional (2D) cultures as such are established to investigate experimental strategies in cancer and have been used for decades due to their low cost, and straightforward features (Kapałczyńska *et al*., 2016). The cells used in this 2D environment are spontaneously immortal (like cancer cells) or can be mutated to escape senescence (immortalised cell lines) (Segeritz & Vallier, 2017). Alternatively, more sensitive cells such as stem cells and primary cells can be cultured. These are directly isolated from tissues where they can better maintain the original features and morphology of the original environment, although this is lost during 2D culture expansion. This kind of simplified methodology cannot recreate the milieu of TME, resulting in very poor translatability to the complexity of human diseases (Katt *et al*., 2016). Moreover, the dimensionality of the modelling space influences the structural, functional and migratory features of the cells, which has led cancer scientists to rely heavily on animal experiments (Onaciu *et al*., 2020).

Animals have been used for a long time in the study of diseases, since similar complexity, such as cell-to-cell and cell-to-ECM interactions in a multicellular environment, together with considerations of drug delivery and metabolism are similar across mammals (De-Souza & Costa-Casagrande, 2018). However, animal-based experiments are complex, long-term and expensive. Besides, the use of different species, such as mice and rats, for the study of human diseases in preclinical phases has very poor compatibility and reproducibility, leading to poor translation into human clinical trials (90% of cases fail) (Van Norman, 2019).

In cancer research, these species-related differences, together with the difficulty in reproducing immunological responses to cancer due to the sterile conditions that these *in vivo* models are maintained, cannot be ignored (Cekanova & Rathore, 2014; Van Norman, 2019).

The current ability to obtain a more relevant biological environment through three dimensional (3D) *in vitro* experiments has shown advantages over both canonical 2D cultures and animal models (Riedl *et al*., 2016; Yamada & Sixt, 2019).

## 1.4.2 3D models used in cancer research

A wide range of 3D models have been developed to address specific biological questions, achieve more realistic responses and reduce the reliance for animal experiments. They can be categorised as scaffold-free systems, such as spheroids, or scaffold-based systems in which a physical structure sustains the organisation of the cells (Figure 1.5). Ultimately, 3D models can also reach different levels of cellular complexity, from simple co-culture to miniature organs derived from patients or complete tissue structures.

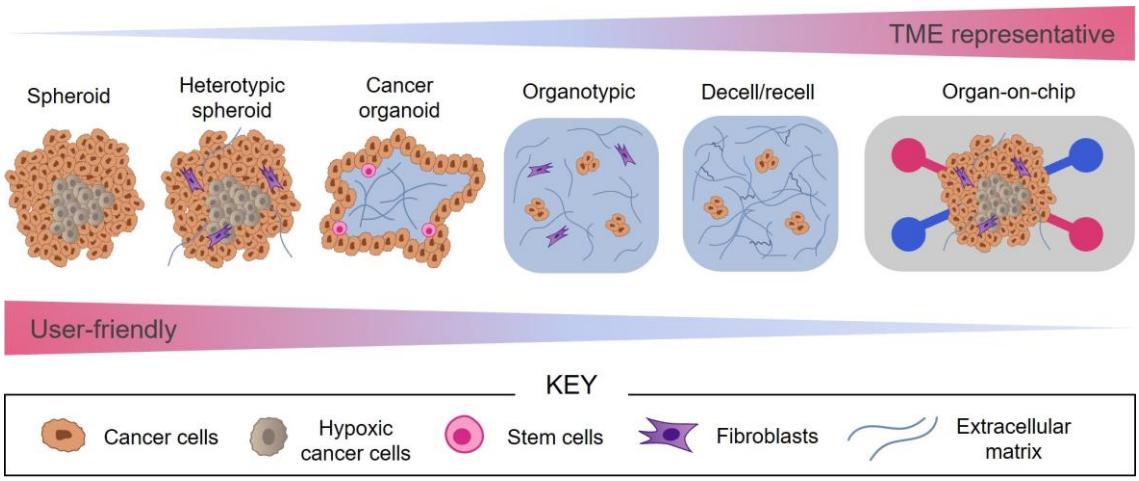


**Figure 1.5. 3D models used in cancer.** Schematic representation showing the different types of 3D models adopted in cancer research. User-friendly 3D models (straight-forward techniques, which are less costly) are generally less representative of the TME.

### *1.4.2.1 Multicellular cancer spheroids as first step of complexity*

Spheroids can be considered the first step of complexity from the monolayer culture since they consist of spherical arrangements of cells and can be generated from a single cell type. Spheroids in cancer research are generally defined as multicellular tumour spheroids (MCTS) and can be obtained by different techniques of culturing, such as hanging drop, liquid overlay or spinner flasks (Han *et al*., 2021). Multicellular tumour spheroids have contributed to the

discovery of biological mechanisms, as well as more accurately modelling the response to specific targeted drugs (Bhave *et al*., 2015; Sant & Johnston, 2017). Spheroids show decreased drug responses compared to 2D culture, emphasising the importance of cell space arrangement in drug efficacy (Bhave *et al*., 2015; Filipiak-Duliban *et al*., 2022; Nowacka *et al*., 2021). The fast growth that cells assumed in a spheroid model is close to the metabolic environment seen *in vivo* during tumour growth, developing a necrotic and hypoxic inner core, while the outer layers are well nourished (Sant & Johnston, 2017). However, whilst *in vivo* such a hypoxic environment would trigger angiogenesis and other mechanisms relevant to cancer progression, this does not happen in spheroid cultures, due to the absence of other cellular and stromal components (Han *et al*., 2021). Thus, the hypoxic feature of the spheroid is an end point for the evolution of the model. To approach a TME system, a step of complexity can be added by attempting co-culture of different cell types. Bacteria such as the CRC linked *F. nucleatum* have also been successfully co-cultured with MCTS and have given important information on the behaviour of bacteria in the presence of cancer cells (Kasper *et al*., 2020).

#### *1.4.2.2 Organoids and modelling healthy intestine in vitro*

With the growth in understanding stem cells and the ability to culture them, 3D cultures took a step further when organoids were first developed. The term organoid refers to a cluster of cells with the ability to self-differentiate and organise into different cell types. Both pluripotent stem cells and tissue-specific adult stem cells can be cultured in specific conditions and mimic the essential functionality of the organ (Zhao *et al*., 2022). Stem cells can also be obtained from patients, adding the organoid the possibility of addressing disease heterogeneity. A key study in the field of organoids was published in 2009, where leucine-rich repeat-containing G-protein coupled receptor 5 (Lgr5+) adult ISCs, found at the bottom of the intestinal crypts, were able to form crypt-like organoids without the need of a mesenchymal niche (Sato *et al*., 2009). The only cell requirements were matrigel embedding and basal growth factors such as R-spondin and epithelial growth factor (EGF). Physiologically, Lgr5+ ISCs are essential for the elevated cell turnover in the gut, but they have been also proposed as the potential cell progenitors of CSCs (Morgan *et al*., 2018; Xu *et al*., 2019). This first organoid was then followed by multiple studies aimed at

recapitulating the intestinal niche and further increasing the complexity of the *in-vitro* system with the help of new engineering approaches (Hinman *et al*., 2021; Spence *et al*., 2011).

### 1.4.3 Recapitulating the wider tumour microenvironment

Despite their ability to represent native features of the organ, stem cell-derived organoids lack in key components of the TME, such as stroma and immune cells. Cellular interactions in the stroma can be addressed in *in vitro* models by developing heterotypic tumour spheroids, which can be seen as an extension of the 2D co-culture, as for the MCTS previously described. Heterotypic spheroids can be obtained with the traditional methods for spheroid culture, such agitation culture (Franchi-Mendes *et al*., 2021). Nutrient and oxygen gradients, kinetics and morphological features resemble the environment of a non-vascular TME with the advantage of partially mimicking the interactions between a specific stromal cell-type and the cancer cells. These types of models can be used to investigate the key exchanges between cells and how these exchanges can impact on therapeutic resistance (Weydert *et al*., 2020). Cellular interactions between cancer cells and cells of the TME such as CAFs can be crucial when assessing a treatment, especially when the drug target can interact with the TME (Lamberti *et al*., 2019; Stock *et al*., 2016). Due to the relatively effortless preparation, triple cultures spheroids can be further developed to evaluate the interactions of different stromal cells in the presence of the tumour. There are TME events that are the result of coincidental interactions between different types of cells. It was previously mentioned how cancer cells/CAFs/TAMs crosstalk leads to the activation of determined cancer phenotypes and this can be observed in the development of heterotypic spheroids (Bauleth-Ramos *et al*., 2020).

#### *1.4.3.1 The introduction of scaffolds to mimic cancer extracellular matrix*

Spheroids and organoids have been shown to produce a small amount of native ECM to support cellular interactions (Glimelius *et al*., 1988). However, the ECM architecture and its physical and mechanical properties can be addressed by adding further steps of complexity. Support matrices of different origins have been introduced in *in vitro* modelling. They can have a natural origin or they can be engineered using synthetic polymers (Unnikrishnan *et al*., 2021; Xie *et al*., 2022). Matrices not only can mimic the complexity of the ECM, but they also allow the culture to grow for a longer period due to their biophysical support. While

artificial scaffolds are generally manufactured to address specific biomechanical conditions, natural scaffolds, which originate directly from ECM compounds, preserve biocompatibility and can better represent the TME, although are often over simplified (Xu *et al*., 2021). Thus, the choice of matrix needs to meet a balance between following the research hypothesis and addressing physiological relevance. The type of matrix may change the results of the experiment, as shown in a recent study, in which the content and the concentration of the matrix chosen affected the cell invasion of different types of cancer spheroids (Liu *et al*., 2020). Widely used scaffolds that ensure long-term culturing include natural plant-based scaffolds, such as agarose and alginate, which lack physiological ECM binding sites, making these scaffolds relatively inert (Chaicharoenaudomrung *et al*., 2019; Yamada *et al*., 2020). Biological matrices often have animal origin and the most common include basic gel systems composed of collagen type I, or basement membrane compounds (e.g., Matrigel or Geltrex$^{TM}$) or a mixture of these.

Another important feature for the selection of the matrix for cancer research is tissue stiffness. Matrices can be tuned to mimic healthy and pathological as well as tissue-specific stiffnesses (Baruffaldi *et al*., 2021). Collagen-based matrices cannot address tissue-specific biomechanical features per se, but can be mixed with other matrices (hydrogels, alginates, polyethylene glycols) or cross-linked with enzymes such as TG2 to obtain targeted physical properties (Okawa *et al*., 2022).

Scaffold embedding techniques can be implemented as a support of 3D cell culture in what is referred as organotypic model, which aims to retain both cellular and mechanical features of the tissue (Hayden & Harbell, 2021). Organotypic models generally need the aid of bioengineering methodologies to achieve architectures that lead to the recapitulation of a tissue-like structure. In cancer, organotypic models are useful to investigate the relationship between malignant cells and stromal fibroblasts, which is also deeply influenced by the ECM (Froeling *et al*., 2009; Gaggioli *et al*., 2007). Organotypic models based on co-culturing CRC and fibroblasts in collagen gels have been developed to investigate the role of the cross-linking enzyme TG2 on collagen remodelling, which contributes to the biomechanical alterations found in CRC, such as matrix increased stiffness (Delaine-Smith *et al*., 2019). Similar models have been

developed in the field of tumour-stroma interactions to evaluate the contribution of activated fibroblasts to migration and invasion, but also to assess the response of different combined drugs in the TME (Cattin *et al*., 2018; Henriksson *et al*., 2011; Zoetemelk *et al*., 2019). Consequently, the establishment and optimisation of new organotypic cultures is time consuming, but due to the clear advantages of such systems, the development around tissue engineering continued, leading to the employment of new materials and compounds.

Tissue decellularisation, developed as an innovative technique in regenerative medicine, has been used in 3D engineering to obtain tissue-specific ECM (Hoshiba, 2019). Decellularisation methods aim to eliminate the cellular components from the tissue while maintaining the ECM and its biological and biomechanical properties (Hoshiba, 2019). Tissues originate from patients, also giving the advantage of obtaining patient-specific decellularised matrices. Once decellularised matrices are obtained, they can be recellularised to achieve new 3D models and evaluate the contribution of altered ECM in the TME. Primary monocytes differentiated into macrophages, successfully repopulating the decellularised matrix coming from normal and cancerous colon (Pinto *et al*., 2017). Interestingly, macrophages subjected to only tumour-derived ECM differentiate into an anti-inflammatory M2-phenotype and an increased stiffness was observed in the decellularised ECM, which may eventually play a role in macrophage polarisation. Deriving decellularised matrices from patient tissues requires resources often with a limited access as tissues are generally requested for pathology purposes, but it is also true that they represent a great advantage and could be considered the optimum strategy as ECM scaffold in cancer. With tissue bioengineering strategies being constantly evolving for cell culture, for example using complex model designs through 3D printing systems or electrospinning, which can use both natural and synthetic matrices according to the specific research aim (Lerman *et al*., 2018).

### 1.4.4 3D models for EVs

As the behaviour of cells in 3D differs from culture in monolayer, so EV production is impacted by the dimensionality of the space. For instance, the cell membrane morphology and the surface, crucial for the release of EVs, do not organise in the same way in 2D and 3D. In 2D cells grow flat, with elongated structures and with the adhesion only to the bottom plastic and adjacent cells, while in 3D models,

cells are smaller, spherical and have interactions around the entire surface (Breslin & O'Driscoll, 2016; Riedl *et al*., 2016). Evidence of variations in the production of EVs in 2D or 3D were found in recent years, where only EVs secreted by cells in *in vitro* 3D models possessed miRNA profiles similar to EVs found *in vivo* (Thippabhotla *et al*., 2019).

#### *1.4.4.1 In vitro models for investigating the functional role of EVs*

Currently, functional roles of cancer EVs are still mainly observed either in 2D cultures or in murine models. Functional research on the role of EVs and cancer EVs would therefore benefit from 3D approaches like spheroids and organoids. It was demonstrated that hypoxia drives release of EVs with functions leading to cancer cell survival and proliferation (Ren *et al*., 2019). Spheroids mimic *in vivo*-like cancer-related hypoxia and therefore they can produce high yield EVs with the same hypoxic features. Furthermore, spheroids could also be conditioned with cancer EVs to evaluate the impact on the regulation of the hypoxia and on the regulation of tumour growth. EVs from CRC were found to increase growth and altered colonic mesenchymal stromal cells (Lugini *et al*., 2016). Similarly, organoids have unique characteristics, as they are constituted by a pool of patient-derived undifferentiated stem cells, which then differentiate over time. Organoids from different CRC patients produced EVs with only 45% of miRNA in common, showing the variability between patients that correlates with individual disease heterogeneity (Szvicsek *et al*., 2019). CRC organoids have been used to investigate the induction of EV secretion by different factors involved in promoting CRC, which showed that collagen deposition was able to increase the EV release from the organoid (Szvicsek *et al*., 2019).

When EVs are released by cells and perform paracrine or endocrine functions, they need to travel through ECM. EVs have been found actively interacting with ECM components, including collagen (Lenzini *et al*., 2020; Palmulli *et al*., 2023). EVs movement in the matrix is also supported by the biomechanical and biophysical properties of the ECM, with stiffer environment promoting a faster transport (Lenzini *et al*., 2020). Since EVs found in the ECM are secreted by all the cell types present in the tissue, a lot of interest has grown around the idea of extracting interstitial EVs from tissues. In cancer, these EVs can provide a snapshot of cellular activities within the TME and can be an alternative to EVs from liquid biopsies with higher specificity (Li *et al*., 2021). Considering the crucial

role of ECM in cancer and in interaction with EVs, physiological matrices need to be considered in the development of 3D models for the study of EV roles. A recent development in the field of 3D engineering is also very relevant for evaluating EV functions. Organ-on-chip models aim to mimic the whole tissue structure, which can include scaffolds, but also they are combined with microfluidics technologies to enable flow of liquids at microscale (Bhatia & Ingber, 2014). Microfluidics add the feature of constant fluid exchange, which is crucially relevant in tumour progression. For instance, EVs can be introduced in the flow to reach the organ-on-a-chip and simulate the arrival of EVs to the PMN. A microfluidic human liver-on-a-chip was indeed developed to emulate the formation of a PMN and explore the roles of breast cancer EVs in liver metastasis, unlocking new functional mechanisms for the establishment of the PMN (Kim *et al*., 2020). However, the establishment and optimisation of these complex 3D models to assess specific hypothesis is time consuming and requires expensive resources. Organotypic models can still offer an alternative as established constructs for the evaluation of EV crosstalk between cells. In combination with the presence of ECM-like structure, it is possible to evaluate the role of EVs without ignoring TME components. Moreover, it is relatively unexpensive in terms of costs and time.

## 1.5 Aims and objectives

The aim of this project was to utilise organotypic models to mimic tissue in order to explore the role of CRC EVs in CRC progression towards metastasis and to evaluate their potential as markers of specific steps of cancer progression. To achieve this, the following objectives were investigated:

Main hypothesis: cancer EVs drive CRC progression and stromal remodelling in organotypic models.

1. Develop a 3D organotypic model of cancer invasion to evaluate the impact of CRC EVs on patterns of invasion.

2. Develop a 3D organotypic model of CRC lung metastasis to investigate the effect of CRC EVs on components of TME.

3. Evaluate the role of CRC EVs in the regulation of cells and proteins involved in ECM remodelling, focussing on crosslinking enzymes such as TG2.

4. Develop a preliminary screening platform based on the responses to stage-dependent CRC EVs using patient samples.

# 2 Impact of colorectal cancer extracellular vesicles on a 3D model of cancer invasion

## 2.1 Introduction

The acquisition of invasive behaviour by cancer cells is a crucial step for malignancy and disease advancement. Since invasion is required not only to penetrate a new tissue, but also in leaving the primary tumour towards extravasation, the process is generally considered an early step of cancer progression (Lusby *et al*., 2022). A combination of factors from the tumour microenvironment (TME) influence and modify cancer cells that are destined to detach from the primary tumour and migrate into the surrounding matrix. One of the most described events linked to invasion is the ability of cancer cells to undergo epithelial to mesenchymal transition (EMT). By appropriating EMT, cancer cells acquire the plasticity of mesenchymal cells, facilitating the movement through the stroma (Pearson, 2019; Ribatti *et al*., 2020). EMT is highly regulated by cells in the TME, such as cancer-associated fibroblasts (CAFs), through the secretion of chemokines and cytokines (Goulet *et al*., 2019). A common marker of EMT is the loss of E-cadherin (E-cad), a transmembrane protein involved in cell-to-cell interactions (Bruner & Derksen, 2018; Na *et al*., 2020). By losing adhesion, cells can individually detach from the primary tumour and invade the surrounding stroma. Increase in N-cadherin (N-cad) expression mirrors the loss of E-cad and it is directly associated with increased cell motility and the ability to degrade the extracellular matrix (ECM) (Cao *et al*., 2019).

Extracellular vesicles (EVs) can be secreted by cancer cells to exert functions in both paracrine and endocrine ways, and therefore they can contribute to cancer progression at the primary site as well as in metastasis (Chang *et al*., 2021; Kogure *et al*., 2020). Furthermore, EVs and their cargo are dependent on the phenotype of the cell of origin, suggesting that EVs deriving from primary or metastatic cells might reflect the stage of the disease (Chen *et al*., 2019; Depciuch *et al*., 2020; Nakurte *et al*., 2018). Cancer EVs have shown to be involved in cancer progression. They can contribute to the choice of pro-survival and more resistant cancer cell phenotypes, yet it is still unclear whether they directly impact on the invasion of cancer cells (Akao *et al*., 2014). One of the mechanisms with which cancer EVs act is to contribute to the EMT process (Greening *et al*., 2015). Cancer EVs have been observed contributing to EMT by specifically decreasing E-cad expression and migratory activity of cells in bladder cancer (Franzen *et al*., 2015).

Originally, single cancer cell migration was thought to be the mechanism to escape the primary tumour and to move through the stroma. In recent studies, alternative modalities of invasion represented by clusters of cancer cells have been observed in colorectal and in other types of cancer and presented in Section 1.2.1 (Fujiyoshi *et al*., 2020; Kato *et al*., 2023). Tumour budding and poorly differentiated clusters have been found as collective way of invasion in CRC and are generally linked to a more aggressive invasion and better chances to succeed in the extravasation process (Reggiani Bonetti *et al*., 2016). EMT is also partially observed in poorly differentiated clusters (PDCs) and invasive clusters, where only border cells leading the invasion are undergoing EMT, and the core maintains the contact between the cancer cells. According to these recent findings, it is becoming pivotal to investigate whether different invasive patterns can be associated with specific stages of cancer progression and therefore could be used as stage-dependent hallmarks.

*In vitro* models have contributed to the understanding of the complex milieu forming the TME at different steps of cancer progression, denoting the possibility of investigating the effects of EVs in cancer invasion.

### 2.1.1 Characterisation of extracellular vesicles deriving from colorectal cancer cell lines

SW480 primary and SW620 metastatic adenocarcinoma cell lines offer a great advantage as an *in vitro* model in CRC studies as they are derived from the same patients at two different stages of the disease (Leibovitz *et al*., 1976). Studies based on these two cell lines have contributed to obtain information on the molecular signatures, unbiased by the well-established disease heterogeneity. As such, phenotypic variations and whole proteomic and miRNA profiles of SW480/SW620 EVs have been also extensively investigated in the discovery of new biomarkers (Chen *et al*., 2019; Ji *et al*., 2013; Suwakulsiri *et al*., 2019, 2023). These differences in the EV contents have also been linked to different functions, thus showing that cancer derived EVs play a role at different stages of CRC progression (Endzelins *et al*., 2018; Rai *et al*., 2019).

### 2.1.2 3D models to mimic cancer invasion

With the knowledge of the TME contributing to cancer mechanisms such as invasive behaviour, *in vitro* studies must adapt to recapitulate the interactions

between cancer cells and stroma. Movement of cells can be observed through 2D migration experiments, but the polarity of cells and the biophysical forces involved in the process differ when cells move within tissue matrices. Monolayer culture experiments cannot distinguish the pattern of single cells or cluster invasion (Duval *et al*., 2017; Yamada & Sixt, 2019). Widely used cancer spheroids are also not suitable since they lack the major structural components necessary for cancer cells to interact when migrating in the ECM.

Transwell assays have been broadly exploited to observe cell invasion in biological matrices. Different matrices have been employed, but they are generally inert due to the absence of cells that actively maintain and produce ECM, such as fibroblasts (Christianson *et al*., 2013; Franzen *et al*., 2015). Organotypic 3D models allow the embedding of more than one type of cells into different kinds of matrix. In this context, they can provide a suitable system to study the relationship between CRC cells, fibroblasts and ECM in the mechanism of invasion. In previous works, when CRC cells were mixed with fibroblasts into a biological matrix, they naturally formed spheroids growing over time, with invasive events also occurring (Delaine-Smith *et al*., 2019). However, a considerable number of spreading spheroids would make the invasive patterns difficult to quantify in a reproducible way, which would also be time consuming. An organotypic model with similar components was developed for squamous cell carcinoma, where invasion patterns were quantifiable through imaging techniques (Nyström *et al*., 2005).

The study of EVs in cancer has been prevalently performed in 2D cultures with the limitations already discussed (Section 1.4.4) and where possible, the findings were translated into *in vivo* animal models to achieve a more physiological response. Recent studies have highlighted the relevance of environmental conditions when analysing the role of EVs in cancer. Just by looking at EV biogenesis, changes were observed between cells in monolayer and cells in 3D. EVs produced by more physiological models not only differ in size, but they also express a diverse biological activity (Christianson *et al*., 2013; Franzen *et al*., 2015). Therefore, the microenvironment is crucial for EV production, as well as for the evaluation of their effects on cells and components in the stroma. When exercising paracrine functions, EVs are released in the ECM and they can interact

with it towards attaining the recipient cells. But they have also been shown to be retained by the ECM and modified by it (Al Halawani *et al*., 2022).

## 2.2 AIMS

The aim of this chapter is to optimise and develop a biologically relevant organotypic 3D model, based on previous work, to evaluate the influence of CRC EVs on cancer invasion patterns and molecules associated with cancer progression. The model was designed to obtain quantification based on imaging analysis. Optimisation and characterisation were required for the 3D model, as well as for the isolation of EVs. Two types of CRC EVs were investigated, deriving from the patient-matched cell lines SW480 and SW620 to obtain information on changes in the invasion according to the stage of the disease.

## 2.3 Materials and Methods

### 2.3.1 Experimental design

First, a 3D model of CRC invasion was developed based on collagen gel mixture in which SW480 cancer cells and MRC5 fibroblasts were added in different templates (Figure 2.1). Once the best template was chosen, the 3D model was characterised to assess morphological and cellular properties. At the same time, bioreactor conditions were evaluated for the high-yield isolation of EVs from two CRC cell lines, SW480 and SW620. EV characterisation was then performed according to the field guidelines. Finally, CRC EVs were used to condition the 3D model of CRC invasion. Semi-quantitative data on invasive pattern were based on imaging analysis. Molecular markers related to invasion and EMT were evaluated with immunohistochemical approaches.

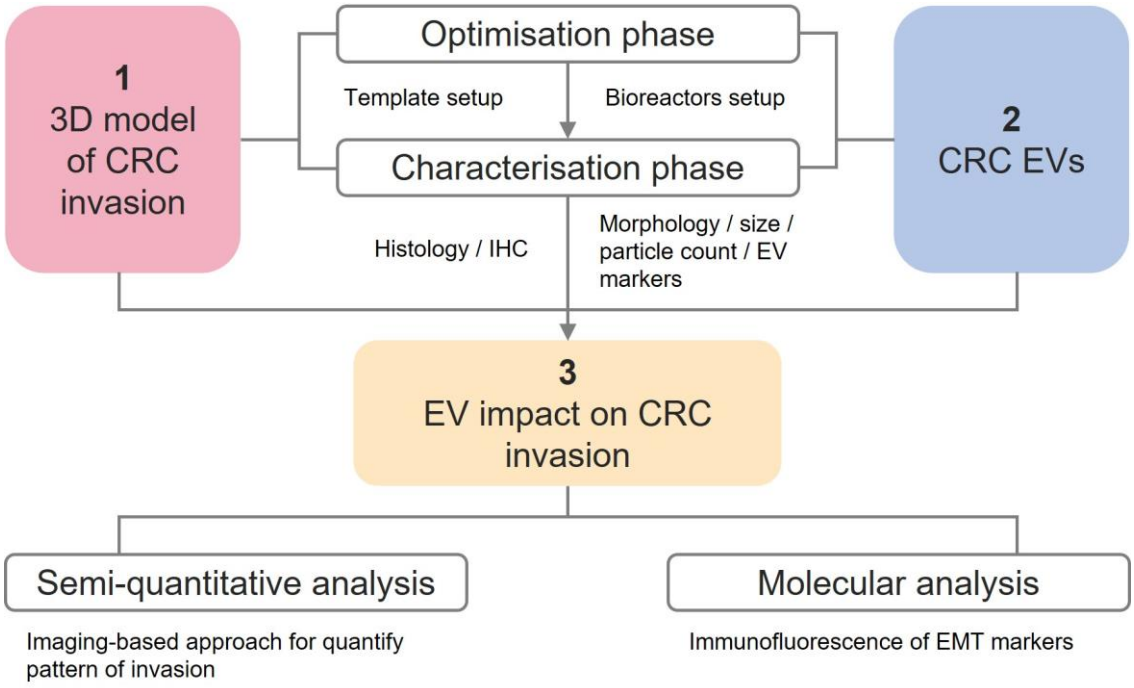


**Figure 2.1. Schematic of Chapter 2 experimental design.** IHC=immunohistochemistry.

### 2.3.2 2D Cell culture

Primary adenocarcinoma SW480 cell line and patient-matched secondary adenocarcinoma SW620 cell lines were purchased from the European Collection of Authenticated Cell Cultures (ECACC), while human lung fibroblast cell line (MRC5) and human foreskin foetal fibroblasts cell line (HFF2) were purchased from Sigma Aldrich (Gillingham, UK). All cells were cultured in complete Dulbecco's Modified Eagle Medium (cDMEM), which was comprised of high

glucose DMEM with GlutaMAX with pyruvate (Gibco, Thermo-Fisher, UK), 10% v/v foetal bovine serum (FBS; Gibco, Thermo-Fisher, UK) and 1% v/v penicillin/streptomycin (P/S; Lonza Ltd., UK). The cells were maintained in a humidified incubator at 37°C and 5% $CO_2$ in air. Culture medium was replaced every 3-4 days and cells sub-cultured (ratios 1:10 SW480/SW620, 1:5 HFF2/MRC5) with Trypsin-EDTA (Thermo-Fisher, Loughborough, UK) when reaching 70-80% of confluence. Cells were checked for mycoplasma with MycoAlert© Detection kit (Lonza Ltd., UK) every 6 months and were shown to be negative throughout.

## 2.3.3 3D Cell Culture

Three different *in vitro* models of invasion were compared to assess which was the most suitable for showing invasive patterns, all based on the preparation of a collagen-based gel mixture (Figure 2.2).

### *2.3.3.1 Transwell model*

For the first 3D model (Figure 2.2A), the gel was composed of 57.5% v/v collagen type I (3 mg/ml, BD Bioscience, Wokingham, UK) and 17.5% v/v GelTrex™, which is a mixture of basement membrane components (Life Technologies, Thermo-Fisher, UK). The mixture was prepared in cDMEM to which fibroblasts (HFF2 or MRC5) were mixed at a concentration of 528,000 cells/ml. Gels were cast using 125 µl/well in the upper compartment of a 24-well plate Transwell™ insert (0.4 µm pore size) for 1 hour at 37°C and 5% $CO_2$. Then, 100 µl of SW480 at 264,000 cells/ml in serum-free DMEM were added to the top of the gel. Complete DMEM (600 µl) was added in the compartment underneath, so that the growth factors present in the FBS could act as chemoattractant for the cancer cells.

### *2.3.3.2 Gel spheroid model*

The second 3D model (Figure 2.2B) utilised the same gel composition in which fibroblasts were mixed at a concentration of 528,000 cells/ml. The gels were cast on ultra-low attachment 96-well plates (Greiner Bio, UK), to create a spheroid gel. SW480 cells (100 µl) were then applied to the top of the gel in serum-free DMEM at a cell density of 264,000 cells/ml.

#### *2.3.3.3 Cancer cell spheroid model*

In the third 3D model (Figure 2.2C), 100 µl SW480 (264,000 cells/ml) were added at the bottom of ultra-low attachment multiple 96-well plates and left overnight (ON) to form spheroids. The gel containing HFF2 cells (528,000 cells/ml), was prepared in serum-free DMEM as described in Section 2.3.3.1 and cast on the top of the spheroid. Once set, 200 µl of cDMEM was overlaid.

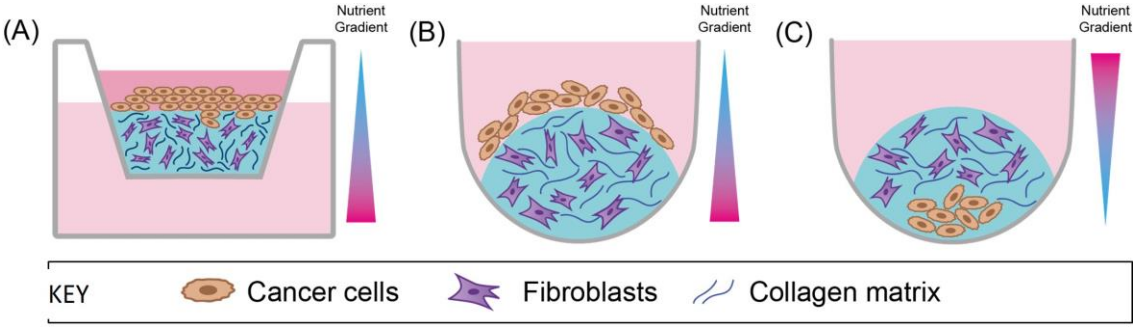


**Figure 2.2. 3D models of invasion** (A) Transwell model (B) Gel spheroid model; (C) Cancer cells spheroid model. A nutrient gradient was present in each model to drive cancer cell invasion.

### 2.3.4 Sample preparation for histology/IHC/IF

Samples from Section 2.3.3 were processed at different time points (day 1, 3, 7 or 14) for paraffin embedding according to the standard protocols. Briefly, samples were fixed for 12-24 hours in 10% neutral buffered formalin (Merck, UK), then dehydrated in graded industrial methylated spirit (IMS; Merck, UK), cleared in xylene substitute (Sub-X, Leica Microsystems, UK) and embedded in molten paraffin wax (Leica Microsystems, UK). Tissue sections of 4 µm were mounted onto X-tra™ adhesive glass slides (Leica Microsystems, UK) and dried for a minimum ON and for a maximum of a week at 37°C. The sections were stored at room temperature (RT) until further analysis. Prior to any staining, deparaffinisation was performed by washing in Sub-X (3x5 min). Then, sections were rehydrated in graded passages of IMS (100% x 2 min, 90% x 2 min, 70% x 2 min) and rinsed in water.

All the histological and immunohistochemical images were observed with an Olympus BX60 microscope and images captured by a digital camera Olympus XC30 and Olympus CellSens software (Media Cybernetics, Buckinghamshire, UK).

#### *2.3.4.1 Haematoxylin & Eosin staining*

Haematoxylin and eosin were performed to evaluate the morphology of the cells in the 3D models. Sections were stained with Mayer's Haematoxylin (Merck, UK) for approximately 3 min to counterstain cell nuclei (dark purple), blued in running tap water for 6 minutes prior to 1% aqueous Eosin Y solution (Leica biosystems, UK) staining (4 min) for the cytoplasmic regions of the cells (pink). Sections were dehydrated in IMS (5 min, 3 times), and then IMS was cleared by Sub-X (5 min, 3 times). Finally, sections were mounted with 1 drop of Pertex (Leica Biosystems, UK) per slide and coverslips were applied.

#### *2.3.4.2 Masson Trichrome staining*

Masson Trichrome staining was applied to the sections according to the manufacturers protocol (Atom Scientific, UK) to evaluate the matrix structure within the 3D model. With this staining, collagen is stained in blue, cell nuclei in dark red/brown, muscle tissue in red and cytoplasm in pink. Briefly, nuclei were stained with Weigert's Iron haematoxylin for 20 min, rinsed in 1% acid alcohol solution and blued in tap water. Ponceau fuchsin was applied for 5 min and differentiated in phosphotungstic acid for 15 min. Then, the samples were transferred without rinsing into methyl blue solution for 5 min. Sections were finally rinsed, dehydrated in IMS and cleared by Sub-X (2.3.4). Finally, sections were mounted with 1 drop of Pertex (Leica Biosystems, UK) per slide and coverslips were applied.

#### *2.3.4.3 Immunohistochemistry*

Dehydration, clearing and mounting were performed as described in Section 2.3.4. Immunohistochemistry (IHC) for rabbit primary antibody Ki67 (1:200, ab15580 polyclonal; Abcam, Cambridge, UK) was performed to observe the degree of actively proliferating cancer cells in the 3D model and visualised using biotinylated secondary goat anti-rabbit antibody (1:500, Abcam, Cambridge, UK). After deparaffinisation and rehydration, endogenous peroxidases were blocked by submerging the slides in 3% v/v hydrogen peroxide (Merck, UK) in IMS. After two washes in $dH_2O$, heat-induced antigen retrieval (HIAR) was performed to remove formalin cross-links. Slides were placed into citrate buffer (10 mM citric acid, pH 5.9) and irradiated for 5 min at 40% pwr with a 900W microwave. After 1 min of rest, slides were irradiated again for 5 min at 20% pwr. Slides were left to rest for 15 min and then washed with tris-buffered saline (TBS; 20 mM Tris,

150 mM NaCl, pH 7.5). Secondary antibody host interactions were blocked with a solution containing 1% w/v bovine serum albumin (BSA; Merck, UK), 75% v/v TBS and 25% v/v normal goat serum (Merck, UK). Ki67 primary antibody (1% BSA/TBS) was applied ON at 4°C in a humidified environment. Three washes in 0.5% v/v Tween-20/TBS were performed before applying the secondary antibody (1% BSA/TBS) for 30 min at RT. Then, three washes in 0.5% v/v Tween-20/TBS were performed followed by the treatment with horseradish peroxidase avidin-biotin complex (HRP ABC kit, Vector Laboratories, Peterborough, UK) for 30 min at RT. Three more washes with 0.5% v/v Tween-20/TBS were performed and then a solution of 0.65 mg/ml of 3,3-diaminobenzidine tetrahydrochloride (DAB; Merck, UK), 0.08%v/v in TBS was added for 20 min or until brown colouration was visualised under the microscope. Slides were washed in $dH_2O$ for 5 min prior to the dark purple nuclei counterstain in Mayer's haematoxylin (approximately 3 min) and then blued under tap water for 6 min.

#### *2.3.4.4 Immunofluorescence*

To evaluate ECM-stroma interactions, immunofluorescence (IF) was performed for primary antibodies α-SMA (1:500, ab7187 mouse monoclonal 1A4, Thermo-Fisher, UK) as CAF marker, N-cad (1:50, CD325 mouse monoclonal 8C11; Thermo-Fisher, UK), E-cad (1:100, ab40772 rabbit monoclonal EP700Y; Abcam, Cambridge, UK) and catenin delta-1 (p120) (1:100, ab92514 rabbit monoclonal EPR357(2), Abcam, Cambridge, UK) as EMT markers. Goat anti-mouse secondary immunoglobulin (IgG) antibody labelled with Alexa Fluor® 488 (1:500, Abcam, Cambridge, UK) and goat anti-rabbit secondary IgG antibody labelled with Alexa Fluor® 555 were used to visualise the staining. After deparaffinisation and rehydration, HIAR was performed followed by the blocking step in goat serum (2.3.4.3). For p120, a permeabilisation step in 0.1% Triton-X/TBS for 10 min was necessary. Sections were incubated with primary antibodies (1%BSA/TBS) ON at 4°C in a humidified environment. Three washes in 0.05% v/v Tween-20/TBS were performed followed by the incubation with secondary antibodies (1%BSA/TBS) for 1 hr at RT. Three more washes were performed and then VECTASHIELD® HardSet™ Antifade Mounting Medium with 4′,6-diamidino-2-phenylindole (DAPI) (Vector Laboratories, Peterborough, UK) was used to mount the coverslips. Images were acquired with Olympus IX81 inverted microscope (Media Cybernetics, Buckinghamshire, UK). Confocal images were acquired with

Zeiss Axio LSM800 (Zeiss, Germany, UK). Mean fluorescence intensity was obtained.

## 2.3.5 CRC-derived Extracellular Vesicles

### *2.3.5.1 Isolation of CRC-derived Extracellular Vesicles*

SW480 or SW620 cells were cultured in WHEATON® CELLine™ AD-1000 Bioreactor flasks (DWK Life Sciences, GmbH). Briefly, the cells (2.5 x $10^7$) in 15 ml of DMEM with 10% FBS, 1% P/S were added to the inner cell compartment. 500 ml of DMEM with 10% FBS, 1% P/S was then added to the media compartment. The cells were left to grow and adhere to the membrane for 10 days. Then, the conditioned media (CM) was replaced after washes in phosphate buffered saline (PBS) with two alternative conditions: serum free (DMEM with 1% P/S) or EV-depleted FBS media, in which normal FBS was substituted with 10% of Gibco EV-depleted FBS (Thermo-Fisher, UK) (Figure 2.3). In the latter condition, media in the outside compartment was replaced with 5% normal FBS and 1% P/S in DMEM. The outside media was replaced weekly in both conditions. The EV-enriched CM, harvested weekly, was centrifuged at 300×g for 5 min (21 °C). The supernatant was collected and centrifuged again at 2000×g for 5 min (21 °C). The supernatant was then stored at - 80 °C until further use.

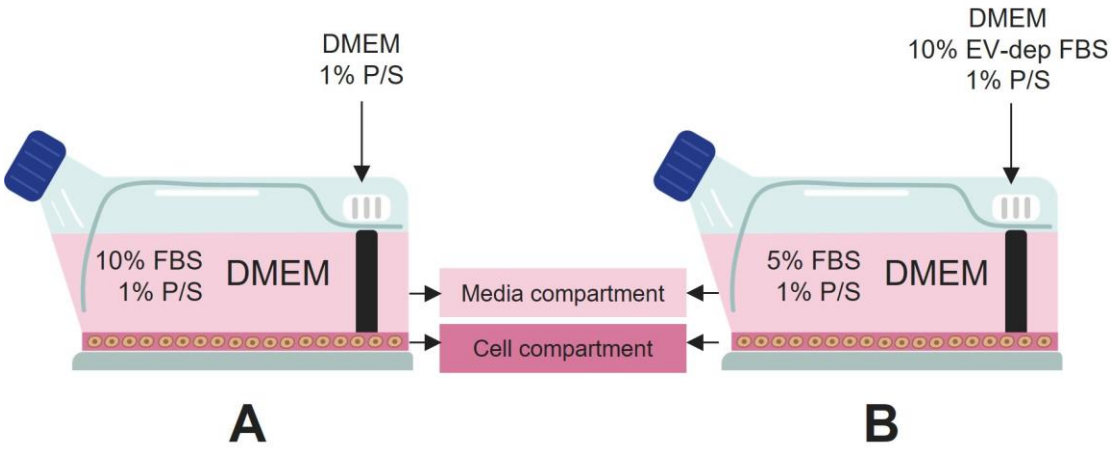


**Figure 2.3. Serum free condition and EV-depleted serum-enriched condition in bioreactor flasks.** Schematics of Wheaton® CELLine™ Adherent bioreactor flasks showing the two alternative conditions investigated. (A) Serum free CM was replaced to the cell compartment after 10 days of equilibration. (B) EV-depleted media was replaced to the cell compartment after 10 days of equilibration. The media in the outside compartment was also replaced with DMEM with 5% FBS media instead of 10%.

#### *2.3.5.2 EV purification by size-exclusion chromatography*

The conditioning media was concentrated through Vivaspin® 20 (100 kDa MWCO) (Sartorius, Germany) to reach a volume of 0.5 ml at 3000g. EVs were separated from soluble factors by size exclusion chromatography in 14 ml of sepharose CL-2B (GE Healthcare, Uppsala, Sweden) loaded in disposable Econo-Pac columns (Biorad, Watford, UK) and eluted in PBS. Twenty fractions of 0.5 ml were obtained from each column.

#### *2.3.5.3 Protein quantification with BCA assay*

Protein quantification assay was performed on fractions 1-20 using bicinchoninic acid (BCA) assay to evaluate the protein content in each SEC fraction and pooled SEC fractions. BSA was used to generate 1:2 serial dilutions between 15.625 - 2000 µg/ml as a standard curve. Then, 10 µl of samples and standard were placed in 96 well-plate in duplicate, with 100 µl of working reagent, consisting of copper sulphate II solution (Sigma-Aldrich®) and BCA solution (Sigma-Aldrich®) in a 1:50 ratio. The plate was incubated at 37° C for 1 hour. Absorbance was read at 570 nm (0.1 s) with a Wallac Victor2™ 1420 multilabel counter (Perkin-Elmer, USA). Absorbance from standards was used to create a standard curve and protein concentration was calculated for each fraction.

#### *2.3.5.4 Transmission electron microscopy*

To evaluate EV morphology, membrane integrity and size, transmission electron microscopy (TEM) was performed at the Electron Microscopy facility, Faculty of Science, University of Sheffield. EVs were transferred through absorption onto carbon-coated copper grids for 1 minute, quickly dried with filter paper and then washed twice with water. Then filtered 2% uranyl acetate was used for 2 min to negatively stain the EVs. Excess liquid was removed with filter paper, and the grid was allowed to dry for 10 min, the grids were then stained in Uranyl Formate. Grids were visualised on a FEI Tecani G2 Spirit BioTwin (PennState, USA) TEM, and images were recorded using a Gatan Orius 1000B CCD camera and Gatan Digital Micrograph software (Gatan, USA) at the University of Sheffield facility.

#### *2.3.5.5 Western Blot for TSG101 and GM130*

To confirm the presence of EVs in the SEC fractions, positive (TSG101) and negative (GM130) markers of EVs were investigated by western blots. Cell lysates were used as negative controls to evaluate marker specificity. Antibodies against TSG101 (ab2386 mouse monoclonal [CUB 7402]; Abcam, UK; 1:1000

dilution) and Golgi matrix protein GM130 (ab52649 rabbit monoclonal [EP892Y]; Abcam, UK; 1:1000 dilution) were used. A volume of 15 µl of determined SEC fractions was loaded in 10% sodium dodecyl sulphate (SDS)-polyacrylamide resolving gels and electrophoresed in running buffer (0.25 M Tris, 1.92 M Glycine, 1% w/v SDS) at 120 V for 1.5 hr. The resolved proteins were transferred onto the nitrocellulose membrane in transfer buffer (1:1:5 RTA Transfer Kit: EtOH:dH2O) (Bio-Rad, UK) using Trans-Blot® Turbo™ transfer system (Bio-Rad, UK) for 7 min. The membrane was then blocked with blocking buffer 5% w/v non-fat dried milk (Marvel, UK) in washing buffer 0.05% Tween20 in Tris Buffered Saline) at RT for 1 hr. TSG101 and GM130 primary antibodies were added to the blocking solution and left ON at 4°C. The membrane was rinsed and washed three times for 10 min each with washing buffer before IRDye 800RD goat anti-mouse or IRDye 680RD donkey anti-rabbit secondary antibodies (1:10000 dilution; LI-COR Biosciences, UK) were added and incubated at RT for 1 hour. The membrane was washed again three times in washing buffer and then analysed using Li-Cor® Odyssey® instrument.

#### *2.3.5.6 Nanoparticle Tracking Analysis*

Nanoparticle tracking analysis (NTA) of EV fractions from serum free bioreactor isolations was performed to evaluate particle count and size with Zetaview® (ParticleMetrix, Germany) available at the department of Oncology and Metabolism (Medical school) at University of Sheffield. Briefly, EV fractions were diluted to obtain an ideal concentration between 1 – $5x10^8$ particles/ml. Then, 15 ml of particles were introduced in the instrument. 11 positions were taken for each analysis.

#### *2.3.5.7 NanoFCM*

To confirm the EV size and content, pooled fractions were further characterised in particle count, size and tetraspanin markers (CD9, CD81, CD63) using a nanoanalyser instrument based on nanoflow cytometry (nanoFCM) through collaboration with NanoFCM Co., Ltd (MediCity, Nottingham, UK). Briefly, 10 µl of unlabelled EVs were first analysed to assess particle count and size. EVs were compared to QC beads (250 nm silica standard) and size beads (68, 91, 113 and 155). Then, $2x10^8$ particles were labelled with FITC/APC conjugated antibodies for CD9, CD81 and CD63 (1:10) and incubated at RT for 30 min. Finally, 10 µl was run on the instrument.

### 2.3.6 Conditioning with SW480/SW620 EVs

Routine treatments with EVs were based on protein concentration assessed by the BCA assay. To observe EV uptake, SW480 and SW620 EVs were labelled with 500 nM CellTracker™ Deep Red (Thermo-Fisher, UK) for 30 min and then ultracentrifuged for 1 hour at 100,000g with an Optima™ MAX Ultracentrifuge (Beckman-Coulter, High Wycombe, UK) to remove the excess of dye. Then, 50 µg/ml of SW480 EVs or SW620 EVs were introduced in serum free DMEM in the upper compartment of the transwell model at day 0, after the invasion of cancer cells, and at day 4 of the cultures described before (Section 2.3.3.1). A control treatment of only PBS with the same volume of EVs introduced was also performed. The bottom compartment of the transwell was replaced by DMEM with 10% EV-depleted FBS. For this treatment, the 3D cultures were maintained until day 7 exclusively. The 3D models were then fixed and processed accordingly (Section 2.3.4).

### 2.3.7 Quantitative measurements of CRC invasion

Tile images from the histological staining sections were taken at 20x magnification, to obtain a high resolution of all the samples. All the analyses were performed with ImageJ 1.5i software. Scale bars from the images were used to set the scale of the measurements. The horizontal set point was taken considering the invasive front of cancer cells always at the top of the sample (Figure 2.4). The perimeter dividing cancer cells and matrix was defined as front of invasion. Freehand selections were drawn following the area of the SW480 cells or cluster cells invading the matrix and area size were acquired. A threshold of 70 $\mu m^2$ (which corresponded to a single nuclei observation) was considered when separating between single cells and cell clusters. Five measurements of the length of invasion were taken where the clusters were found at the furthest distances from the invasive front. The five biggest clusters observed in the samples were also measured in their vertical length to see whether EVs impacted on the direction of invasion towards the matrix.

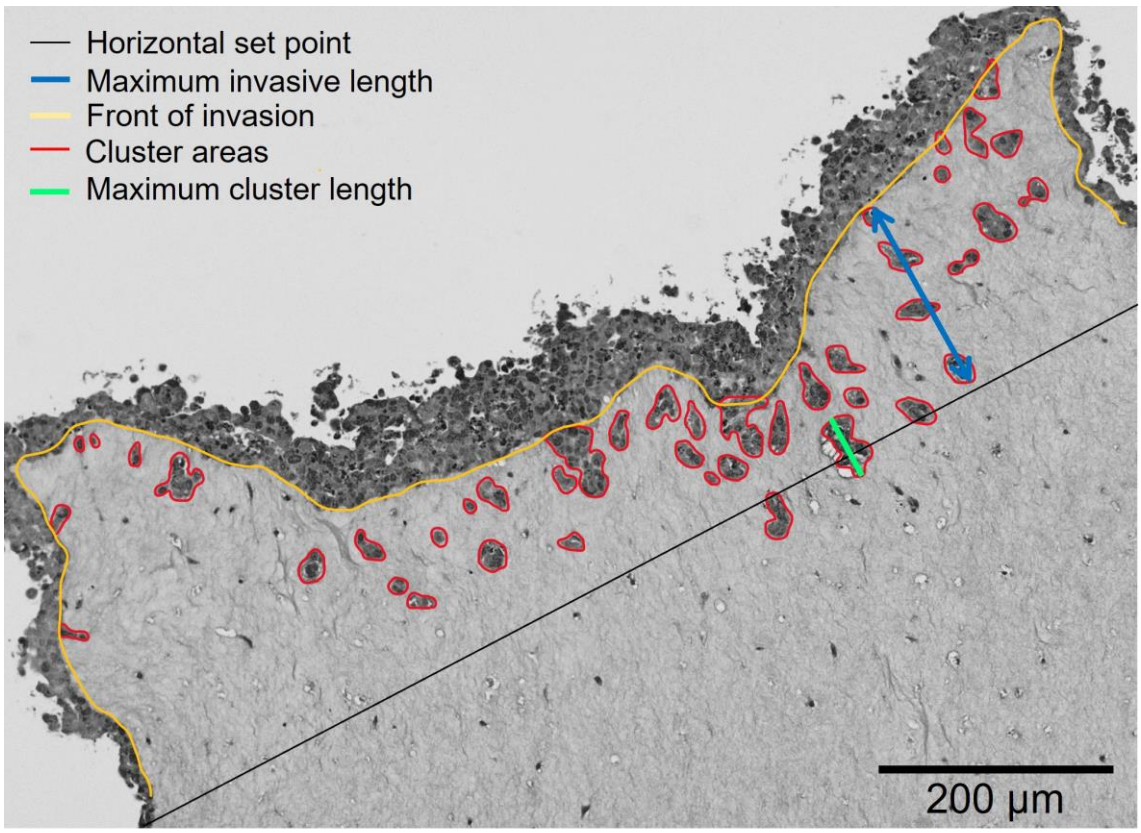


**Figure 2.4. Setting of quantitative measurements of invasion.** Representative histological image showing the measurements on the invasion of SW480 cells in the stroma. Measurements were performed with ImageJ software (n≥2 for each condition).

### 2.3.8 Statistical analysis

Statistical analysis was performed using Prism 8.1.1. Data were tested for normality (gaussian distribution) with two modalities: D'Agostino & Pearson test (for data with n > 3) and Shapiro-Wilk test (for data with n ≤ 3).

As the groups tested were 3, multiple comparison tests were employed for all the dataset of this chapter. Multiple comparison through ordinary one-way analysis of variance (ANOVA) with Tukey's test as post-hoc analysis was performed for parametric data, while Kruskal-Wallis (KW) test with Dunn's test as post-hoc analysis was performed for non-parametric data. P-values < 0.05 were considered significant.

Data representation varied according to the number of replicates and the normal distribution. For data with n ≤ 6, individual values were shown. When data were shown as summary, mean ± standard error of the mean (SEM) was used for parametric data, whereas media ± 95% confidence interval (CI) was used for non-parametric data.

## 2.4 Results

### 2.4.1 Optimisation of a 3D model of colorectal cancer invasion

Initially, the three different models were compared to obtain a system showing a reproducible layer of invasion. Samples were collected at day 1 and day 3. The size of all the gels prior to processing was around 2-3 mm. Once processed, all the models were subjected to shrinkage (about 1 mm) due to dehydration during the tissue processing (data not shown). Histological analysis of the samples was performed to evaluate the gel conditions and the cancer cell layer (Figure 2.5). The transwell model and gel spheroid model showed a thin layer of SW480 cells at the top of the gel (Figure 2.5A, B). In the embedded spheroid model at day 1 no spheroid was found, while at day 3 a cancer cell spheroid was present surrounded by a highly fibrotic area (Figure 2.5C). Evenly distributed foci indicating the presence of HFF2 fibroblasts were found in the transwell model, but they were scarce in the gel spheroid and in the embedded spheroid.

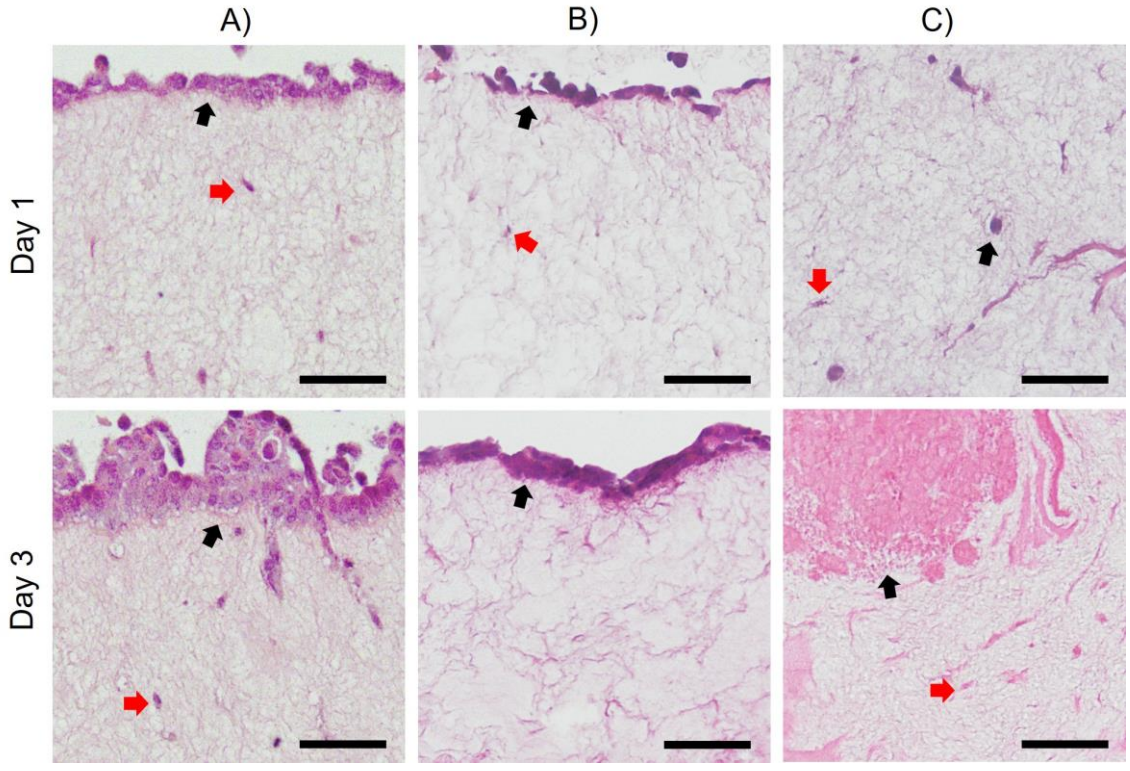


**Figure 2.5. 3D models of CRC invasion.** H&E of sections from day 1 and day 3 3D cultures. (A) Transwell model; (B) Gel spheroid model; (C) Embedded spheroid model. Cancer cells indicated by the black arrows; fibroblasts indicated by the red arrows. Scale bar = 50 µm.

The transwell model was chosen as it showed a measurable and reproducible layer of cancer cell invasion. Cultures from this model were progressed for 7 days and 14 days. A decrease in size was observed during the time of the culture due to the presence of fibroblasts progressively contracting the gels (Figure 2.6).

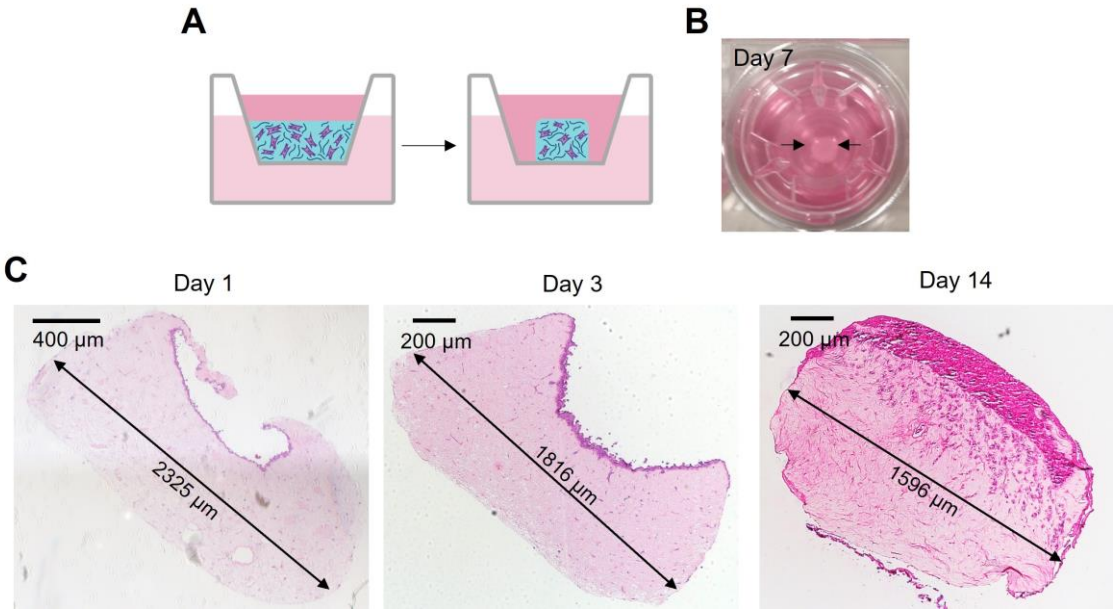


**Figure 2.6. Gel contraction**. (A) Schematic representation of gel contraction in the Transwell™ inserts. (B) Photograph of contraction of the gel at day 7. (C) Representative H&E from 3D models at day 1, day 3 and day 14 of culture (n=1). Maximum diameter length measured with Image J software.

MRC5 fibroblasts were used in gels as an alternative to HFF2 fibroblasts for two reasons; first, to observe whether differences in the behaviour of fibroblasts in the gel are depending on the cell line. Secondly, MRC5 cells derive from lung, relevant for adapting the model for future analysis on lung metastasis. At day 7 of culture, clusters of invasive SW480 were observed and were morphologically discernible from the fibroblasts in the matrix (Figure 2.7A). While some of these clusters appeared to remain connected to the compact front of invasion, others were detached from it at different distances. Maintaining the culture until day 14 showed an increase in number and size of the cancer cell masses (Figure 2.7A). The rich collagen-based matrix was observable by blue staining of the Masson's Trichrome stain, which highlighted the fibrillar structure of collagen (Figure 2.7B).

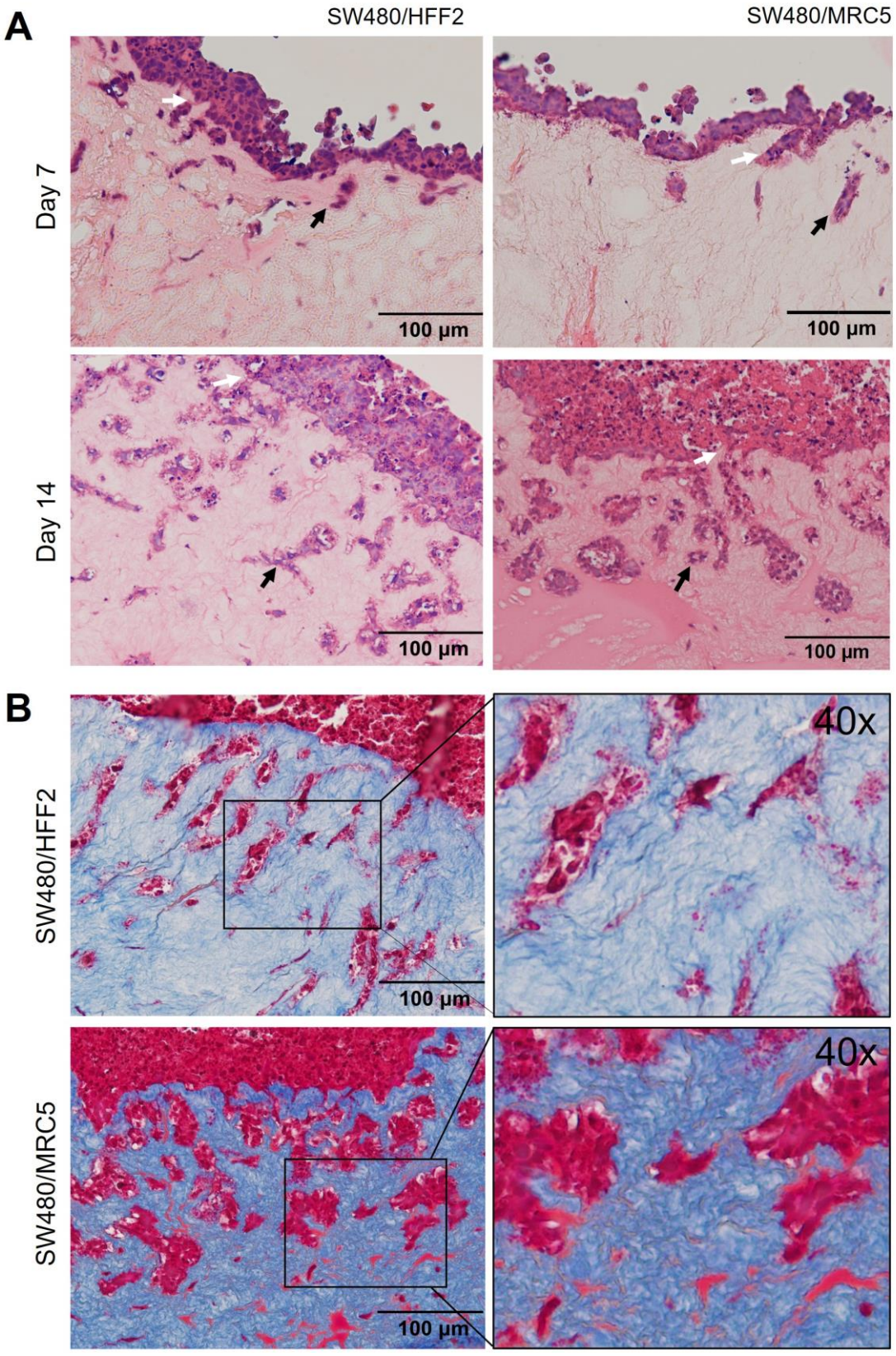


**Figure 2.7. Example of histological staining of CRC invasion 3D models.** (A) H&E of sections from day 7 and day 14 of the 3D culture showing the areas of cancer invasion (20X). Clusters of SW480 cells that invaded in the collagen matrix are indicated with arrows: white arrows = clusters attached to the front of invasion, black arrows = distant clusters. (B) Masson's Trichrome staining of sections from day 14 of 3D culture. Higher magnification images shown in inserts.

Immunohistochemical staining for Ki67, a proliferative marker, was observed only at day 7 of the cultures, with the protein strongly expressed by SW480 at the front of invasion and occasionally by the clusters closer to the front (Figure 7). At day 14, Ki67 was not expressed by SW480.

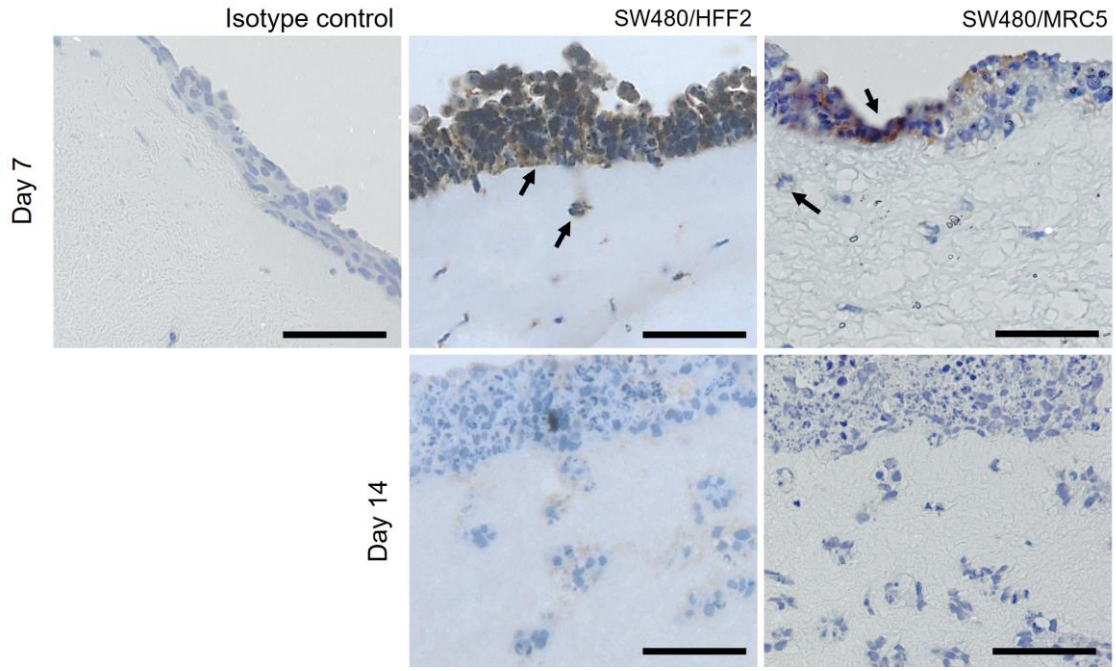


**Figure 2.8. Proliferation of SW480 in the 3D model of invasion.** Representative image of IHC for Ki67 (brown staining) marker of proliferation at day 7 and day 14 of the culture. Black arrows indicate the cells positive for Ki67. Haematoxylin as nuclei counter stain (blue). Scale bar = 50 µm.

## 2.4.2 Characterisation of SW480 and SW620 EVs from CELLine™ Bioreactor

### *2.4.2.1 Size and particle count of SW480 and SW620 EVs from serum free culture*

SW480 and SW620 EVs from serum-free bioreactors were characterised for protein concentration, size and particle count. To obtain a high yield of EVs, cells need to be cultured at densities not achievable with a normal 2D monolayer. For this reason, SW480 and SW620 cells were cultured in Wheaton® CELLine™ adherent bioreactor flasks, which allow cells to grow into a system of 3D membranes increasing the surface area 50-fold (Artuyants *et al*., 2021). The membrane has a molecular weight cut-off of 10 kDa that separates the cells from the media chamber and allows the enrichment of cell derivatives (EVs, larger soluble proteins). Once injected, adherent and viable cells cannot be removed until the end of the bioreactor culture. Once every week, conditioning media (CM)

was harvested from the cell compartment and SEC was chosen as the isolation method, following minimum information for the study of extracellular vescicles (MISEV) guidelines (Théry *et al*., 2018). BCA assay was performed on the fractions from the two bioreactor conditions tested to evaluate the protein concentration at different stages of the life of the bioreactor (Figure 2.9A, Figure 2.10). At later fractions, soluble proteins were generally present at high concentrations. Nanoparticle tracking analysis was performed to evaluate size and particle count of the EV fractions. Mean size decreased from F8 to F10, with SW480 EVs bigger than SW620 EVs (Figure 2.9B). The number of particles was high for EVs derived from both cell lines, with SW620 EVs generally higher, which aligned with the BCA assay data.

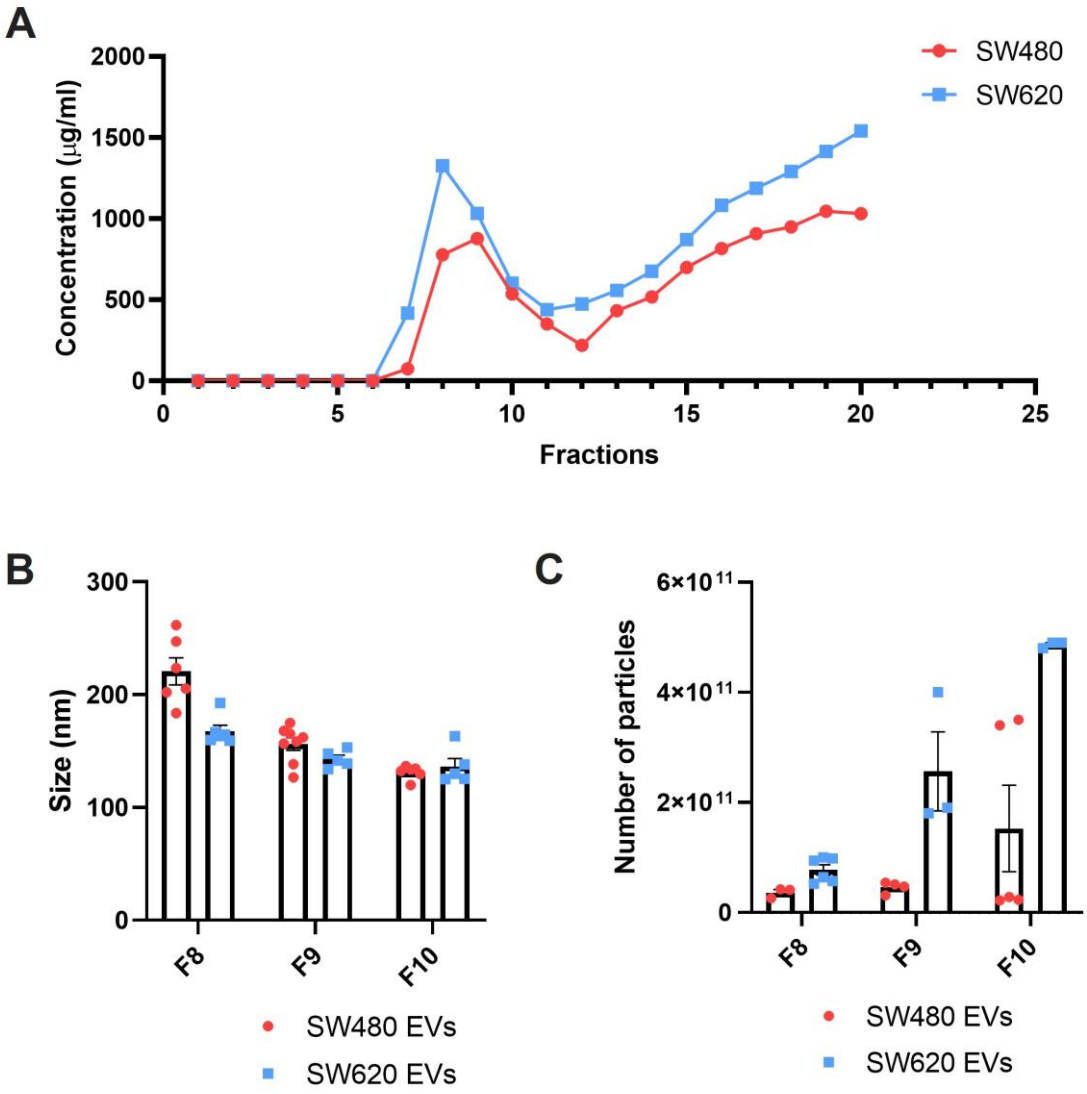


**Figure 2.9. Protein concentration, size and particle count and marker of SW480 and SW620 EV fractions from serum free conditioning.** (A) BCA assay of fractions from SEC for SW480 and SW620 CM. (B) Size obtained with nanoparticle tracking analysis (NTA) of the three fractions

with highest protein concentration; Mean ± SEM (n=3). (C) Particle counts obtained with NTA of the three fractions with highest protein concentration; Mean ± SEM (n=3).

#### *2.4.2.2 EV production from serum free media and EV-depleted serum enriched media cultures*

During the first four/six weeks of both conditions, EVs were enriched in protein, with the highest concentration generally around 1000 µg/ml (Figure 2.10A, B). After two months of culture, a sharp drop in protein concentration could be observed in the serum-free bioreactors (Figure 2.10A). In the EV-depleted serum-enriched bioreactors, proteins were still detectable with the assay, although the separation between the EVs peak and the soluble proteins peak was less evident due to a further increase in the soluble protein fractions (Figure 2.10B). EV-depleted serum-enriched condition was chosen for maintaining bioreactors in the long term.

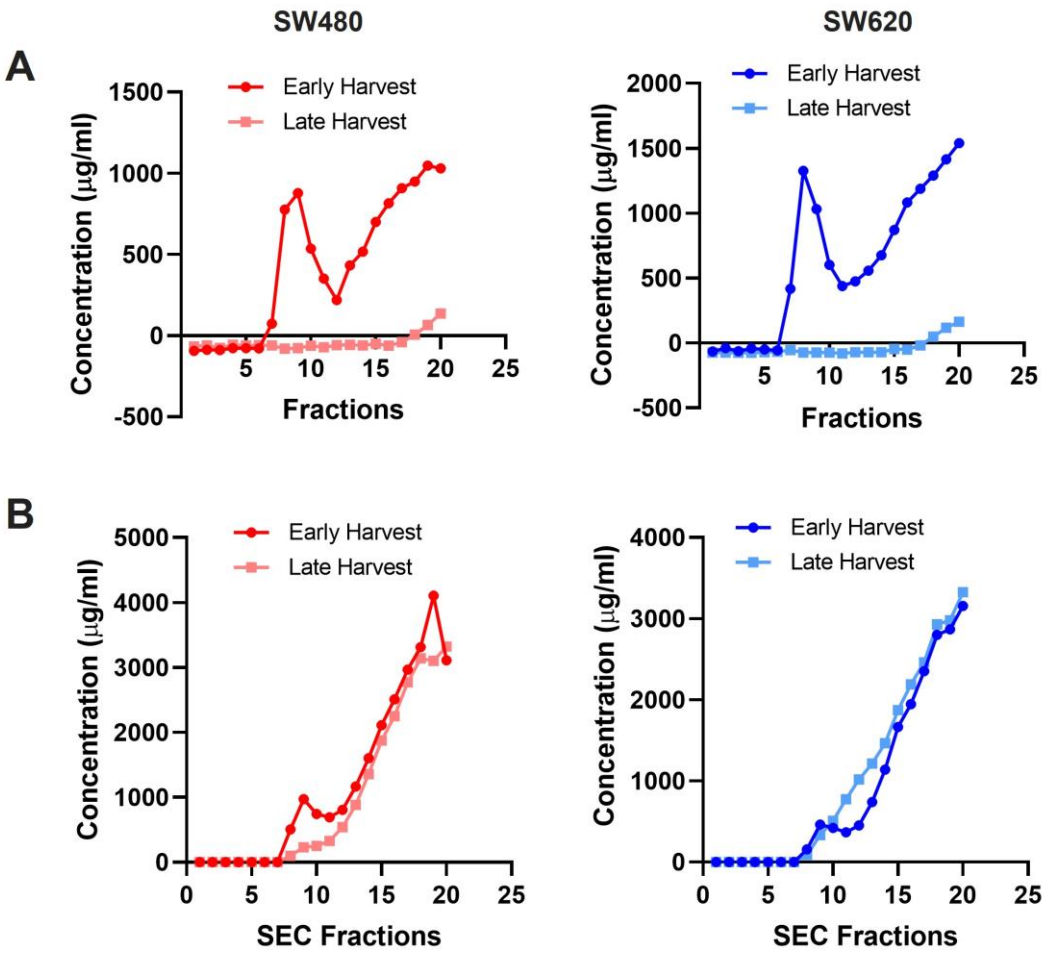


**Figure 2.10. BCA Assay of CM from serum free bioreactors and EV-depleted serum-enriched bioreactors.** Early harvest indicates CM collected in the first two weeks of the bioreactor life. Late harvest indicates CM collected after two months of the bioreactor life. (A) BCA

Assay of the CM from serum free bioreactors. (B) BCA Assay of the CM from EV-depleted serum-enriched bioreactors.

#### *2.4.2.3 Size, particle count and EV markers in EVs derived from SW480 and SW620 cultured in EV-depleted FCS media*

TSG101 is involved in EV biogenesis, and GM130, a protein associated to Golgi intracellular membranes, were used respectively as positive and negative markers for the isolated EV fractions deriving from the bioreactors with EV-depleted media (Figure 2.11A). Fraction 20 deriving from SEC showed high concentration of soluble proteins, thus was used to compare against the effects of EVs. GM130 was absent in all the EV fractions and soluble proteins fractions but present in the cell lysate (Figure 2.11A). TSG101 was found in the EV fractions, the lysates, but not in the soluble protein fraction. Results were comparable between the two cell lines. For all the experiments involving SW480 and SW620 EVs as treatment, the three EV fractions with the highest protein concentrations from each SEC isolation were combined (8-10). Particle size, count and three most common tetraspanins (CD9, CD31, CD81) were analysed by NanoFCM to confirm the preservation of EVs in the pooled solution and throughout the bioreactor culture time (Figure 2.11D). CD9 was the most prevalent marker in both EV types, while CD63 and CD81 were found stably at around 10% positivity. While small variations were observed in terms of size, particle count dropped from $10^{11}$ to $10^{10}$ after one month for SW620 EVs. A similar decrease was observed in SW480 EVs at the end of the bioreactor life, which was about three months after seeding (Figure 2.11E).

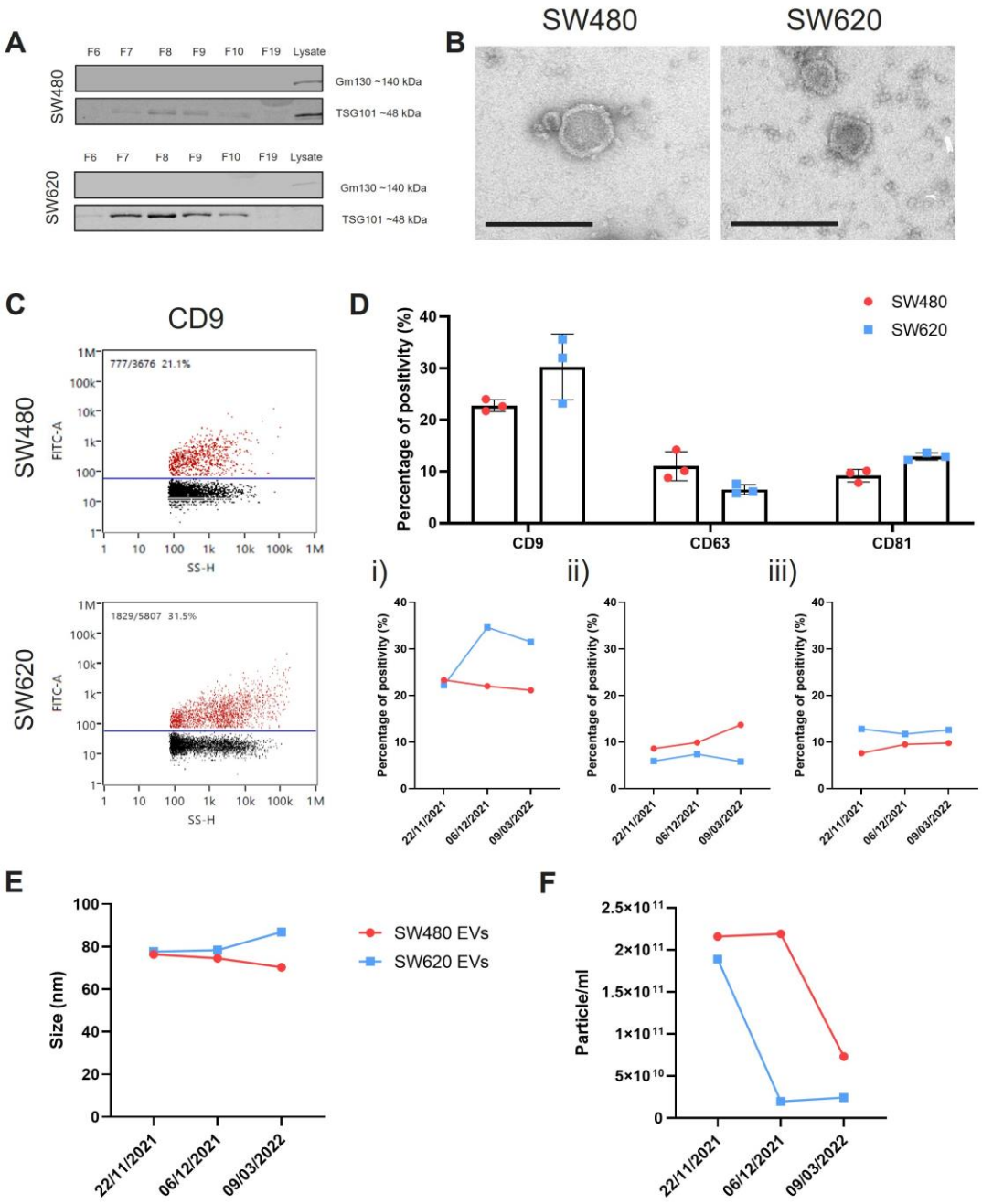


**Figure 2.11. SW480 and SW620 EVs from EV-depleted bioreactors.** (A) Western blot for TSG101 and GM130 of SW480 and SW620 EV fractions. (B) TEM images of CRC EVs. Scale bar = 200 nm. (C) Example of dot plots from NanoFCM analysis. CD9 expression population gated and coloured in red. (D) Summary of EV markers. Mean ± SEM (n=3); (i) CD9, (ii) CD63, (iii) CD81 at three timepoints of the bioreactor life. (E) NanoFCM particle size at three timepoints of the bioreactor life. (F) NanoFCM particle count at three timepoints of the bioreactor life.

## 2.4.3 Impact of CRC EVs on cancer cell invasion

First, the retainment of EVs in the matrix was assessed by observing labelled EVs in the 3D models. After 7 days, fluorescence was observed in both treated gels, whereas no staining was identified in the untreated gels (Figure 2.12).

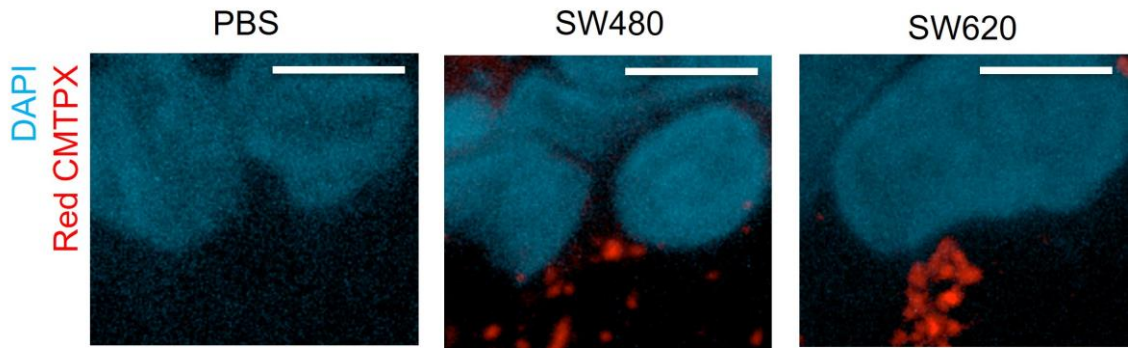


**Figure 2.12. EV labelling showed presence of EVs in the 3D model of invasion.** Confocal images of SW480/SW620 EVs pre-labelled red with CellTracker™ Red CMTPX inside the 3D model at day 7 of culture. Nuclei counter stained with DAPI (blue). Scale bar = 5 µm.

To investigate whether EVs had an impact on the invasion profiles of SW480, quantitative measurements were taken based on stained sections from the 3D invasive culture treated with CRC EVs for 7 days. In particular, the ratio between single cells and larger clusters of cells, the length of the clusters and the depth of the invasion were quantified. Upon treatment with SW620 EVs, less single cell invasion was observed ($P \leq 0.01$) in favour of an increase of cell clusters ($P \leq 0.01$) (Figure 2.13B). Measurements were taken in the regions where the invasion was found > 50 µm in the matrix. SW620 EVs significantly increased the depth of invasion compared to PBS control ($P \leq 0.001$) and SW480 EVs ($P \leq 0.01$) (Figure 2.13C). Both primary and metastatic EVs impacted on cluster length and areas, although only the SW620 EVs increase was significant ($P \leq 0.0001$) (Figure 2.13D, E). Interestingly, the effects on depth of invasion and cluster length deriving from the two types of EVs were also significantly different ($P \leq 0.05$) (Figure 2.13C, D).

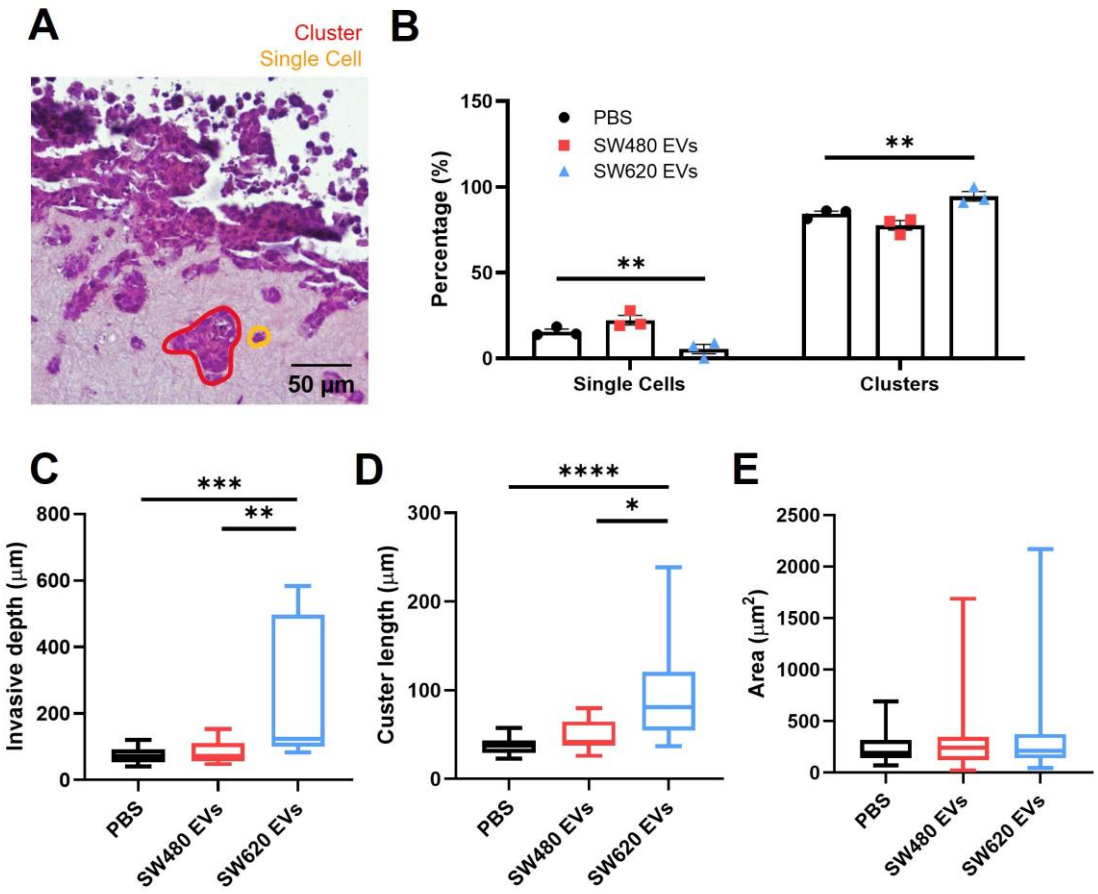


**Figure 2.13. Quantitative measurements of SW480 invasion upon treatment with CRC EVs.** (A) Representative image of cluster cells (red), single cells (yellow). (B) Ratio between single cell and cluster invasion in percentage. Particles ≤ 70 µm$^2$ were considered single cells. Particles > 70 µm$^2$ were defined as clusters. Mean + SEM (n = 3); ANOVA, ** P ≤ 0.01. (C) Depth of invasion. Measurements were taken in the regions where the invasion was > 50 µm inside the matrix. Min to max (n=3); Kruskal-Wallis ** P ≤ 0.01, *** P ≤ 0.001 (D) Length of clusters invading in the matrix. Measurements were taken of the 10 biggest clusters that were detached from the invasive layer per sample. Min to max (n=3); Kruskal-Wallis * P ≤ 0.05, **** P ≤ 0.0001. (E) Areas of cluster cells. Min to max (n=3); Kruskal-Wallis.

Expression of markers of invasion was investigated in the single cells/clusters region of interests (ROIs). E-cadherin expression significantly increased in both SW480/SW620 EV treated cultures compared to the control (P ≤ 0.0001) (Figure 2.14B). Increase in N-cad was identified in 3D models treated with SW620 EVs, statistically significant from the PBS control (P ≤ 0.01) and the SW480 EVs condition (P ≤ 0.0001). Similarly, p120 increased with SW620 EVs, significantly compared to the PBS control and SW480 EVs treatment (p<0.0001).

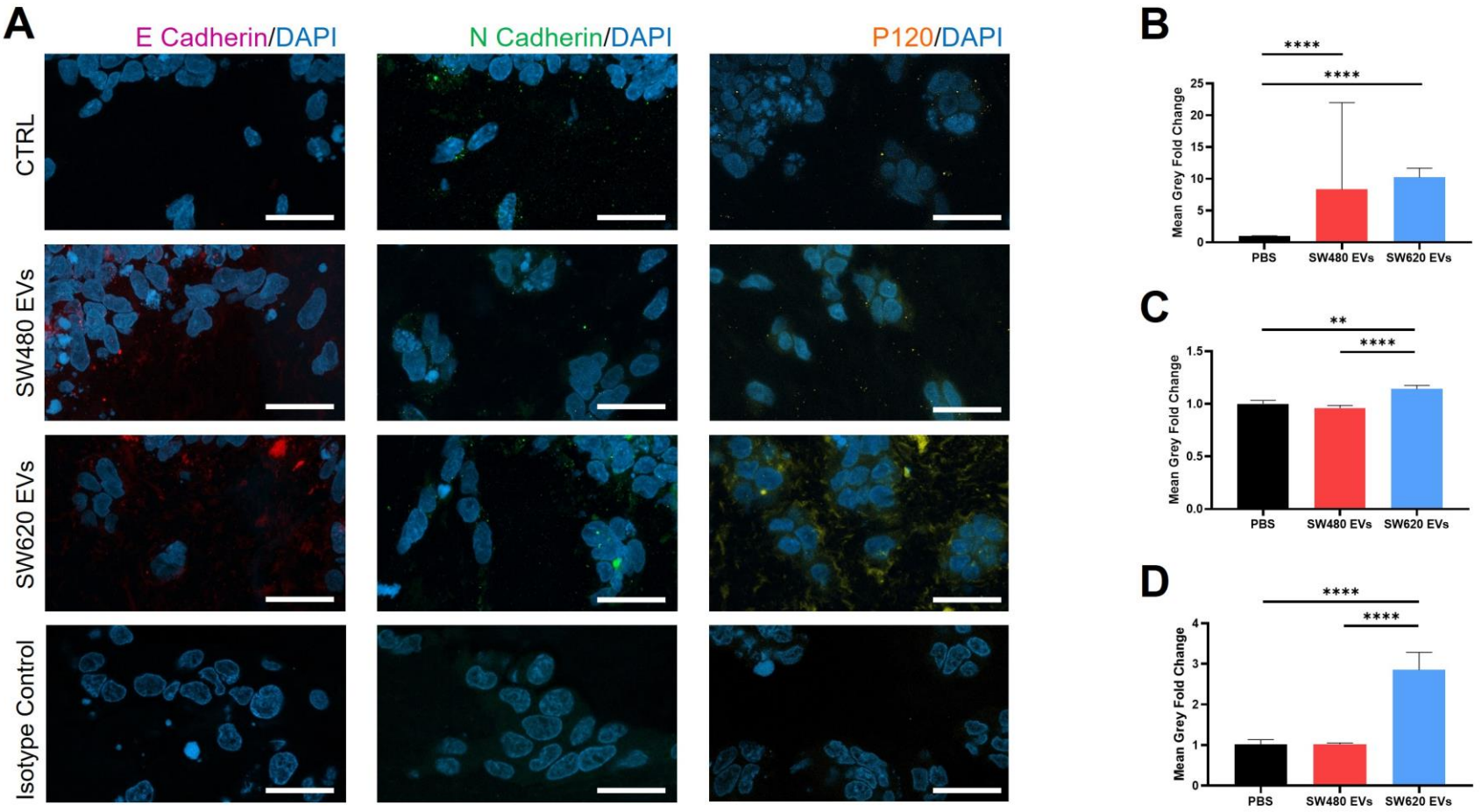


**Figure 2.14. EMT proteins expression in conditioned 3D models of invasion.** (A) Representative images of IF staining for E cad (red), N cad (green) and P120 (yellow) in CRC EVs treated 3D models. DAPI (blue) was used as counterstaining for nuclei. All the captured images show the layer between the front of invasion and the stroma. Scale bar = 20 µm. (B) E cadherin (555 nm wavelength) mean grey intensity. Median with 95% CI (n=3); Kruskal-Wallis **** P ≤ 0.0001.(C) N cadherin (488 nm wavelength) mean grey intensity. Mean ± SEM (n=3); ANOVA ** P ≤ 0.01, **** P ≤ 0.0001. D) P120 (555 nm wavelength) mean grey intensity. Median with 95% CI (n=3); Kruskal-Wallis **** P ≤ 0.0001.

## 2.5 Discussion

Invasion is a key event in the progression of cancer towards metastasis. With this chapter, a reproducible organotypic 3D model of quantifiable CRC invasion was optimised and characterised. The main aim was to obtain a 3D model to evaluate the involvement of CRC EVs in patterns and mechanisms of cancer invasion.

### 2.5.1 Selection and characterisation of 3D organotypic models of invasion

Of the three 3D model templates initially developed to create a reproducible front of invasion, the template based on transwell inserts was the most robust in the representation of an invasive layer of cancer cells. A lack of development of a homogeneous matrix and absence of fibroblasts at day 3 was observed in the gel spheroid model, whereas in the embedded spheroid model, cancer cells poorly adhered to the matrix. In the transwell template, the 3D culture was placed in the upper compartment and the cancer cells were invading in serum free conditions. The presence of the bottom well allowed the formation of a nutrient gradient that worked as a chemoattractant for the cancer cell to invade in the matrix. The matrix conditioned by the presence of fibroblasts was prepared before the invasion of cancer cells, thus allowing a window of time to treat the gels with EVs and mimicking the PMN in future studies.

Matrix stiffness is a relevant factor in cancer invasion and for this reason, it is crucial to work with an *in vitro* model able to preserve biomechanical properties. Collagen type I at the concentration of 3 mg/ml polymerises to give a stiffness of about 2000 Pa, which is the minimum requirement for tissues (Wells, 2013). Further matrix contraction was observed after day 3 of the culture, with the gel visibly shrunken in the inserts. This has been previously observed and linked to the biomechanical activity of fibroblasts, and it is a fundamental feature when studying stromal interactions (Liu *et al*., 2020). At the end of the cultures, samples were treated as formalin-fixed paraffin-embedded (FFPE) tissue for further immunohistochemical and histological analysis. The choice was mainly due to the practicality in orientating the samples for the cross-sectional cut. One of the main disadvantages of FFPE is tissue shrinkage, which can lead to incorrect size measurements. The contracting feature linked to fibroblasts observed prior to

processing was however unaffected and observable also in the microtome sections, thus confirming FFPE processing was suitable for these 3D models. Higher magnification of Masson's Trichrome staining also allowed observations on the structure and orientation of the collagen fibrils in the matrix, which however were not quantified, but may be of interest in future work now that the model system is established.

Histological images showed cancer cell invasion increased from day 7 to day 14. Along with the increase in invasion, a decrease in proliferation was indicated by the downregulation of Ki67. Even though the two mechanisms can be present at the same time, and they identify the most aggressive cancer cells, it has been shown that cells tend to switch between proliferative and invasive phenotype due to their high plasticity (Lattmann *et al*., 2021; Rabie *et al*., 2021). Considering that Ki67 is commonly used as a cancer cell marker, particularly for SW480, the absence of Ki67 could also mean that the serum free condition was reducing cancer cell activity, thus making it difficult to use day 14 to obtain quantitative measurements. For further quantitative experiments, the 3D models were therefore cultured for 7 days.

### 2.5.2 Isolation and characterisation of CRC EVs

EVs were isolated from the patient-matched primary and metastatic CRC cell lines SW480 and SW620. Low yield is a common issue when working with EVs. Functional studies are often limited by the amount of EVs that monolayer culture produces. Here a cell culture bioreactor, previously used for EV studies (Artuyants *et al*., 2021), was optimised for the study needs. The bioreactor allows the culture of a high number of proliferative cells into a 3D membrane for a long period. At every media change (weekly), the secretome with a cut-off of 10 kDa can be extracted as it is retained in the inner chamber where cells grow. High particle count and protein concentration were observed in the SEC fractions deriving from the weekly harvest, allowing accumulated storage of EVs needed for the study.

Another concern when working with functional EV studies is the EV contamination in common nutrients used in cell culture. EV yields in animal sera, such as FBS, are generally quite high, resulting in data misinterpretation (Lehrich *et al*., 2021). Thus, the cells must be cultured in a medium free from EV contaminants. Initially,

SW480 or SW620 were introduced in the inner compartment of the bioreactor in a starvation condition, without serum. To compensate for the lack of nutrients, 10% serum was introduced in the outside compartment where serum EVs could not interfere with EVs from the culture. Particle size and count were found quite high throughout, while protein concentration profiles of the EVs drastically dropped for both cell lines after a month-long culture, thus suggesting a change in the cells and in the EV phenotype (Figure 2.10). This could derive from the long-term starvation that cells were subjected to in the bioreactor, but also by the harsh osmotic gradient created between the two membranes.

Starvation was then avoided by the introduction of 10% EV-depleted FBS in the inner compartment. The gradient was also inverted by lowering the normal FBS in the media compartment to 5%. Consequently, protein levels in EV fractions were consistent for a longer period, aligning with particle count analysis. EVs deriving from EV-depleted FBS media were then fully characterised following the minimum requirements stated by the MISEV guidelines (Witwer *et al*., 2021). Presence of TSG101 compared to the absence of anti-Golgi marker GM130 from the WB confirmed that the particles in the SEC fractions were of extracellular nature. The intact structure and morphology of the isolated EVs were observed through TEM, highlighting the lipid bilayer. The three tetraspanins tested with nanoFCM in the pooled fractions showed that the positivity was generally lower than 50% with variation between the different tetraspanins, which is due to the heterogeneity and subpopulations of the EVs isolated (Lees *et al*., 2022; Mizenko *et al*., 2021) (Figure 2.11D). To confirm the feasibility of long-term culture of the adapted bioreactor, particle size and counts were analysed with NanoFCM, showing no differences in terms of size and a slight decrease of particle count at the end of the culture (Figure 2.11E, F).

### 2.5.3 SW620 EVs increase SW480 cell line invasion

To assess the influence of CRC EVs on the invasive potential of SW480, different measurements based on the images were taken. Cancer cells can invade singularly or in clusters, with the latter attributed to a more aggressive phenotype (Fujiyoshi *et al*., 2020). The concentration of EVs employed for the treatment hasn't been titrated, but it was chosen after literature search (Payton *et al*., 2021; Schillaci *et al*., 2017).

SW620 EVs, which derive from an advanced stage of CRC, increased invasive cluster depth, length and size, compared to the untreated and the earlier stage SW480 EVs, thus suggesting that the stage of the EVs might play a pivotal role in the level of invasion. It was previously demonstrated that in monolayer culture metastatic EVs induced endothelial permeability (Schillaci *et al*., 2017), but invasion patterns have never observed in 3D. N-cad and p120 are proteins strictly associated with invasion and the ability to degrade the ECM (Cao *et al*., 2019; Kourtidis *et al*., 2013). Increased expression of N-cad and p120 were observed in the treatment with SW620 EVs, confirming their activity on inducing an aggressive phenotype. SW480 EV treatment didn't significantly affect any of the measurements, although an increase in size and depth of the clusters was observed.

In addition to these measurements, the ratio between single cells and clusters of cells invading was investigated. It is important to note that the ratio analysis adopted was semi quantitative, and dependent on the cross sections taken for the measurement. To avoid mistakes in the data interpretation, the measurements were taken from multiple cuts from each sample, to reduce variability. In all the treatments the number of single cells was lower than the number of cancer cells invading the matrix as aggregates, denoting an important feature and possible finding of the 3D model in mimicking single cell invasion. Despite this, differences on the percentages of single cells/clusters were observed after cancer EV treatments, with the opposite trend. While the increase of clusters lead by SW620 EVs could be linked to their advanced stage, the increase of single cell invasion with SW480 is harder to associate to a biological function. Since invasion of single cells was observed mainly with SW480 EVs, it was hypothesised that higher loss of cell-to-cell adhesion and E-cad decrease would be found, thus implying cells undergoing EMT. Nonetheless, E-cad expression was significantly higher with both EV treatment when analysed with IF. It was previously demonstrated that E-Cad can be a component of the cancer EV surface proteins. When present in the EVs, the protein was linked to cancer progression, by promoting angiogenesis through interactions with another type of adhesion molecule named VE cadherin (Tang *et al*., 2018). The high expression of E-cad in the treated cultures was indeed observed as a general increase of noise in the gel, non-specific to the invasive layer, thus suggesting a possible

expression of E-cad in the EVs. Proteins from the same family were observed in proteomic analysis of both cell types (Suwakulsiri *et al*., 2019). Therefore, a follow-up study should be conducted to confirm E-cad expression in CRC EVs.

## 2.6 Conclusions

The aim of this chapter was to develop a biologically relevant *in vitro* 3D model, suitable for analysing the role of EVs in patterns and mechanism of CRC invasion. The organotypic culture based on transwell inserts was able to recapitulate a reproducible front of invasion. By culturing patient matched SW480 and SW620 cell lines in bioreactors, a high yield of EVs was obtained.

The treatment with advanced stage SW620 EVs led to increased invasion of primary SW480 cells in the matrix, suggesting a change into a more aggressive behaviour. Further analysis focussed on phenotypical changes of the conditioned SW480 cells are needed to confirm the observations. The treatments with the two CRC EVs differed in their influence on invasive mechanisms of cells, suggesting a stage-dependent effect and a potential use of cell responses to EVs as cancer biomarkers.

The expression of proteins linked to invasion was influenced by the presence of CRC EVs. N-cad and p120 were found to increase after SW620 treatment. Gain of E-cad expression was however contradictory to previous studies and further investigations must be conducted to understand the role of E-cad in EVs and in EV driven invasion.

# 3 Impact of CRC EVs on a 3D model of lung metastasis

## 3.1 Introduction

Metastatic progression is the primary cause of treatment failure and high mortality in cancer patients. For a cancer to metastasise, cancer cells that have successfully detached from the primary site need to encounter the physical pressure of the circulation, extravasate towards the new tissue and adapt to a completely new microenvironment. Of the cells that reach the new tissue, only a few will succeed. The seed and soil hypothesis, initially proposed by Paget in 1889, has been extensively demonstrated in the last decades, emphasising that malignant cancer cells are supported by the new microenvironment (Akhtar *et al*., 2019; Paget, 1989). These changes have been observed to happen early in the disease, before the invasion of cancer cells, with the formation of the pre-metastatic niche (PMN) (Peinado *et al*., 2017). To date, the events known to contribute to shaping the PMN include alterations to vascular permeability, angiogenesis, remodelling of the extracellular matrix (ECM) and the deregulation of the immune features of the tissue (Doglioni *et al*., 2019).

Extracellular vesicles (EVs), alongside other soluble factors such as chemokines and cytokines, are released by cancer cells into the circulation, they reach distant sites and are hypothesised to favour the future establishment of metastases. Cancer EVs act selectively by expressing surface integrins which are recognised by target cells, mediating their role in metastatic organotropism (Hoshino *et al*., 2015). A major feature that allows the invasion of cancer cells is ECM remodelling and above all matrix degradation driven by matrix metalloproteinases (MMPs), which has been observed already in the PMN (Paolillo & Schinelli, 2019). Matrix metalloproteinases have been found in cancer-associated EVs, contributing to ECM remodelling, alongside activation of tumour microenvironment (TME) components such as cancer-associated fibroblasts (CAFs), which further secrete MMPs (Shimoda, 2019). Extracellular matrix proteins and collagens vary according to the specific organ; for example, lung interstitial matrix is mainly composed of collagen type I and III, but it is also enriched by other minor type of collagens which might be targeted by specific MMPs present in the EVs (Liu *et al*., 2021). Understanding the tissue-specific changes in the ECM at PMN stage can reveal early biomarkers and new targets for the treatment of specific metastasis.

A lot of the current knowledge about the PMN was obtained by investigating lung metastasis. The lungs are the second most recurrent site of colorectal cancer (CRC) metastasis (10-20%) and they are the site of metastasis most shared between different types of cancer (Riihimäki *et al*., 2018). In CRC, patients with lung metastasis showed higher overall survival compared to patients presenting with metastasis to other organs, such as liver and brain (Prasanna *et al*., 2018). Despite the main findings being based on animal models, *in vivo* preclinical models cannot be used to study syngeneic metastasis, which means metastasis with the same genetic background of the host (Francia *et al*., 2011). Once again, *in vitro* 3D models can prove useful to fill the gaps of animal-based research. With the most recent technologies, they also allow innovative ways to follow all the steps of malignancy, from the early PMN to fully developed metastasis.

### 3.1.1 Existing 3D models of lung metastasis

Recently, developments in *in vitro* 3D models were focussed on the establishment of a relevant representation of the metastatic niche (Goliwas *et al*., 2021; Ramamoorthy *et al*., 2019; Shinde *et al*., 2020). For example, a 3D model of lung metastasis based on a fully engineered perfusion bioreactor was created to assess the EV-mediated crosstalk between metastatic cancer cells and TME cells (Goliwas *et al*., 2021). This model was able to show that EVs secreted from fibroblasts in the lung TME support the deregulation of the immune response mediated by cancer cells. In another study, cancer EVs were added to a primitive lung organoid, where increased colonisation of CRC cells was observed, demonstrating that the 3D model developed was suitable to be used as a support in the evaluation of treatment for personalised medicine (Ramamoorthy *et al*., 2019). Little is known about the ability of *in vitro* 3D models to show proteomic and cellular changes in the PMN and in metastasis. To address this, the model requires a relevant representation of the site-specific ECM and the cellular components with the main influence on matrix modifications.

### 3.1.2 MALDI mass spectrometry for the study of ECM proteins

Matrix-assisted laser desorption/ionisation mass spectrometry (MALDI-MS) is a high-throughput approach that has been useful in exploring proteomic changes in several diseases, including cancer (Merlos Rodrigo *et al*., 2014). MALDI-based proteomic studies generally employ *in situ* digestion of proteins coupled with imaging to obtain information on analyte localisation. The identification of the

proteins present in the tissue is then obtained by a bottom-up approach, where proteins are enzymatically digested before mass spectrometry (MS) analysis. Spectral profiling of peptides enables the identification of proteins present in the sample with the help of database matching. MatrisomeDB, a specific database for ECM proteins, has been developed and collects information for the detection of ECM alterations in many diseases (Naba *et al*., 2012).

Notably, collagens - key components of the ECM - are not easily accessible to enzymes, such as trypsin, which is commonly used in bottom-up MS approaches. This is due to post translational modifications and collagen cross-linking. Bacterial collagenase III (COLase III) is an MMP that shows unbiased cleavage of collagens (Angel *et al*., 2019). Combined MS analysis derived from these enzymatic digestions has also led to the enrichment of matrix information (Clift *et al*., 2021). Metabolic studies of 3D models have been successfully carried out by MS technologies (Flint *et al*., 2020; Russo *et al*., 2018). However, the evaluation of proteomic changes in ECM relevant 3D models hasn’t been achieved to date.

### 3.1.3 Aims of the chapter

In this chapter, a 3D model of lung stroma was developed to study cellular and proteomic changes driven by CRC EVs in the PMN and metastasis. The first aim was to develop a relevant model of lung TME and characterise its stability and cellular content. After the treatment with CRC EVs, immunohistochemical approaches were adopted to assess whether EVs impacted on alteration on the cellular phenotypes and viability. MALDI-MS was also employed to screen proteomic differences between the treatments. Lastly, metastatic invasion was introduced in the model after the conditioning with SW480 or SW620 CRC EVs to understand the onset of the PMN remodelling and the support of EVs for the invasion of cancer cells in the lung metastasis.

## 3.2 Materials and Methods

### 3.2.1 Experimental design

A lung 3D model was first developed based on the composition of Chapter 2 (Figure 3.1). Density of MRC5 was adapted and two more cell lines were introduced: THP-1 as macrophages and HULEC-5a as endothelial cells. Viability, markers expression and inflammatory cytokines were assessed to characterise the model. Then, SW480/SW620 EVs were used to condition the model and mimic the PMN. Cellular marker alterations were evaluated, along with proteomic signatures with MS profiling. After 7 days of EV conditioning, labelled SW620 cancer cells were added in suspension in the model and invasion was assessed alongside cellular markers alteration. Finally, secreted collagens and cytokines were compared between pre- and post-invasion.

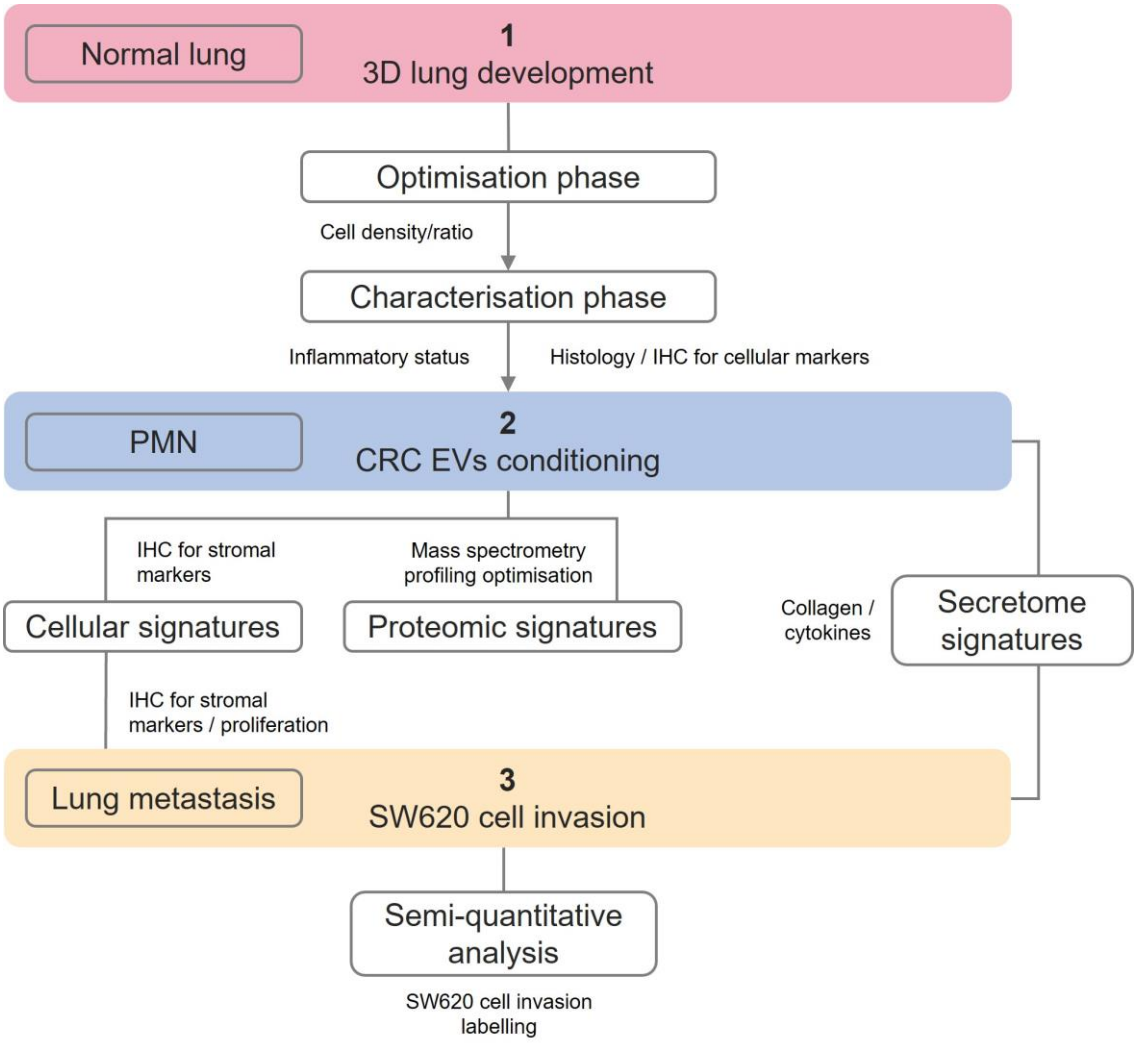


**Figure 3.1. Schematic of Chapter 3 experimental design.**

### 3.2.2 2D Cell culture

Culturing procedures for SW480, SW620 and MRC5 cell lines were performed as described in Section 2.3.2. The human leukaemia monocytic cell line THP-1 and microvascular endothelial cell line HULEC-5a were purchased from ECACC. THP-1 cells were cultured in RPMI 1640 basal media (Gibco, Thermo-Fisher, UK) with 10% v/v FBS and 1% v/v P/S. HULEC-5a cells were cultured in basal MCDB131 (Gibco, Thermo-Fisher, UK), supplemented with 10 ng/ml Epidermal Growth Factor (EGF; Fisher Scientific; Loughborough, UK), 1 µg/ml hydrocortisone (Merck, UK), 10 mM Glutamine (Gibco, Thermo-Fisher, UK) 10% v/v FBS and 1% v/v P/S. The cells were maintained in a humidified incubator at 37°C and 5% $CO_2$ in air. Culture medium was replaced every 3-4 days and cells sub-cultured (ratio 1:5) with Trypsin-EDTA when reaching 70-80% confluence. Cells were checked for mycoplasma with MycoAlert© Detection kit (Lonza Ltd., UK) every 6 months and were shown to be negative throughout.

### 3.2.3 3D Cell Culture

A 3D model of lung stroma was developed by adding cells in the same matrix components described in Section 2.3.3. MRC5, THP-1 and HULEC-5a were co-cultured in the mixture of collagen type I/Geltrex™ to recreate the lung stromal tissue. MRC5 density was compared between 528,000 cells/ml, 1,056,000 and 2,112,000 cells/ml. THP-1 monocytes were differentiated in M0 macrophages (dTHP-1) 72 hours before the 3D culture with 50 ng/ml of phorbol 12-myristate 13-acetate (PMA). To monitor the cell ratio, cells were stained for 30 min with fluorescent probes before the inclusion in the gel; for MRC5, 10 µM of CellTracker™ green CMFDA (ThermoFisher, UK), for HULEC-5a, 10 µM of CellTracker™ Red CMTPX (ThermoFisher, UK) and 500 nM of CellTracker™ Deep Red dye (ThermoFisher, UK) for differentiated THP-1 in serum free culture media were used. Ultimately, the three cell lines were added to the gel mixture at appropriate experimental density and ratio. The gel was left to set for 1 hour at 37°C and 5% $CO_2$, and then cultured for 1, 7 or 14 days in cDMEM supplemented with 0.05 mM ascorbic acid 2-phosphate (Sigma). The growth media was changed every 3-4 days.

#### *3.2.3.1 CRC EVs conditioning*

SW480 or SW620 EVs were isolated according to Section 2.3.5.1 and pooled EVs fractions (7-9) were added to the lung 3D model at a concentration of 50 µg/ml. Control gels (PBS) were simultaneously cultured, where the treatment was replaced with equal volume of PBS. The first treatment was introduced after the gels were set. The treatment was repeated at every media change until day 7 of culture. To evaluate EV uptake, EVs were labelled as described in Section 2.3.6.

#### *3.2.3.2 Invasion of SW620 cells in conditioned lung 3D model*

After 7 days of EV conditioning, the lung 3D models were placed in ultra-low attachment 96-well plates (Figure 3.2). SW620 were labelled with 10 µM Red CMTPX dye for 30 min and then introduced in the 3D model at a concentration of 264,000 cells/ml. The cells were left to invade the gel for 3 days before being fixed.

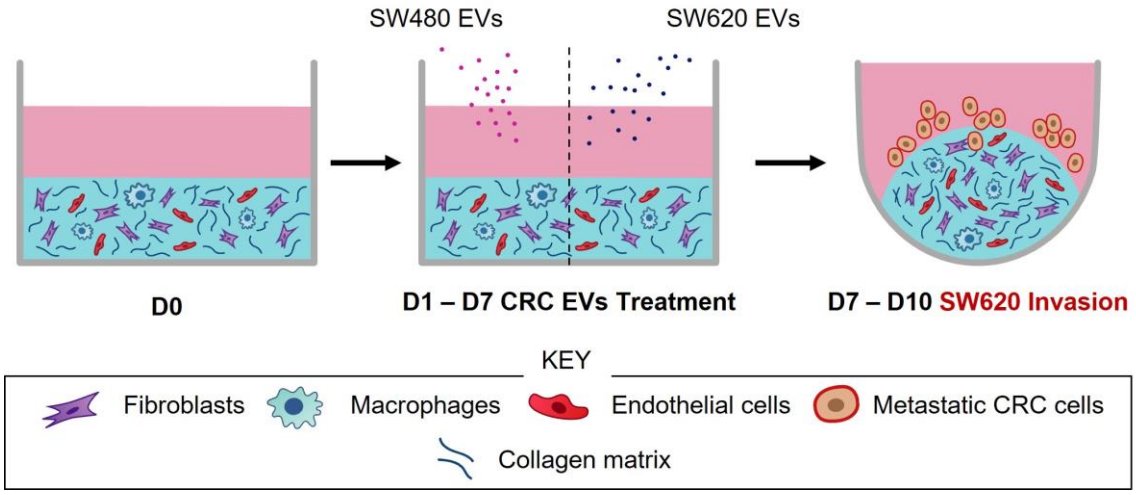


**Figure 3.2. EV pre-conditioning and SW620 invasion in the lung 3D model.** Schematic representation of the culture steps for the evaluation of EV pre-conditioning and SW620 invasion.

### 3.2.4 Sample preparation

The lung 3D models were processed as FFPE and stained with H&E and Masson's Trichrome as described in Section 2.3.4.

#### *3.2.4.1 Immunohistochemistry*

IHC was performed following the method described in Section 2.3.4.3. Sections of 3D lung were incubated with primary antibodies for: Ki67 to measure cancer cells proliferation, alpha-smooth muscle actin (α-SMA) (1:1000; ab7817 mouse monoclonal [1A4]; Abcam, Cambridge, UK) as CAF marker, CD68 (1:8000; ab213363 rabbit monoclonal [EPR20545]; Abcam, Cambridge, UK) as

macrophage marker and Von Willebrand factor (vWF) (1:300; ab9378 rabbit polyclonal; Abcam, Cambridge, UK) as endothelial marker and visualised using 0.04% v/v biotinylated secondary goat anti-rabbit antibody (1:500; ab207995; Abcam, Cambridge, UK) or rabbit-anti mouse antibody (ab6727; Abcam, Cambridge, UK) followed by DAB until brown staining was observed (Section 2.3.4.3). Nuclei were counterstained dark purple with Mayer's Haematoxylin. For CD68, enzymatic antigen retrieval with 0.01% w/v α-chymotrypsin (Sigma) in 0.1% w/v was performed and incubated for 30 min at 37°C. Secondary antibody host interactions were blocked with a solution containing 1% w/v BSA, 25% v/v normal goat serum or normal rabbit serum (Merck, UK) to match the species of the secondary antibody in TBS.

## 3.2.5 MALDI mass spectrometry analysis

To evaluate proteomic features of the lung 3D model, FFPE sections were analysed with MALDI-MS profiling and MALDI-MS imaging.

### *3.2.5.1 Sample preparation for mass spectrometry*

For MALDI-MS analysis, paraffin was removed from the sections by incubating for 20 min at 60°C, followed by washes in high-performance liquid chromatography (HPLC) grade toluene (Merck, UK) (3 x 4 min). Sections were rehydrated through washes in 100%, 90% and 70% (3 min each) of HPLC-grade ethanol and then rinsed in de-ionised water (2 x 3 min). HIAR was performed using 10 mM Citric Acid at 97°C in a water bath for 30 min. Sections were then left to stand for 5 min within the hot buffer and placed in $dH_2O$ for 5 min. MS-grade Trypsin Gold (Promega, UK) at 20 µg/ml or collagenase type III (Rockland Immunochemicals, Pottstown, USA) at 100 µg/ml was spotted (1-5 µl). Sections were then left in a humidity chamber ON at 39° C.

### *3.2.5.2 Mass spectrometry profiling*

Alpha-cyano-hydroxy-aminic acid matrix (α-CHCA) was spotted (0.8 µl) onto the whole sample at a concentration of 5 mg/ml in a 70:30 acetonitrile:$H_2O$ with 0.4% v/v of trifluoroacetic acid (TFA). Analysis were performed using two different instruments; the first, MALDI HDMS Synapt G2 mass spectrometer (Waters Corporation, Manchester, UK) equipped with a neodymium/yttrium aluminium garnet (Nd:YAG) laser operated at 1 kHz and coupled with time of flight (TOF) mass analyser. External calibration was performed by using peptide calibration

standard II (Bruker Daltonics GmbH). MALDI-MS profiling was acquired in positive ion mode at a range of *m/z* 800 to 3000 (resolution 10 000 fwhm), without ion mobility function. The second instrument was MALDI Select Series MRT (Waters Corporation, Manchester, UK) quadrupole TOF (qTOF). External calibration was performed by using phosphorus red (Merck, UK). Similarly, MALDI-MS profiling was acquired in positive ion mode at a range of *m/z* 0 to 2400.

#### *3.2.5.3 Peptide mass fingerprint*

To obtain putative identifications of protein from the profiling, Mascot Peptide Mass Fingerprinting was employed. MALDI HDMS SynaptG2 average spectra obtained for each profiling was exported as *.txt files in mMass open-source software. Baseline correction was performed as pre-processing algorithm. Automated peak picking was then performed (S/N = 3) and the *m/z* features found were inserted in Mascot Peptide Mass Fingerprinting (v 2.7.0, Matrix Science, London, UK) for the identification of putative proteins in *Homo sapiens* SwissProt database. Trypsin was selected as cleaving enzyme with 2 missed cleavages. Carboxymethylated cysteine was set as fixed modification, while methionine oxidation as variable modification. Monoisotopic masses were searched with charges set at 1+ and peptide tolerance at 0.05 Da. Mascot probability-based scoring results to be significant when $P \leq 0.05$.

#### *3.2.5.4 In silico digestion*

MALDI HDMS SynaptG2 average *m/z* features from the previous peak picking were then compared to *in silico* digestion of some ECM collagens of interest to see the level of collagen digestion in the 3D model. Collagen type I (CO1A1), collagen type III (CO3A1), collagen type VI (CO6A1), collagen type VII (CO7A1) and collagen type XI (COBA1) aminoacidic sequences were taken from UniProt and inserted into Protein Digest feature in mMass. Trypsin was selected as cleaving enzyme with 2 missed cleavages. Monoisotopic masses were searched with charges set at 1 with peptide tolerance at 10 ppm.

#### *3.2.5.5 Multivariate analysis*

To evaluate how the spectra clustered and separated between the different conditions, multivariate analysis was performed. MALDI-MRT average spectra were exported as *.txt files from the instrument and transformed into .csv as requested by MetaboAnalyst, the open-source online platform for MS multivariate

analysis. Then, statistical analysis (one factor) was selected and peaks were aligned through pre-processing with mass tolerance of 0.025. Data filtering was applied with interquartile range (IQR) filters to discard variables that were unlikely to be of use. Finally, normalisation was obtained by sum and auto-scaling. Partial component analysis (PCA), Partial least squares discriminant analysis (PLS-DA) and hierarchical clustering were automatically performed.

### 3.2.6 Cytokine Release (ELISA)

Enzyme-linked immunosorbent assay (ELISA) was performed on culture media of the 3D lung models at day 0, day 7 and day 14 to evaluate the levels of anti- and pro-inflammatory cytokines and the 3D organotypic model stability. All the sandwich ELISA assays were performed according to manufacturer's instructions of commercially available kits (PeproTech EC Ltd., UK; Bio-Techne, UK) and concentrations for each target antibody are summarised in Table 3.1. Capture antibody, detection antibody and Streptavidin-HRP concentrations, alongside the supernatant dilutions are reported in Table 3.1. ELISA assay antibody concentrations and standard curve ranges. Nunc 96 well MaxSorp™ ELISA plates (Thermofisher, UK) were coated with 50 µl/well of capture antibody and incubated ON at RT. Between every incubation step, plates were washed four times with 200 µl/well of washing buffer (0.05% Tween-20 in PBS) and blotted on clean paper towel to remove all the buffer. The following morning the plates were incubated with 200 µl/well of block buffer (1% BSA in PBS) for 1 hr at RT. Then, the plates were incubated with 50 µl/well of samples/standards ON at 4°C. Dilution antibody (50 µl/well) was incubated for 2 hours at RT, followed by 30 min RT incubation with 50 µl/well of Streptavidin-HRP. The final incubation step was performed with 50 µl/well of tetramethylbenzidine (TMB) substrate (Fisher Scientifics, UK). Without washing the plates, the reaction was stopped by adding 50 µl/well of 1M hydrochloric acid (HCl). Ultimately, the optical density of the reaction was analysed with the Clariostar plate reader at 450 nm wavelength, with correction set as 620 nm wavelength.

**Table 3.1. ELISA assay antibody concentrations and standard curve ranges.**

| Cytokine | Capture antibody (µg/ml) | Detection antibody (µg/ml) | Standard curve (pg/ml) |
|---|---|---|---|
| IL-4 900-T14 (Peprotech, UK) | 0.5 | 0.25 | 7.81-2000 |
| IL-6 900-T16 (Peprotech, UK) | 0.5 | 0.125 | 7.81-2000 |
| IL-8 900-T18 (Peprotech, UK) | 0.125 | 0.25 | 0.78-200 |
| IL-10 900-K21 (Peprotech, UK) | 1 | 0.5 | 11.71-3000 |
| MCP-1 DY279 (Bio-Techne, UK) | 1 | 0.025 | 15.6-1000 |
| TIMP-1 DY970 (Bio-Techne, UK) | 2 | 0.05 | 31.2-2000 |
| TIMP-2 DY971 (Bio-Techne, UK) | 2 | 0.0125 | 31.2-2000 |

### 3.2.7 Dot blot

Antibodies against collagen type III N-terminal (1:2000, 22734-1-AP, rabbit polyclonal; Proteintech, UK), collagen type VI (1:2000, 66824-1-Ig, mouse monoclonal [3H10B1]; Proteintech, UK) and collagen type XI (1:2000, 21841-1-AP, rabbit polyclonal; Proteintech, UK) were used on supernatants from 3D lung cultures, to confirm the presence of signature collagens found by mass spec profiling. Briefly, 2 µl of samples were spotted onto a nitrocellulose membrane; the distance between each sample was 1 $cm^2$. The membranes were left to dry for 10 minutes before being blocked with 5% (w/v) non-fat dried milk in TBST at RT for 1 hour. Primary antibodies were diluted in blocking buffer and the membranes incubated at 4°C ON. The membrane was rinsed and washed three times for 10 min each with washing buffer before IRDye 800RD goat anti-mouse or IRDye 680RD donkey anti-rabbit secondary antibodies (1:10000 dilution) were added and incubated at RT for 1 hour. The membrane was washed again three times in washing buffer and then imaged using Li-Cor®Odyssey®. Densitometry values were obtained with Image Studio™.

### 3.2.8 Statistical analysis

Statistical analysis was performed using Prism 8.1.1 software. First, data were tested for normality as previously described (Section 2.3.8).

When the groups tested were 2 (lung pre- vs. post-invasion), T test was performed for parametric data, whereas Mann-Whitney (MW) test was performed for non-parametric data. When the groups tested were ≥ 3, multiple comparisons tests were employed. For unpaired data (lung EV conditioning) ANOVA with Tukey's post-hoc analysis was performed for parametric data, while KW test with Dunn's post-hoc analysis was performed for non-parametric data. For paired data (lung optimisation time points), which were all parametric, repeated measures ANOVA (RM-ANOVA) with Geisser-Greenhouse correction and Tukey's post-hoc was performed. P-values less than 0.05 were considered significant.

Data representation as previously described (Section 2.3.8).

## 3.3 Results

### 3.3.1 Development of a 3D model of lung stroma

To obtain the fibroblasts cellularity present in the connective tissue of lungs, three different concentrations of fibroblasts were tested. No main differences were observed in MRC5 morphology and cells were distributed homogeneously in all the gels (Figure 3.3). No differences in matrix structure were found. The density of 2,112,000 cells/ml was chosen as the closest to the normal interstitial histology images found in literature (Kamp *et al*., 2022; Matsushima *et al*., 2020).

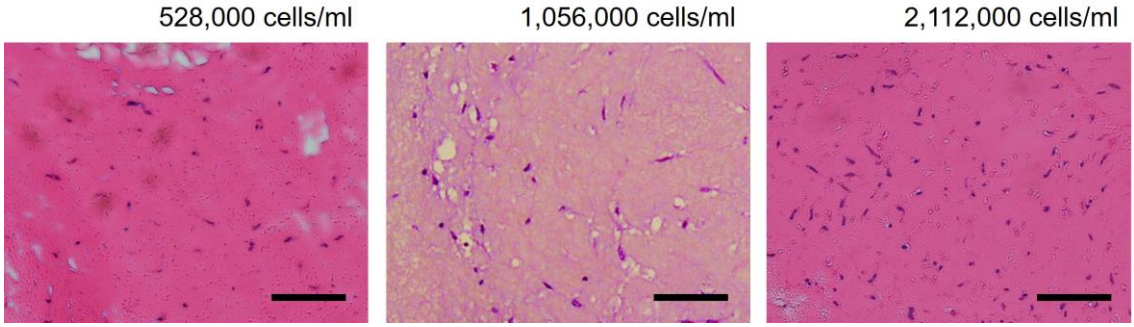


**Figure 3.3 Optimisation of MRC5 density in collagen/Geltrex gels.** Representative H&E images of MRC5 concentrations to mimic the density in the connective tissue of the lung.

HULEC-5a and dTHP-1 were then mixed with MRC5 in the gel to mimic the stroma of the lung and cultured for 7 or 14 days. The ratio chosen between the three cell lines was 52.5:30:17.5 according to literature (Crapo *et al*., 1982; Travaglini *et al*., 2020). Morphology was investigated with H&E and Masson's Trichrome (Figure 3.4A, B). Cells homogeneously occupied the space in the gel. A decrease in cellularity was observed in the gels from day 7 to day 14. A monolayer of elongated cells could be observed covering the border of the gels (Figure 3.4A).

Release of monocyte chemoattractant protein-1 (MCP-1), IL-6, IL-4 and IL-10 into the culture media were investigated to evaluate the inflammatory condition of the 3D model; MCP-1 decreased non-significantly from day 4 to day 7($P = 0.6002$) and from day 7 to day 14 ($P = 0.2314$) (Figure 3.4C). IL-6 levels were significantly lower at day 7 compared to day 4 ($P \leq 0.01$). A complete loss of IL-6 was observed at day 14, thus significantly differentiating from day 4 ($P \leq 0.0001$) and day 7 ($P \leq 0.001$) (Figure 3.4D). IL-4 showed an opposite trend, with gradual increase from day 4 to day 14, although this failed to reach significance ($P = 0.19$

day 4-day 14) (Figure 3.4E). No significant differences were seen for IL-10 (Figure 3.3F).

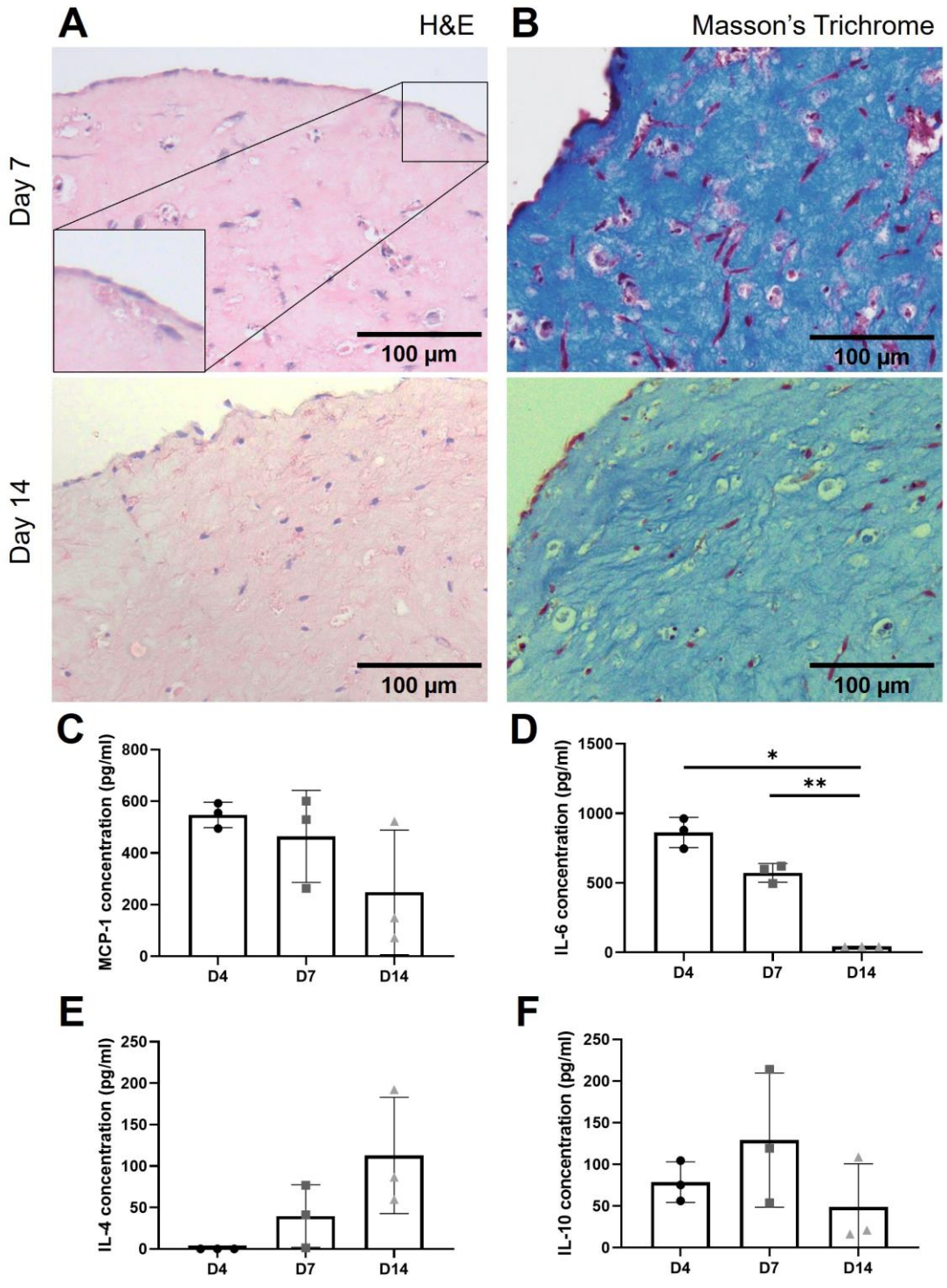


**Figure 3.4 Histology and cytokine profile in 3D model of lung.** (A) Representative H&E staining of 3D lung at day 7 and day 14 of the culture. At day 7, magnification of the border of the gel enriched by elongated cells. (B) Representative Masson's Trichrome staining of 3D lung at day 7 and day 14 of the culture. (C) MCP-1 expression; Mean ± SEM (n=3). RM-ANOVA. (D) IL-6 expression. Mean ± SEM (n=3). RM-ANOVA, * $P \leq 0.05$, ** $P \leq 0.01$. E) IL-4 expression; Mean ± SEM (n=3). RM-ANOVA. (F) IL-10 expression; Mean ± SEM (n=3). RM-ANOVA.

Three markers associated with the cell lines introduced in the lung 3D model were evaluated with IHC, α-SMA for MRC5, CD68 for dTHP-1 and vWF for HULEC-5a. High positivity for α-SMA was found at day 0, gradually decreasing at day 7 and at day 14 (Figure 3.4). Cells in the border of the gels were positive throughout. CD68 was identified only in large round shaped cells, which is the typical morphology of macrophages. Lastly, vWF was found in a small number of cells, occasionally creating clusters of two or three cells around holes in the matrix. Isotype controls were negative for all the three markers.

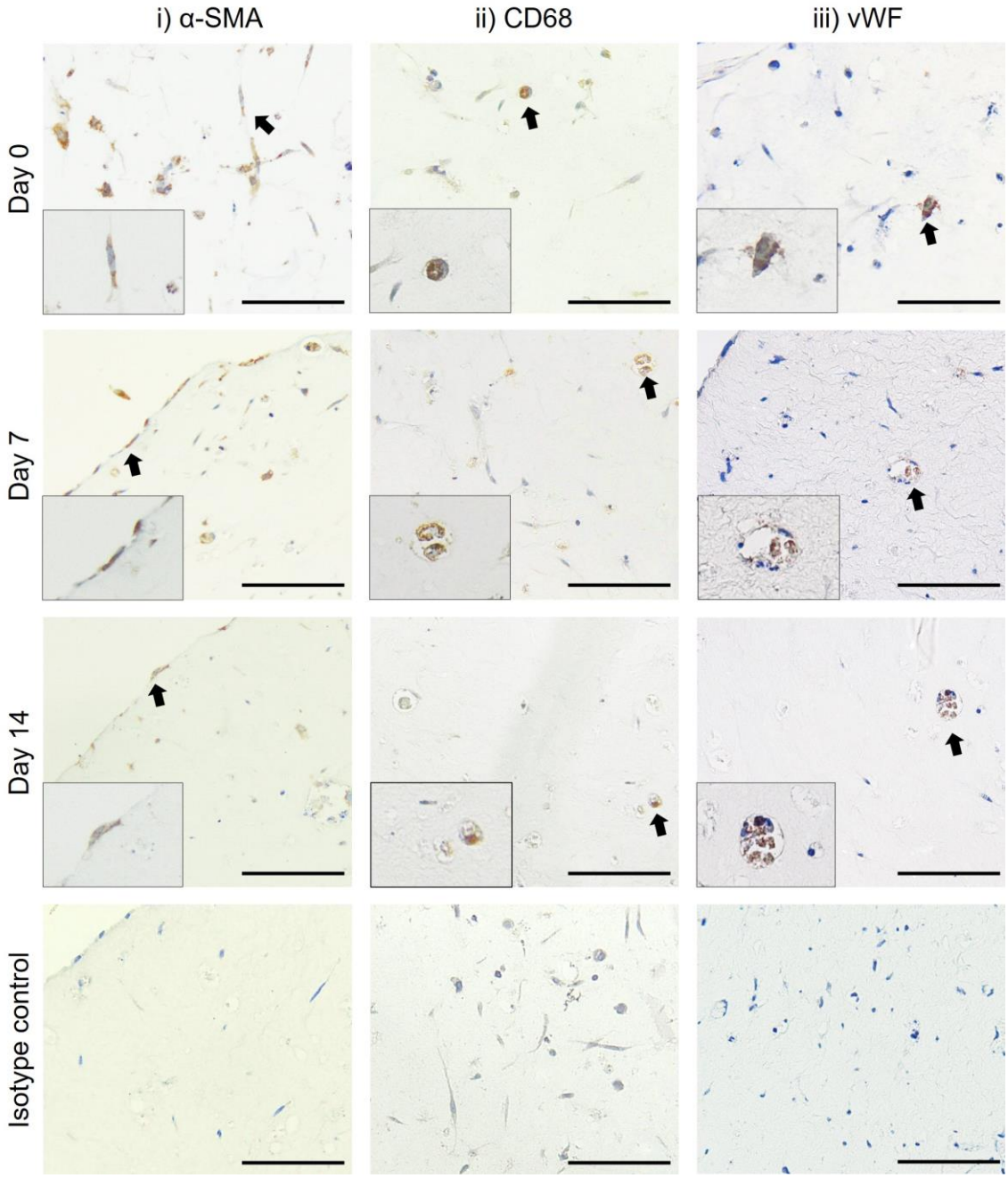


**Figure 3.5 Cell markers IHC in the 3D model of lung.** Representative images of (i) α-SMA, (ii) CD68 and (iii) vWF expression, all stained brown. Examples of positive cell staining are indicated by the black arrows. Haematoxylin as nuclei counter stain (blue). Scale bar = 100 µm.

Due to the instability of the cultures at day 14, for the next experiments cultures were maintained for 7 days only. Staining with passive dyes was also investigated to monitor the ratio of cells in the gel (Figure 3.6). Positive living nuclei were counted with DAPI. Alongside living cells, apoptotic bodies and necrotic cells were also found in the gels. At day 7, the three cell lines maintained the same ratio as when first introduced in the gel. However, most living cells lacked specific staining, thus were difficult to identify and indicated some loss of the stains during the 7 days of culture.

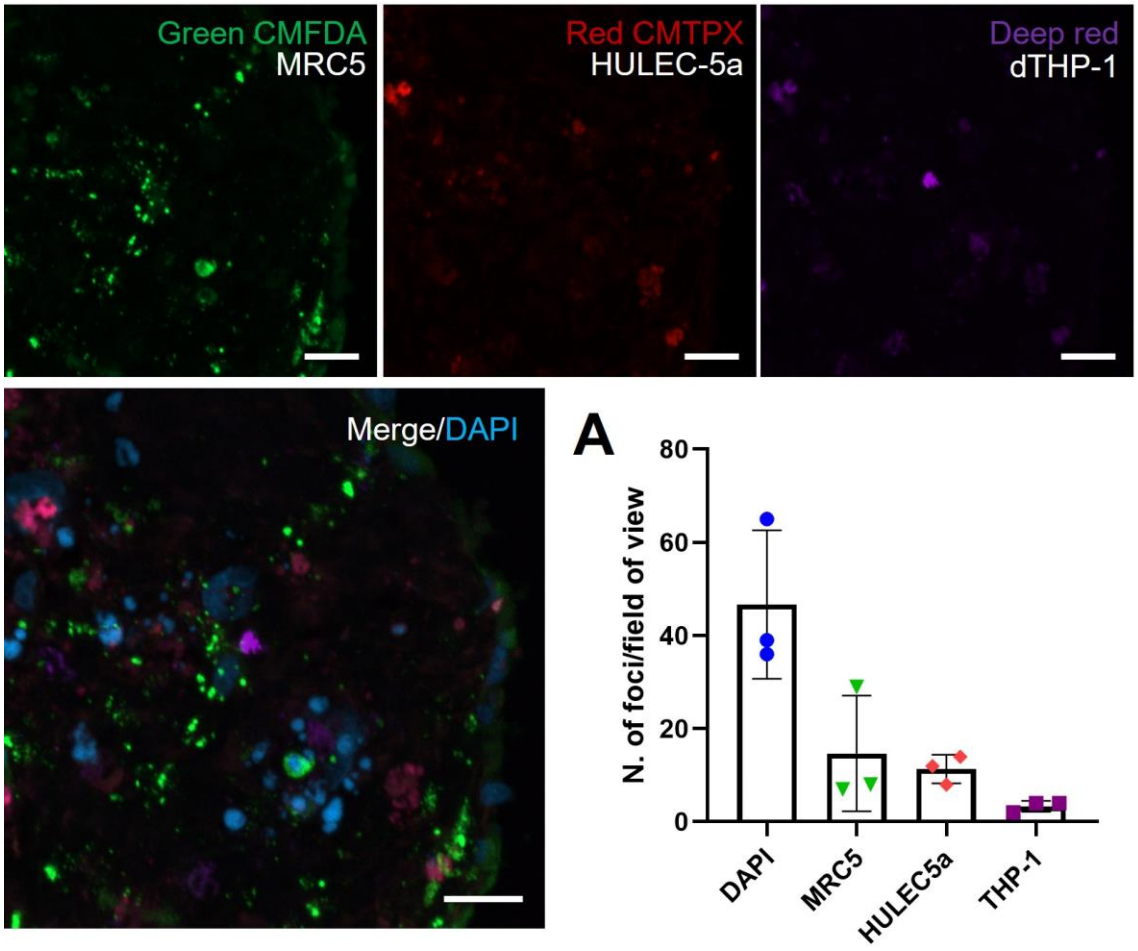


**Figure 3.6. Staining of cells in the 3D model of lung with Cell Tracker probes.** Representative images of lung fibroblasts (green), endothelial cells (red), macrophages (purple). Scale bar = 20 µm. (A) Living cell count from the staining compared to the number of foci found with DAPI blue stain (n=3).

### 3.3.2 Conditioning of lung stroma 3D model with CRC EVs

SW480 and SW620 EVs were added to the culture media of the lung from day 1 to day 7. Morphological, cellular, and proteomic alterations were evaluated. At the end of the culture, major differences in the opacity of the gels were observed. Both SW480 and SW620 EV treatments reduced the opacity of the gels compared to the control (Figure 3.7A). EV uptake by the gel was confirmed as previously described (Section 2.4.3). Labelled EVs were found in the middle of the gel in both conditions (Figure 3.7B). H&E was performed to check for differences in morphology and cellular organisation in the gel. Gels treated with SW480 and SW620 EVs contained cell aggregates, which were not found in the control (Figure 3.7C).

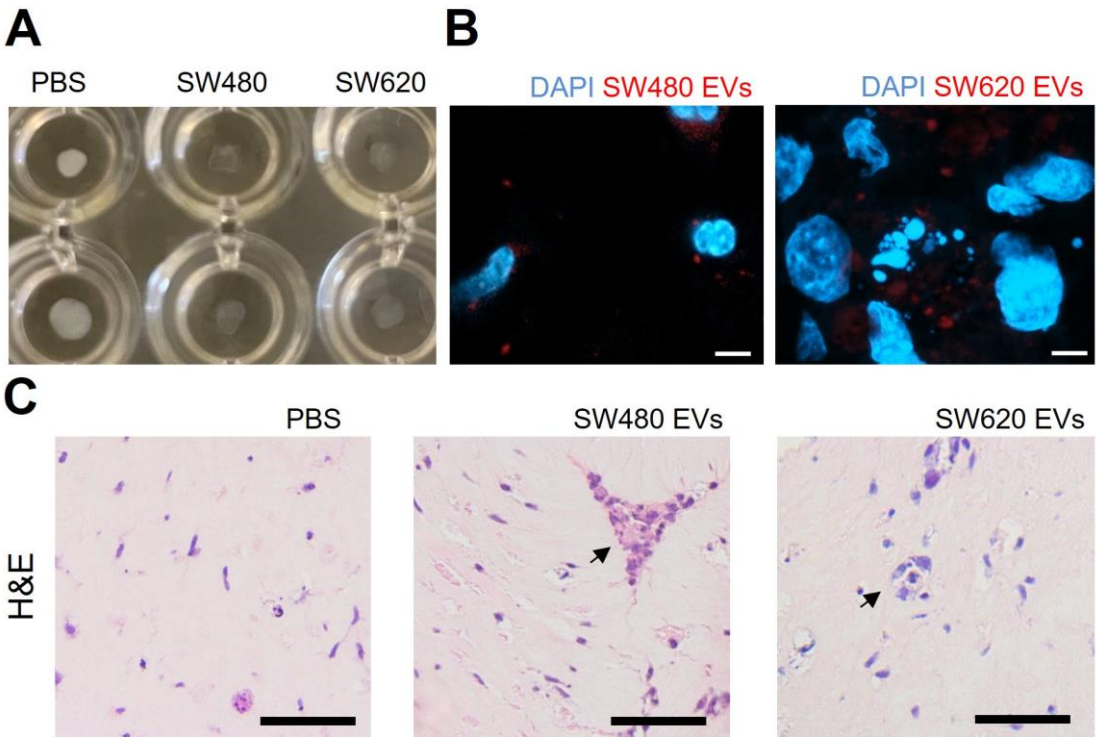


**Figure 3.7. EV uptake and cell morphology in lung stroma 3D model after CRC EVs treatments.** (A) Photograph of the lung stroma 3D model in the well-plate. (B) Representative images of SW480 and SW620 EV uptake in the gel (red). Cell nuclei counterstained with DAPI (blue). Scale bar = 5 µm. (C) Representative images of H&E staining. Black arrows = cell aggregates Scale bar = 50 µm.

Immunohistochemistry for the three cell markers was then performed to investigate the effect of EVs on marker expression. Decrease of expression of α-SMA was observed with SW620 EVs (Figure 3.8A). However, statistical analysis could not be performed as the biological replicates for SW480 EV treatment were limited. Non-significant increase of vWF was observed in cultures treated with both CRC EVs, which was higher following SW620 EV stimulation (P = 0.1152) (Figure 3.8B). CD68 expression was not affected by the EV conditioning (Figure 3.8C).

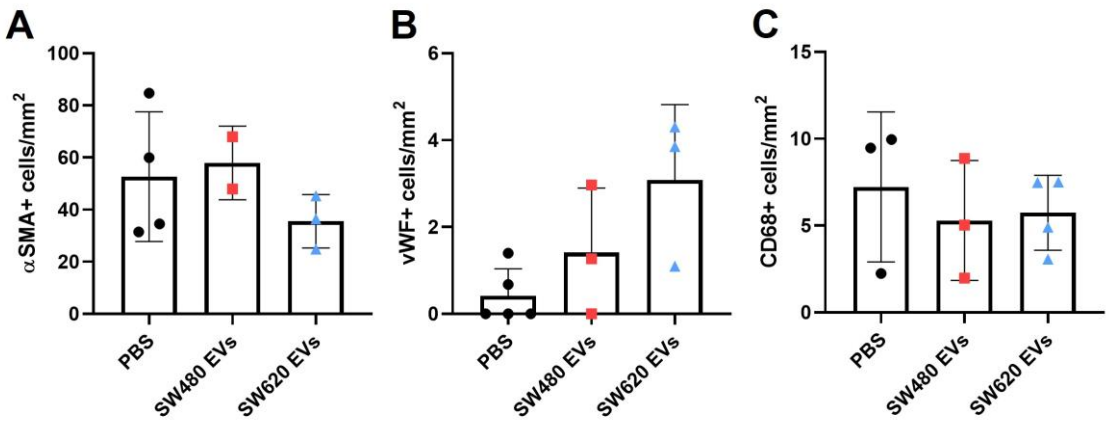


**Figure 3.8. Cell count based of IHC of cell markers.** Cell count normalised to $mm^2$. (A) α-SMA expression. Mean ± SEM (n≥2). (B) vWF expression. Median ± 95% CI (n=3). Kruskal-Wallis. (C) CD68 expression. Mean ± SEM (n≥3). ANOVA.

### 3.3.3 Optimisation of MALDI mass spectrometry profiling of peptides of the lung stroma 3D model

Changes in the proteomic profile of the lung 3D model were assessed with MALDI-MS. Initially, optimisation of the method was performed with MRT. The untreated lung 3D models were digested with trypsin or COLase III to determine the digestion methodology which produced enriched proteomic profiling based on the average spectra (Figure 3.9A). With trypsin, intense *m/z* signals were found within the range of 1200-2000 *m/z*, whereas with COLase III, *m/z* signals with the highest intensities were limited to 800-1100 *m/z*. Tryptic digestion average spectra from the two MALDI instruments employed (SynaptG2 and MRT) were compared, showing higher intensity and higher mass resolution with MRT (Figure 3.9B).

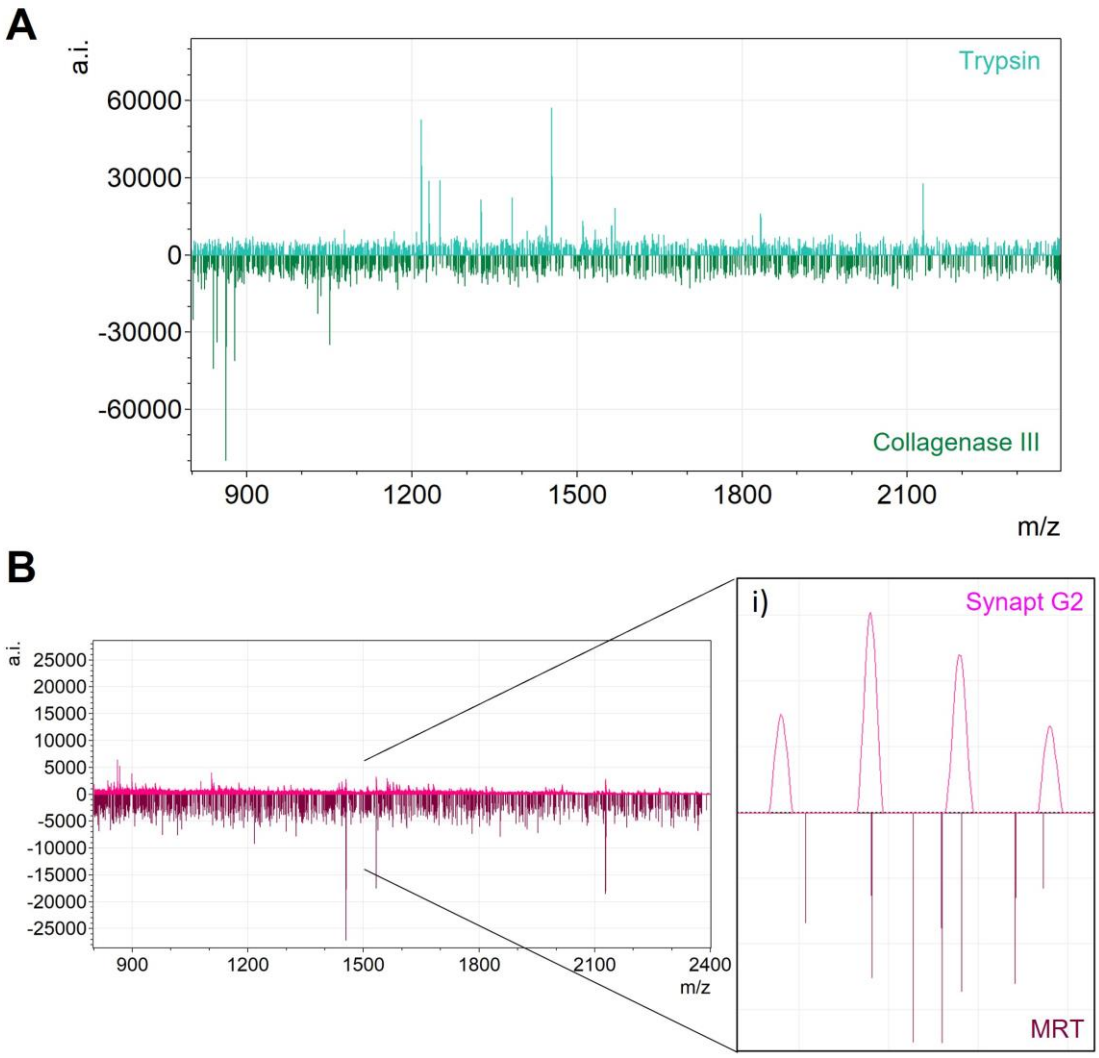


**Figure 3.9. MALDI-MS profiling spectra comparison of different techniques.** (A) Comparison of spectra from the digestion with trypsin and the digestion with COLase III. (B) Comparison of mass resolution and intensity with Synapt G2 and MRT instruments; (i) Magnification of the ion cluster at *m/z* 1562.

Peptide mass fingerprint was performed for the mass spectra obtained with SynaptG2 for putative identification of proteins in the samples. Recurring identifications in the samples with statistically significant matches were shown (mass tolerance higher than 0.05 Da) (Table 3.2).

**Table 3.2 Peptide mass fingerprint with MASCOT search.** List of putative proteins found in the mass spectra from 3D lung stroma through PMF. The list was limited to proteins with mascot score equivalent to $p<0.05$; *****=Monoisotopic mass ($M_r$).

| Protein Name | Gene | Mass* | Protein sequence coverage (%) |
|---|---|---|---|
| Nebulin-related-anchoring protein | NRAP | 197936 | 66 |
| Ciliary rootlet coiled-coil protein 2 | CRCC2 | 186690 | 63 |
| Serine/arginine repetitive matrix protein 2 | SRRM2 | 300192 | 50 |
| TBC1 domain family member 2B | TBD2B | 110508 | 48 |
| Golgin subfamily A member 4 | GOGA4 | 261908 | 63 |
| Coiled-coil domain-containing protein 90B | CC90B | 29545 | 73 |
| Fibroblast growth factor 2 | FGF2 | 31099 | 72 |
| Centlein | CNTLN | 162110 | 77 |
| Nuclear distribution protein nudE homolog 1 | NDE1 | 37872 | 77 |
| Collagen alpha-1(VII) | CO7A1 | 296027 | 44 |
| Partitioning defective 3 homolog B | PAR3L | 133109 | 48 |
| Peroxiredoxin-like 2A | PXL2A | 25863 | 68 |
| Src substrate cortactin | SRC8 | 61723 | 67 |
| Zinc finger protein 169 | ZN169 | 70184 | 50 |
| Citron Rho-interacting kinase | CTRO | 233374 | 62 |
| Nebulin | NEBU | 775445 | 60 |

*In silico* protein digestion of collagens linked to cancer were then performed and compared to the average spectra of the lung 3D model. Small differences between the sample replicates in terms of sequence coverage were observed for all the collagens. Also, sequence coverages were all lower than 20%, with collagen I (CO1A1) being the highest with 15-18/82%. The lowest coverages were identified in collagen VI (CO6A1) (5% in R1) and collagen XI COBA1 (8% in R2). Of the *m/z* covering the sequence, only the ones that were shared between the two sample replicates were presented. Error (ppm) lower than 1 were found in CO1A1 and COBA1.

**Table 3.3. *In silico* digest of collagens related to cancer.** Protein coverage in percentage = coverage in the sample/maximum coverage for the cleavage method used. Relevant *m/z* were the peaks in common between R1 and R2. Error showed in part per million (ppm).

| **Protein** | **Coverage** | | **Relevant m/z** | |
|---|---|---|---|---|
| | **R1** | **R2** | ***m/z*** | **Error (ppm)** |
| CO1A1 | 15/82% | 18/82% | 817.4097 | 7.7 |
| | | | 1226.6012 | 0.6 |
| | | | 2639.2597 | 0.2 |
| CO3A1 | 11/76% | 13/76% | 954.4752 | 2.3 |
| | | | 982.5065 | -2.4 |
| | | | 1492.7139 | 6.7 |
| CO6A1 | 5/86% | 10/86% | 1104.5718 | -7.3 |
| | | | 1991.9842 | 8.1 |
| CO7A1 | 13/85% | 16/85% | 864.4356 | 6.8 |
| | | | 954.4752 | 2.3 |
| | | | 1137.5759 | 5.6 |
| | | | 1356.6913 | -1.6 |
| COBA1 | 9/84% | 8/84% | 914.4578 | 0.1 |
| | | | 1095.5654 | -6.1 |
| | | | 1186.6062 | -5 |

### *3.3.3.1 Detection of proteomic changes induced by CRC EVs in the lung 3D model*

3D models from Section 3.3.2 were profiled with MALDI MRT. Differences in the profiling were observed in the average spectra (Figure 3.10). Specifically, SW620 EVs treatment showed intense signals between 900 and 1100 *m/z* which were absent in both control and SW480 EVs treatment.

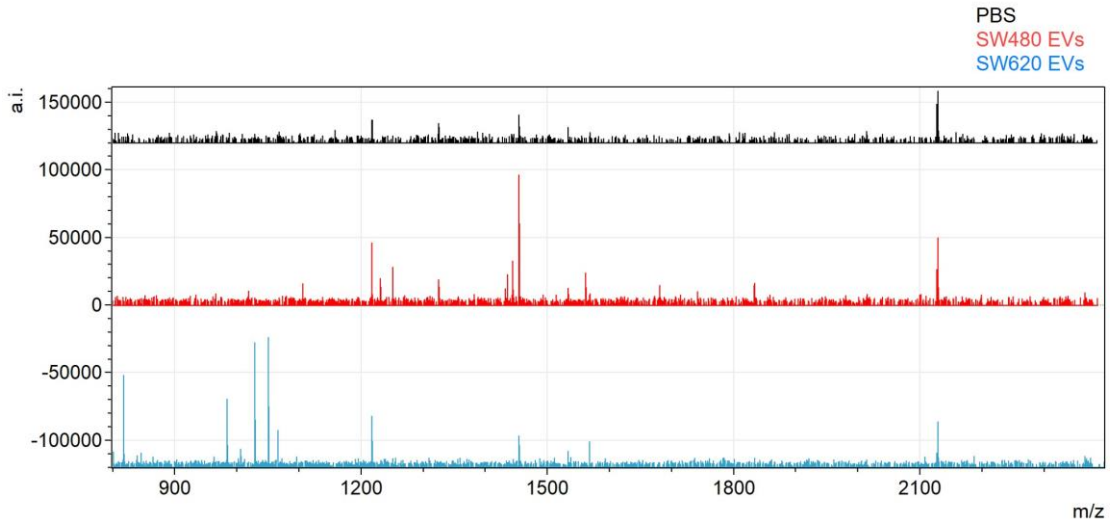


**Figure 3.10. MALDI MRT average spectra of lung 3D model treated with CRC EVs.** Average spectra visualised with mMass. Mass range 800 – 2400 *m/z.* CTRL spectrum in positive offset, SW620 EVs spectrum in negative offset.

Multivariate analysis was then performed to evaluate the differences in the proteomic profiling induced by the treatments (Figure 3.11). Separation of SW620 EVs treatment from the other two groups was observed due to principal component 1 (PC1) (Figure 3.11A). SW480 EVs treated and control groups did not separate. Within the groups, samples clustered together for PC1 in both SW480 EVs treated and control groups. PLS-DA showed better separation between all the groups for component 1 compared to PCA (Figure 3.11B). Also, within each group, better clustering was observed, especially for the SW480 EVs treated group. Variable importance in projection (VIP) scores were obtained from PLS-DA (Figure 3.11C), with significant variables > 1. Signals that distinguished between the three groups of samples ranged from 992 to 2369 *m/z*. The *m/z* peaks with the highest VIP scores were 1850.87 and 2164.54 *m/z*. Five *m/z* peaks were close to the score of 2 (2307.33, 1740.09, 2068.44, 2200.64 and 2301.44 *m/z*).

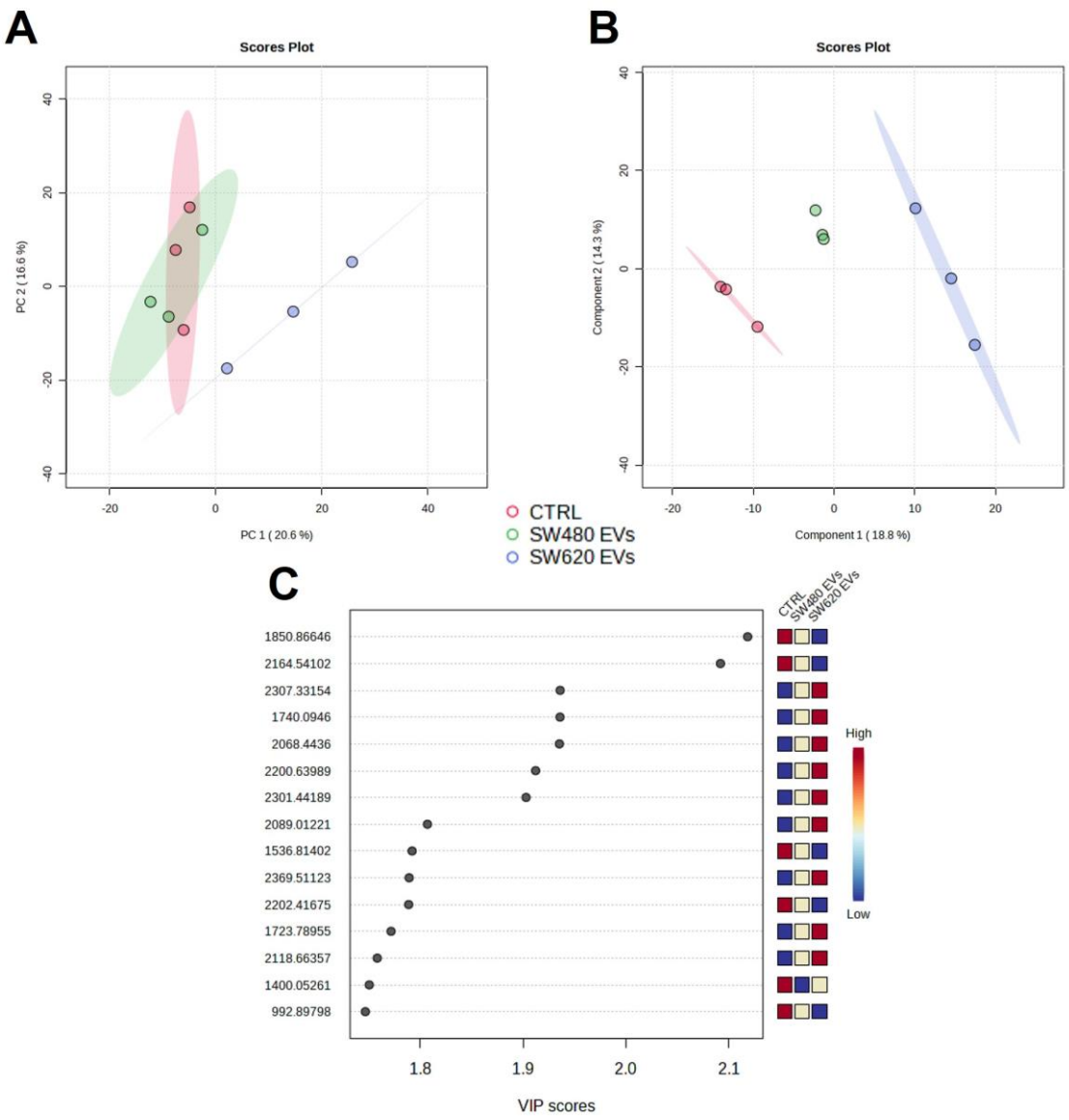


**Figure 3.11. Multivariate analysis on MS profiling of lung 3D model.** (A) PCA unsupervised, treatment groups not considered for the analysis. (B) PLS-DA supervised, treatment groups considered for the analysis. (C) VIP score showing the top 15 discriminatory *m/z* signals between the groups. CTRL = PBS control.

### 3.3.4 CRC EVs increased SW620 cells invasion

To investigate whether CRC EVs effects on the PMN had an impact on the invasive power of metastatic cells, pre-labelled SW620 were added onto the lung 3D model after 7 days of EV conditioning and kept invading for 4 days before sample processing. After 4 days, clusters of SW620 EVs were found to adhere to the border of the gel. The mean fluorescence intensities for the red channel were higher when gels were treated with SW480 and SW620 EVs, with the latter being statistically significant ($P \leq 0.05$) (Figure 3.12).

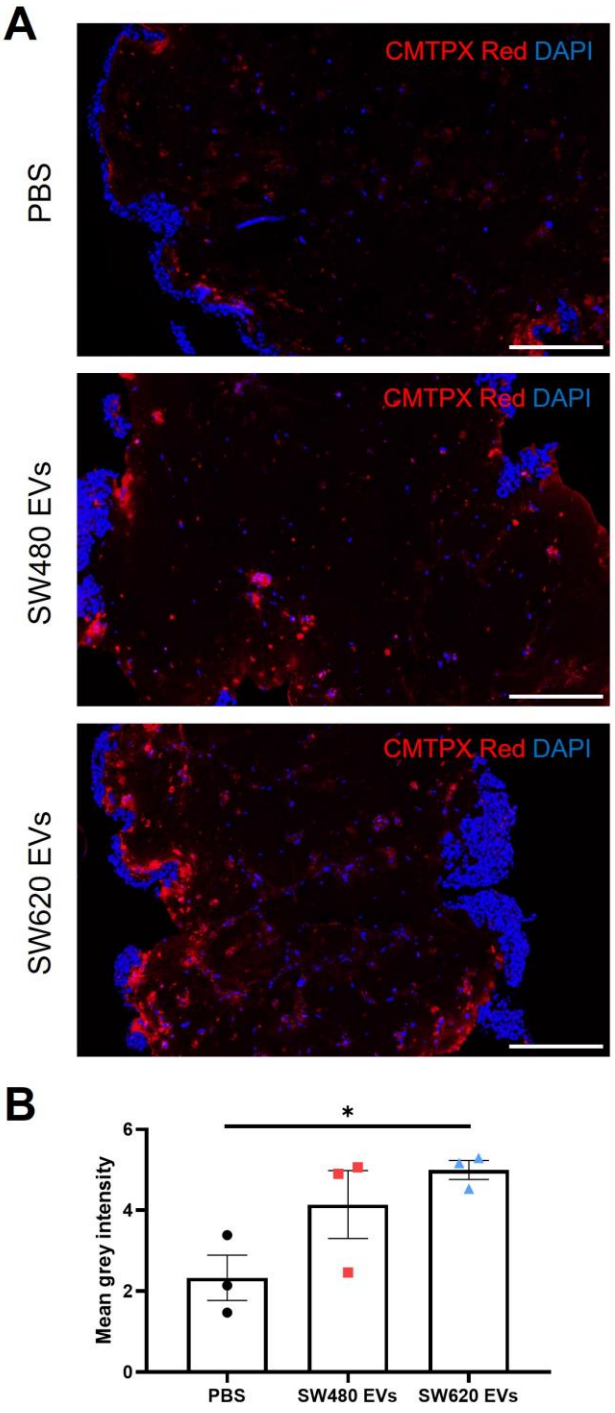


**Figure 3.12. SW620 cells invasion after the treatment with CRC EVs.** (A) Representative images of the lung stroma 3D model after the CRC EVs conditioning and the SW620 cells invasion (red cells). (B) Mean grey intensity of celltracker™ CMTPX Red staining. Individual values and mean ± SEM (n=3); ANOVA, * P ≤ 0.05.

Expression of α-SMA, vWF, CD68 and Ki67 were investigated again after the invasion of SW620 cells. CRC EVs induced an increase in α-SMA expression, in both cases statistically significant (P ≤ 0.05) (Figure 3.13A). An increase in the expression of vWF was also observed but failed to reach significance (P = 0.3927) (Figure 3.13B). Variable expression of CD68 was observed, especially

with SW480 EVs (Figure 3.13C). Expression of Ki67 was evaluated only in the cluster of SW620 cells (Figure 3.13D). SW620 EVs significantly decreased Ki67 positivity compared to PBS control (P ≤ 0.05), but the biological replicates for SW480 EV treatment were too limited to apply statistical analysis.

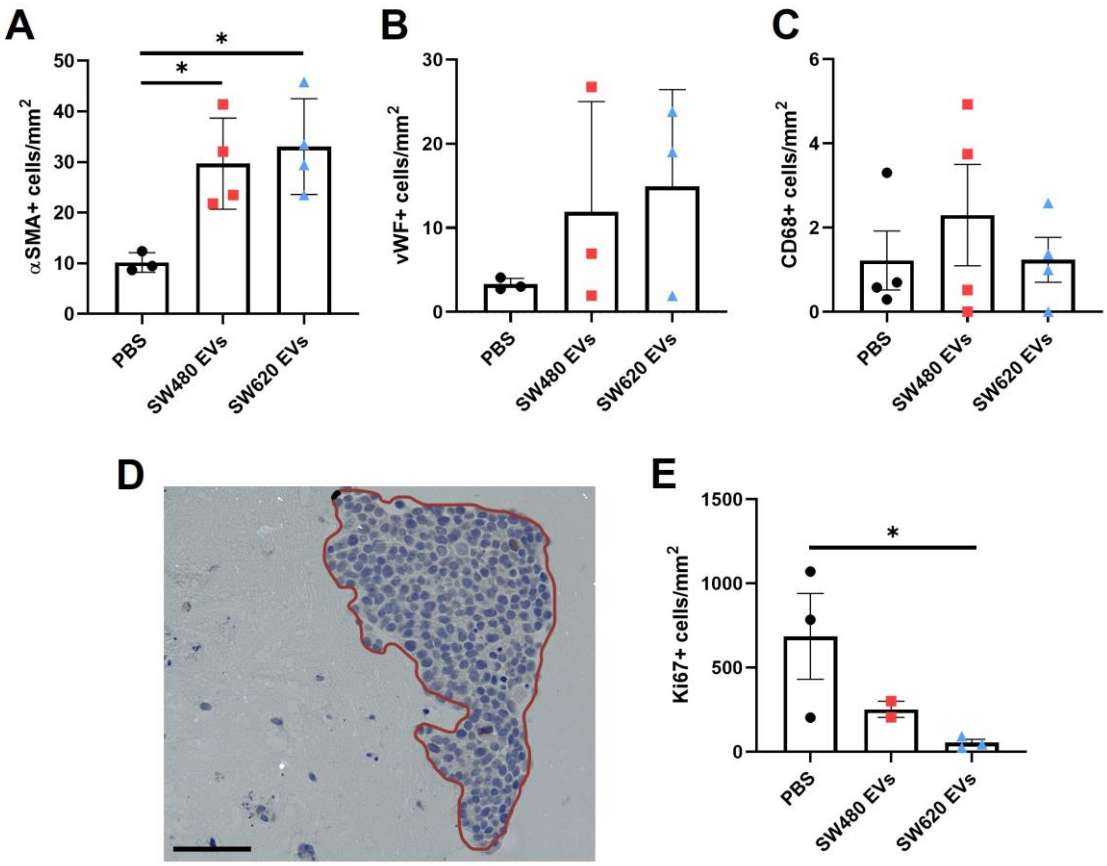


**Figure 3.13. Expression of cell markers based on IHC positivity after SW620 invasion.** Lung cell count normalised to $mm^2$. (A) αSMA expression. Individual values + mean (n≥3); ANOVA * P ≤ 0.05. (B) vWF expression. Individual values + mean (n=3). ANOVA. (C) CD68 expression. Individual values + median (n=4). Kruskal-Wallis. (D) Representative image of ROI selected for the Ki67 cell count (brown). (E) Ki67 expression in the SW620 clusters. Individual values + mean (n≥2). T test on PBS vs SW620 EVs, P ≤ 0.05.

### *3.3.4.1 Secreted factors in the lung 3D model pre and post SW620 invasion*

Pro-inflammatory cytokine expression was monitored before and after the invasion of SW620 cells, to see whether cancer EVs affected the inflammatory status of the 3D model. No evident alterations were observed in the secreted factors between the three conditions, thus statistical analysis was performed only on the pre- and post-invasion comparison, independently of the treatments. Although not significantly, IL-6 was high in the pre-invasion with SW480 EVs but then decreased post-invasion (P = 0.7) (Figure 3.14A). IL-8 expression was lowered after the invasion of SW620 cells in all the conditions, which reached

significance in the 3D models treated with SW480 EVs (P ≤ 0.05) (Figure 3.14B). A small increase in the expression of MCP-1 was observed in all the treatments from pre- to post-invasion, although failed to reach significance (P = 0.6618 for PBS, P = 0.7486 for SW480 EVs, P = 0.4818 for SW620 EVs) (Figure 3.14C). TIMP-1 increase from pre- to post-invasion was not significant in the control (P = 0.4) and SW620 EVs (P = 0.1) (Figure 3.14D). Interestingly, the levels of TIMP-1 were similar from pre- to post-invasion when the 3D models were treated with SW480 EVs. TIMP-2 was higher after SW620 cell invasion compared to the pre-invasion in both SW480/SW620 EV conditioning (P ≤ 0.05).

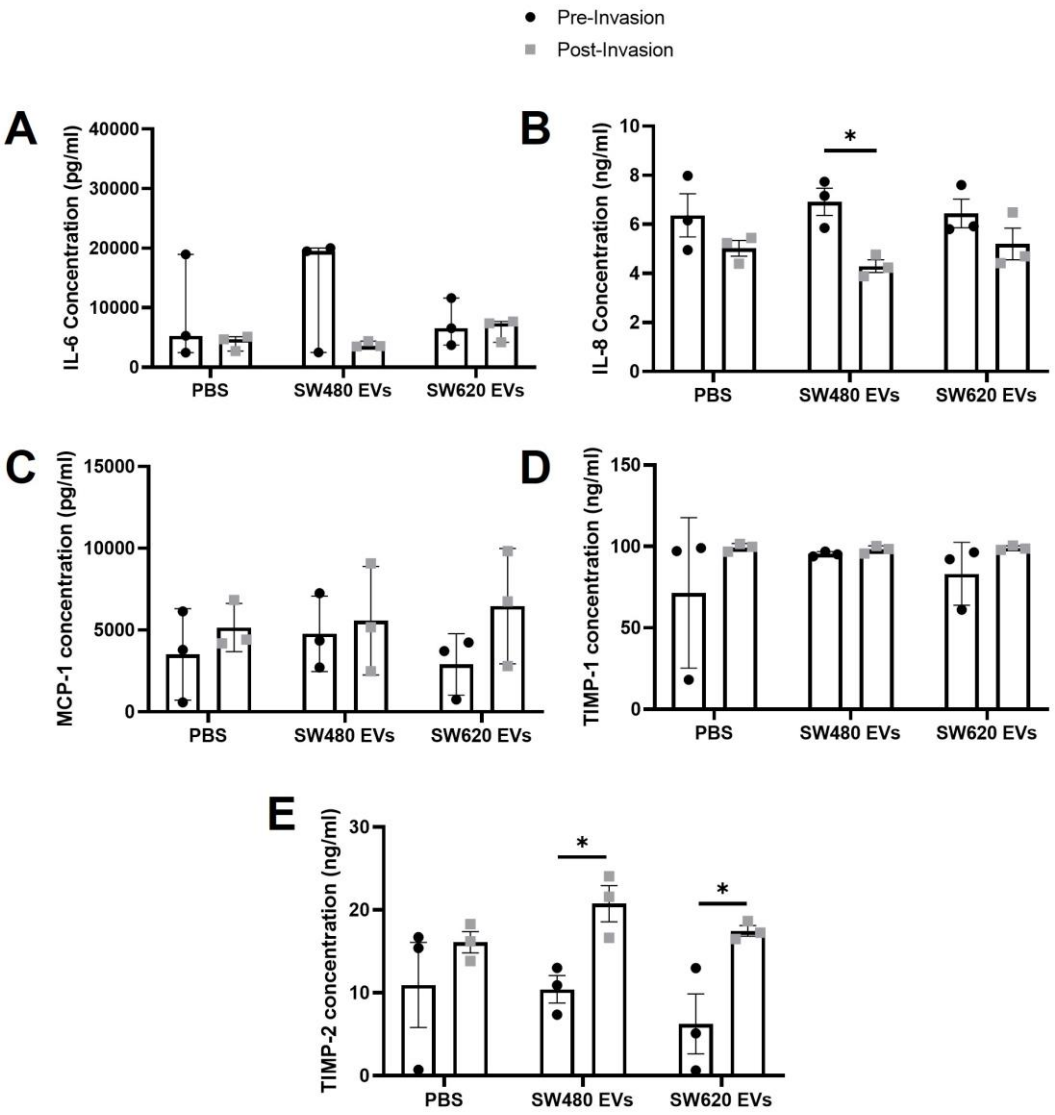


**Figure 3.14. Pro-inflammatory cytokines expression in the secretome of the lung stroma 3D model.** Comparisons conditioning/post-invasion were performed on the three treatments individually. (A) IL-6 concentration. Median with 95% CI (n=3); MW. (B) IL-8 concentration. Mean ± SEM (n=3); T test, * P ≤ 0.05. (C) MCP-1 concentration. Mean ± SEM (n=3). T test. (D) TIMP-1 concentration. Median with 95% CI (n=3). MW. (E) TIMP-2 concentration. Mean ± SEM (n=3); T test, * P ≤ 0.05.

### *3.3.4.2 Colorectal cancer EVs influence on ECM in the lung 3D model*

Of the collagens putatively identified with MS (Section 3.3.3), collagen III, collagen VI and collagen XI were screened through dot blots. Statistical analysis was not performed due to the loss of replicate (n ≥ 2). In general, SW620 cell invasion reduced collagen secretion regardless of the treatments (Figure 3.15). The conditioning with CRC EVs limited collagen III decrease post-invasion (Figure 3.15B). Despite the low levels, collagen XI was more reduced by the treatment with SW620 EVs, with complete loss of expression post-invasion (Figure 3.15D).

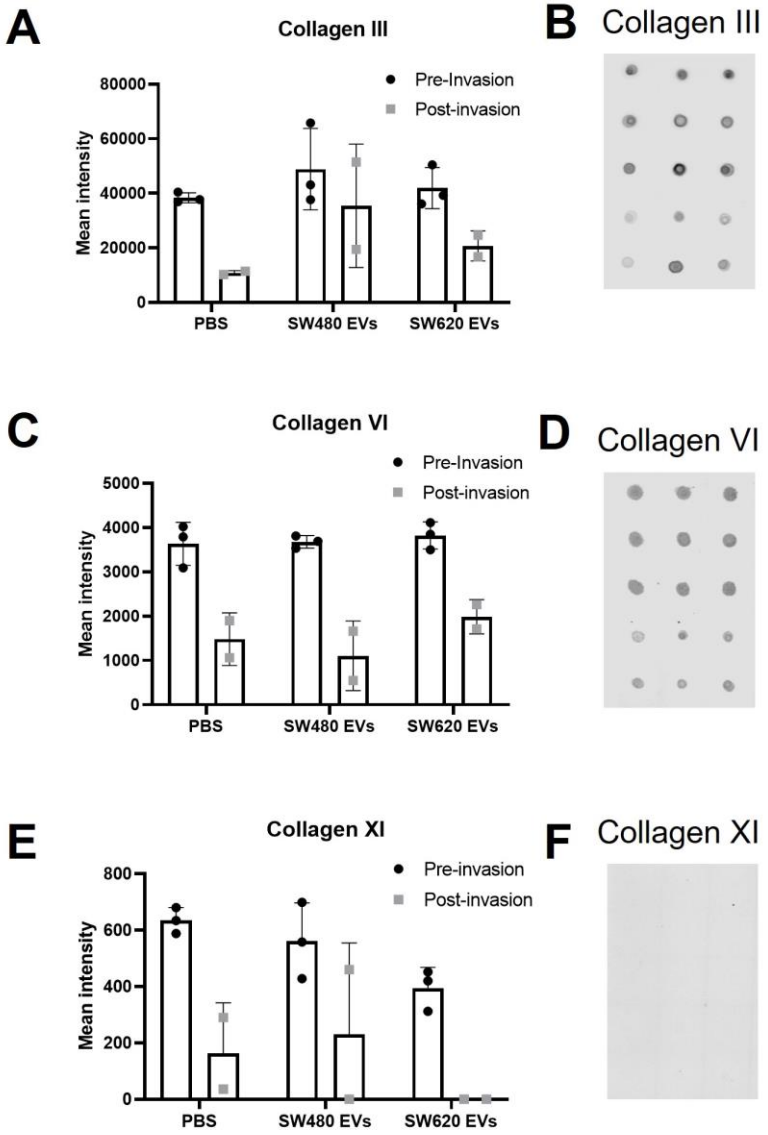


**Figure 3.15. Dot blots of cancer-related collagens.** (A) Collagen type III expression. Mean ± SEM (n ≥ 2). (B) Dot blots of collagen type III. (C) Collagen type VI expression. Mean ± SEM (n ≥ 2). (D) Dot blots of collagen type VI. (E) Collagen type XI expression. Mean ± SEM (n ≥ 2). (F) Dot blots of collagen type XI.

## 3.4 Discussion

The establishment of the PMN is a crucial intermediate step in malignancy that often goes unobserved by the screening tools currently employed due to the late stage of diagnosis. Investigating the events surrounding the PMN is of significant current interest to improve diagnosis, as well as to find therapeutic targets that act to prevent the progression towards metastasis. As a step building on the TME model developed in Chapter 2, a 3D model of lung was created to evaluate the cellular and proteomic changes driven by cancer EVs in the PMN.

### 3.4.1 Development of a 3D model of lung stroma

As the focus of the study was to determine EV mediated changes in the stroma of the lung, the *in vitro* 3D model was developed to mimic the denser areas of the lungs, where the ECM and fibroblasts reside. These areas are also the first areas exposed to cancer cells from the vasculature. Most of the research around PMN modulation by cancer EVs showed alterations in fibroblast phenotype and immune regulation (Dong *et al*., 2023; Patras *et al*., 2023). Normal lung fibroblasts, macrophages alongside endothelial cells were considered as the main representative cells which interact with metastatic colonisation first. From the previous model, MRC5 cells were maintained to represent normal lung fibroblasts, but the density was adapted to histological images of the *interstitium* found in literature (Kamp *et al*., 2022; Matsushima *et al*., 2020). Fibroblast density is a very important feature subjected to alterations in metastasis, correlated to tumour associated matrix stiffness and fibrosis (Doolin *et al*., 2021; Knops *et al*., 2020).

Long-term culture of the lung 3D model was tested for 7 or 14 days. While day 7 showed high cellularity and morphological heterogeneity of the cells, after 14 days the model was affected by the loss of these features. Cytokines released in the supernatant of the cultures, showed a lack of IL-6 and decrease in MCP-1, which may indicate a decline in viability. However, an increase in the anti-inflammatory cytokine IL-4 at day 14 could represent a slow stabilisation of the culture. From the histological images, intact nuclei could still be observed at day 14, suggesting that the alteration of cytokines did not completely impact on the cell survival.

Specific cell markers were chosen to confirm the presence of the three cell lines in the lung 3D model alongside passive staining. Normal lung fibroblasts have been known to express high levels of α-SMA when cultured (Dugina *et al*., 1998). At day 0, α-SMA was expressed in most cells in the model. It was indeed previously demonstrated that upon determined conditions, monocytes and macrophages can also produce α-SMA (Meng *et al*., 2016). This unspecific expression was however lost at day 7, suggesting that the culture was stabilising and differentiating over time. At day 7 and day 14, fibroblasts were distributed mainly at the border of the gels, showing their ability to migrate towards denser and stiffer areas of the gel (Hadjipanayi *et al*., 2009). For dTHP-1, the marker selected was CD68, abundantly expressed in all macrophages, regardless of their phenotype (Chistiakov *et al*., 2017). CD68+ macrophage like cells were found homogeneously expressed in the 3D model at the different time points and they did not correlate with the decreased expression of pro-inflammatory markers. HULEC-5a are an immortalised cell line deriving from lung endothelium, used as a site-specific alternative to the commonly used human umbilical vein endothelial cells (HUVECs). At first, CD31 was considered as endothelial marker. When first optimised on cytospin preparations of HULEC-5a, the cell line did not express CD31 (data not shown). Thus, vWF was selected as a marker for endothelial cells, which is a glycoprotein secreted during homeostasis, angiogenesis and immune response (Dmitrieva & Burg, 2014; Nakhaei-Nejad *et al*., 2019). Recently, it has been associated with cancer and metastatic advancement (Patmore *et al*., 2020; Yang *et al*., 2018). Although the amount of vWF expression remained similar throughout the culture, the highest expression of the marker was found on endothelial cells clustering together and shaping capillary-like structures.

Pre-stained cells were then counterstained with DAPI to enable numeration of viable and apoptotic cells in the models based on nuclear morphology. DAPI highlighted the presence of apoptotic events in the gel, even at day 7, which might lead to the decrease of cell density at day 14. Nevertheless, the time point at day 7 was chosen as a suitable length of time for the pre-conditioning since it to correlated with stabilisation of the culture. It is important to state that apoptosis is a physiological event in tissues, it is not only associated with a pathologic

condition, thus presence of apoptosis in the 3D model might just imply an intrinsic feature of the tissue (Mondello & Scovassi, 2010).

### 3.4.2 CRC EVs mediated induction of a pre-metastatic niche

Cancer EVs have been extensively linked to the paracrine remodelling of PMN. To observe the functional EV changes *in vitro*, relevant 3D models need to be developed, which can be pre-treated with cancer EVs. The lung stroma 3D model developed was treated with SW480 and SW620 EVs for 7 days. At the end of the culture, the treated gels showed higher transparency compared to the control, suggesting relevant modification on the structure and density of the collagen matrix. Histological staining did not reveal morphological changes in the matrix, but further biomechanical testing might better characterise any alterations in tissue stiffness and density of the EV conditioned gels. Presence of cell aggregates upon treatment with CRC EVs might also be a cause or an effect of the increase of transparency and potential ECM remodelling. MMPs have been investigated as they can be associated with cancer-EVs and degrade specific ECM components to facilitate cancer cell invasion (Shimoda, 2019).

Despite the extensive research around EVs and CAF activation, the results of α-SMA IHC raised an interesting observation. SW620 EVs, but not SW480 EVs, induced a decrease in the expression of α-SMA. This might indicate that the activation of CAFs is related to the early stage of the disease rather than late. HULEC-5a released more vWF upon conditioning with late SW620 EVs, which might correlate with increased angiogenic signalling. In CRC, the role of CD68+ macrophages varies according to the type and the location of the macrophages. Many studies observed a positive contribution and a better disease outcome with increased presence of CD68+ TAM around the invasive front (Koelzer *et al*., 2016; Li, *et al*., 2020). However, CD68+ cells have been also correlated to metastatic progression and chemoresistance (Wei *et al*., 2019; Yin *et al*., 2017). Here, CRC EVs did not affect the levels of the markers in the tissue. In future, markers specific to M1 (like CD86) or M2 (likeCD206) phenotypes could help in identifying whether EVs alter macrophages phenotype (Jayasingam *et al*., 2020).

To initially screen ECM and proteome modification in the 3D models, a MALDI-MS approach was employed. It was first imperative to evaluate whether the lung 3D model, due to its collage-dense matrix, was resistant to enzymatic digestions

by the enzymes commonly used in MS proteomics, which generally results in low data intensity (Clift *et al*., 2021). Surprisingly, the 3D model was more sensitive to trypsin degradation rather than COLase III. The list of putative identifications of lung showed that with trypsin digestion, many matrix derivatives were identifiable, including collagen VII. Recent work has shown the potential role of collagen VII as a biomarker of immune infiltration in pancreatic cancer (Ding *et al*., 2023). Future work is required to confirm the presence of collagen VII in the 3D model and evaluating possible alteration by cancer EVs. *In silico* digestion of collagens linked to cancer was also performed to evaluate the sequence coverage and the ability to obtain information on ECM proteins. Even though the coverage was never over 20%, *m/z* signals attributed to the collagens were always identified with low errors. Taken together, these results demonstrate that the 3D model was suitable for the MS profiling of ECM proteins.

Differences in the spectra deriving from the conditioning of the lung 3D model were then evaluated. The high mass resolution that features MRT mass spectrometer is not recognised by mMass software and its peak picking. Thus, the automated PMF algorithm and *in-silico* digestion of protein of interest could not be performed. For this reason, the differences were investigated by multivariate analysis, which showed separation of the samples treated with SW620 EVs with both supervised and unsupervised analysis. Two *m/z* signals were identified to be the main peptides responsible for the separation, but the identification would require further tandem MS/MS approaches. However, this preliminary study demonstrates the potential of MALDI-MS technology to investigate ECM proteins in 3D models. However, more work needs to be done to confirm the putative identifications and to validate the multivariate analysis.

### 3.4.3 SW620 invasion is regulated by the pre-metastatic alterations linked to CRC EVs

SW620 cells derive from CRC lymph nodes metastasis, so they are a good model for studying events leading to metastasis. Pre-conditioning of the lung TME with CRC EVs led to an increased adherence and presence of SW620 cells at the border of the gels, which confirmed previous data (Ramamoorthy *et al*., 2019). Additionally, the comparison offered by the SW480/SW620 EVs model showed that the invasion is induced by early EVs as well as late. This might not be a surprise, given that PMN is suspected to be an early event. Alteration in the

expression of cellular markers was also evaluated. Interestingly, increased α-SMA was observed with both EV treatments. This might indicate that CRC EVs do activate CAFs, but only when cancer cells are invading, implying a synergistic activity between the EVs and the cancer cells. vWF levels were increased by the EV treatments, but the general expression was still low. The expression of vWF was found frequently close to the area of invasion, which might indicate that more than an increased expression, endothelial cells are relocated towards the cancer cells. No main changes were observed in CD68 expression, but it is known that cancer induces a change in the phenotype rather than increase or loss of cells. Finally, Ki67 was utilised to evaluate whether increased invasion corresponded to decreased proliferation of SW620, as previously observed with SW480. A decrease was observed with both treatments, but statistical analysis could not be performed due to the loss of SW480 EVs treated replicate.

To evaluate whether CRC EVs induced the phenotypic M1 to M2 changes of THP-1 in the 3D model, inflammatory cytokines were also investigated pre- and post-invasion. It is important to note that the cancer cells were left to invade for four days after the seven days of pre-conditioning with EVs. A decrease of inflammatory cytokine secretion was expected, as previously observed in the optimisation of the 3D model from day 7 to day 14. The 3D models without exogenous EVs showed that the invasion of SW620 cells is able alone to reduce or even revert the decrease. Only upon SW480 EV conditioning the expression of pro-inflammatory cytokines, especially IL-8, was reduced, thus showing that the EV induced anti-inflammatory activity is promoted from early stage EVs rather than metastatic EVs.

Dot blots can be a useful technique for the qualitative screening of proteins of interest. Three of the collagens investigated with MS were screened in the lung 3D models Collagen III rich ECM has been previously associated with cancer dormancy, while its disruption showed increased proliferation and metastasis (Brisson *et al*., 2015; Di Martino *et al*., 2021). Collagen VI and collagen type XI are highly associated with cancer progression (Li *et al*., 2022; Wu & Chou, 2022). For all three collagens, the expression in the 3D models was decreased following SW620 invasion. This could indicate that loss of collagen is mediated by the invading cancer cells rather than the EVs, but could also relate to the extended time point of the culture. Interestingly, cancer EVs impacted the expression of

only collagen XI, with a decrease with SW620 EVs conditioning. Further analysis combining these results to tissue expression are necessary to clarify whether the presence of collagens in the supernatant is linked to increased presence in the tissue, turnover or degradation.

## 3.5 Conclusions

A lung 3D model was successfully developed to investigate the role of EVs in the PMN. Even though the *in vitro* model was limited in the length of culture duration, it was able to demonstrate that CRC EVs altered the PMN and that these alterations can happen at different stages of the disease. MALDI-MS profiling showed promising preliminary results for the investigation of ECM molecules in the 3D models. Finally, CRC EVs increased the invasion of SW620 cells in the gels, altered the biophysical structure and the cells of the PMN. Further research is needed to confirm the role of CRC EVs in ECM proteomic modification.

# 4 The role of colorectal cancer EVs in the modulation of Transglutaminase 2 and extracellular matrix remodelling

This chapter was undertaken in collaboration with the group of Dr. Luca Urbani's group at the Institute of Hepatology (King's college, London). The work was shared with the PhD candidate Lai Wei. Data obtained by collaborators will be appointed in the figure legends.

## 4.1 Introduction

Among the proteins that play a role in the biological and biomechanical regulation of cancer invasion and progression, transglutaminase 2 (TG2) is a relatively new discovery in the field. Transglutaminase 2 is a protein linked to a wide array of functions and can either function in an enzymatic or non-enzymatic role (Fesus & Piacentini, 2002; Tempest *et al*., 2021). The already ubiquitous protein has been linked to many cancers and has shown context dependent actions for the establishment of the tumour and its metastases. While this can be seen contrasting, the differential activities likely relate to the different configurations and multiple variants of TG2 (Beninati *et al*., 2017; Lai *et al*., 2007). Furthermore, TG2 expression is not limited to cancer cells, but can be produced and regulated by other cellular and non-cellular components of the TME, such as cancer-associated fibroblasts (CAFs) and the extracellular matrix (ECM) (Tempest *et al*., 2021). For these reasons, TG2 is now considered a crucial player in all the hallmarks of cancer. In the most recent years, research on TG2 activity in cancer has been focussed on the role in chemotherapy resistance and in the development of TG2 inhibitors as anti-cancer agents (Eckert, 2019; Parvatikar *et al*., 2022; Shinde *et al*., 2022). However, due to its multifunctional properties and heterogeneous activity, the modulation of TG2 cannot lead to a single solution for treatment of all cancers. Thus, understanding the specific cellular and tissue related TG2 activities is still an important area to explore.

### 4.1.1 Transglutaminase 2 role in cancer invasion and metastasis

The dysfunctional remodelling of the ECM is a very important step for the migration and invasion of cancer cells in the tissue. From one side, collagen deposition and cross-linking of the matrix by enzymes like lysyl oxidase (LOX) act in favour of the cancer spread and produce a stiffer environment commonly observed in the primary tumour (Ramos *et al*., 2022). On the other hand, degradation of the ECM by matrix metalloproteinases (MMPs) and impairment of its turnover are also essential for cancer cell migration (Botta *et al*., 2012; Zeng

*et al*., 1999). There has been key interest in the exploration of TG2 extracellular activity, where TG2 binds to and cross-links ECM proteins (Bhedi *et al*., 2020; Stamnaes *et al*., 2016). The cross-linking function has physiological roles, as well as disease-related roles. In cancer, it has been strongly associated with matrix remodelling which occurs during cancer invasion (Delaine-Smith *et al*., 2019; Lee *et al*., 2015).

The mechanism of secretion of TG2 by cells into the ECM is not completely understood; however, secretion can occur through extracellular vesicles (EVs) and controlled via heparan sulfate (Furini *et al*., 2020). The presence of TG2 on EVs is correlated with fibronectin (FN), one of the proteins through which TG2 expresses its functions. The link between TG2 and EVs is not limited to TG2 secretion into the ECM, but the presence of TG2 on the surface of EVs has both intracellular and extracellular functions in many processes including cancer progression (Antonyak *et al*., 2011; Diaz-Hidalgo *et al*., 2016). For example, cancer microvesicles-linked TG2 and FN have been shown to transform normal fibroblasts in cancer-like phenotypes (Antonyak *et al*., 2011). In another study, it has been shown that cancer EV-associated TG2 facilitates the establishment of the metastatic niche (Shinde *et al*., 2020). Finally, cancer cells with low migratory potential have been shown to communicate with fibroblasts via the release of TG2-enriched MVs to escape the primary tissue and metastasise (Schwager *et al*., 2022).

Cell surface TG2 is also found in a strict complex with FN and is responsible for the binding with integrins to promote cell adhesion, cell migration and the deposition of FN extracellularly (Nurminskaya & Belkin, 2012). Attachment of ovarian cancer spheroids to the stroma was inhibited upon targeting the TG2/FN/integrin complex (Condello *et al*., 2018). Furthermore, surface TG2 expression increased invasion and survival of metastatic breast cancer cells (Mangala *et al*., 2007).

Despite the numerous evidence of this pro-tumorigenic activity, inhibition of TG2 via mi-RNA 19 has also been associated with cancer progression, thus highlighting the heterogeneous and controversial role of TG2 in cancer (Cellura *et al*., 2015).

### 4.1.2 Transglutaminase 2 and cancer-associated fibroblasts

Fibroblasts and CAFs are an important target for the TG2 driven mechanisms in cancer progression. As already introduced, the transformation from normal fibroblasts to CAFs is key for ECM remodelling and the generation of the stiffer microenvironment, which is linked to the advancement of the disease. As TG2 main activity is to cross-link collagen and ECM-related proteins, there is a natural link in investigating TG2 involvement in the establishment of CAFs.

A well-known activator of CAFs by cancer cells is tumour growth factor-beta (TGF-β), which is expressed by many cancerous cells (Chen *et al*., 2023; Ishimoto *et al*., 2017; Lewis *et al*., 2004). TGF-β is a major inducer of TG2 (Nunes *et al*., 1997) and exists in a positive feedback loop, where TG2, in return, can activate TGF-β (Shweke *et al*., 2008).

Once CAFs are activated, they exert many pro-tumorigenic functions, through the secretion of growth factors, cytokines and ECM proteins (Kalluri, 2016). Excessive matrix deposition (desmoplasia) is a feature commonly associated with CAFs activity and is associated with the increased tissue stiffness of advanced tumours (Cannon *et al*., 2018; Naba *et al*., 2012; Zeltz *et al*., 2020). Tissue stiffness is a result of matrix deposition, but also of increased cross-linking activity conducted by different enzymes including TG2 (Delaine-Smith *et al*., 2019; Lee *et al*., 2015).

Aside of matrix deposition, CAFs contribute to the phenotypic behaviour of cancer cells needed for disease progression. CAFs have a role in the induction of EMT of cancer cells (Yang *et al*., 2023). In hepatocellular carcinoma, the EMT driven by CAFs is promoted by the overexpression of TG2 alongside the production of IL-6 and hepatocyte growth factor (HGF) cytokines (Jia *et al*., 2020).

### 4.1.3 Transglutaminase 2 role in liver fibrosis

The excess of matrix deposition and the enzymatic cross-linking activity of collagen in the ECM lead to pathological fibrosis. In fact, fibrosis has been frequently associated with advanced cancer stages, especially in organs with a physiological dense matrix, such as liver (Affo *et al*., 2017). Moreover, fibrosis linked to different types of disease like non-alcoholic steatohepatitis (NASH) and non-alcoholic fatty liver disease (NAFLD) have been explored in understanding the high incidence of liver metastasis in CRC (Kondo *et al*., 2016). Among the

cells responsible for liver fibrosis, hepatic stellate cells (HSCs) are the main contributors, as they are the main progenitor of the myofibroblasts responsible for matrix synthesis, which is a CAF-like feature (Zhang *et al*., 2020). For this reason, common markers of activated HSCs are α-SMA and vimentin (Carpino *et al*., 2005; Wang *et al*., 2019). Activation of the myofibroblast phenotype is associated with TGF-β and IL-6 secretion (Xiang *et al*., 2018). As such it is hypothesised that TG2 is also involved in the cross-linking activity present in liver fibrosis (Tatsukawa *et al*., 2020).

The complexity of TG2 functions as well as the intricate feedback pathways that connect TG2 to molecules responsible of TME activity are yet to be clarified.

### 4.1.4 Aim of the chapter

In this chapter, the role of TG2 in CRC invasion and metastasis is explored in relation to CRC EVs. First, the *in vitro* 3D model of invasion previously developed was used to evaluate the EVs driven expression of TG2 and the relationship with cancer invasion. Then, it was evaluated whether the expression of TG2 in the mutual communication between CRC cells and fibroblasts was supported by CRC EVs. Finally, HSCs isolated from fibrotic livers were used to evaluate the involvement of CRC EVs in myofibroblasts activation and TG2 expression.

## 4.2 Materials and Methods

### 4.2.1 Experimental design

The chapter is divided into two main sections (Figure 4.1). In the first section, the role of EVs in the mediation of TG2 was evaluated in the 3D model of CRC invasion. Flow cytometry was applied to investigate the origin of TG2 found in the 3D model and its modulation driven by cancer cells and CAFs cross-talk. Cells in mono- and co-culture were compared in the TG2 expression. Then, CAFs were treated with EVs and soluble proteins deriving from CRC cells to assess which of the factors were responsible for TG2 modulation. The second part analyses the role of CRC EVs and TG2 in HSC activation and in fibrosis linked to CRC liver metastasis. Three patient-derived HSCs were utilised and treated with CRC EVs. IF analysis along with gene expression were performed on TG2 and proteins related to fibrosis.

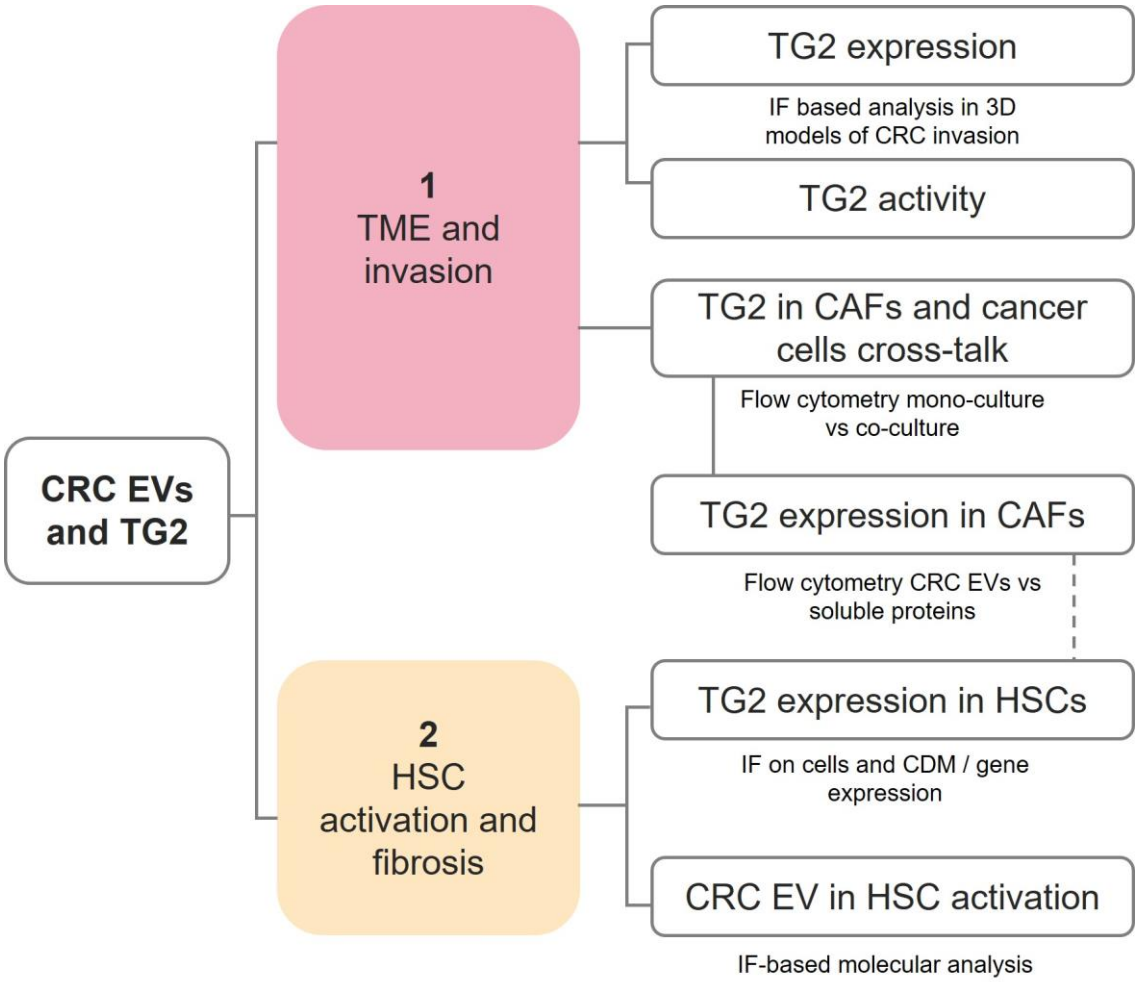


**Figure 4.1. Schematic of Chapter 4 experimental design.**

### 4.2.2 2D Cell culture

The general subculturing procedure of SW480 and MRC5 cell lines can be found in Section 2.3.2. Hepatic stellate cells (HSC073, HSC088, HSC215) were isolated from tissue samples of CRC patients with liver metastasis who had undertaken surgery at King's College Hospital and *maintained by the collaborators at the Foundation for Liver Research, Institute of Hepatology, London* (Table 4.1). The cells were cultured in growth media (DMEM, 1% v/v P/S, 10% v/v FBS) with 0.01% epithelial growth factor (EGF). The cells were maintained in a humidified incubator at 37°C and 5% $CO_2$ in air. The media was replaced every 4 days and cells were sub-cultured with trypsin (Merck) when reaching 70-80% of confluence. Cells were checked for mycoplasma and were shown to be negative throughout.

**Table 4.1. HSC primary cells.** F-Score = Fibrotic score.

| Patient number | Collection date | F-Score | Gender | Age |
|---|---|---|---|---|
| 73 | 09/04/2019 | F1-F2 | F | 64 |
| 88 | 26/07/2019 | F0 | F | 36 |
| 215 | 30/06/2022 | F0-F1 | M | 51 |

### 4.2.3 3D Cell culture

For this chapter, TG2 expression was observed in the 3D model of invasion developed in Chapter 2.

### 4.2.4 CRC-derived extracellular vesicles

Isolation, purification and quantification of CRC EVs (from SW480 and SW620 cell lines) was done according to Section 2.3.5.

### 4.2.5 Hepatic stellate cells treatment with SW480/SW620 EVs

*Plate setup of HSCs was performed by the collaborators at the Foundation for Liver Research, Institute of Hepatology in London.* HSC073, HSC088, HSC215 cells were cultured into 24 well-plates with coverslips and left for a day to adhere. Then, starvation media (DMEM with low serum) was replaced until cells were ready to undergo treatments. For immunofluorescence (IF), cells were plated at density of 12000 cells/ml. For ECM deposition, the coverslips were coated with 0.2% gelatin (Merck, UK) for 60 min at 37°C, rinse and then 1% glutaraldehyde was replaced for 30 min at RT. After rinsing, quenching was performed using 1M

glycine in PBS for 20 min at RT. Cells were plated at density of 36000 cells/ml. At day 2 of the culture, media was replaced with growth media and 50 µg/ml of SW480 or SW620 EVs was added to the culture. The cells were incubated for 48 hours and then supernatant was collected and cells were fixed with 4% paraformaldehyde (PFA) for 20 min. After fixation, PBS was replaced in the culture and the cells were kept at 4°C until further use.

## 4.2.6 Immunofluorescence

### *4.2.6.1 Immunofluorescence in 3D*

To evaluate the presence of TG2 around the invasive clusters in the 3D model of invasion, IF was performed using a primary antibody to TG2 (1:200, mouse monoclonal CUB 7402; Abcam, UK). Goat anti-mouse secondary IgG antibody labelled with Alexa Fluor® 488 was used to visualise the staining in green. For the more detailed method, see Section 2.3.4.3. After deparaffinisation and rehydration, HIAR was performed followed by the blocking step in goat serum. Sections were incubated with primary antibody (1:200) overnight at 4°C in a humidified environment. Three washes in 0.05% v/v Tween-20/PBS were performed followed by the incubation with secondary antibody (1:500) for 1 hr at RT. Three more washes were performed and then VECTASHIELD® HardSet™ Antifade Mounting Medium with DAPI was used to mount the coverslips. Confocal images Zeiss Axio LSM800 and mean fluorescence values were acquired.

### *4.2.6.2 Immunofluorescence in 2D*

Immunofluorescence was used to measured TG2, vimentin and SMA expression of hepatic stellate cell. Vimentin and α-SMA are markers of hepatic stellate cell activation. Hepatic stellate cells were placed on coverslips within a humidity chamber. Blocking buffer (PBS, 1% BSA) was left on the coverslips for 30 min at RT, then replaced with the following primary antibodies: anti-TG2 (mouse monoclonal CUB 7402), anti-Vimentin (1:100, MAB2105 rat monoclonal 280618; R&D, Abingdon, UK) and anti-SMA (1:100, ab5694 rabbit polyclonal; Abcam, UK). The coverslips were incubated overnight at 4°C. The day after, 3 washes with PBS (5 min each) were performed before adding secondary donkey anti-mouse Alexa Fluor® 488, donkey anti-rabbit Alexa Fluor® 555 donkey anti-rat Alexa Fluor® 647 (1:500, ThermoFisher, UK) for 1 hour at RT. The slides were mounted with Fluoroshield with DAPI (Merck, UK) and left to dry for 2 hours before imaging.

#### *4.2.6.3 Immunofluorescence for decellularised matrix*

*2D decellularisation to obtain cell derived matrix (CDM) was performed by the collaborators at the Foundation for Liver Research, Institute of Hepatology in London.* 2D decellularisation was employed to investigate the presence of fibrotic markers in the CDM after the conditioning with CRC EVs. Extraction buffer (10 mM $NH_4OH$, 0.25% Triton X-100 in PBS) was introduced in the plates with the HSCs and incubated at 37°C for 4 min to lyse the cells. To remove the cells, half of the buffer was removed and replaced with PBS. This process was repeated until no visible cells remained. Then, IF was performed as described in Section 4.2.6.2. Primary antibodies: anti-TG2 (1:200 mouse monoclonal CUB 7402), anti-FN (1:100, ab23750 rabbit polyclonal, Abcam, UK) and anti-Pancollagen (1:100, NBP2-67538 rabbit monoclonal ST58-04, Novus Biologicals, UK). Secondary antibodies: donkey anti-rabbit Alexa Fluor® 647, donkey anti-rabbit Alexa Fluor® 555 and donkey anti-mouse Alexa Fluor® 488 (1:500, ThermoFisher, UK).

### 4.2.7 TG2 activity with biotin-monodansylcadaverine staining

To evaluate the cross-linking activity of TG2 on the invasion in the CRC 3D models, biotinylated monodansylcadaverine (biotin-MDC; Invitrogen, molecular probes, UK), which is a TG2 cross-linked substrate, was employed. At the end of the 3D model culture, the gels were placed in 0.2M CaCl in PBS to equilibrate for 15 min at 37°C, 5% $CO_2$. Then, the gels were treated with 10µl/ml of biotin-MDC in the same solution for 2 hours at 37°C, 5% $CO_2$. Controls without the substrate were also performed for 2 hours (data not shown). Samples were then fixed and processed as FFPE and sections cut with microtome. After deparaffinisation and rehydration steps, HIAR was performed as previously described (Section 2.3.4.3). Then, 20 µg/ml of Alexa Fluor™ 488 Streptavidin Conjugate (Invitrogen, UK) was used to visualise the complex. After two washes in PBS, VECTASHIELD® HardSet™ Antifade Mounting Medium with DAPI was used to mount the coverslips and counterstain.

### 4.2.8 Quantitative measurements for TG2 expression

Measurements of the invasive length and size of invasive clusters (single cells/clusters) as described in Section 2.3.7, were used for investigating TG2 expression in the invasive SW480 cells found in the 3D model of invasion.

## 4.2.9 Flow cytometry

### *4.2.9.1 SW480/MRC5 Co-culture experiments*

SW480 and MRC5 cells were used to evaluate differences in the expression of surface TG2 between single and co-culture. To be able to distinguish the two cell types, SW480 cells were labelled with 500 nM CellTracker™ Deep Red Dye and MRC5 cells with 5 µM CellTracker™ Green CMFDA for 30 min in serum free condition prior to trypsinising and counting. Fluorescence images of the passive staining performed in the co-culture was obtained to confirm the absence of cross-reactivity of the passive dyes. For single cells culture, $1x10^6$ cells, while 250000/750000 SW480/MRC5 were added in co-culture. To determine whether the expression was EV mediated, dimethyl amiloride (DMA), inhibitor of EV secretion, was introduced at 15 nM in the co-culture condition (Savina *et al*., 2003). Cells were incubated for 2 days in T75 flasks at 37°C and 5% CO2 in air. At the end of the culture, cells were resuspended and fixed in 4% PFA for 20 min. Then cells were washed in PBS three times. For every washing cycle, the cells were centrifuged at 300 g for 5 min to discard supernatant. To prevent non-specific binding, the pellets were resuspended in PBS with 10% EV-depleted FBS for 20 min followed by three washes in PBS. Then, cells were incubated with primary antibody mouse to mAb to TG2 (dilution 1:100, Abcam, USA) for 2 hours at RT. Pellets were washed again two times before donkey to mouse IgG secondary antibody conjugated to AlexaFluor® 750 was added (dilution 1:100, Abcam, USA) for 1 hr at RT in the dark. Pellets were ultimately washed twice in PBS before reaching the final suspension for the analysis (PBS with 10% EV-depleted FBS) with CytoFlex flow cytometer (Beckman Coulter Life Sciences, UK).

TG2 expression was evaluated in a SW480/MRC5 co-culture with flow cytometry and compared to the TG2 expression by the cells in monoculture. Since the type and the number of staining differed between the co-culture and the monoculture, different gating strategies were applied (Figure 4.2). For the co-culture, a first gate isolating live cells was created. In this gate, two populations were observed being separated by the FITC-A and APC-A channels, identifying MRC5 and SW480 respectively. TG2 positivity was evaluated by setting thresholds on the graphs where the cell channel was on the y axis and the TG2 channel (APC-A750-A) was on the x axis. In the monocultures, after the gating of live cells (data

not shown) a single population was observed. Staining threshold of the co-culture was calculated independently from the mono-culture thresholds.

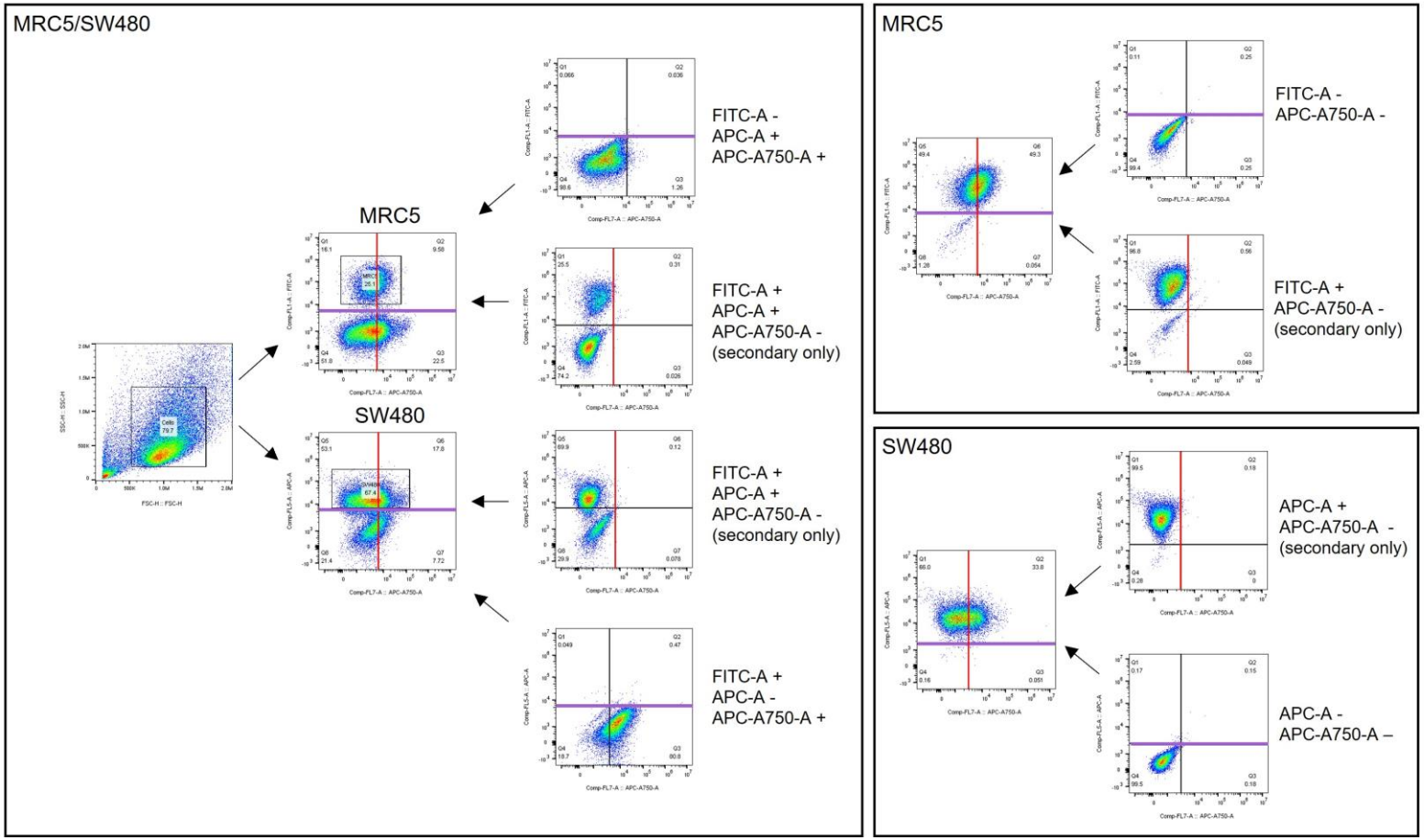


**Figure 4.2. Gating strategy for the evaluation of co-culture induced TG2.** Co-culture (MRC5/SW480) and mono-culture expression of TG2 with flow cytometry. After the selection of the living cells, MRC5 were distinguished by SW480 in the co-culture model according to staining positivity. FM0 controls were employed to determine the threshold of passive staining positivity. Secondary only controls were employed to determine the positive TG2 cells.

#### *4.2.9.2 Treatment of MRC5 cells with SW480/SW620 EVs*

For flow cytometry, 500,000 MRC5 cells were cultured for 24 hours and then treated for 48 hours with 50 µg/ml of either SW480 EVs, SW620 EVs (deriving from pooled SEC fractions 7-9), SW480 or SW620 soluble proteins (SEC fraction 19). The treatment was added in DMEM with 10% EV depleted serum. At the end of the culture, cells were resuspended and fixed in 4% PFA for 20 min. Then cells were washed in PBS three times. For every washing cycle, the cells were centrifuged at 300 g for 5 min to discard supernatant. To prevent non-specific binding, the pellets were resuspended in PBS + 10% EV-depleted FBS for 20 min followed by three washes in PBS. Then, cells were incubated with primary antibody mouse to mAb to TG2 (dilution 1:100, Abcam, USA) for 2 hours at RT. Pellets were washed again two times before donkey to mouse IgG secondary antibody conjugated to AlexaFluor® 750 was added (dilution 1:100, Abcam, USA) for 1 hr at RT in the dark. Pellets were ultimately washed twice in PBS before reaching the final suspension for the analysis (PBS with 10% EV-depleted FBS) with CytoFlex flow cytometer (Beckman Coulter Life Sciences, UK).

#### *4.2.9.3 Data analysis*

Data were analysed with FlowJo 10.7 software (BD Biosciences, USA). Flow dot plots and histograms were created. Quantitative analysis based on median fluorescent intensity (MFI) and cell populations were obtained and graphically represented using GraphPad Prism 8.

### 4.2.10 Cytokine Release (ELISA)

ELISA assay for IL-6, IL-8 and MCP-1 were performed according to manufacturer's instructions using commercially available kits, as described in Section 3.2.6.

### 4.2.11 Real time quantitative PCR for genes linked to HSC activation

*Polymerase chain reaction (PCR) was performed by the collaborators at the Foundation for Liver Research, Institute of Hepatology in London.* RNA was extracted from HSCs using ReliaPrep™ RNA Miniprep Systems (Promega, UK), following manufacturer's instructions. RNA concentration was measured using Nanodrop1000 (ThermoFisher, USA). Then, RNA was converted into cDNA

using GoScript™ Reverse Transcriptase kit (Promega, UK) and a cDNA concentration of 10 ng/µL was obtained. Quantitative (q)PCR was performed on 25 ng of cDNA using PCR master mix (PrecisionPLUS-R, from Primerdesign Ltd., UK) with low-ROX and Taqman qPCR probes (Integrated DNA Technology, Coralville, USA.) in MicroAmp Fast Optical 96 well Reaction Plates (Starlab, Milton Keynes, UK) using the ABI7500 Real-Time PCR System (Applied Biosystems, CA, USA).

For the analysis, ribosomal protein lateral stalk subunit 0 (RLP0) housekeeping gene threshold cycles (Cq) were used to calculate ΔCq for each gene in each sample. Then, ΔΔCq was calculated by normalising against the ΔCq of the untreated controls.

### 4.2.12 Statistical analysis

Statistical analysis was performed using Prism 8.1.1 software. First, data were tested for normality as previously described (Section 2.3.8).

When the groups tested were 2 (0-50 µm vs > 50 µm clusters), Student T test was performed. When the groups tested were ≥ 3 (CRC EV conditionings), multiple comparisons tests were employed. ANOVA with Tukey's post-hoc analysis was performed for parametric data, while KW test with Dunn's post-hoc analysis was performed for non-parametric data. P-values less than 0.05 were considered significant.

Data representation as previously described (Section 2.3.8).

## 4.3 Results

### 4.3.1 Surface transglutaminase 2 expression depends on the relationship between cancer cells and fibroblasts

Passive dyes did not cross-react, with MRC5 maintaining the green and SW480 maintaining the red staining (Figure 4.3A). Transglutaminase 2 was non significantly decreased on MRC5 in the co-culture compared to monoculture (P = 0.0757) (Figure 4.3 Bi and Ci). The opposite trend was observed in SW480 TG2 expression, showing a non-statistically significant increase (P = 0.1802) when placed in co-culture with MRC5 (Figure 4.3 Bii and Cii). To evaluate whether the changes in the TG2 expression were EV mediated, DMA, inhibitor of EV secretion, was introduced in the co-culture. DMA did not revert the expression of TG2 in MRC5. However, SW480 TG2 expression decreased (non-significantly, P = 0.4985) and reached a similar level of the monoculture.

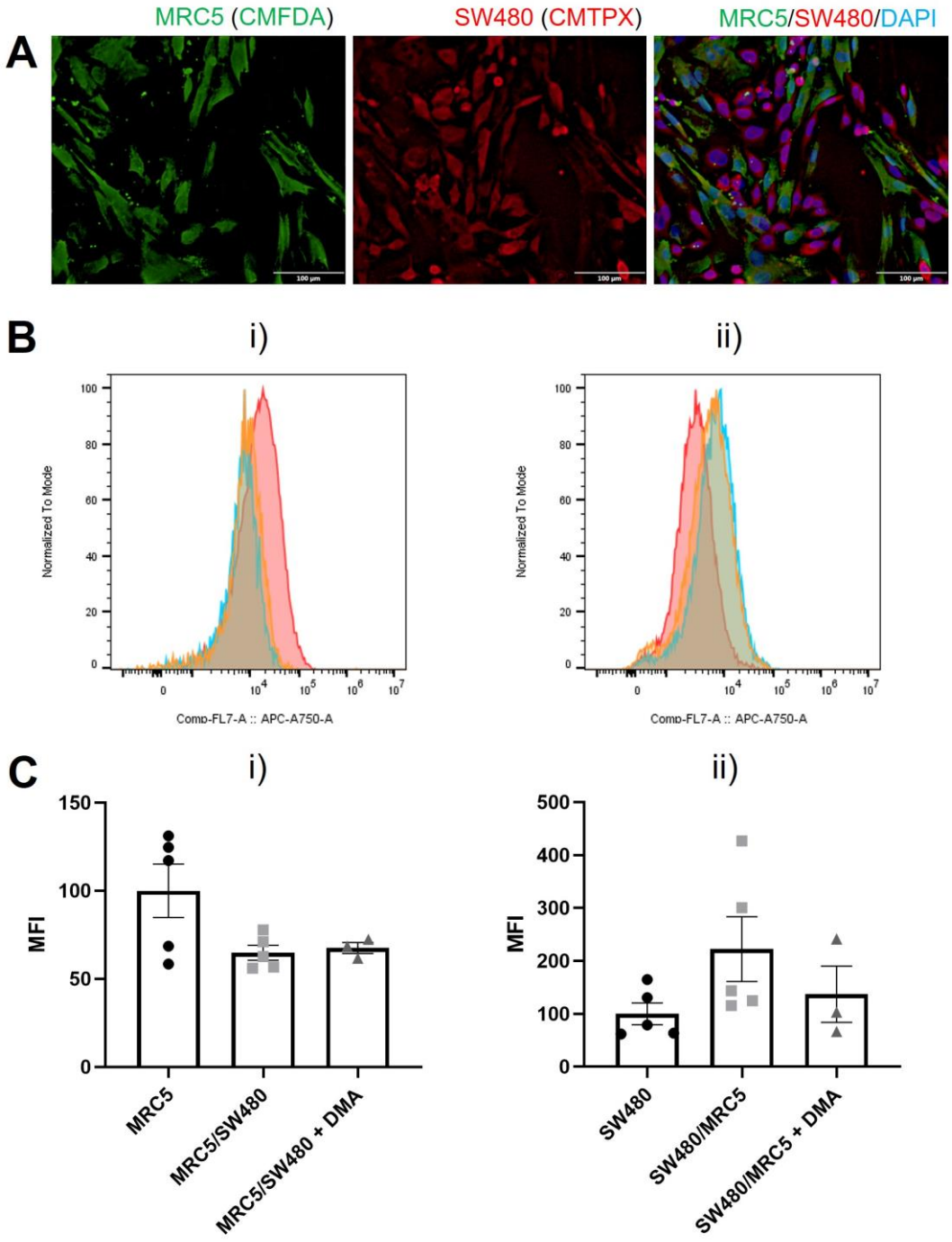


**Figure 4.3. MRC5/SW480 co-culture altered expression of TG2.** (A) Representative images of passive co-culture staining with CellTracker™ dyes. Green CMFDA used for MRC5 staining and Red CMTPX used for SW480. DAPI counterstain. (B) FlowJo histograms of TG2 levels. Modal overlay scaling. Red = monoculture, blue = co-culture, yellow = co-culture with DMA; (i) MRC5, (ii) SW480. (C) Median fluorescence intensity of TG2; (i) MRC5. Mean ± SEM (n ≥ 3). ANOVA, (ii) SW480. Mean ± SEM (n ≥ 3). ANOVA.

### 4.3.2 Transglutaminase 2 expression in MRC5 is mediated by cancer cells secretome

CRC secretome was used to evaluate the modification in TG2 expression by fibroblasts. MRC5 fibroblasts treated with CRC EVs or soluble proteins were stained for TG2 and analysed with flow cytometry. TG2 positivity was identified after selecting the threshold with the secondary only control. A decrease in TG2 expression was observed with all the treatments, which reached significance for treatments with SW480 or SW620 soluble proteins ($P \leq 0.01$), but failed to reach significance in cells treated with CRC EVs ($P = 0.7$ for SW480 EVs, $P = 0.7022$ for SW620 EVs) (Figure 4.4).

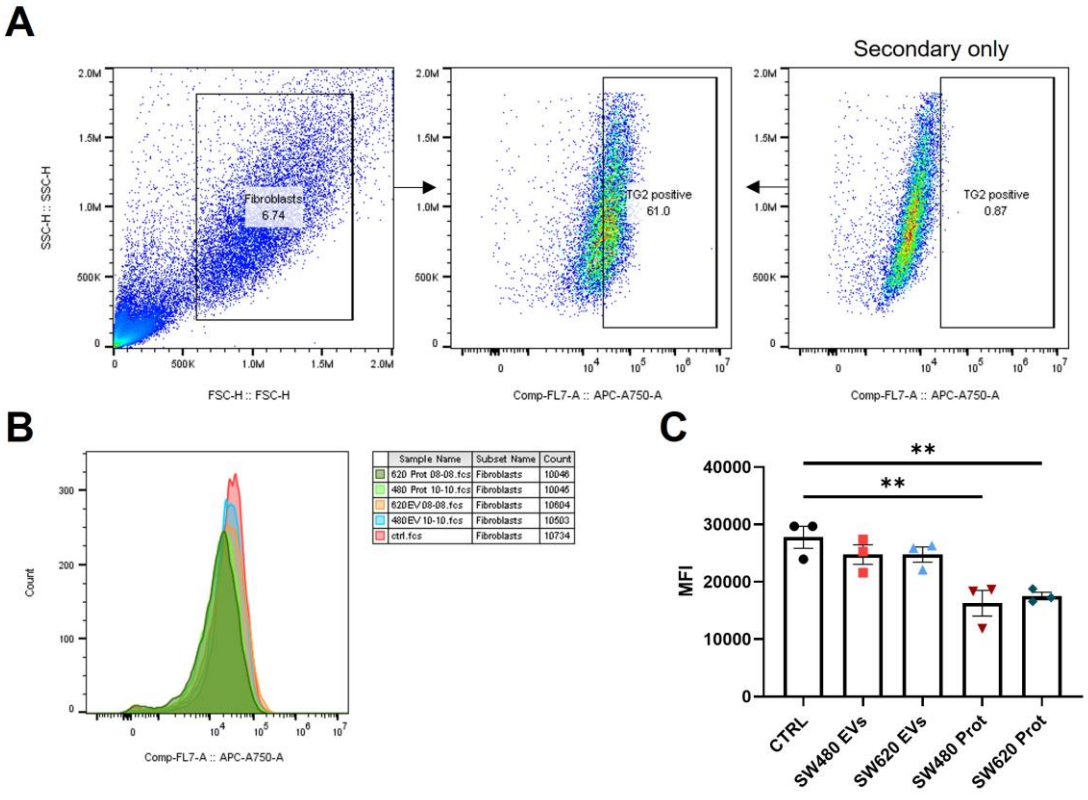


**Figure 4.4. TG2 expression in MRC5 mediated by CRC proteins.** (A) Gating strategy for the evaluation of TG2 expression in MRC5. Threshold of positivity selected from the secondary only control. (B) FlowJo histogram of TG2 expression. Smoothing applied. Modal overlay scaling. (C) Median fluorescence intensity of TG2 expression. Mean ± SEM (n=3). ANOVA, ** $P \leq 0.01$.

### 4.3.3 Transglutaminase 2 expression induced by CRC EVs

Since TG2 levels were increased in SW480 upon co-culture with MRC5, TG2 was investigated in its impact on cancer cell invasion in the TME. TG2 expression found in the invasive SW480 cells was investigated upon treatment with SW480 or SW620 EVs (Figure 4.5). To evaluate whether TG2 expression was dependent

on the cell depth in the tissue, clusters close to and distant from the front of invasion were separately considered (Figure 4.5C). No statistically significant differences were observed ($P > 0.05$), even if in the control models, TG2 was expressed less by clusters > 50 µm distant compared to the ones close to the front of invasion (0-50 µm). TG2 expression in single cell invasion significantly increased when the 3D model was treated with SW620 EVs, compared to the control ($P \leq 0.05$) and SW480 EVs conditioning ($P \leq 0.01$) (Figure 4.5Di). Similarly, TG2 significantly increased in the invasive clusters with SW620 EVs conditioning compared to the control ($P \leq 0.001$) and SW480 EVs ($P \leq 0.01$) (Figure 4.5Dii). Preliminary data on TG2 expression were also obtained (n=2). In a similar way, the mean grey values in the invasive region were evaluated, and a significant increase in TG2 activity was observed following treatment with SW480 EVs only when compared to SW620 EV treatment ($P \leq 0.05$) (Figure 4.5E).

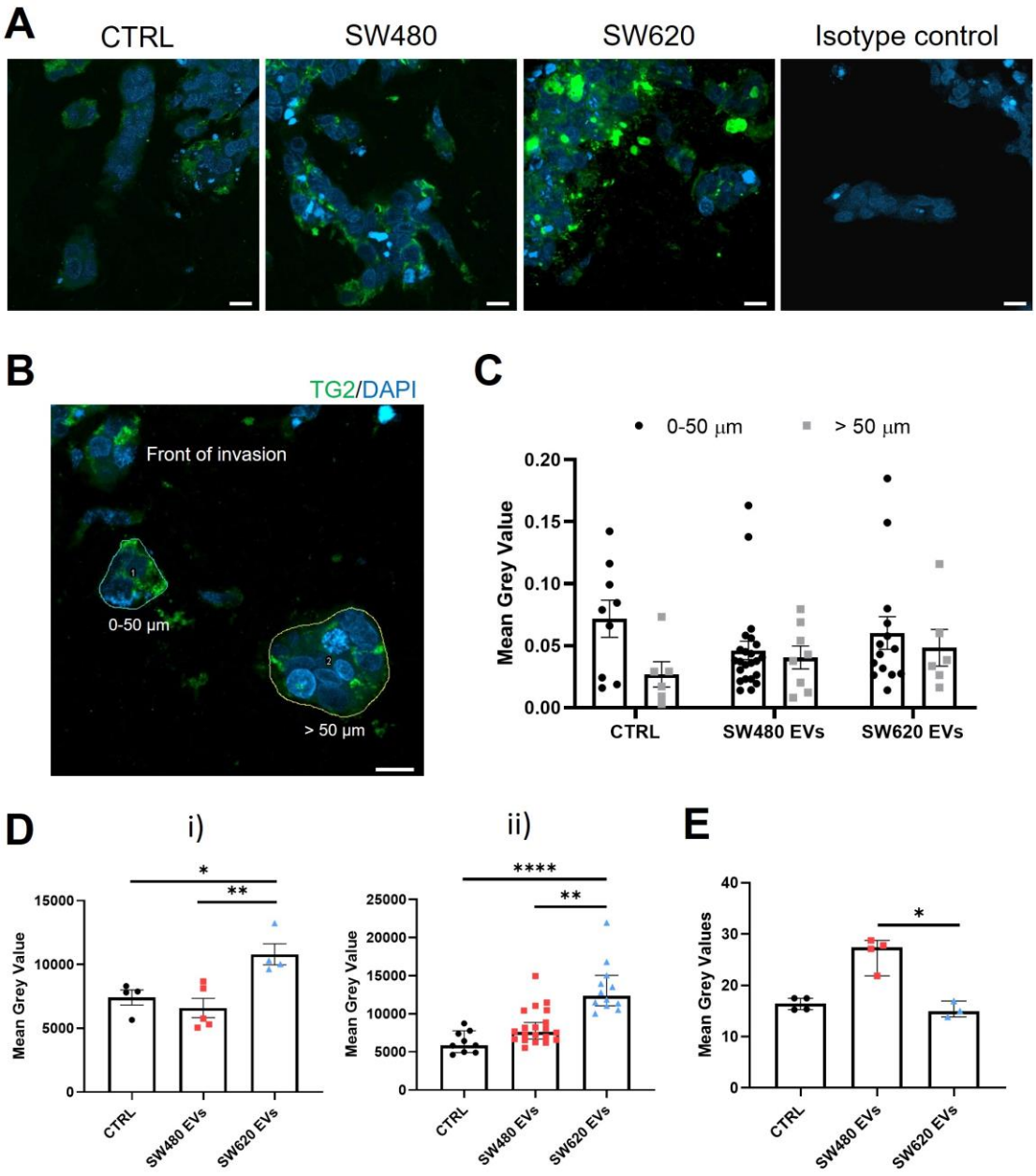


**Figure 4.5. TG2 expression in the 3D model of CRC invasion.** (A) Representative images of TG2 IF (green) around SW480 clusters. Dapi as counterstaining (blue). Scale bar = 10 µm. (B) Region of interest selected for the quantitative measurements. Invasive cluster close (0-50 µm) and distant (> 50 µm) from the invasive layer. Mean Grey Values normalised to the areas. Scale bar = 10 µm. (C) Comparison of TG2 expression between close and distant clusters of invasion. Mean ± SEM (n=3). T test. (D) TG2 in single cells or clusters of invasion; (i) TG2 on single cells. Mean ± SEM (n=3). ANOVA * P ≤ 0.05, ** P ≤ 0.01. (ii) TG2 on clusters. Median ± 95% CI (n=3). Kruskal-Wallis ** P ≤ 0.01, **** P ≤ 0.001. (E) TG2 activity on total invasion. Median ± 95% CI (n=2). Kruskal-Wallis * P ≤ 0.05.

### 4.3.4 Colorectal cancer EVs activate hepatic stellate cells

The role of CRC EVs and TG2 were evaluated in HSC activation, which correlates with fibrosis and metastasis (Huang *et al*., 2019; Lee & Friedman, 2011). For all HSCs results, the proteins levels were represented individually (according to the

three cell lines) and as combined result for statistical analysis. Levels of α-SMA, marker of HSC activation, were investigated. Tumour growth factor-beta treatment increased the expression of α-SMA in all patient-derived HSCs (Figure 4.6A). Colorectal cancer EVs induced a stronger increase in HSC073 and HSC088, with the highest levels reached with SW480 EVs. In HSC215, α-SMA levels upon CRC EVs were similar to TGF-β treatment. Combined data showed that SW480 EVs significantly increased α-SMA expression in HSCs compared to the untreated ($P \leq 0.005$) (Figure 4.6B). SW480 EV treatment was significantly higher than SW620 EV treatment ($P \leq 0.05$). When the gene expression of α-SMA was evaluated, a higher level was found with TGF-β in all the patients HSCs (Figure 4.6D). Alpha-smooth muscle actin was decreased with CRC EVs in all the HSC cells. The TGF-β increase was statistically significant compared to the untreated control ($P \leq 0.005$), to SW480 EVs and SW620 EVs ($P \leq 0.001$) (Figure 4.6E).

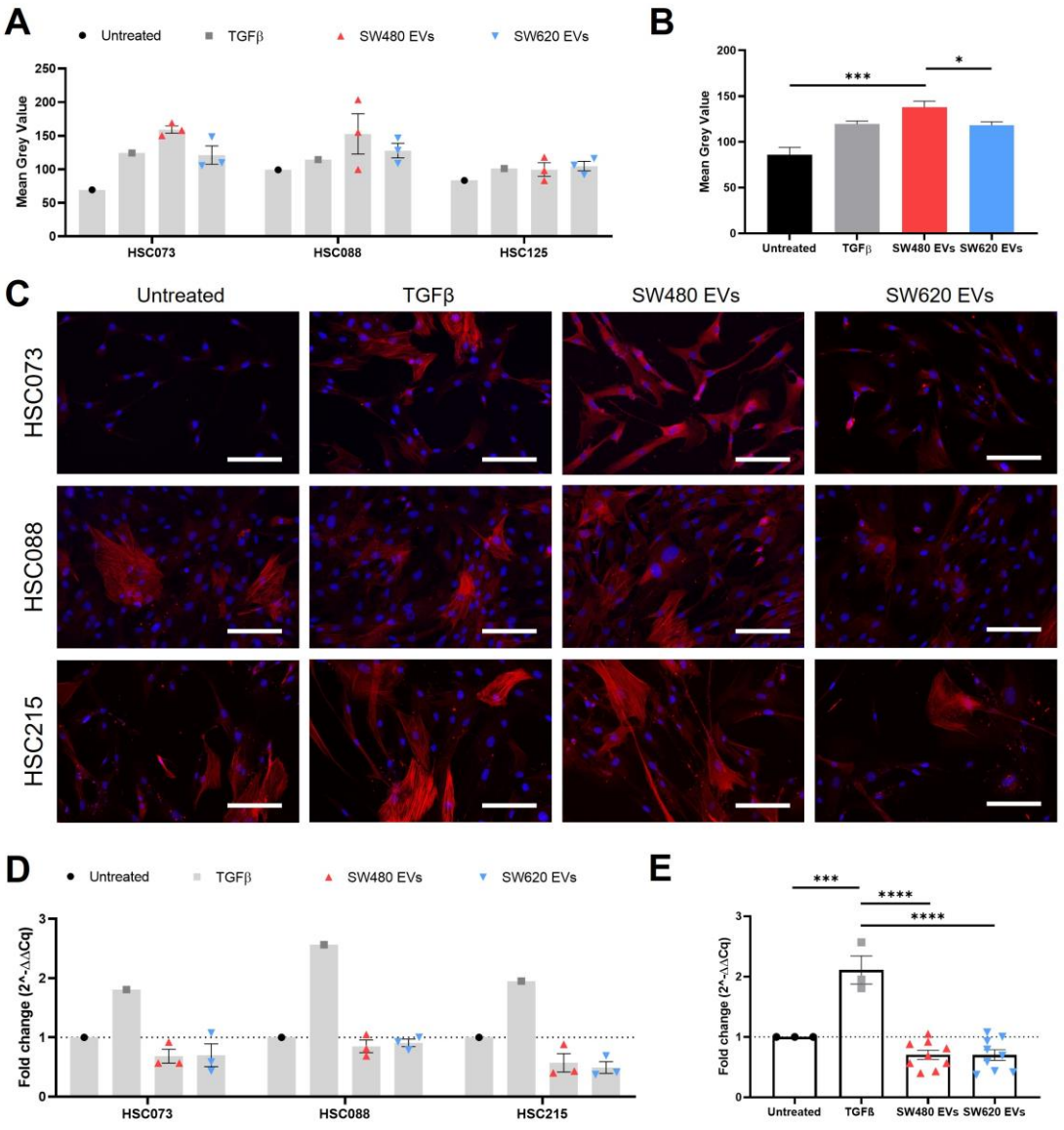


**Figure 4.6. α-SMA protein expression with IF and gene expression in HSCs.** (A) Levels of α-SMA in the three patient derived HSCs. Mean ± SEM.(B) Summary of the levels of α-SMA expression (mean grey value). Mean ± SEM (n ≥ 3). ANOVA, * P ≤ 0.05, *** P ≤ 0.005. (C) Representative images of α-SMA expression (red) with DAPI as counterstaining (blue). Scale bar = 100 µm. (D) qPCR data of α-SMA expression in patients HSCs. ΔΔCq normalisation to housekeeping gene RLP0. Mean ± SEM. (E) Summary of TGM2 expression. Mean ± SEM (n ≥ 3). ANOVA *** P ≤ 0.005, **** P ≤ 0.001.

Vimentin is another marker of HSC activation (Wang *et al*., 2019). Protein expression of vimentin was analysed with IF. All the treatments varied according to the HSC type. No changes were found with TGF-β for HSC073 and HSC215, while vimentin increased in HSC088 (Figure 4.7A). EV treatment didn't follow the same trend; HSC073 cells showed higher levels of vimentin with both CRC EVs, but for HSC088 and HSC215 the two EV treatments induced a decrease in

vimentin expression. None of these changes were found statistically significant (P > 0.05) (Figure 4.7B).

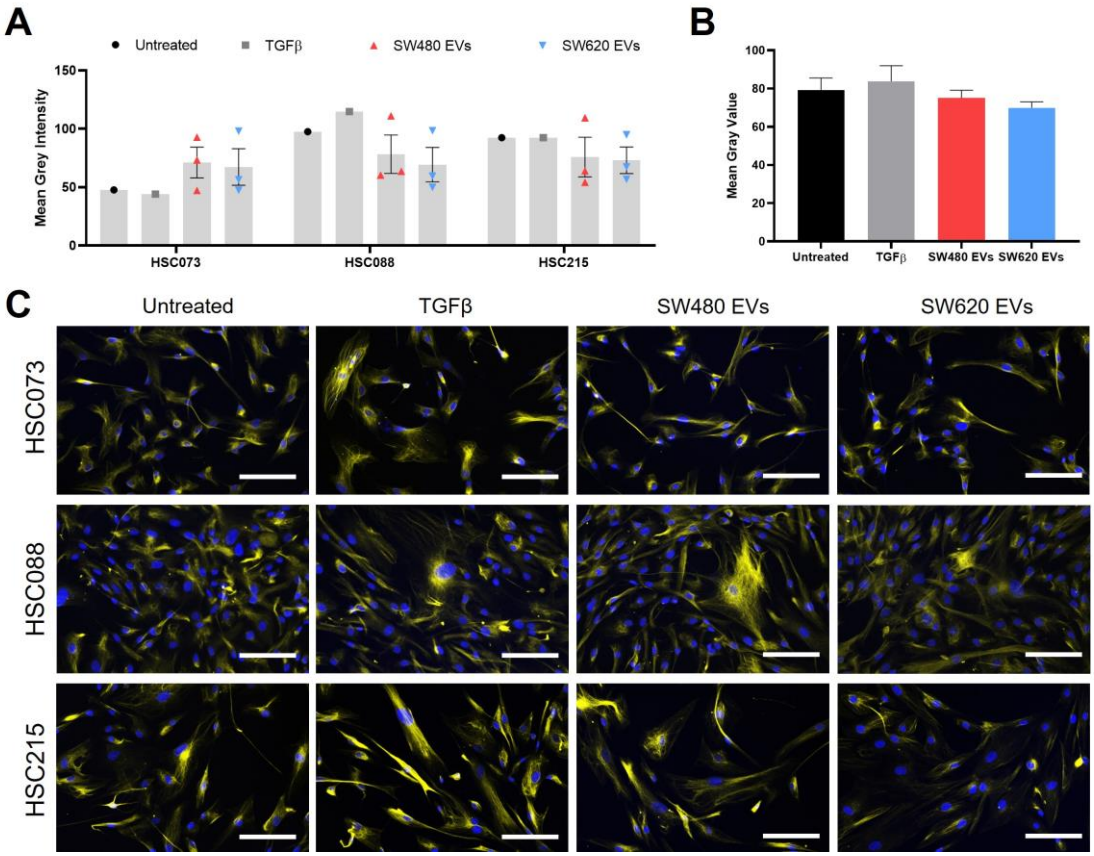


**Figure 4.7. Vimentin expression with IF in HSCs.** (A) Levels of vimentin in the three patient derived HSCs. Mean ± SEM. (B) Summary of the levels of α-SMA expression (mean grey value). Mean ± SEM (n ≥ 3). ANOVA. C) Representative images of α-SMA expression (yellow) with DAPI as counterstaining (blue). Scale bar = 100 µm.

### 4.3.5 CRC EVs mediated TG2 expression in primary hepatic stellate cells

To evaluate whether CRC EVs regulate TG2 in HSCs, in the same way as was found in MRC5 cells, TG2 expression was assessed in HSCs deriving from patients with liver fibrosis. Changes in TG2 expression upon treatment with CRC EVs were dependent on the patient (Figure 4.8A). HSC073 did not show any change in TG2 when treated with TGF-β. Both CRC EVs induced an increase in TG2 expression. HSC088 and HSC215 showed comparable TG2 expression: higher with TGF-β, but lower with SW480 and SW620 EVs. When the HSCs data were combined, no significant changes were found (P > 0.05), although a non-significant increase of TG2 was observed with TGF-β (Figure 4.8B). From the IF

images, high cell density was found in HSC088 compared to the other two cells (Figure 4.8C).

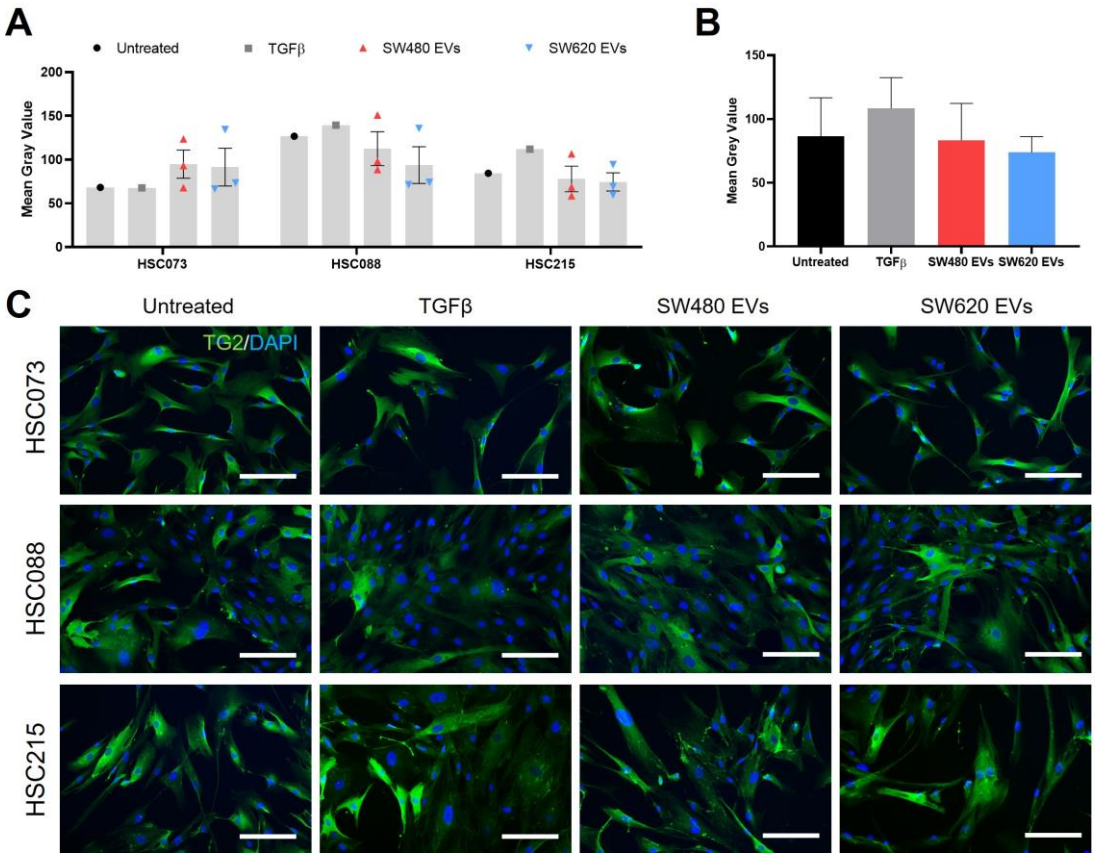


**Figure 4.8. IF TG2 expression in primary HSCs.** (A) Levels of TG2 in the three patient derived HSCs. Mean ± SEM. (B) Summary of the levels of TG2 expression (mean grey value). Median ± 95% CI (n ≥ 3). Kruskal-Wallis. (C) Representative images of TG2 expression (green) with DAPI as counter staining (blue). Scale bar = 100 µm.

As TG2 can also be an ECM protein, TG2 was evaluated in HSC cell-derived matrix. Transglutaminase 2 expression was patient specific when the HSC were treated with TGF-β; HSC073 showed total loss of TG2 expression, whereas a small decrease was found in HSC088 compared to the untreated control (Figure 4.9A); in HSC215 matrix TG2 increased upon TGF-β treatment. CRC EVs decreased the expression of matrix TG2 in all the patient cells, except of a slight increase in HSC073 when treated with SW480 EVs. When the measurements were combined, no statistical significance was found ($P > 0.05$) (Figure 4.9B). However, TG2 expression was globally lower after the CRC EVs treatments compared to the untreated control and TGF-β treatment (Figure 4.9B). To observe whether the CRC EVs induced decrease was present at a gene level, qPCR was performed for the TG2 gene (Figure 4.9D). Surprisingly, only HSC073 were found with a lower TG2 gene expression after EV treatment compared to

untreated control. Both HSC088 and HSC215 showed an increase expression, especially with SW480 EVs. Combined data confirmed a non-significantly increased TG2 expression after treatment with CRC EVs (P > 0.05) (Figure 4.9E).

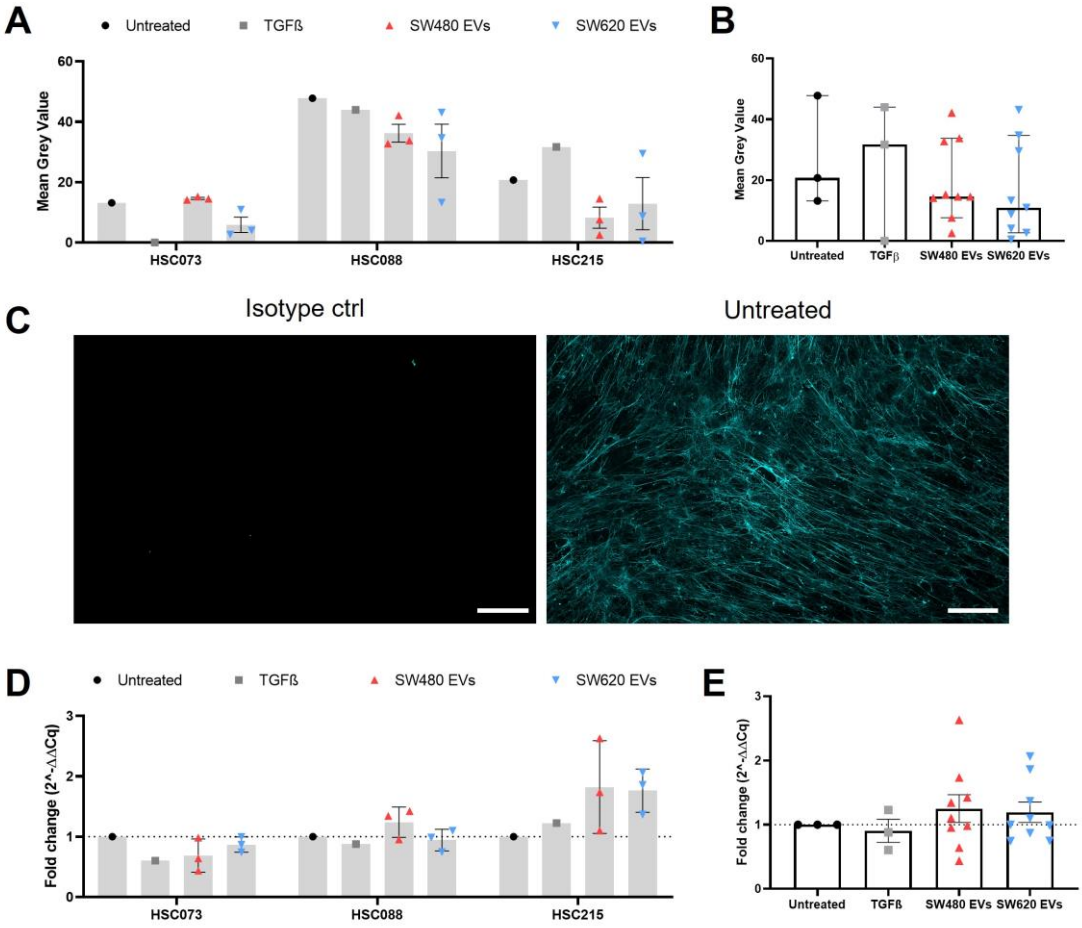


**Figure 4.9. TG2 expression in HSCs decellularised matrix and TG2 gene expression.** (A) Levels of TG2 in decellularised matrix in patients HSCs. Mean ± SEM. (B) Summary of the TG2 levels in decellularised matrix (mean grey value). Median ± 95% CI (n ≥ 3). Kruskal-Wallis. (C) Representative images of isotype control for the staining and TG2 expression in decellularised matrix (blue) (untreated). Scale bar = 100µm. (D) qPCR data of TG2 expression in patients HSCs. ΔΔCq normalisation to housekeeping gene RLP0. Mean ± SEM. (E) Summary of TG2 expression. Mean ± SEM (n ≥ 3). ANOVA.

Fibronectin was increased in all the patients HSCs upon TGF-β treatment, however the increase was not statistically significant (P > 0.05). CRC EVs induced very different results in the three HSC cells and the values also varied within the replicates. This resulted in no significant changes in FN expression overall.

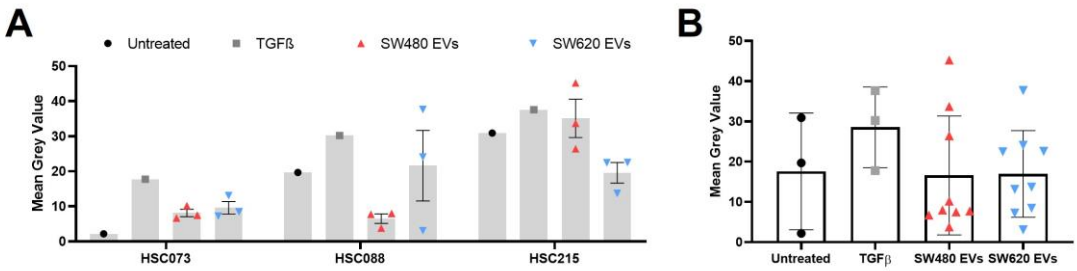


**Figure 4.10. Fibronectin gene expression in liver fibrosis patients HSCs.** (A) qPCR data of COL1 expression in patients HSCs. ΔΔCq normalisation to housekeeping gene RLP0. Mean ± SEM. (B) Summary of FN expression. Mean ± SEM (n ≥ 3). ANOVA.

### 4.3.6 Impact of colorectal cancer EVs on proteins linked to hepatic fibrosis

Collagen expression as a marker of fibrosis was assessed using a pan-collagen antibody in the CDM. The expression of pancollagen was strictly related to the patient origin of the HSC cells. Loss of pancollagen was found in HSC073. The level in HSC088 did not change from the untreated, but they increased in HSC215. As for CRC EVs, pancollagen expression was not affected. No significance was observed when the data was combined. Gene expression of collagen I (COL1), the most abundant collagen in liver ECM (Nyström, 2021), was then evaluated. COL1 was increasingly expressed with TGF-β treatment, although non significantly, as in HSC088 the level was similar to the untreated control (P = 0.4301). SW480 EVs decreased COL1 expression in HSC073, increased it in HSC215, but did not affect its expression in HSC088. SW620 EVs induced and increase in COL1 only in HSC088 and HSC215. The increase was not statistically significant compared to the untreated control when combined (P = 0.8408).

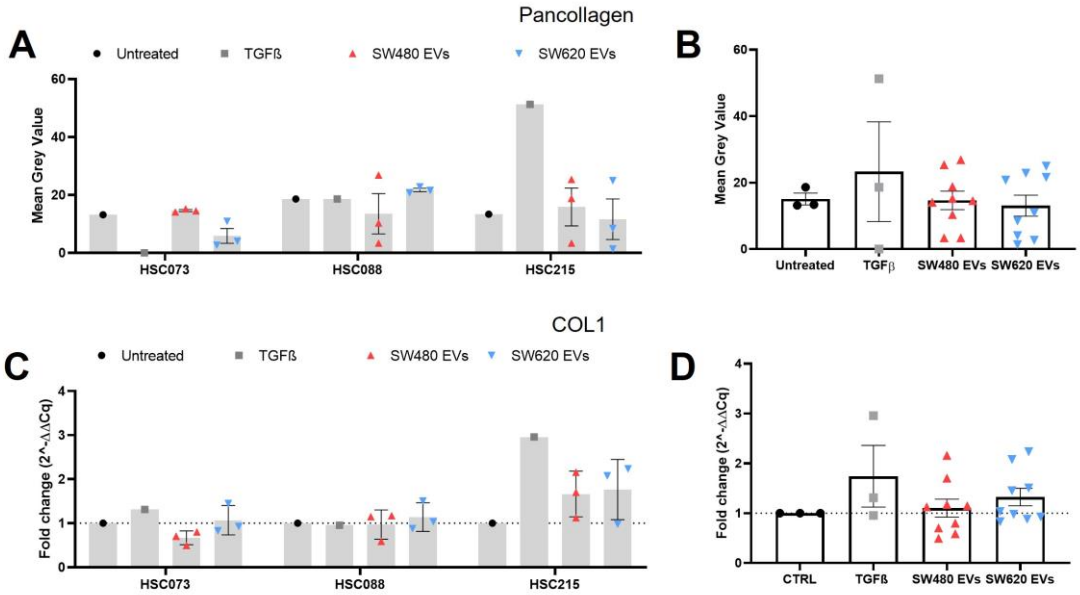


**Figure 4.11. Matrix proteins expression in liver fibrosis patients HSCs decellularised matrix.** (A) Levels of pancollagen in decellularised matrix in patients HSCs. Mean ± SEM. (B) Summary of the pancollagen levels in decellularised matrix (mean grey value). Mean ± SEM (n ≥ 3). ANOVA. (C) Levels of FN in decellularised matrix in patients HSCs. Mean ± SEM. (D) Summary of the pancollagen levels in decellularised matrix (mean grey value). Median ± 95% CI (n ≥ 3). Kruskal-Wallis.

Pro-inflammatory cytokines secreted by the HSCs were also evaluated. IL-6 secretion was higher from HSC215 cells compared to the other two cells. While the levels of IL-6 with TGF-β varied in the three HSCs, the treatment with CRC EVs led to increased IL-6 (Figure 4.12A). For the combined data, fold change was applied due to the differences in intensity (Figure 4.12B). The data were normalised against the untreated controls. Fold change values confirmed the increase of IL-6 upon treatment with SW480 EVs and SW620 EVs, but not statistically significant (P = 0.1829 for SW480 EVs, P = 0.7855 for SW620 EVs). A similar trend was observed for IL-8 (Figure 4.12C). TGF-β induced an increase in IL-8 secretion only in HSC088, decreased in HSC073 and was not affected in HSC215. IL-8 levels were increased by CRC EVs, but not statistically significant (P = 0.2727 for SW480 EVs, P = 0.0858 for SW620 EVs) (Figure 4.12D). MCP-1 was lower with TGF-β for all the HSCs (Figure 4.12E). SW620 EVs induced a slight decrease of monocyte chemoattractant protein-1 (MCP-1) secretion, especially in HSC088. The decrease expression of MCP-1 by TGF-β was statistically significant compared to the untreated control and SW480 EVs treatment (P ≤ 0.05) (Figure 4.12F).

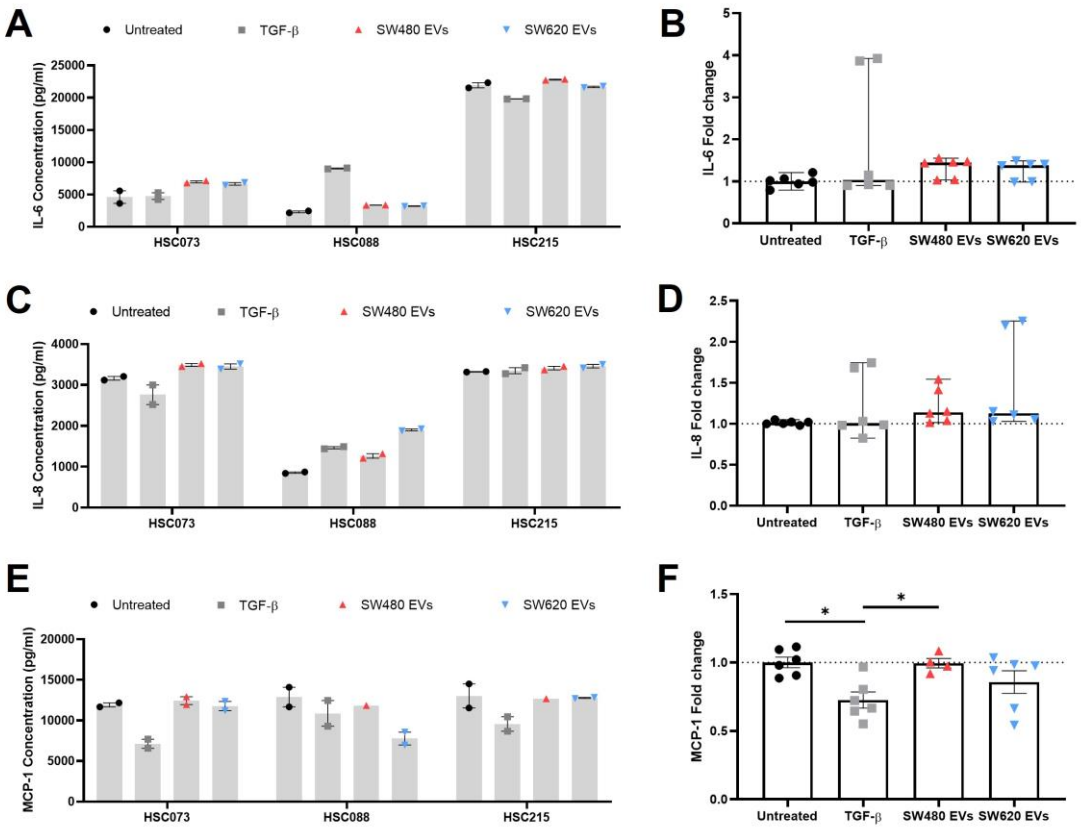


**Figure 4.12. Pro-inflammatory cytokine release by liver fibrosis patients HSCs.** (A) IL-6 secreted by patient HSCs. Mean ± SEM. (B) Fold change values of IL-6. Median ± 95% CI (n = 6). Kruskal-Wallis. (C) IL-8 secreted by patient HSCs. Mean ± SEM. (D) Fold change values of IL-8. Median ± 95% CI (n=6). Kruskal-Wallis. (E) MCP-1 secreted by patient HSCs. Mean ± SEM. (F) Fold change values of MCP-1. Mean ± SEM (n=6). ANOVA, * P ≤ 0.05.

## 4.4 Discussion

In this chapter, the influence of CRC EVs on TG2 and proteins involved in ECM remodelling was investigated and extended to a model of liver CRC metastasis. Due to the multifunctional nature of TG2, it is pivotal to clarify the role of TG2 in the specific mechanisms surrounding CRC progression. The evaluation of TG2 expression in different studies has highlighted the complexity and heterogeneity of its functions; either pro- or anti-tumorigenic (Beninati *et al*., 2017; Tempest *et al*., 2021).

To assess whether the relationship between cancer cells and fibroblasts plays a role in the expression of surface TG2, a SW480/MRC5 co-culture was compared to monocultures of the two cell lines. It was observed that the TG2 linked to MRC5 in co-culture with SW480 CRC cells was lower than MRC5 monoculture. TG2 has been found to be expressed in CAFs of different cancers (Jia *et al*., 2020; Torres *et al*., 2015). However, little is known about CAFs expression of TG2 in relation to cancer cells. Therefore, it was important to further understand whether this decrease was mediated by a specific kind of communication between the cell types, such as EVs. However, when the inhibition of the EV secretion was introduced, the level of TG2 was unaffected in the co-culture. Instead, when MRC5 were treated with soluble proteins derived from SW480 and SW620 cells, this decreased TG2 levels compared to SW480/SW620 EV conditioning.

Surface TG2 is often found in a complex with FN, which is known to promote cell adhesion to ECM and cell invasion in cancers (Mangala *et al*., 2007). When SW480 cells were cultured with MRC5 fibroblasts, TG2 expression in SW480 increased compared to SW480 in monoculture, thus showing a role of CAFs in regulating the expression of cancer related TG2. Interestingly, the dimethyl amiloride (DMA) treatment led to TG2 levels similar to the SW480 in monoculture, thus suggesting a role of MRC5 EVs in the regulation of cancer associated TG2 expression. Further studies on fibroblasts derived EVs are necessary to confirm their involvement.

In a previous study carried out on similar organotypic cultures, the role of TG2 in CRC was dependent on the stage of the cancer, as well as on the TG2 derivation (Cellura *et al*., 2015; Delaine-Smith *et al*., 2019). Here, the impact of SW480/SW620 EVs on the influence of TG2 expression on cancer invasion was

assessed in the *in vitro* model of cancer invasion developed in chapter 2. An important signature found in this previously published research was the strong presence of TG2 on the boundaries between spheroids and ECM, which can result from the accumulation of surface TG2 on cancer cells (Delaine-Smith *et al*., 2019). Recently, the overexpression of TG2 in cancers has also been related to chemoresistance (Zhang *et al*., 2023). Therefore, the confinement created by TG2 around the tumour can be hypothesised to serve this purpose and protect the cell cluster from immunity and anti-cancer agents. The analysis on TG2 expression was limited only to region of interests (ROIs) surrounding the invasive clusters. Presence of TG2 was generally observed in the invasive clusters, despite the border being less defined than in the cancer spheroid model (Delaine-Smith *et al*., 2019). TG2 expression was significantly higher when the model was conditioned with SW620 EVs, which also considerably increased the invasion of cancer cells. This confirmed previous studies that related the presence of high TG2 to cancer progression. In the PBS control, invasive clusters were observed to lose TG2 expression as they were further detaching from the original mass. Upon treatment with CRC EVs, the levels of TG2 expression were similar between close and distant clusters, thus suggesting that TG2 expression might be somewhat induced by the primary mass. The increased TG2 expression mediated by SW620 EVs was found in both single cells and invasive clusters, implying no direct link on TG2 expression on pattern of invasion. However, the expression was lower in single cells treated with SW480 EVs, while in the clusters was high. This might indicate that TG2 induced by SW480 EVs is dependent on the ability of cells to aggregate in clusters.

Preliminary analysis on TG2 cross-linking activity were also performed to evaluate whether there is a direct relationship between the presence of TG2 as a protein and the cross-linking activity on the ECM. Despite being unfinished data (n=2), TG2 activity increased only with SW480 EVs, but not with SW620 EVs. In a previous published study, TG2 cross-linking activity has, in fact, being associated to a decrease in invasive behaviour of SW620 cells (Cellura *et al*., 2015). Since the levels of TG2 activity were not increased, it was concluded that SW620 EVs mediated invasion was not dependent on TG2 activity. On the other hand, it was hypothesised that early-stage CRC advances using a cross-linked and stiffer ECM (Cellura *et al*., 2015; Levental *et al*., 2009).

### 4.4.1 Role of CRC EVs in hepatic stellate cells

Liver fibrosis has been associated with poor prognosis in CRC patients with hepatic metastasis and increased relapse, implying that these strong alterations to ECM have a role in seeding and supporting the establishment of metastasis (Hu *et al*., 2020). In this preliminary experiment, HSCs, the main cells involved in liver fibrosis, were treated with CRC EVs to evaluate their potential contribution to the support of liver fibrosis. Three primary HSCs have been isolated from CRC patients with liver metastasis with different fibrotic stages. Although the cohort of HSC cells was limited, this study was designed to obtain preliminary information on the influence of TG2 and CRC EVs on cells active in fibrosis.

Due to the phenotypical similarity with myofibroblasts, α-SMA is one of the main markers for the activation of HSCs. Initially, presence of α-SMA in the cytoskeleton of HSCs was evaluated to confirm that the HSCs isolated were a good phenotypical model. TGF-β treatment was used as a positive control to observe increased activation of HSCs. TGF-β increased the presence of α-SMA in all the three HSCs, confirming to be a good model for HSC activation. Both treatment with CRC EVs induced an increase of α-SMA in the cells. With SW480 EVs especially, the mean grey values were even higher than the TGF-β treatment. Interestingly, whereas the TGF-β increase is reflected by an increase in the expression of the α-SMA, upon SW480/SW620 EV conditioning the α-SMA transcription was reduced. These results indicate that CRC EVs can activate HSCs, but the mechanism of activation is not gene dependent. Analysis on the specific interactions between HSCs and CRC EV, which might involve specific EV cargo, will help in identifying the mechanism of activation.

Among the proteins linked to the matrix stiffening characterising liver fibrosis, TG2 and its cross-linking activity have been found (Grenard *et al*., 2001; Li *et al*., 2019; Tatsukawa *et al*., 2020). TG2 expression in HSC cells was generally increased in response to TGF-β. It was observed that when the cells were treated with CRC EVs, cellular TG2 expression was lower compared to the untreated control, except for HSC073, which showed an increased cellular TG2 expression with both EVs. With this it was concluded that the phenotype and the derivation of the HSCs might lead to differential need of TG2 as protein in the activation of HSC. To evaluate whether was possible to visualise the presence of extracellular TG2, which is likely linked to cross-linking activity, a staining on decellularized CDM

was optimised and TG2 was expressed in the matrix filaments deposited by HSCs. When its expression was investigated after the conditioning, TG2 was variable, including after TGF-β treatment and in the untreated controls. However, matrix deposition is also strongly dependent on the number of cells and the phenotypic differences of the HSCs need to be considered when studying ECM. For example, although the seeding density was the same for the three cell lines, HSC088 showed a higher proliferation rate compared to the other two cell lines, increasing the number of cells in the plates. A TG2 extracellular deposition dependent on the type of HSCs could also mean that TG2 is involved in fibrotic events, but it is not necessary for the events cascade. This was already observed in a study where it was investigated the role of TG2 cross-linking activity in mouse model (Popov *et al*., 2011). Yet, when the expression of TG2 was evaluated, CRC EVs promoted an increase in HSC088 and HSC215. To confirm these results, a wider study including more replicates and more HSCs needs to be performed. Alongside TG2, FN presence in the CDM was evaluated, as FN has been commonly found associated to extracellular TG2 (Antonyak *et al*., 2011; Stamnaes *et al*., 2016). TGF-β increased FN in all the HSCs and this was already demonstrated, showing the production of FN by activated HSCs in *in vivo* and *in vitro* (Liu *et al*., 2016). Treatment with CRC EVs identified a small loss of FN in general. When the values were observed for each of the HSCs, a similar pattern than cellular TG2 was observed, suggesting that the boundary between them is present even in HSCs.

Deposition of collagen was also investigated. Pancollagen antibody was evaluated on the CDM, to observe changes in the deposition of collagen fibrils and then the expression of collagen type I, the most abundant collagen in the liver was also assessed (Nyström, 2021). CRC EVs did not show any specific pattern in the alteration of collagens, with the only exception being COL1 in HSC215 increased expression. This was not enough to conclude a role of CRC EVs in the deposition of collagen by HSCs.

Finally, pro-inflammatory cytokines were assessed. IL-6 is associated with liver regeneration and not commonly found in HSCs, but increased levels of IL-6 were found in hepatic fibrosis linked to cancer (Schmidt-Arras & Rose-John, 2016). This was confirmed by the levels found in HSCs, where IL-6 was higher only after treatment with CRC EVs and not depending on the increase of TGF-β. IL-8 has

not linked before to HSC, but it is a cytokine commonly produced by CAFs (Thongchot *et al*., 2021; Zhai *et al*., 2019). Similarly to IL-6, CRC EVs slightly increased the secretion of IL-8, thus showing that the pro-inflammatory feature in HSC is specifically driven by cancer. On the other hand, MCP-1 is overexpressed and linked to the recruitment of the inflammatory infiltration in chronic injury, but its expression linked to HSC activation is not clear (Kobayashi *et al*., 2018; Sprenger *et al*., 1999; Xi *et al*., 2021). Interestingly, an unexpected significant decrease in MCP-1 was found when treated with TGF-β. As the chemokine is a recruiter of neutrophils and macrophages, the levels of MCP-1 might not be dependent by HSC activation but by the microenvironment. Further studies in 3D models would be useful to confirm the decrease.

The HSCs analysed originated all by patients found with liver fibrosis as a feature of different pathologies. To an extent, all the three HSCs had a background activation. Comparing these results with normal HSCs can indicate whether CRC EVs effects are more defined and can induce by themselves the activation of HSCs.

## 4.5 Conclusions

TG2 alteration in the CRC TME is the result of crosstalk between cancer cells and fibroblasts. Differential TG2 expression in cancer cells and fibroblasts are linked to different TG2 roles, with reduced TG2 in MRC5 and increased TG2 in SW480. The decrease in MRC5 was not EV mediated but induced by soluble proteins. On the contrary, CRC EVs, in particular SW620 EVs, increased the presence of TG2 in the invasive clusters. CRC EVs contribute to the activation of HSCs in a different way compared to TGF-β dependent activation, but the mechanism of activation needs to be explored. TG2 was not necessary in the activation of HSCs driven by CRC EVs, as it was heterogeneously present both cellularly and extracellularly. Abundance of proteins linked to HSC activation and liver fibrosis were modulated by CRC EVs in a manner dependent on the HSC origin, thus suggesting different sensitivities in different types of hepatic fibrosis.

# 5 Cell responses to EVs as CRC screening biomarkers

## 5.1 Introduction

Cancer is still a challenging disease with high mortality rates and effective treatment strategies. For many types of cancers, including colorectal cancer (CRC), the methodology used for diagnosis is often invasive and time consuming, requiring the presence of a specialised clinician. In CRC for example, colonoscopy is the gold standard diagnostic method, which requires preparation for the patient the day before and the uncomfortable invasive procedure. Combined with the financial burden of the surgical procedure, the patients' compliance is low in undergoing colonoscopy, especially at early stage when the cancer is asymptomatic (Kamel *et al*., 2022). However, the diagnosis of more CRC patients at early stage would greatly improve the prognosis since the survival rate at stage 1 is about 90% and decreases to less than 10% at stage 4 (Keane & Johnson, 2012).

Alongside the development of new therapeutics, non-invasive modalities of screening CRC have helped in reducing the levels of patients' death in the past decades (Bretthauer *et al*., 2022; Doubeni *et al*., 2018). The implementation of screening strategies, such as the faecal occult blood test (FOBT) and faecal immunochemistry test (FIT) has shown to be beneficial in reducing cancer mortality (Gupta, 2022). However, there is a continuous effort in researching new biomarkers for the improvement of the screening methods, as they often lack in sensitivity and specificity. Therefore, the prospect of liquid biopsies, such as blood, urine and saliva, could provide additional advantage of offering non-invasive detection alternatives to the traditional invasive approaches. The long progression of CRC offers a promising window for the development of improved screening biomarkers, from the long time required in the formation of the polyp, to the asymptomatic transition from early to late stage (Gupta, 2022). Furthermore, specific biomarkers can also be used to monitor targeted therapies. Kristen rat sarcoma virus (KRAS) is currently the most reliable marker in CRC and it has been implemented for patients under targeted chemotherapy treatment towards epithelial growth factor (EGFR) (Sepulveda *et al*., 2017). By combining promising biomarkers, it is possible to obtain a highly sensitive, specific screening test, which can also determine known variations of the disease and help in personalised therapy.

### 5.1.1 Extracellular vesicles as cancer biomarkers

As extracellular vesicles (EVs) are found in all biofluids and contain bioactive cargo defined by the donor cell and its environment, they are considered as promising for use in liquid biopsies. In fact, the lipid bilayer characterising EVs confer stability during circulation, making them one of the most interesting approaches to researchers developing new and improved biomarkers (Gupta, 2022; Liu *et al*., 2021; Ogata-Kawata *et al*., 2014).

Once isolated, EVs contain a heterogeneous range of enriched cargo, which can be profiled with omics techniques and introduced in online databases, such as EVpedia (http://evpedia.info/) and ExoCarta (http://www.exocarta.org) (Shiromizu *et al*., 2017; Zheng *et al*., 2020). Within the various biological fluids, circulating EVs do not always maintain the same phenotype, even when deriving from the same cell type. In a study on lung cancer, differences in the proteome contained in the EVs isolated from saliva and EVs isolated from serum were identified (Sun *et al*., 2017). This potential lack of robustness and the heterogeneity of circulating EVs does pose serious limitations, slowing the process of introducing them into clinical workflows for diagnosis. Also, information deriving from EVs is strongly dependent on the method of isolation chosen (Akbar *et al*., 2022; Brennan *et al*., 2020). To investigate cancer EVs components and cargo, the isolation needs to overcome two main steps: the high non-EV protein and lipoprotein content present in the biofluids, which can compromise the purity of the EVs and introduce bias in the analysis; and the isolation of specific cancer EVs from the EVs produced by all the other cells in the body. The yield of cancer-related biomarkers contained in a heterogeneous population of biofluid EVs is generally low and thus hard to determine. This requires sensitive techniques that are generally expensive, but also time consuming, therefore incompatible with clinical procedures and timelines.

These limitations can become less influential if the EV bioactivities, rather than the EV profiling, is considered as biomarker. The wide number of EV functional roles on targeted tumour microenvironment (TME) cells and the extensive research around their functional roles could help in identifying specific cell responses working as cancer biomarkers. For example, it was shown that blood EVs in women affected by breast cancer can induce angiogenesis in human umbilical vein endothelial cells (HUVEC) compared to blood EVs from healthy

women (Garcia-Hernandez *et al*., 2022). However, a singular cell response would not be specific and reliable enough to be implemented as alternative screening techniques, but it would be necessary to consider a panel of cell responses. Due to the enriched and specialised EV cargos, specific EV types generally induce more than one effect in cells, thus providing an interesting new perspective in the research of EV related biomarkers.

## 5.2 Aims

Here, a screening approach based on the evaluation of multiple cellular responses to CRC derived EVs was investigated. In the previous chapter, differences in the bioactivity of cells in *in vitro* 3D models were observed upon treatment with early or late-stage CRC EVS. This study tested the hypothesis that cell responses to CRC derived EVs can determine the stage of the disease. First, SW480 and SW620 EVs were used to treat SW480 cancer cells and MRC5 lung fibroblasts to determine a panel of potential biomarkers, which were then applied *ex vivo* with patients derived EVs. Finally, multivariate analysis was developed to evaluate the strength of the preliminary screening model.

## 5.3 Materials and Methods

### 5.3.1 Experimental design

Cellular responses upon SW480/SW620 EV conditioning were evaluated in MRC5 and SW480 cells, following the previous findings on the 3D models. Cell migration, proliferation and metabolic activity were initially tested and then, cytokine arrays were employed to widen the panel of responses. Plasma was isolated from CRC patients and from healthy control (HC) blood. EVs were then isolated and characterised according to the Minimal Information for studies of EVs (MISEV) guidelines. The selected bioactive markers were then used to perform a blind preliminary study to evaluate plasma EV influence. A multivariate analysis model was then developed using the cell responses as variables.

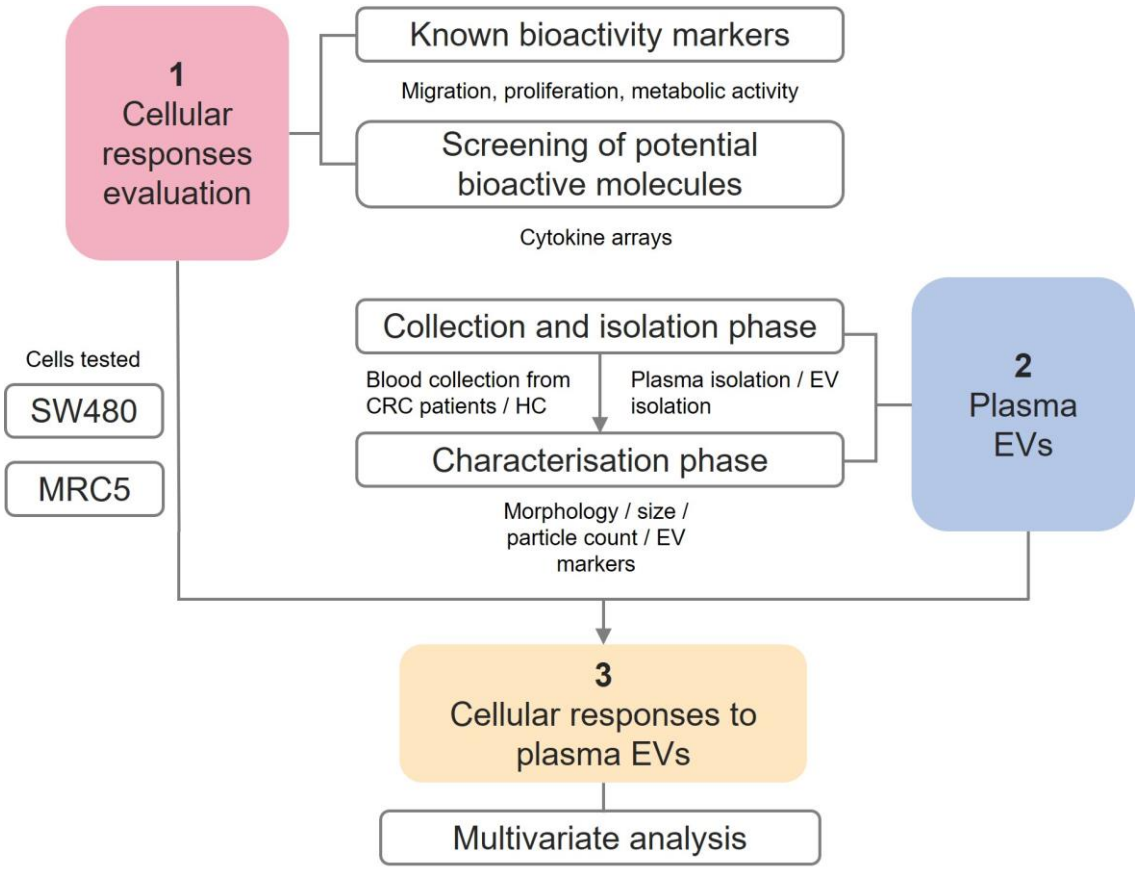


**Figure 5.1. Schematic of Chapter 5 experimental design.**

## 5.3.2 2D Cell culture

General subculturing procedure of cell lines can be found in Section 2.3.2.

## 5.3.3 Conditioning with CRC EVs and CRC soluble proteins

SW480 or SW620 EVs were isolated according to Section 2.3.5.1 and size exclusion chromatography (SEC) fractions 7-9 pooled. SW480 and SW620 SEC fraction 19/20 which showed high content of soluble proteins were also collected.

### *5.3.3.1 Alamar blue assay*

Alamar blue assay was performed to evaluate the metabolic activity of the cells after the treatment with CRC EVs. SW480 or MRC5 cells (20,000 cells/well) were cultured in a 96 well plate and left growing until 50% confluent. Then, cells were treated with 50 µg/ml of SW480 or SW620 EVs, SW480 or SW620 soluble proteins (SEC fraction 19/20) in DMEM with 10% EV-depleted serum for 48 hours. A control condition (PBS) was also created for each experimental replicate. Supernatant was collected from the wells at the end of the experiment and stored at -80°C for further assays. Resazurin sodium salt was resuspended in EV-dep media to reach a concentration of 0.03 mg/ml to replace the conditioning media of the cultures and left for 4 hours. Finally, absorbance readings were taken with excitation wavelength (λex) at 530-560 nm and emission wavelength (λem) at 590 nm using Clariostar (BMG Labtech, UK).

### *5.3.3.2 Scratch assay*

Scratch assay was performed to investigate the rate of migration of SW480 and MRC5 cells after the treatment with CRC EVs. SW480 or MRC5 cells (500000 cells/well) were cultured in a 24 well plate and left growing until 100% confluent. Then, a pipette tip was used to obtain a vertical scratch in the middle of the culture of about 1 mm. After three PBS washes to remove the detached cells, adherent cells were treated with 50 µg/ml of SW480 EVs or SW620 EVs, SW480 or SW620 proteins in DMEM with 10% EV-depleted serum. A control condition (PBS) was also created for each experimental replicate. Brightfield images were acquired with Cytation™ 5 Cell Imaging Multi-Mode Reader (BioTek, UK) at 0, 8, 24 and 36 hours of culture. Supernatant was collected from the wells at the end of the experiment and stored at -80°C for further assays. Images of the scratch time points were analysed with ImageJ 5.1i. Ten measurements of the distance in the

scratch gap were taken at each time point and the difference was calculated to evaluate the migration length of the cells.

### 5.3.4 Propidium Iodide staining

Propidium iodide staining, a fluorescent dye which labels dead cells (ex 535/em 615nm), was performed on SW480 and MRC5 cells to evaluate the changes in cell death after the treatment with CRC EVs. Media of SW480 cells in 96 well plates was replaced after the Alamar blue assay and cells left for a further day to expand in normal growing media condition (Section 2.3.2) to let the cells re-equilibrate. Then, 10 µl of propidium iodide solution (10% in PBS) was added to each well and incubated at 37°C for 30 min. Texas Red (λex = 596, λem = 615) fluorescent images were acquired with Cytation™ 5 Cell Imaging Multi-Mode Reader and count of red foci (death cells) was performed with ImageJ.

### 5.3.5 Glucose metabolism pathway

Supernatant from SW480 cells was used to evaluate the glucose uptake by the cells after the treatment with CRC EVs. Glucose consumption in the conditioned supernatant (Section 5.3.3.1) was assessed through glucose oxidase assay (Gox). Briefly, glucose oxidase reagent was prepared by adding 1mg/ml of 2,2'-azino-bis (3-ethylbenz-thiazoline-6-sulfonic acid) disodium salt (ABTS), 1000 ul/mg of Peroxidase Type VI-A and 40.3 u/mg of Glucose oxidase Type II-S into a 0.1 M phosphate buffer solution (pH 7). A standard curve of glucose (0 µM–100 µM) was generated and 50 µl of each standard or sample was added into a 96 well-plate. Glucose oxidase reagent was added to the solution and colorimetric optical density (OD) was taken at 570 nm.

Lactic acid production was measured through L-Lactic Acid (L-Lactate) assay kit (Megazyme, UK) as per the manufacturer's instructions. Briefly, a standard curve was prepared with L-lactic acid (0-15 µg/ml). Standards and samples were mixed with solution buffer (pH 10.0) plus D-glutamate and sodium azide (0.02% w/v), Nicotinamide adenine dinucleotide+/Polyvinylpyrrolidone (NAD+/PVP) and D-glutamic pyruvic transaminase (D-GPT). Then, L-lactate dehydrogenase (L-LDH) was introduced and incubated for 10 min before the OD was taken at 340 nm.

### 5.3.6 Cytokine arrays

Cytokine arrays were employed for the discovery of differential expression of cytokines upon EV treatment. Human cytokine arrays (ab133998 and ab169815,

Abcam, UK) were performed according to the manufacturer's protocol, 80 targets were tested for MRC5 and 51 targets for SW480. Membranes were initially blocked with blocking buffer at RT for 30 min. The buffer was replaced by 1 ml of supernatant from scratch assay (PBS control and SW620 EVs treatment) and left at 4°C overnight. For each incubation step, 6 washes (5 min each, RT) were performed with two different washing buffers. After the sample incubation, a large volume wash was also performed to remove the excess (45 min). The membranes were incubated overnight at 4°C with biotin-conjugated anti-cytokines. Then, washing steps were performed and HRP-Conjugated Streptavidin added to the membrane for 2 hours at RT. To detect the signals, detection buffers were mixed 1:1 and added to the membrane for 2 min before chemiluminescent images were obtained with LI-COR OdysseyFc. Imager (LI-COR Biosciences, USA). Semi-quantitative densitometry analysis was performed with Image Studio Lite (LI-COR Biosciences, USA).

To choose relevant cytokines for further analysis, density values and fold change compared to the PBS treatment were considered. Only cytokines with density values over 0.01 were further considered. Fold changes with opposing results between the biological replicates were discarded (Supplementary 7.1).

### 5.3.7 Cytokine Release (ELISA)

An assessment was made of eight cytokines (IL-6, IL-8, MCP-1, TIMP-1, TIMP-2, GDF-15, VEGF-165 and Nidogen-1) using a sandwich ELISA. All the ELISAs assays were performed according to manufacturer's instructions of commercially available kits (PeproTech EC Ltd., UK; Bio-Techne, UK). Capture antibody, detection antibody and Streptavidin-HRP concentrations, alongside the supernatant dilutions are reported in Table 5.1. ELISA assay antibody concentrations and standard curve ranges. For VEGF-165, concentrations were approximately calculated as information was not provided by the supplier. Nunc 96 well MaxSorp™ ELISA plates (Thermofisher, UK) were coated with 50 µl/well of capture antibody and incubated overnight at RT. Between every incubation step, plates were washed four times with 200 µl/well of washing buffer (0.05% Tween-20 in PBS) and blotted on clean paper towel to remove all the buffer. The following morning the plates were incubated with 200 µl/well of block buffer (1% BSA in PBS) for 1 hr at RT. Then, the plates were incubated with 50 µl/well of samples/standards overnight at 4°C. Dilution antibody (50 µl/well) was incubated

for 2 hours at RT, followed by 30 min RT incubation with 50 µl/well of Streptavidin. The final incubation step was performed with 50 µl/well of TMB substrate (Fisher Scientifics, UK). Without washing the plates, the reaction was stopped by adding 50 µl/well of 1M HCl. Ultimately, the optical density of the reaction was analysed with Clariostar plate reader at 450 nm wavelength, with correction set as 620 nm wavelength.

**Table 5.1. ELISA assay antibody concentrations and standard curve ranges.** For VEGF-165, concentrations were approximately calculated as information was not provided by the supplier.

| Cytokine | Capture antibody (µg/ml) | Detection antibody (µg/ml) | Standard curve (pg/ml) |
|---|---|---|---|
| IL-6 900-T16 (Peprotech, UK) | 0.5 | 0.125 | 7.81-2000 |
| IL-8 900-T18 (Peprotech, UK) | 0.125 | 0.25 | 0.78-200 |
| MCP-1 DY279 (Bio-Techne, UK) | 1 | 0.025 | 15.6-1000 |
| TIMP-1 DY970 (Bio-Techne, UK) | 2 | 0.05 | 31.2-2000 |
| TIMP-2 DY971 (Bio-Techne, UK) | 2 | 0.0125 | 31.2-2000 |
| GDF-15 DY957 (Bio-Techne, UK) | 2 | 0.0125 | 7.81-500 |
| VEGF-165(A) 900-T10 (Peprotech, UK) | ≈ 0.1 | ≈ 0.1 | 3.125-800 |
| Nidogen-1 RK07569 (Universal biologicals, UK) | Provided by the manufacturer | | 0.075-10000 |

## 5.3.8 Plasma EV isolation

Blood from CRC patients was collected after written informed consent following ethical approval (REC reference: 19/NI/0221, Supplementary 7.3) from the Department of General Surgery, Sheffield Teaching Hospitals. Similarly, HC blood from donors working at Sheffield Hallam University was collected after written informed consent following the same ethics approval (Table 5.2). Blood was collected in EDTA vacutainers (Fisher Scientific, UK) which have been reported as the optimal for plasma derived EV stability (Buntsma *et al*., 2022). Within three hours from collection, the blood was centrifuged at 1,000 g for 10 min to obtain whole plasma. The plasma was diluted 1:1 and centrifuged at 1,500

g for 15 min. Again, supernatant was centrifuged at 2,500 g for 15 min before storing it at -80°C. EVs were isolated within 6 months of storage. Once defrosted, 0.5 ml of plasma was centrifuged to remove the lipoproteins at 10,000 g for 30 min and then applied to SEC columns as previously described (Section 2.3.5.2).

## 5.3.9 Blood EVs characterisation

### *5.3.9.1 Protein quantification with BCA assay*

Protein quantification assay was performed on fractions 1-20 using BCA assay as previously described (Section 2.3.5.3).

### *5.3.9.2 Transmission electron microscopy*

Transmission electron microscopy images to evaluate the EVs morphology, structure and size were obtained following the protocol described in Section 2.3.5.4.

### *5.3.9.3 DELFIA© for tetraspanins EV markers*

To confirm tetraspanins expression, blood EVs were tested for CD9 (ab2215 mouse monoclonal [MEM-6]; Abcam, UK; 1:5000 dilution), CD63 (MCA2142 mouse monoclonal [MEM-259]; Bio-Rad Ltd, UK; 1:5000 dilution) and CD81 (MCA1847 mouse monoclonal [1D6]; Bio-Rad Ltd, UK; 1:5000 dilution) with dissociation-enhanced lanthanide fluorescence immunoassay (DELFIA©). The technique exploits time-resolved fluorescence allowing higher sensitivity and stability. Then, 100 µl EV fractions (5-12) were incubated overnight at 4°C into Nunc 96 well MaxSorp™ ELISA plates. Between every incubation step, plates were washed four times with 200 µl/well of washing buffer (10 mM Tris-HCl, 0.05% v/v Tween-20, 130 mM NaCl) and blotted on a clean paper towel to remove all the buffer. Blocking of non-specific sites was performed by adding 300 µl per well of 1% w/v BSA in PBS for 2 hours at RT. Primary antibody (100 µl) for CD9, CD63 and CD81 (0.1% w/v BSA in PBS) was incubated overnight at 4°C. The plate was then incubated with 100 µl/well of biotinylated anti-mouse IgG secondary antibody (1:2500, Perkin-Elmer Life Sciences, UK) in 0.1% w/v BSA in PBS for 1 hour at RT onto a plate shaker. Eu-N1 streptavidin conjugate (Perkin-Elmer Life Sciences, UK) was diluted (1:1000) in assay buffer (50 mM Tris-HCl, 0.9% v/w NaCl, 0.2% v/w BCA, 0.1% v/v Tween-20, 20 µM pentetic acid) and 100 µl added to the wells for 45 min at RT on a plate shaker. The plate was washed six times in wash buffer before the last incubation in DELFIA© enhancement

solution (Perkin-Elmer Life Sciences, UK) for 5 min at RT on a plate shaker. Time-resolved fluorescence was measured with Europium protocol (ex/em 320/615 nm) with Wallac Victor2™ 1420 multilabel counter.

#### *5.3.9.4 Particle size, count and tetraspanin markers with NanoFCM*

Pooled EV fractions deriving from CRC patients and HCs were analysed with using a Nanoanalyzer instrument by NanoFCM Co., as previously described in Section 2.3.5.7

### 5.3.10 Statistical analysis

Statistical analysis was performed using Prism 8.1.1 software. First, data were tested for normality (gaussian distribution) with two modalities: D'Agostino & Pearson test (for data with n > 3) and Shapiro-Wilk test (for data with n ≤ 3).

As the groups tested (CRC EV, soluble proteins and blood EV treatments) were ≥ 3, multiple comparison tests were employed for all the dataset of this chapter. Multiple comparison through ordinary one-way ANOVA (ANOVA) with Tukey's test as post-hoc analysis was performed for parametric data, while Kruskal-Wallis (KW) test with Dunn's test as post-hoc analysis was performed for non-parametric data. P-values less than 0.05 were considered significant.

Data representation varied according to the number of replicates and the normal distribution. For data with n ≤ 6, individual values were shown. When data were shown as summary, mean ± SEM was used for parametric data, whereas media ± 95% CI was used for non-parametric data.

#### *5.3.10.1 Multivariate analysis*

Multivariate analysis from the cell responses assays tested on SW480 and MRC5 cells after blood EV conditioning was performed with SIMCA® 16 Multivariate Analysis software (Sartorius, UK). Results from the cell response assays tested with plasma EVs were formatted and imported in the software. No pre-processing normalisation was operated. Unsupervised partial component analysis (PCA) and supervised PLS-DA were performed, with variable considered < 3. From the partial least squares discriminant analysis (PLS-DA), variable important projections (VIP) score was obtained with a confidence level of 95%.

## 5.4 Results

### 5.4.1 Comparison between SW480 EVs and SW620 EVs effects on cellular activity

#### *5.4.1.1 SW480 cells responses to treatment with CRC EVs*

To establish potential bioactivity markers, migration, cell viability, and metabolic activity of SW480 cells were evaluated after treatment with SW480 and SW620 EVs for 48 hours. Cancer cell viability was not affected by the treatment with CRC EVs as indicated by the Alamar blue assay (Figure 5.2A). However, a small non statistically significant increase in cell death from the PI staining was found when the cells were treated with SW620 EVs ($P = 0.5074$) (Figure 5.2B). CRC EVs did not affect the glucose uptake of the cells, whereas SW620 EVs significantly decreased the SW480 production of lactic acid ($P \leq 0.05$) (Figure 5.2C, D). VEGF-165 (VEGF-A) was also tested. VEGF levels were significantly increased with the CRC EVs treatments compared to the control ($P \leq 0.05$), with SW620 EVs significantly higher compared to SW480 EVs ($P \leq 0.01$) (Figure 5.2E).

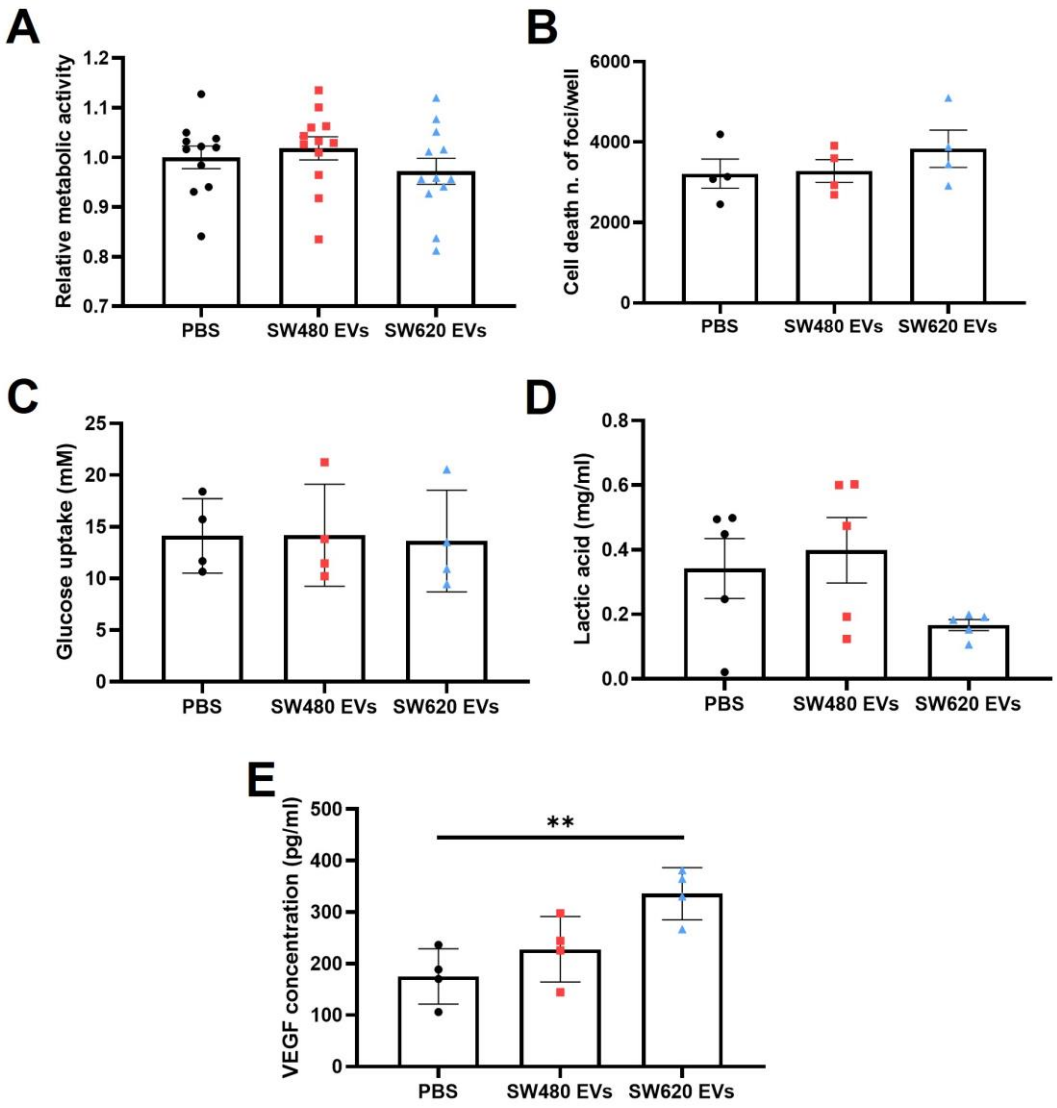


**Figure 5.2. Metabolic assays on SW480 after treatment with CRC EVs.** (A) SW480 proliferation with Alamar blue assay. Data were normalised to the PBS group; Mean ± SEM (n > 3). ANOVA. (B) SW480 cell death with PI staining; Mean ± SEM, (n = 4). ANOVA. (C) SW480 glucose uptake; Mean ± SEM (n = 4). ANOVA. (D) SW480 production of lactic acid; Mean ± SEM (n > 3). ANOVA. (E) VEGF-A expression in SW480. Mean ± SEM (n=3). ANOVA, ** P ≤ 0.01.

Cell migration was next assessed by scratch assay at four time points: 0, 8, 24 and 36 hours. Length measurements were taken from the border of cells still adhering, as the single cell migration was undistinguishable from cells detaching or cell death. Interestingly, while no differences were observed in the first 8 hours, at 24 hours (P = 0.0599) and 36 hours both CRC EVs induced a decrease in the migration of SW480 cells (Figure 5.3B), which was statistically significant at 36 hours (Figure 5.3C). The effect was higher with SW620 EVs (P ≤ 0.01) compared to SW480 EVs (P ≤ 0.05).

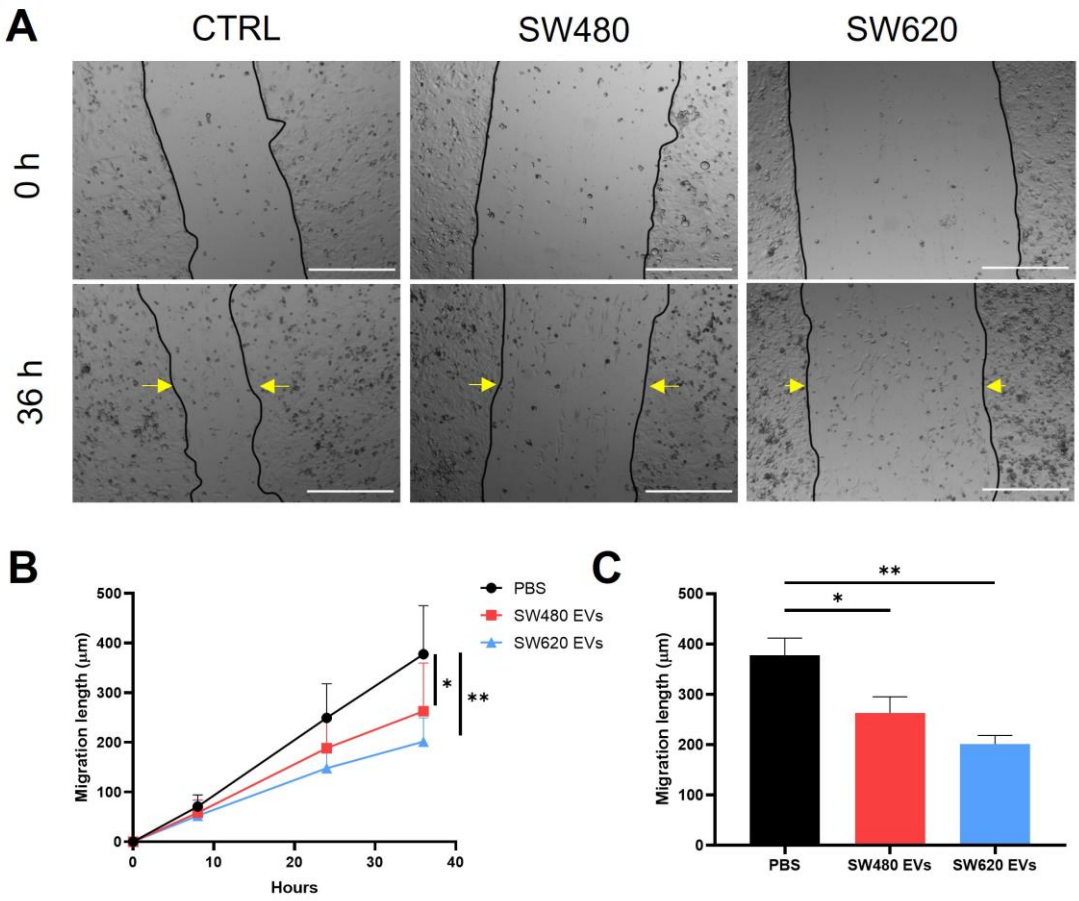


**Figure 5.3. Scratch Assay on SW480 after treatment with CRC EVs.** (A) Representative images of scratch wound assay on SW480 cells. Black lines indicate the perimeter of the wound area. Scale bar = 500 µm. (B) Summary graph of scratch wound assay showing wound healing ability of SW480 cells. Data were normalised to T0 (0 hour). (C) Scratch length at 36 hours timepoint; Mean ± SEM (n = 5). ANOVA, * P ≤ 0.05, ** P ≤ 0.01.

To expand the panel of potential measures that could show responses to CRC EVs, supernatants from the control and the treatment with SW620 EVs were tested with a cytokine array of 51 targets (including proteolytic enzymes) and the full list of non-significant results can be found in Supplementary 7.1. Signal intensity and fold change between the control and the treatment were considered for the selection of the most differentially expressed markers (Figure 5.4). Five cytokines (GDF-15, PAI-I, Ferritin, N-CAM1 and Nidogen-1) reached a normalised densitometry value of 0.05 (Figure 5.4B). Differences between control and SW620 EVs treatment were considerably higher (over 0.5 fold change) for 6 cytokines: GDF-15, MMP-2, NCAM-1, Nidogen-1, RANK and VEGF-C (Figure 5.4C).

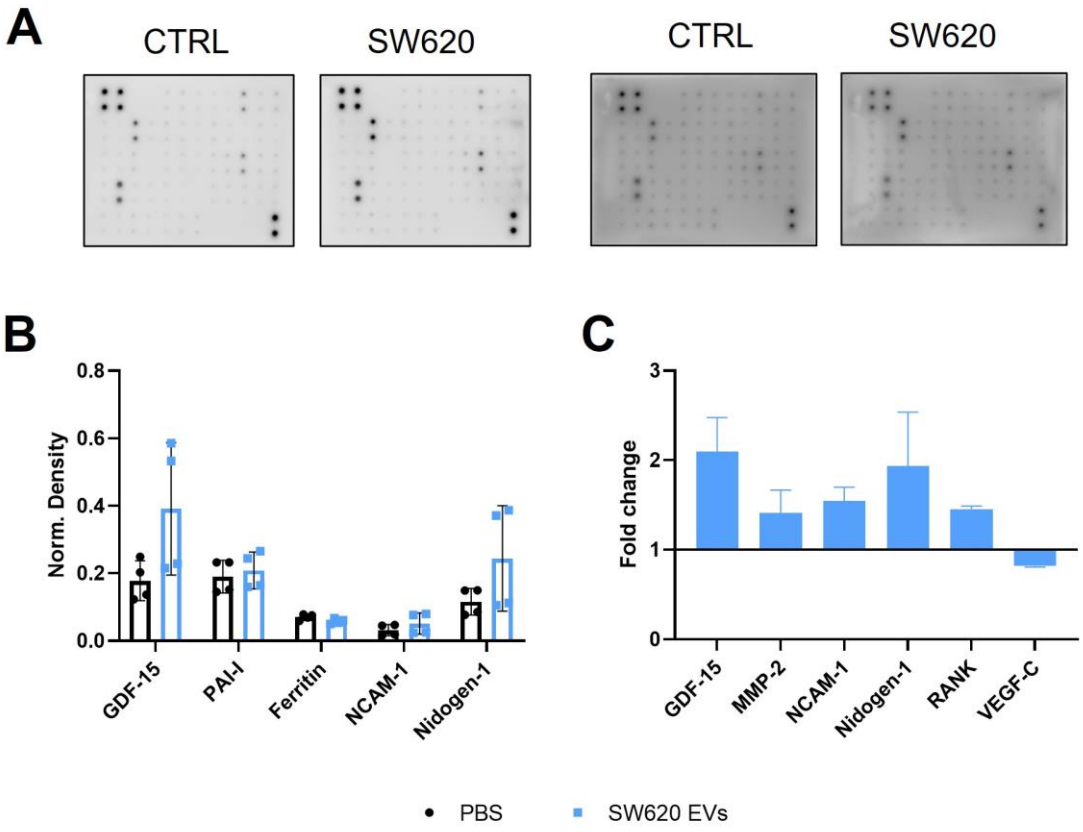


**Figure 5.4. SW620 EVs effects on SW480 cytokine expression.** (A) Representative chemiluminescent acquisition of the cytokine array membranes. (B) Cytokines found with the highest signal. Densitometry data normalised to the control membrane (n=2). (C) Cytokines found with the greatest differences between the control and the treatment with SW620 EVs (n=2).

#### *5.4.1.2 MRC5 cell response to treatment with CRC EVs*

Similarly, cell viability, cell death and migration of MRC5 were tested. Alongside, secretion of pro-inflammatory cytokines IL-6 and IL-8 was investigated as they have previously been associated to the activation of CAFs (Zhai *et al*., 2019; Zhong *et al*., 2021). MRC5 treated with both CRC EVs showed a statistically significant increase ($P \leq 0.001$ SW480 EVs, $P \leq 0{,}0001$ SW620 EVs) in metabolic activity compared to the control, together with a decrease of cell death (n = 2) (Figure 5.5A, B). IL-6 was upregulated when the cells were treated with SW620 EVs compared to the control ($P = 0.2382$) and SW480 EVs ($P = 0.3972$), but the increase was not statistically significant. SW480 EVs treatment also resulted in a small increase in secretion of IL-6 (not statistically significant, $P = 0.9204$) (Figure 5.5C). Similarly, IL-8 levels were higher in cells treated with SW480 EVs ($P = 0.8331$), but even more with the SW620 EVs conditioning ($P = 0.3447$), despite no statistical significance was observed (Figure 5.5D).

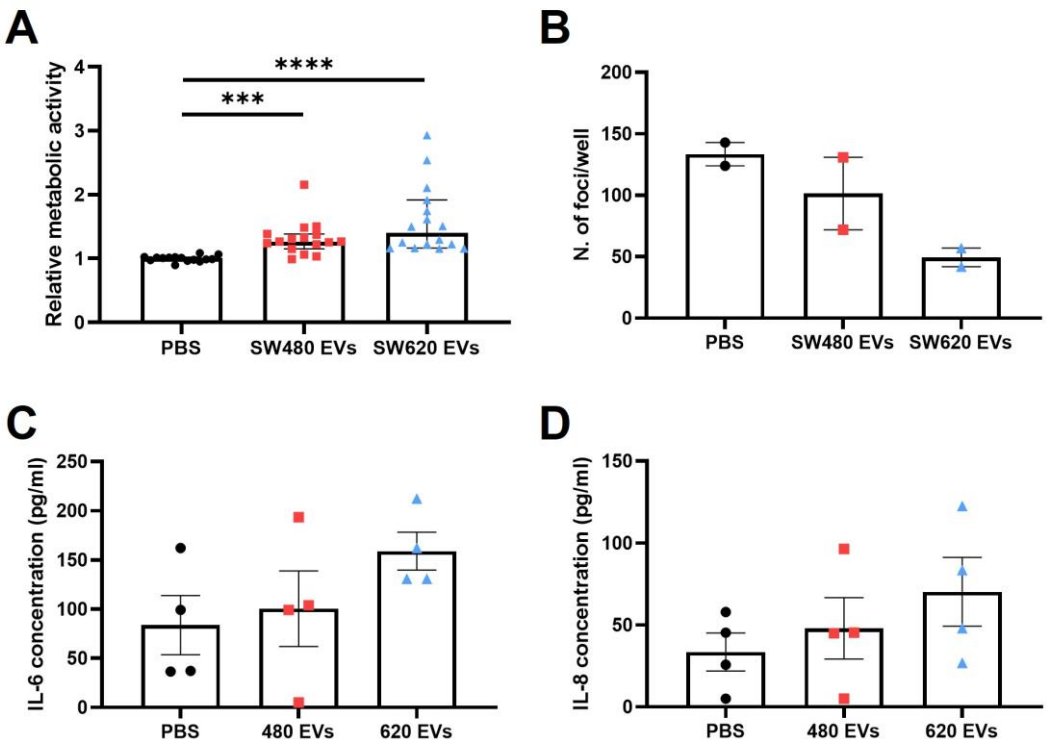


**Figure 5.5. Metabolic assay and cytokine release of MRC after treatment with CRC EVs.** (A) MRC5 cells metabolic activity with Alamar blue assay. Data were normalised to the control; Median with 95% CI (n = 5); Kruskal-Wallis, *** P ≤ 0.001, **** P ≤ 0.0001. (B) SW480 cell death with PI staining. Mean ± SEM, (n = 2). (C) IL-6 concentration; Mean ± SEM (n = 4). ANOVA. (D) IL-8 concentration; Mean ± SEM, n = 4. ANOVA.

Both SW480 and SW620 EVs increased MRC5 migratory ability, but the increases were not statistically significant (Figure 5.6B). When the scratch was analysed at 36 hours, a higher effect was linked to the SW620 EVs (P = 0.0707) compared to SW480 EVs (P = 0.3577) (Figure 5.6C).

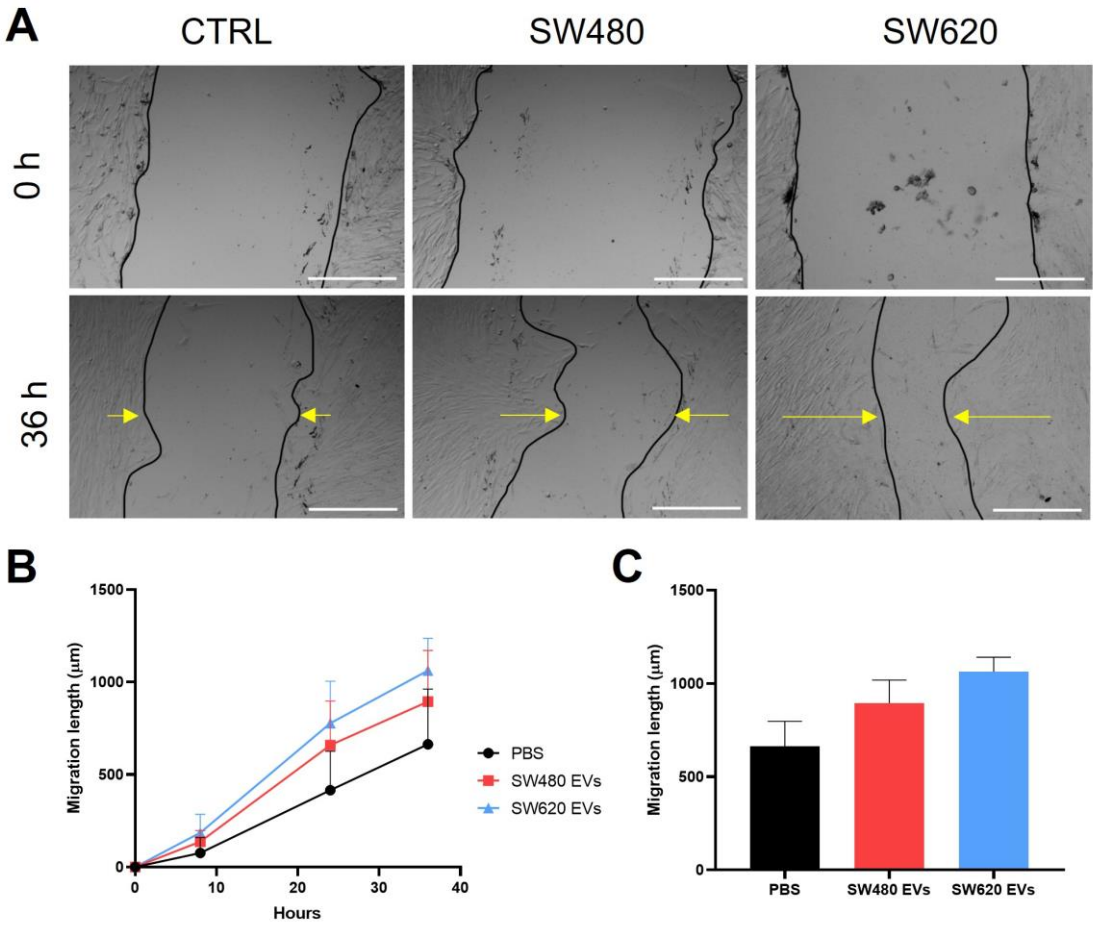


**Figure 5.6. Scratch Assay on MRC5 after treatment with CRC EVs.** (A) Representative images of scratch wound assay on MRC5 cells. Black lines indicate the perimeter of the wound area. Scale bar = 500 µm. (B) Summary graph of scratch wound assay showing wound healing ability of SW480 cells. Data were normalised to T0 (0 hour), n = 5. (C) Scratch length at 36 hours timepoint. Mean ± SEM (n = 5); ANOVA.

A cytokine array containing 80 immune related cytokines was performed to obtain a wide panel of MRC5 cell responses to CRC EVs. The arrays were once again limited to the comparison between the control and the treatment with SW620 EVs. Seven cytokines were found to be highly expressed by MRC5: IL-6, IL-8, MCP-1, HGF, TIMP-1, TIMP-2 and Osteoprotegerin (Figure 5.7B). When the difference between control and treatment was considered, 9 cytokines (IL-6, MCP-1, BDNF, TIMP-1, osteopontin, osteoprotegerin, TGF-β3 and PARC) were found to have fold change between the biological replicates (Figure 5.7C).

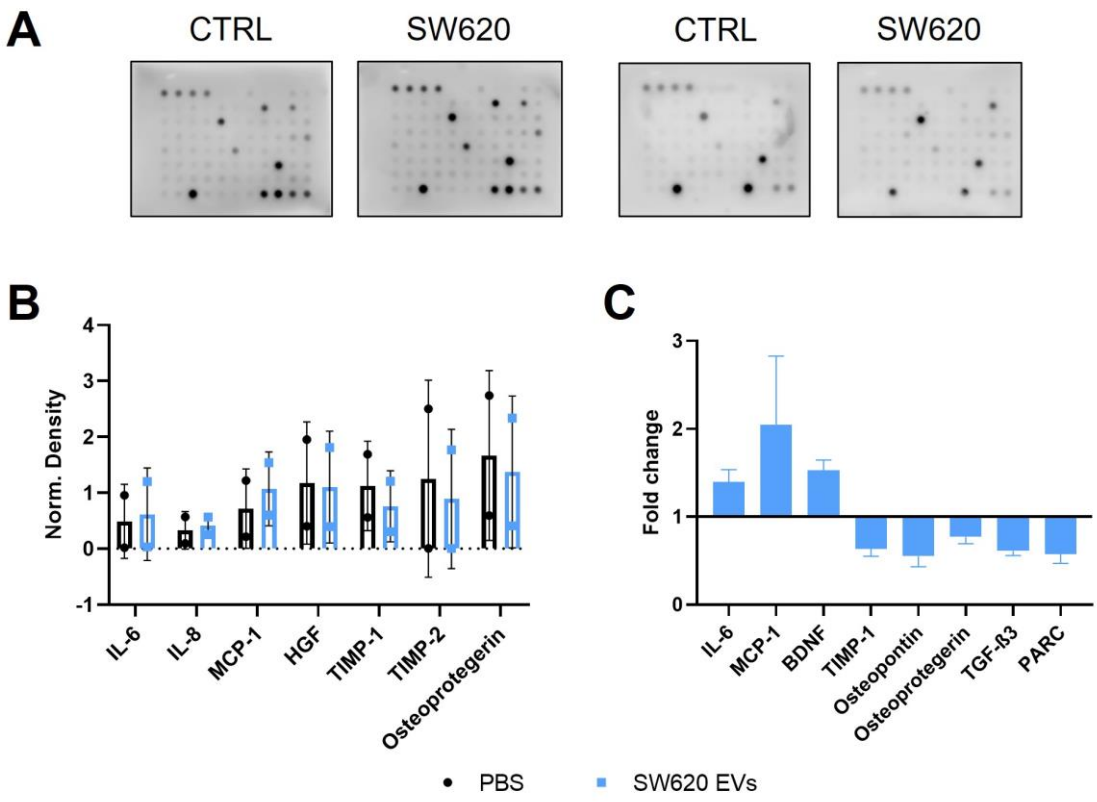


**Figure 5.7. Cytokine array on MRC5 supernatant.** (A) Representative chemiluminescent acquisition of the cytokine array membranes. (B) Cytokines found with the highest signal. Densitometry data normalised to the control membrane (n=2). (C) Cytokines found with the greatest differences between the control and the treatment with SW620 EVs (n=2).

#### *5.4.1.3 Comparison between the effect of CRC EVs and CRC soluble proteins*

To assess whether the changes observed in the cellular responses were specific to the EVs, the treatments with CRC EVs were compared to the effects of soluble proteins derived from the size exclusion chromatography in the two main assays used previously, Alamar blue and scratch assay. A statistically significant decrease in metabolic activity of SW480 ($P \leq 0.05$) was induced by SW620 derived proteins, whereas no changes were observed in MRC5 activity with SW620 proteins compared to the control (Figure 5.8A, B). On the other hand, a statistically significant increase in metabolic activity of MRC5 with SW480, SW620 EVs ($P \leq 0.0001$) and with SW480 proteins ($P \leq 0.05$) was found. A decrease in migratory activity of cancer cells was statistically significant only upon treatment with SW480 ($P \leq 0.05$) and SW620 EVs ($P \leq 0.01$) (Figure 5.8C). On the contrary, increased migration was significant only in fibroblasts treated with SW620 proteins ($P \leq 0.05$) (Figure 5.8D).

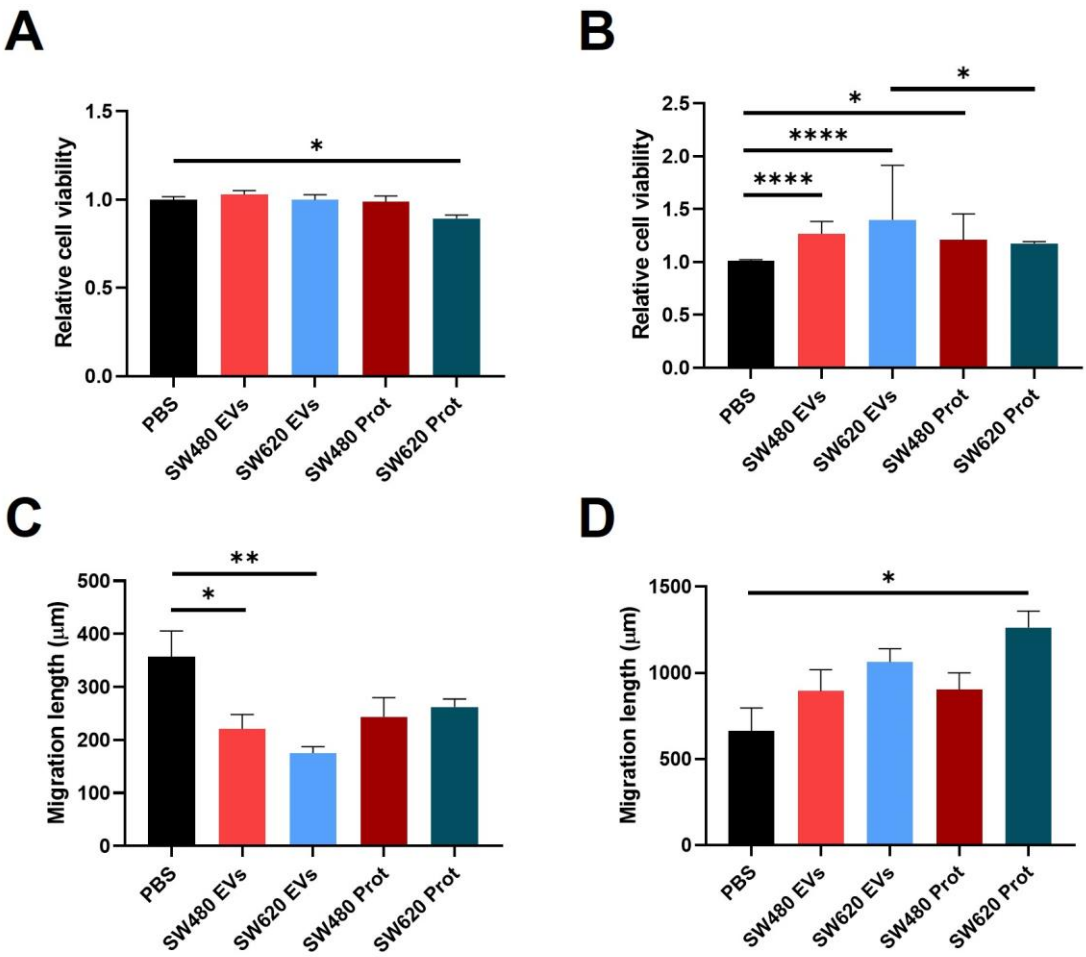


**Figure 5.8. Comparison between the effects of CRC EVs and CRC soluble proteins on cell activities.** Data were normalised to the PBS control for Alamar blue, for T0 (0 hour) for Scratch. (A) Alamar blue on SW480. Mean ± SEM (n > 3). ANOVA * P ≤ 0.05. (B) Alamar blue on MRC5. Median with 95% CI (n > 3). Kruskal-Wallis * P ≤ 0.05, **** P ≤ 0.0001. (C) Scratch assay on SW480. Data were normalised to T0 (0 hour); Mean ± SEM (n > 3). ANOVA * P ≤ 0.05, ** P ≤ 0.01 (D) Scratch assay on MRC5. Mean ± SEM (n > 3). ANOVA * P ≤ 0.05.

## 5.4.2 Characterisation of plasma EVs

Preliminary analysis on cells treated with EVs deriving from 3 CRC patients and 3 HC plasma suggested changes in cellular responses (data not shown). Blood EVs were characterised before comparing their effects with cell lines EVs. BCA assay did not detect proteins from fraction 0 to 8 and showed low abundance of proteins from fractions 8 to 10 (Figure 5.9A). High concentrations of proteins were however observed from fraction 11 to 20 (Figure 5.9A). NanoFCM analysis for CD9, CD63 and CD81 for the pooled fractions previously used (7-9) revealed low percentages of the three markers, with only CD9 occasionally reaching 1% (Figure 5.9B). To confirm the presence of EVs in the fractions, CD9, CD63 and CD81 markers were investigated in fractions 5-12 with DELFIA immunoassay.

The markers were highly expressed by fractions 8, 9, 10, 11 and 12, but absent or low from fractions 5 to 7 (Figure 5.9C).

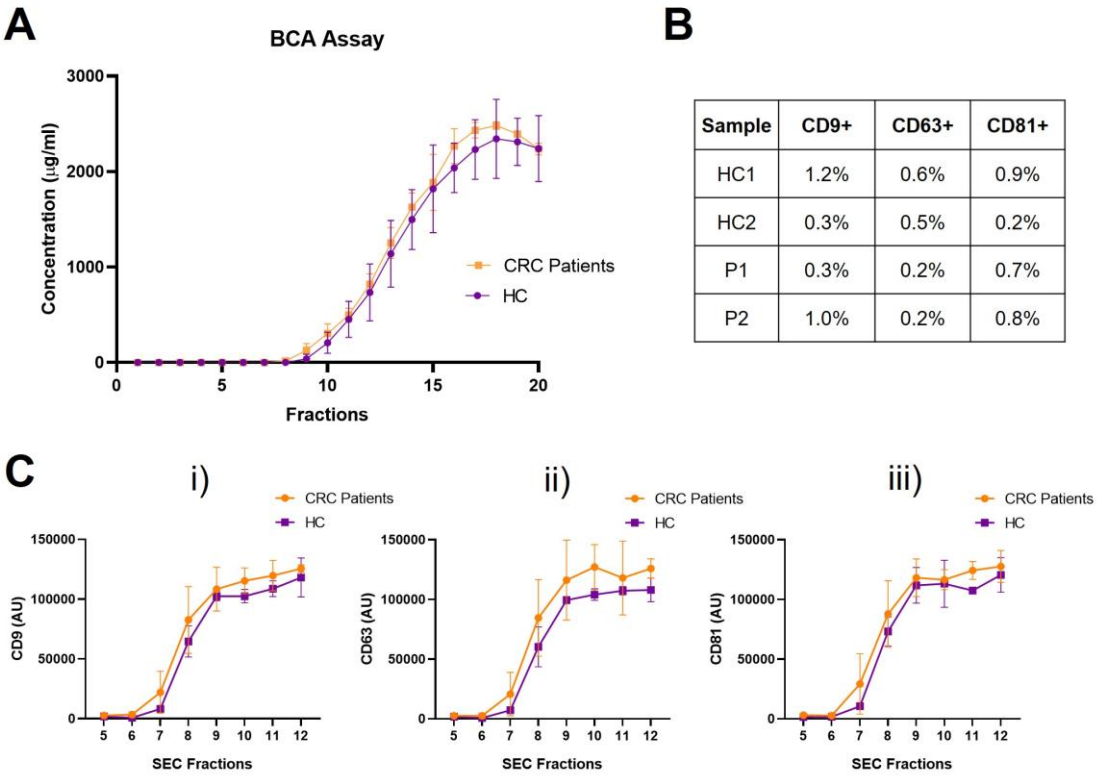


| Sample | CD9+ | CD63+ | CD81+ |
|---|---|---|---|
| HC1 | 1.2% | 0.6% | 0.9% |
| HC2 | 0.3% | 0.5% | 0.2% |
| P1 | 0.3% | 0.2% | 0.7% |
| P2 | 1.0% | 0.2% | 0.8% |

**Figure 5.9. Characterisation of SEC fractions and pooled EVs.** (A) BCA assay of fractions from SEC for CRC patients and HC derived EVs (n=3). (B) Tetraspanins percentage of positivity of SEC fractions 7-9 derived from CRC patients and HC. (C) DELFIA assay of the three tetraspanins markers of EVs (CD9, CD63, CD81). CRC patients and HC derived EVs (n=3).

DELFIA showed presence of CD9, CD63 and CD81 markers at fractions 8 – 12. Since fraction 12 was close to smaller soluble proteins, it was decided to pool only SEC fractions 8-11. The new pool of EVs was obtained from three patients and then characterised again to obtain information about morphology, particle count, size, protein concentration and marker expression (Figure 5.10). Double membrane particles of different sizes (30-150 nm) were identified with TEM (Figure 5.10A). Percentage of positivity of CD9 did not increase compared to the previous pool, whereas CD63 and CD81 were higher in pooled EV fractions from 8-11 than pooled EV fractions from 7-9 (Figure 5.10B). Particle size showed an average size of 60 nm and the concentration was between $10^9$ and $10^{10}$ in all the samples (Figure 5.10C).

A

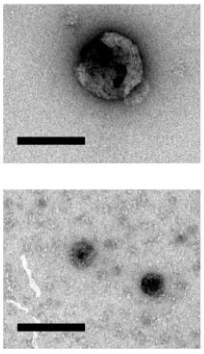

B

| Sample | CD9+ | CD63+ | CD81+ |
|---|---|---|---|
| P1 | 1.5% | 5.2% | 3.0% |
| HC1 | 0.8% | 3.2% | 2.5% |

C

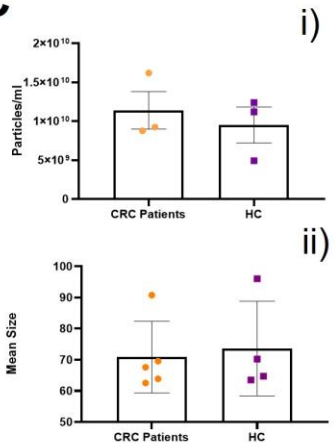


**Figure 5.10. Characterisation of plasma EVs pooled from fractions 8-11.** (A) Representative TEM images of EVs with different sizes. Scale bar = 100 nm. (B) Tetraspanins percentage of positivity of EVs derived from CRC patients and HC. (C) Particle concentration and size with NanoFCM; (i) Particles concentration; Mean ± SEM (n=3, (ii) Particle size; Individual values + mean (n=3).

## 5.4.3 Cell responses to plasma EVs

### *5.4.3.1 Selection of the participants cohort*

Pooled plasma EVs (fractions 8-11) from 18 participants (12 CRC patients and 6 HC) were then used to treat SW480 and MRC5 independently, using the methods established using the cell line EVs. During the period of running and analysing these experiments, the study was blinded until all the data were collected and processed. The cohort of patients was chosen and randomly numbered by another member of the research team to maintain blinding. Samples were selected to compare the stage of the disease: 6 HC, 6 patients with early-stage CRC and 6 patients with late-stage CRC (Table 5.2). During the analysis, non-sensitive participant information was revealed to help in data interpretation. Of the 12 CRC patients, only 3 were females. On the contrary, HC 83% were females. Despite the intention to match the cohort in terms of age, HC (mean age 46.17 ± standard deviation 5.67) were all younger than the CRC patients (mean age 73.33 ± standard deviation 10.65).

**Table 5.2. List of patients selected for the blind study.** Blood was collected within the period of 6 months. CRC patients in white, healthy donors in grey. * Age of CRC patients and healthy donors at sample collection. CRC patients classified in two groups according to the stage. CRC patients divided in two groups according to their tumour, node, metastasis (TNM) stage. Early = T2-3, M0; Late = T3-4, M1.

| Patient | Sex | Age* | Date of collection | Stage (TNM) | Classification |
|---|---|---|---|---|---|
| 1 | F | 78 | 26/04/2022 | T2N0M0 | Early |
| 2 | F | 68 | 04/05/2022 | T2N0M0 | |
| 3 | M | 89 | 26/09/2022 | T2N1M0 | |
| 4 | M | 83 | 04/10/2022 | T2N0M0 | |
| 5 | M | 57 | 09/08/2022 | T3N0M0 | |
| 6 | M | 83 | 26/09/2022 | T3N0M0 | |
| 7 | M | 64 | 23/05/2022 | T3N1M1 | Late |
| 8 | M | 80 | 21/07/2022 | T3N1M1 | |
| 9 | M | 85 | 05/08/2022 | T3N0M1 | |
| 10 | M | 63 | 13/09/2022 | T3N2M1 | |
| 11 | M | 58 | 27/07/2022 | T4N2M1 | |
| 12 | F | 72 | 20/09/2022 | T4N0M1 | |
| 13 | F | 45 | 02/09/2022 | / | Healthy controls |
| 14 | F | 43 | 02/09/2022 | / | |
| 15 | F | 49 | 09/09/2022 | / | |
| 16 | F | 57 | 13/09/2022 | / | |
| 17 | F | 39 | 13/09/2022 | / | |
| 18 | M | 44 | 13/09/2022 | / | |

#### *5.4.3.2 Cell responses to plasma EVs*

Migration (scratch assay) and cell viability (Alamar blue) were first evaluated, and statistical analysis were first performed considering also the PBS control. Decreases in proliferation and in the migration of SW480 and MRC5 were generally observed with the plasma EV treatments, unrelated to the patient origin (Figure 5.11). SW480 and MRC5 proliferation resulted in no variation between the treatments (Figure 5.11A, B). Only one outlier in late stage group strongly decreased MRC5 proliferation. SW480 conditioned with late stage EVs migrated less than the HC (non significantly, $P = 0.4418$) and early stage EVs (non significantly, $P = 0.3470$) (Figure 5.11C). The decrease from PBS control of late stage treatment was significant in SW480 scratch ($P \leq 0.05$). A decrease in MRC5 migratory ability was observed with late stage EVs, not statistically significant compared to HC ($P = 0.5985$) and early stage EVs ($P = 0.1423$) (Figure 5.11D).

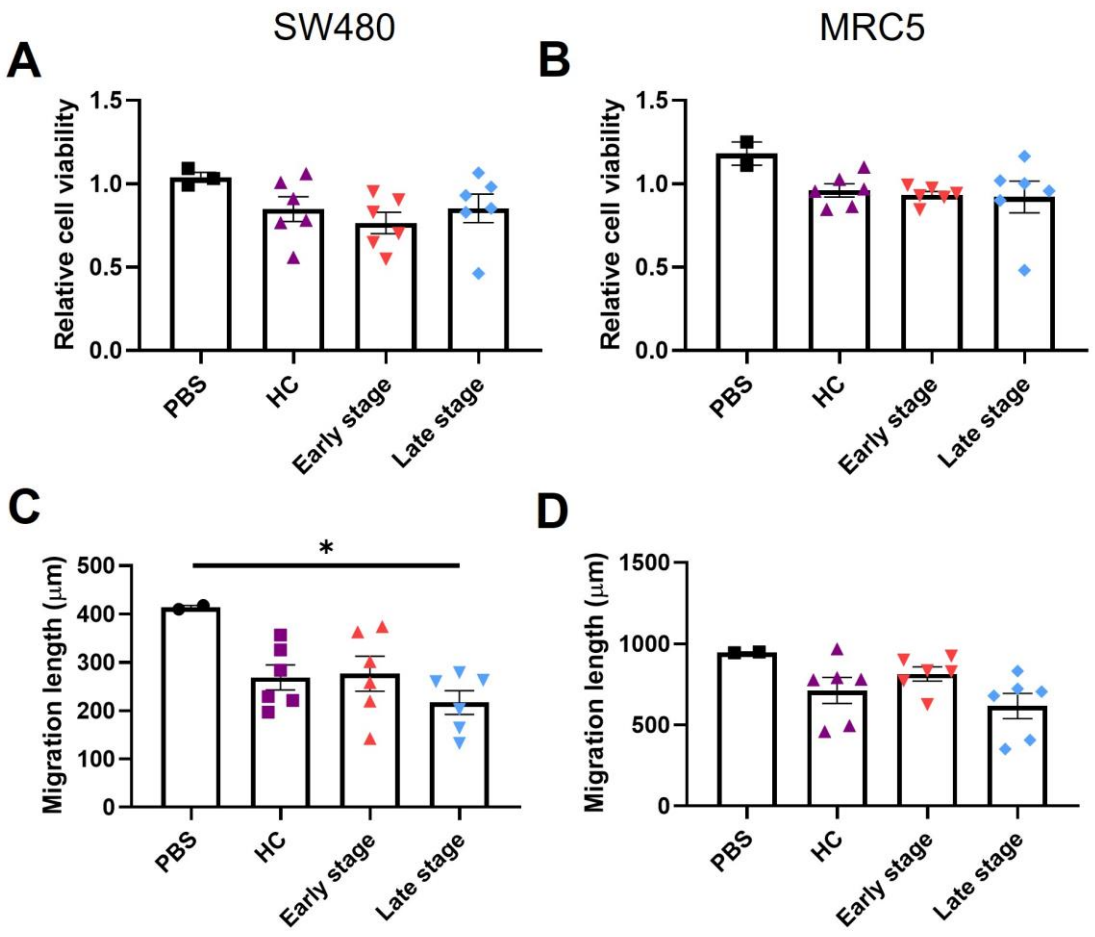


**Figure 5.11. Cell viability and migration of SW480 and MRC5 after plasma EVs treatment.** (A) SW480 Alamar blue. Data normalised to the PBS control. Mean ± SEM; ANOVA. (B) MRC5 Alamar blue. Data normalised to the PBS control. Mean ± SEM; ANOVA. (C) SW480 scratch assay after plasma EVs treatment. Mean ± SEM; ANOVA, * P ≤ 0.05. (D) MRC5 scratch assay after plasma proteins treatment. Mean ± SEM; ANOVA.

Cytokines showing changes upon EV treatment in the cytokine array screening were investigated (5.4.1.1, 5.4.1.2). VEGF, GDF-15 and nidogen-1 were analysed in the supernatant from SW480 cells. A non-statistically significant increase in the levels of VEGF was observed with late-stage EVs conditioning compared to PBS control (P = 0.1509), HC (P = 0.1657) and early stage (P = 0.2114) (Figure 5.12A). GDF-15 significantly increased with late stage EVs conditioning compared to the PBS control (P ≤ 0.05) (Figure 5.12B). The outlier patient was found in GDF-15 and was responsible for the large standard deviation. Nidogen-1 levels were significantly decreased in similar way after all the blood-derived EV treatments compared to the PBS treatment control (P ≤ 0.01 for HC and early stage EVs, P ≤ 0.005 for late stage EVs) (Figure 5.12C).

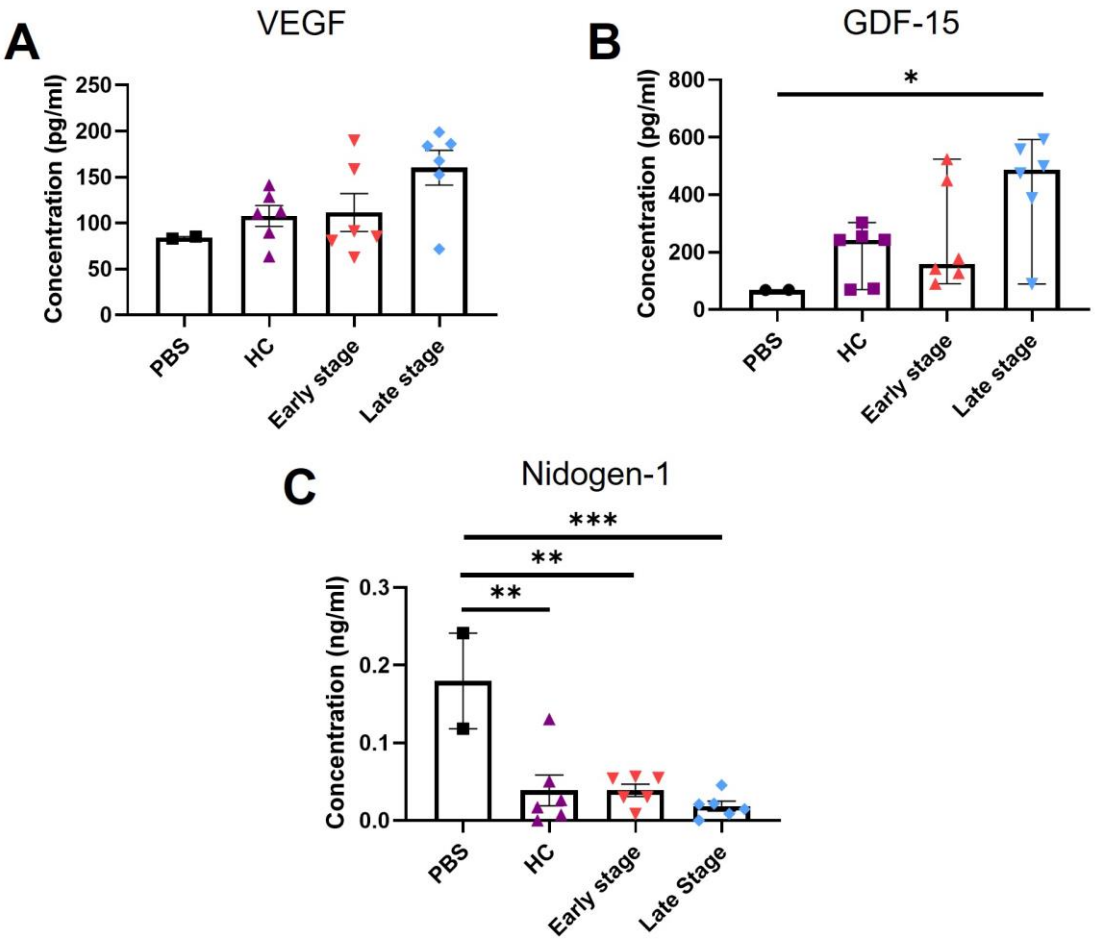


**Figure 5.12. Cytokine release of SW480 and MRC5 after plasma EVs treatment.** (A) VEGF concentration in SW480 supernatant. Mean ± SEM; ANOVA. (B) GDF-15 concentration in SW480 supernatant. Median + 95% CI; Kruskal-Wallis, * P ≤ 0.05. (C) Nidogen-1 concentration in SW480 supernatant. Mean ± SEM; ANOVA, ** P ≤ 0.01, *** P ≤ 0.001.

MRC5 supernatant was analysed for IL-6, IL-8, TIMP-1, TIMP-2 and MCP-1 (Figure 5.13). A general decrease (not statistically significant) in the levels of all the cytokines tested was observed when treated with plasma EVs. The decrease in TIMP-2 with late stage EVs was significantly lower compared to the PBS control (P ≤ 0.01), as well as with early stage EVs (P ≤ 0.05) (Figure 5.13D). Variability in expression after treatments within the different patient groups was present in IL-6, IL-8 and MCP-1, especially after treatment with late stage EVs. One patient from the late stage was distinct from the other data points and for IL-8 was so different to be the only value higher than the PBS control (Figure 5.13B).

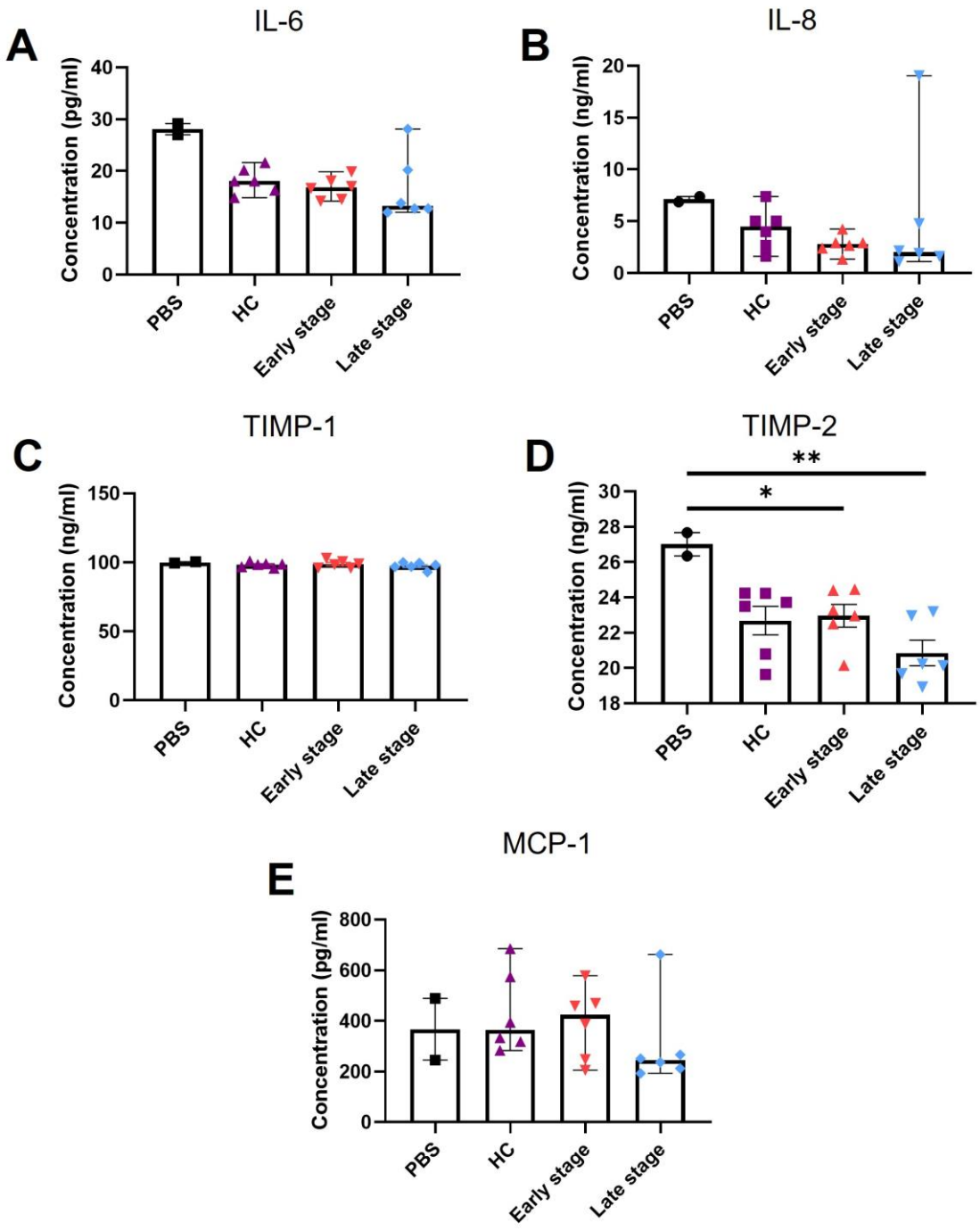


**Figure 5.13. Cytokine expression of MRC5 after plasma EVs treatment.** (A) IL-6 concentration in MRC5 supernatant. Median with 95% CI; Kruskal-Wallis. (B) IL-8 concentration in MRC5 supernatant. Median with 95% CI; Kruskal-Wallis. (C) TIMP-1 concentration in MRC5 supernatant. Mean ± SEM; ANOVA. (D) TIMP-2 concentration in MRC5 supernatant. Mean ± SEM; ANOVA, * $P \leq 0.05$, ** $P \leq 0.01$. (E) MCP-1 concentration in MRC5 supernatant. Median with 95% CI; Kruskal-Wallis.

#### *5.4.3.3 Multivariate analysis approach based on cell responses to plasma EVs*

All the results obtained from the cell response assays (from both SW480 and MRC5 cells) for the evaluation of plasma EVs were then combined to create a multivariate analysis model, excluding the PBS control. Initially, PCA was performed as unsupervised analysis to investigate the ability of the patients to cluster together (Figure 5.14A). No clusters were observed except for one patient from the late-stage EVs group which was separated from the others (P1). When the supervised PLS-DA was performed, which considered the information about the patient group, two main clusters were observed: one formed by early and HC, and one formed by late-stage patients (Figure 5.14B). Despite some overlap, the HC group cluster was tight around the centre of the axis/right side of the x axis; similarly, the late-stage group clustered on the left side of the x axis (PC1) and had only one patient (P5) as outlier. The early-stage group was instead divided into two groups: P10 and P11 close to the left side of the x axis and P4, P6, P15, P16 on the right side of the axis.

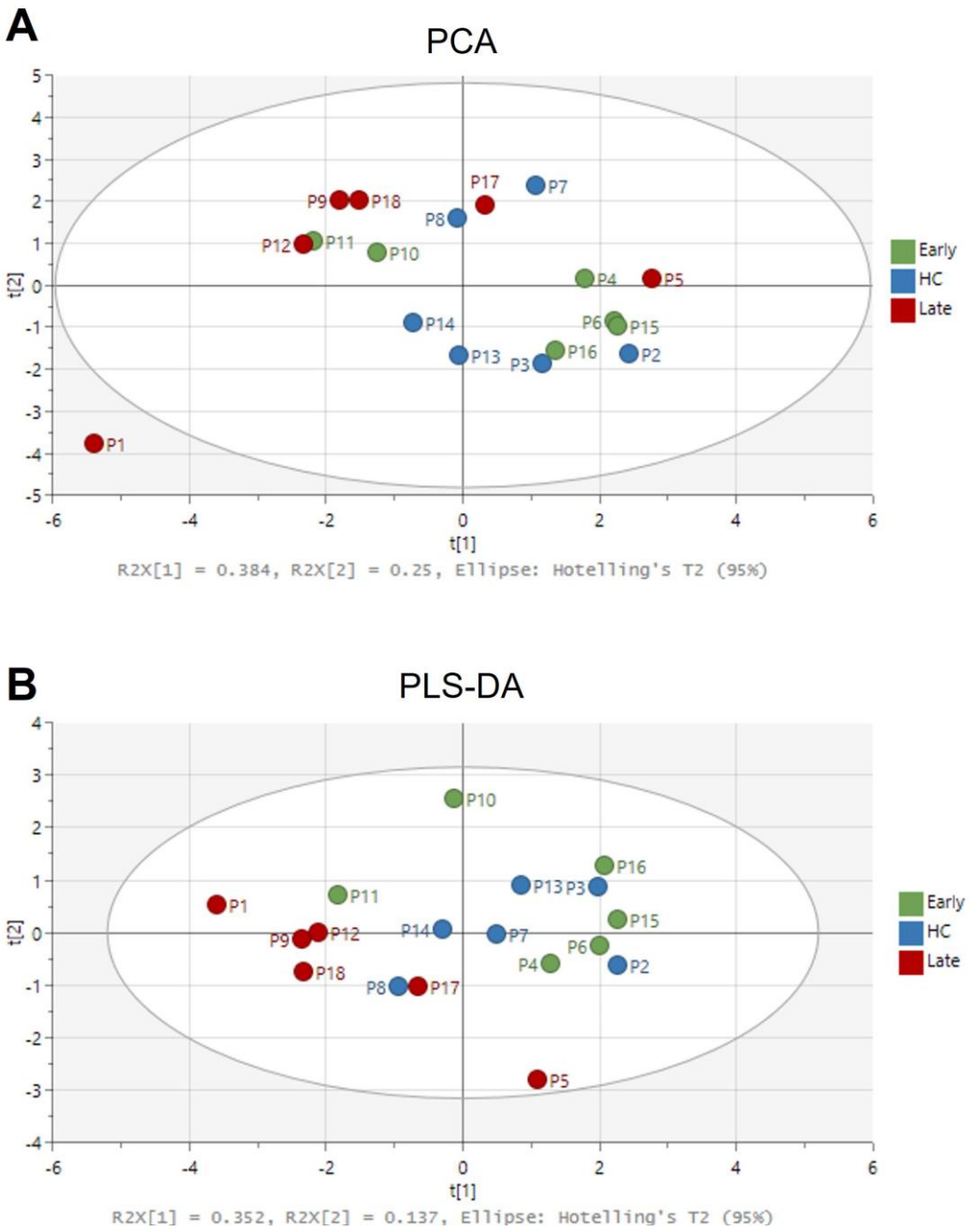


**Figure 5.14. Principal component analysis and partial least squares discriminant analysis score plots.** Cell responses assays on SW480 and MRC5 were combined to evaluate the results of the treatment with plasma EVs. Each point corresponds to a patient (A) PCA unsupervised, patient groups not considered for the analysis. (B) PLS-DA supervised, patient groups considered for the analysis. HC=healthy control.

From the PLS-DA, VIP scores can be obtained to evaluate the variables that contributes more to the separation according to the groups (Figure 5.15). Variables with VIP larger than 1 are most relevant for the separation. GDF-15, TIMP-1, Scratch MRC5, VEGF, TIMP-2, IL-6 and MCP-1 were over 1. However, TIMP-1, Scratch MRC5 and IL-6 were characterised by large uncertainty bars.

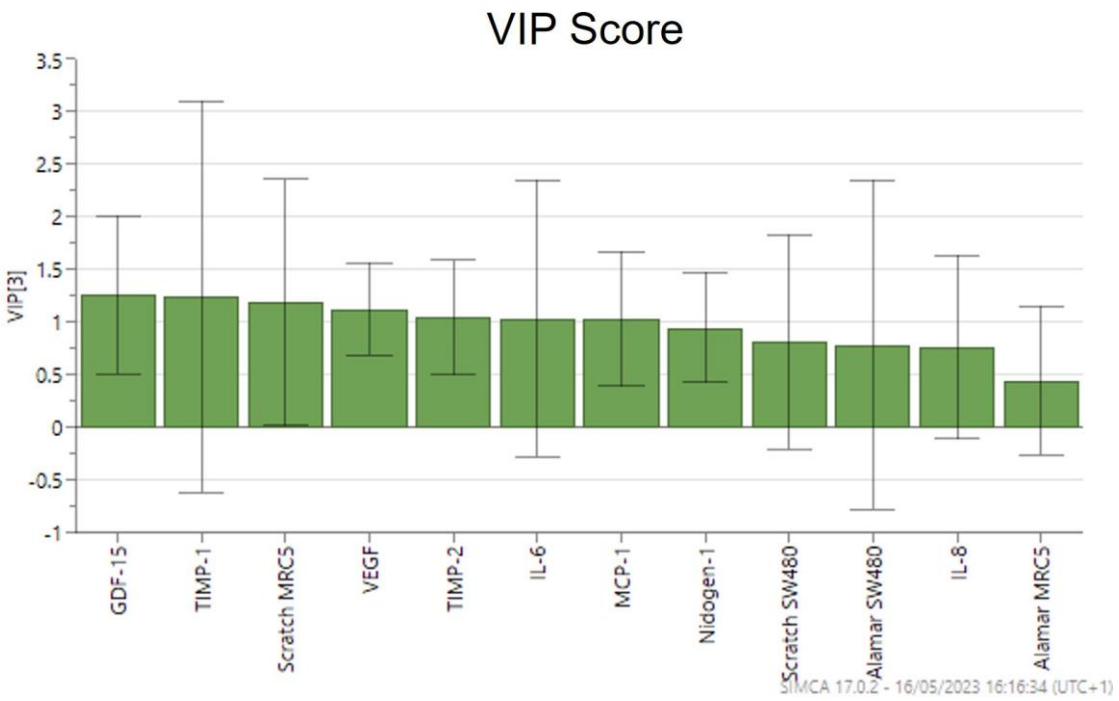


**Figure 5.15 VIP Score based on PLS-DA.** All the variables introduced in the multivariate analysis are represented in order of importance for the clustering of the PLS-DA.

## 5.5 Discussion

Despite recent advances in screening for CRC, diagnosis is still frequently made in later stages of disease where prognosis is poor. The discovery of new modalities of screening for cancer is therefore essential to support patient diagnosis, prognosis, and therapeutic strategies. EVs have huge potential as circulating biomarkers due to their disease-relevant cargo and their translation into clinical use is currently being explored (Ogata-Kawata *et al*., 2014; Sepulveda *et al*., 2017; Shiromizu *et al*., 2017). Since the EV cargo is bioactive, the aim of this Chapter was to build on EVs as potential biomarkers by evaluating the potential for cellular responses to EVs from differential CRC stage using multiplexed cell-based bioassays.

### 5.5.1 Cell responses to CRC cell lines EVs

In the previous chapters, the difference in invasion of SW480 when treated with their own EVs or SW620 EVs suggested that other basal cellular activities can be modified by the effect of CRC EVs. Due to the isogenic origin, SW480 and SW620 cell lines offer an interesting *in vitro* model in which to observe differences in the effect of stage dependent EVs on cells of the TME (Palmieri *et al*., 2015; Slater *et al*., 2018).

EV responses were investigated on SW480 cells. Despite invasion in the 3D model being driven by CRC EVs in a stage dependent way (section 2.4.3), migration in the scratch assay showed the opposite trend. SW620 EVs significantly decelerated the migration of SW480 cells. This was in line with a recent study, where an increase in migration in a scratch assay was induced only by hypoxic SW480/SW620 EVs and not by the normal phenotype (Endzelins *et al*., 2018). However, when migration was investigated via transwell assay, SW480 migratory activity was enhanced by the treatment with metastatic SW620 EVs (Pang *et al*., 2021), indicating that the method is critical when assessing the impact of EVs on migration. It is important to understand the limitation of scratch as a migration assay since it is a 2D assay lacking matrix and biomechanical support. SW480 showed significant proliferation and presence of cells in suspension even after three washes performed after the scratch, which made the measurement of single cell migration difficult. For this reason, the scratch

measurement was limited to the cohesive cell front and may not be representative of the migratory events *in vivo*.

Cancer cells adapt their metabolism to address the requirements of the continuously changing TME during the steps leading to metastasis (Wei *et al*., 2020). A small increase in cell death was observed after treatment with SW620 EVs, but the proliferation remained unchanged, implying a minimum loss of cell viability. Lactic acid production, which is an indicator of anaerobic glycolysis, was considerably lower after treatment with SW620 EVs compared to the control and SW480 EVs. This can indicate a change in the metabolic pathways being utilised, which has been previously representative of phenotypical changes towards aggression in other types of cancer (Yao *et al*., 2022; Zhou *et al*., 2022).

Several factors were considered when supernatant from conditioned SW480 (similarly for MRC5) was analysed with cytokine arrays; first, signal intensity was a crucial feature in the selection of the cytokine of interest. Multiplexed cytokine arrays are generally more sensitive compared to ELISA bioassays, therefore only the cytokines with high signal intensity were considered for further ELISA-based analysis. Then, the difference between the control and SW620 conditioning needed to be relevantly high and consistent between the two biological replicates performed. Two key cytokines were identified with both features: GDF-15 is a member of the TGF-β family and has been extensively linked to metastasis in different cancers (Li *et al*., 2016; Li *et al*., 2018; Siddiqui *et al*., 2022); nidogen-1 has also previously related to poor clinical outcomes and metastasis (Alečković *et al*., 2017). Interestingly, EVs from metastatic hepatocellular carcinoma were found to be enriched in nidogen-1 (Mao *et al*., 2020). VEGFs are a group of growth factors playing a key role in angiogenesis and vascular remodelling necessary for cancer invasion and metastasis development (Yang & Cao, 2022). VEGF-C was the only cytokine to decrease after the treatment with SW620 EVs. Not much is known on the role of this growth factor in cancer, but the most recent study showed increased production associated with lymphoangiogenesis in metastasis, thus aligning it with growth factors from the same family (Akagi *et al*., 2000). As the signal was too low to consider it for further investigation, we tested whether the same effect was observed with the more abundantly expressed VEGF-A. Interestingly, both EVs induced an increase in VEGF-A expression, in line with previous studies (Ko & Naora, 2020).

The phenotypic switch from normal fibroblasts to CAFs has also been associated with cancer derived EVs in different types of cancer (Giusti *et al*., 2022; Zhang *et al*., 2022). Therefore, cellular responses were also investigated in the MRC5 fibroblast cell line. A significant increase in proliferation and migration of MRC5 was induced by CRC EVs, supporting the idea that fibroblasts are activated by EV cargo (Abdouh *et al*., 2019). Furthermore, higher expression of pro-inflammatory IL-6 after the CRC EVs treatment was observed. The interleukins released by CAFs have been previously found to be responsible for different aspects of cancer progression, from inducing epithelial to mesenchymal (EMT) in gastric cancer, to drug resistance in prostate cancer (Cheteh *et al*., 2020; Wu *et al*., 2017).

When the cytokine array was performed on MRC5 supernatant, the signal between the two replicates performed was variable, thus it was more difficult to identify relevant cytokines. IL-6 present in the assay confirmed the data obtained with the ELISA. Alongside, MCP-1 was increased after SW620 EV treatment. MCP-1 is a crucial chemokine in the activation of tumour associated macrophages and has been previously observed expressed by non-tumour stromal cells (Yoshimura, 2018). As of the other cytokines and secreted factors, TIMP-1 had intense signal and was relevantly inhibited by SW620 EV treatment. As a matrix metalloproteinases (MMP) inhibitor, TIMP-1 decrease might attenuate the MMP activity of cancer cells and subsequent ECM degradation. However, increased expression of TIMP-1 in cancer cells has been also associated with cancer progression (Gong *et al*., 2013). Extravesicular TIMP-1 activity was extensively investigated on stromal fibroblasts, which induced TIMP-1 release by fibroblasts, as well as ECM remodelling and cancer invasion (Rao *et al*., 2022). As part of the TIMP family, TIMP-2 was also found to be highly expressed, although no significant differences were observed when comparing the EV treatments. In cancer literature this protein has a less clear role compared to TIMP-1, therefore evaluating it in relation to TIMP-1 may be of interest. TIMP-2 inhibition was found to be increased with MMP-9 activity in CRC and leading to poorer patient survival; in triple-breast cancer, increased levels of TIMP-2 were found with EMT and metastasis (Peeney *et al*., 2020; Wang *et al*., 2019). In other types of cancers, TIMP-2 expression, as well as TIMP-1, was linked to worse outcome (Escalona *et al*., 2020). The increased expression of TIMPs might be a

consequence of the feedback loop arisen by the increased MMP activity. As such, TIMP-1 and TIMP-2 were selected as potential markers; however, further analysis on the functional mechanism of TIMPs in relation to cancer EVs must be conducted to clarify the variability between studies.

### 5.5.2 Isolation and characterisation of plasma EVs

To align the previous study and maintain consistency, SEC was the method chosen for the isolation of plasma derived EVs. The choice of the isolation technique impacts on the EVs output in terms of yield, purity and reproducibility (Théry *et al*., 2018). When considering EVs derived from blood, the presence of abundant lipoproteins can affect the purity of the isolation. Protocols containing sequential combination of isolation techniques have been developed to attempt to remove contaminants such lipoproteins, however such methods also result in large loss of yield (Brennan *et al*., 2020). Despite the EV community not having a single, standard established method of EV isolation from high protein liquid biopsies, SEC is still one of the most preferred methods for the isolation of blood EVs (Théry *et al*., 2018). Besides providing high EV yield, SEC is also a relatively quick isolation method, ideal when working with patient samples.

BCA didn't detect high concentration of proteins in the fractions from 6 to 12 as previously observed with the cell lines EVs (Section 2.4.2.2). Determination of protein concentration is known to be a challenge in the study of EVs and it varies according to the nature of the EVs (Théry *et al*., 2018). When the pool of fractions previously considered were analysed with NanoFCM for CD9, CD63 and CD81 tetraspanins, the percentage of positivity was lower than 1%. Despite this seeming low positivity, plasma EVs are commonly found with tetraspanin percentages around 3-4 % with this technique (Dong *et al*., 2020). When the markers were examined with the higher sensitivity DELFIA assay, fractions 8 to 12 showed the presence of CD9, CD63 and CD81 tetraspanins. Fraction pooling for experimental treatments was therefore refined to fractions 8, 9, 10 and 11, without the inclusion of fraction 12 as this raised the possibility of contamination with larger soluble proteins eluting from the SEC. Analysis of this EV pool by TEM showed EVs of different size, and measurements with NanoFCM were again analysed, showing an increase in the marker percentage, aligning with previous studies. Despite the increase, the highest percentage of positivity for the three EV linked tetraspanins (5.2% in CD63) was still considerably low, especially

compared to the values found in cell line EVs (Section 2.4.2.3). This might be due to the impurity due to lipoprotein contamination of EV preparations from blood samples. When observing the size of EVs, plasma EVs were slightly smaller than cell lines EVs. Although this might still be due to impurity of the samples, it is also important to note that the pooled fractions of plasma EVs included fractions 10 and 11, which correspond to smaller size in the SEC.

### 5.5.3 Cell responses to CRC plasma EVs

In recent years, EVs and EV cargo derived from biological fluid have been investigated as potential cancer biomarkers. Here, cellular responses to EVs from plasma patients were explored to investigate whether they could be an alternative screening source. It is imperative to consider that plasma EVs are not cancer cell specific, therefore the effects observed cannot be strictly associated to the cancer cells. EVs that circulate in the blood can have different origins and they can be altered according to specific condition. (Yáñez-Mó *et al*., 2015). EVs released during normal homeostasis are secreted in the body fluids and even EVs secreted from the tumour can derive from all the cells of the TME. For this reason, rather than focussing on single response, multiple responses on two different types of cells representing the TME were investigated and multiple comparison analysis were also attempted. Despite the limited differences previously observed with scratch and Alamar blue, the two assays were used as a template to obtain preliminary information on the group of patients investigated. A general decrease in ability of migration and proliferation in both cell lines treated with plasma EVs was observed, independently from the stage of the disease. When cell death was assessed in the preliminary study, treatments with plasma EVs reduced the overall death of the cells compared to the PBS treated control. Thus, it was determined that the loss of proliferation and migration observed was not due to cell death. SW480 cells that underwent the treatment with EVs from late-stage patients were the least migratory, especially compared to the PBS control treatment. However, these differences weren't significant to determine variations linked to the disease stage.

The expression of cytokines identified by arrays following cell line EV treatment were assessed following plasma EV treatment. Higher expression of GDF-15 and VEGF were observed after the treatment with EVs from late stage disease compared to HC EVs. This would have resulted in statistical significance if not for

one considerably lower outlying value. This was not observed in the cytokines released by MRC5, as no main differences between the treatments were found. Pro-inflammatory cytokines such as IL-6, IL-8 and MCP-1, previously attributed to a worsening condition, were actually relatively low when MRC5 were treated with late stage EVs. TIMP-1 and TIMP-2 were the least variable of all the cytokines analysed. Despite the significative differences between the PBS control and the EV treated MRC5 for TIMP-2, the concentration levels ranged on a similar scale (20-30 ng/ml), but were not affected by treatments. Furthermore, for concentrations close to the limit of detection of the assay, differences in expression might be difficult to detect.

Since there were individual outlying values from the cluster in the late-stage group, the patient history and information were considered. In VEGF, GDF-15 and MCP-1, the patient distanced from the late-stage cluster was the only patient with grade IV CRC. The patient was also under levothyroxine medication, which is given to patients with underactive thyroid (Hennessey, 2017). Levels of factors and homeostasis in the blood can indeed be altered by specific treatments and medications (Lone *et al*., 2022). In IL-6 and IL-8, the only two diabetic patients showed values very different from the cluster. Despite the preliminary nature of the study, this suggests important information about the feasibility of considering cell responses to plasma EVs as cancer biomarkers, given co-morbidities and effects of treatments.

Finally, all the cellular responses evaluated on the two cell lines were added into a preliminary multivariate analysis model to assess the strength as a potential screening test. PCA is used to observe multivariate data in a bidimensional setting and helps in observing unsupervised clustering (Zhang & Castelló, 2017). In the PCA, the patient groups and HCs failed to cluster but overlapped within each other. The only feature observed was the separation of one of the late-stage diabetic patients (P1) from the cluster of the late-stage group. In combination with PCA, supervised tests are also generally run, such as PLS-DA, to observe the separation and clustering with the information on samples group (Lee *et al*., 2018). When PLS-DA was assessed, late-stage group separated from the HC and early-stage groups. Again, one outlier sample from the late-stage group was observed, different from the PCA, which was the patient with CRC at grade IV. Although HC and early-stage group did not separate between each other, two

early-stage patients separated from the rest of the cluster. Both patients were in advanced age at sample collection, with P10 being the oldest of the cohort (89 years old). PLS-DA and its VIP score gave also biological information by confirming GDF-15 as principal component and highlighting its potential role in stage-dependent CRC. Exploring different cellular responses to EVs which rely on the stage of the disease is crucial to improve the PCA. Moreover, multivariate analysis gains power with larger amounts of data, thus increasing the patient number in the cohort would also improve the outputs.

## 5.6 Conclusions

The use of cell responses as multiplexed bioassays demonstrates that cancer EVs can determine differential activities in cells according to the disease stage. Despite the complex nature of blood components as liquid biopsies, stage-related effects were also partially observed *ex vivo* with plasma EVs. However, functional effects failed to consistently mirror the effects derived from *in vitro* treatments. Preliminary supervised multivariate analysis showed promising results to use the model based on cellular responses to EVs as screening test. Moreover, it showed GDF-15 release worth of follow-up study. The results obtained were limited in the number of patients and therefore need to be considered preliminary. In future, it is pivotal to expand into larger numbers in the different stages of disease that also account for medication and confounding factors, such as age, sex, and co-morbidities that could influence the outcome.

# 6 Conclusions and future work

## 6.1 Final discussion and future perspectives

Colorectal cancer (CRC) still represents the third most common cause of cancer worldwide. Detection of early CRC is challenging, which leads to a high percentage of patients diagnosed at metastatic stage (Dekker *et al*., 2019). The main aim of this project was to develop and exploit *in vitro* 3D models to obtain information about the role of extracellular vesicles (EVs) in CRC progression and to evaluate EV mediated effects as potential CRC markers.

### 6.1.1 CRC EVs and patterns of invasion

Invasion is a crucial step in the development of metastasis. Cancer cells can escape the primary tumour by invading singularly or in clusters. Because of their plasticity, cancer cells can switch between different modalities of invasion (Friedl, 2004). One of the roles for which cancer EVs support cancer progression is to induce epithelial to mesenchymal transition (EMT) (Franzen *et al*., 2015; Greening *et al*., 2015). However, the role of cancer EVs on invasive behaviour was yet to be explored in a relevant tumour microenvironment (TME) model. EVs have been mainly investigated in 2D cultures or in complex animal models, but neither of these models is able to capture the complex mechanisms of tumour invasion within the TME. In Chapter 1 a 3D model of CRC invasion was developed to evaluate the role of CRC EVs in patterns of invasion.

The 3D model developed in chapter 2 showed increased invasion of cancer cells in the matrix over a relatively limited amount of time (7-14 days), enabled by the presence of a nutrient gradient in the transwell compartments. The 3D models were processed as formalin-fixed/paraffin-embedded (FFPE) tissue which did not compromise the structure and allowed easy handling and orientation of the sample. Collagen fibril orientation could be also observed through histological staining, which would be an important feature to quantify in future work, since extracellular matrix (ECM) remodelling is a crucial event in invasive mechanisms (Winkler *et al*., 2020). Along with the contraction induced by MRC5 on the low-density matrix, this also demonstrates the potential for the 3D model to be employed for future biomechanical testing associated to matrix remodelling, which is an essential feature of cancer progression (Winkler *et al*., 2020). Alterations in biomechanical properties of the tissues have also shown to

influence the EV travelling in the ECM (Lenzini *et al*., 2020) and therefore being of relevance in the study of EV signalling.

By comparing the impact of well characterised SW480/SW620 EVs (Nakurte *et al*., 2018; Suwakulsiri *et al*., 2019) it was possible to compare impact of the stage of disease. To obtain high enough yield for complex 3D model treatment, the cells were cultured in bioreactor flasks, where they grew in a 3D limited space which leads to the enrichment of EV and larger protein (Artuyants *et al*., 2021). The long-term culture of the cells (up to 4 months) was specifically optimised for cancer cells, which have a high degree of proliferation and are adapted to stress conditions. Cells that require specialised or more sensitive conditions may not adapt as readily. Both SW480 and SW620 EVs showed intact structure, high percentage of tetraspanin markers, presence of the tumour susceptibility gene 101 (TSG101) marker and absence of Golgi matrix protein 130 (GM130), thus confirming low contamination of purified EVs with intracellular membranes. Size and particle count was monitored throughout different isolations. This means that the production of EV, which to some extents mirrors the cell conditions, was stable in the bioreactor and that CRC EVs could be used to evaluate biological effects. The bioreactor-based culture method provided a long-term isolation of fully functional cancer EVs at a relatively limited cost.

When CRC EVs were used to treat the 3D model, metastatic SW620 EVs had a major impact on molecular signature and pattern of invasion. With SW620 EV conditioning, invasion of cells in bigger clusters combined with a decrease in proliferation of the invading cells were observed and was associated with a more invasive behaviour (Friedl *et al*., 2012; Lattmann *et al*., 2021). This was confirmed by an increase in N-cadherin (N-cad) and catenin delta-1 (p120), proteins associated with EMT and mesenchymal motility. However, the 3D model did not confirm loss of E-cadherin (E-cad), which is often associated with N-cad increase. This could be potentially linked to the conservation of cell-cell adhesions in the clusters (Ilina *et al*., 2020). However, E-cad was enhanced in the surrounding matrix, suggesting an EV-linked expression and highlighting a limitation of the model in the evaluation of *in situ* molecules simultaneously expressed by EVs and by the tissue.

### 6.1.2 CRC EVs and lung metastasis

Metastatic CRC is a major clinical issue due to the high percentage of patients diagnosed at this stage, inefficacy of treatment and subsequent poorer outcomes on survival. The necessity to find earlier detection signatures is essential because of the poorer survival associated with late-stage CRC. EVs are one of the factors responsible for pre-metastatic niche (PMN) formation (Dong *et al*., 2021). Therefore, establishing *in vitro* models able to investigate these pre-metastatic events may provide important clues that would enable treatments targeting the PMN earlier in the disease progression.

In this work a 3D lung model was developed to represent the stroma undergoing modification into a PMN. The 3D model was able to sustain cellular activity for a period of 7 days, but loss of cell viability at day 14 prevented longer-term cultures. Thus, the 7 day time point was used for PMN modelling through EV treatment. However, after development of this model, there is scope for further optimisation of conditions, for example through supplementation with growth factors, which may sustain longer-term cultures in future work.

CRC EVs increased Von Willebrand factor (vWF) expression by endothelial cells in both PMN and cancer invasion stage, meaning increased angiogenic signalling, which is a hallmark of cancer (Al-Ostoot *et al*., 2021). Cellular marker expression in the lung stroma confirmed the stage-dependant influence of EVs also observed in chapter 2, with SW620 EVs having a substantial impact compared to SW480 EVs. Finding stage-dependant responses can be crucial in identifying disease mediators that could then be considered in screening tests.

A synergistic effect between CRC EVs and invading SW620 cells was observed in the levels of alpha-smooth muscle actin (α-SMA) in the 3D model of lung. A similar effect was observed in collagen XI secreted by the 3D model upon conditioning with SW620 EV, which resulted in the total loss of the protein. This has never been observed before and might indicate that a crucial communication between cancer EVs and cancer cells exists with the aim of improving the success of cancer cells invasion into the PMN.

To date, this is the first study of matrix-assisted laser/desorption ionisation mass spectrometry (MALDI-MS) as a platform to screen proteomic signatures in a 3D model mimicking the TME. Recent research has focussed on the feasibility of MS

and MS imaging in studying cancer spheroids and aggregoids embedded in inert matrices (Flint *et al*., 2020) and so, this study builds on this to contribute towards developing this high-throughput spatial approach for the cancer field. Moreover, putative identification of ECM components, such as collagens, which are considered challenging to detect with MALDI-MS imaging technique, were identified by the application of a high-sensitive profiling approach. The TME has a unique collagen composition and its alteration is crucial in the support of cancer progression, which would support the significance of the development of the MS technique.

### 6.1.3 CRC EVs interactions with TG2 and ECM remodelling in cancer progression

One of the main features driven by the communication between cancer cells and cancer associated fibroblasts (CAFs) is ECM remodelling (Winkler *et al*., 2020). Among the proteins linked to ECM remodelling, transglutaminase-2 (TG2) has been explored in cancer linked with EMT and apoptosis, but also due to its cross-linking activity and compared to other cross-linking proteins such as lysyl oxidase (LOX) (Tempest *et al*., 2021). TG2 cross-linking activity has also been linked to chemoresistance (Shinde *et al*., 2022).

In Chapter 4, analysis on TG2 in the communication between SW480 and MRC5 cells confirmed a context-dependent expression of TG2. When cells were co-cultured, the levels of surface TG2 were different from the levels expressed in monoculture. TG2 decreased in MRC5, whereas it increased in SW480. This demonstrated a cell-dependent expression of TG2 which may also suggest cell-dependent roles of TG2. The evaluation of TG2 expression in CAFs upon conditioning with secreted factors demonstrated that EVs are not the key mediators in the alteration of TG2 in CAFs; instead, a direct communication between the cells or release of specific soluble factors might mediate TG2 expression on CAFs. This was confirmed when soluble non-EV proteins released from CRC cells decreased expression of TG2 in MRC5 fibroblasts rather than CRC EVs. This was further confirmed in hepatic stellate cells (HSCs), where CRC EVs did not have a defined impact on HSC expression of TG2.

Liver fibrosis has been previously associated with CRC and is strongly characterised by activation of HSCs, which assume a myofibroblast-like

phenotype, and drive ECM remodelling (Kondo *et al*., 2016). Of the factors examined, only α-SMA was consistently increased by CRC EVs in the three patient-derived HSCs at protein level, but this was not mirrored at transcriptional level. As next step, it is crucial to investigate the mechanisms and the EV cargos involved in the increased expression of α-SMA, which has been observed previously in other myofibroblast lines (Giusti *et al*., 2022). The evaluated factors involved in HSC activation showed alteration in the expression upon CRC treatment, which did not relate between the three patients examined. Considering the heterogeneity of the fibrotic condition in the three patients, the patient cohort needs widening to confirm the relationship between patient-stage and EV impact.

### 6.1.4 Responses to EVs as a screening platform for CRC

By investigating the SW480/SW620 isogenic model, it was clear that stage-dependent EV effects existed and could be observed in 3D models. This validated the importance of relevant *in vitro* models in pre-clinical research, but it also suggested a potential use of these responses as screening tools. EVs have long been considered as potential screening tools; however, the phenotypic heterogeneity that results from liquid biopsies containing EVs from all cells and tissues in the body prevents a barrier to clinical use.

In this work, cell responses to EVs were evaluated to develop a preliminary screening platform based on multivariate analysis. The cell assays chosen were united by being cost-effective, time saving and straightforward, so they could be implemented without using extensive resources. Cytokine arrays and multiplexed assays are a useful tool to evaluate potential targets, alongside providing biomolecular information.

Markers were refined first with the cell line model and then applied to plasma derived EVs from CRC patients. The multivariate analysis performed on the patients still needs to be considered as a second step in the marker validation and not the final output of the screening. Although the classification of HC/early stage/late stage was aligned with the cell line model, the pattern observed in the assays was not always comparable. For this reason, the multivariate analysis separated between the groups only partially.

This was a preliminary study and demonstrated proof of concept. However, further markers need to be evaluated to improve the analysis score. Also, the age

of the HC cohorts did not match the age of the CRC patients, which may have influenced patient separation in the multivariate analysis. Nonetheless, the multivariate analysis was able to indicate some markers with significant potential, particularly the release of growth/differentiation factor 15 (GDF-15) by CRC cells. When working with liquid biopsies, treatment strategies can lead to alterations in blood components, thus biasing biomarker efficacy (Lone *et al*., 2022). In the cohort of patients selected, outlier patients were observed in both single assays and multivariate model. It was speculated that one of those patients was separating due to therapeutic background. Two patients however, were hypothesised to outlie as they were the patients with the more advanced stage. For further use of this platform as screening, it will be necessary to consider, along with age and absence of other diseases, a similarity in the treatment strategies.

## 6.2 Ongoing work

Although future considerations have been stated for each chapter, here ongoing preliminary work is presented to indicate some steps considered in the project continuation.

### 6.2.1 Development of MS imaging method to evaluate 3D models of invasion

#### *6.2.1.1 Introduction and aim*

Mass spectrometry imaging (MSI) is a powerful high-throughput technique that enables identification of spatial information about molecules via an unlabelled approach (Buchberger *et al*., 2018). Enzymatic digestion for the bottom-up analysis of proteins can be performed by using a deposition method that maintains the analytes localisation on the tissue, such as spraying or sublimation techniques (Huizing *et al*., 2019). Collagens present in the ECM are however hard to detect with MALDI-MSI, due to post-translational modifications, which limit the exposure of trypsin cleavage which is the most frequently used enzyme. Recently, the combination of different enzymes revealed an increase in the sensitivity of MALDI-MSI to ECM detection including collagens (Clift *et al*., 2021). Here, optimisation of a MALDI-MSI method for the analysis of peptides in the 3D model of invasion was attempted.

#### *6.2.1.2 Methods*

For a preliminary observation of the feasible methods for MALDI-MSI analysis of the 3D model, two enzymatic digestions, two spraying techniques and two instruments were compared. The 3D models were processed according to Section 3.2.5.1.

Method 1. Trypsin in 20 µg/mL in 50 mM ammonium bicarbonate was deposited with SunCollect (SunChrom, Germany). Twelve layers of trypsin were deposited at a flow rate of 2 µl/min. The samples were placed in a humidity chamber at 39°C ON. Digestions were stopped with deposition of α-CHCA matrix. Five mg/ml of α-CHCA in 70:30 acetonitrile:$H_2O$ with 0.4% v/v of TFA was deposited with SunCollect (6 layers at 4 µl/min). Tryptic digested samples were analysed with Synapt G2 in positive ion mode at a range of *m/z* 800 to 3000 (resolution 10 000 fwhm) and spatial resolution of 50 µm, without ion mobility function and elaborated with HDI software (Waters Corporation, Manchester, UK).

Method 2. COLase III 100 µg/ml was deposited with HTX M3+ Sprayer™ (HTX Technologies, US) following the parameter found in literature (45°C, 10 psi, 25 µL/min, 1200 m/s, and 15 passes with a 3.0 mm offset) (Clift *et al*., 2021). The samples were placed in a humidity chamber at 39 °C ON. Digestions were stopped with deposition of α-CHCA matrix. Five mg/ml of the same α-CHCA solution was sprayed with HTX M3+ Sprayer™ (77°C, 10 psi, 100µL/min, 1300 m/s, and 10 passes, 2.5 mm offset). Samples digested with COLase III were analysed with MALDI MRT in positive ion mode, spatial resolution of 20 µm.

#### *6.2.1.3 Results*

MALDI-MSI analysis of tryptic peptides conducted with Synapt G2 were able to show *m/z* signals previously found in literature, signals observed were *m/z* 898.5329 and *m/z* 1105.6004, which are putatively identified as collagen α precursor (Figure 6.1B) (Groseclose *et al*., 2008). Average spectra maximum relative intensity was 120000. Analysis of samples digested with COLase III could not be performed due to the lack of matrix deposited onto the samples (Figure 6.1D).

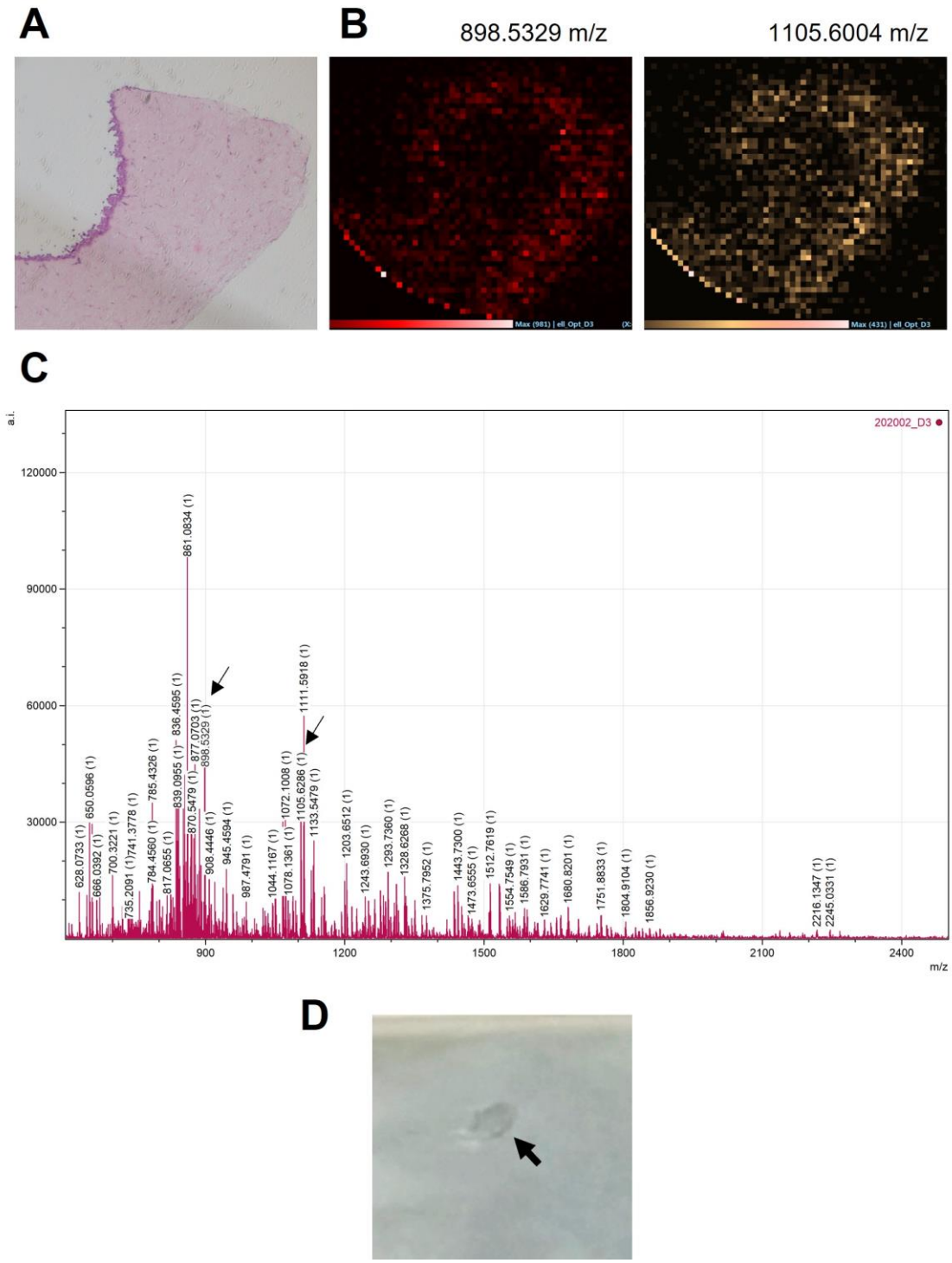


**Figure 6.1. Preliminary optimisation of MALDI-MSI for 3D model of invasion. (**A) Representative H&E image of the 3D model. (B) Representative *m/z* signals found in the 3D model after tryptic digestion. Arbitrary colours: red = *m/z* 898.5329; yellow = *m/z* 1105.6004. (C) Average spectra of tryptic peptides analysed with Synapt G2. D) Picture representing issues with co-crystalisation post matrix α-CHCA deposition with M3+ HTX sprayer™ resulting in heterogeneous coverage.

### *6.2.1.4 Discussion*

MALDI-MSI was attempted to identify ECM proteins in the 3D model of invasion. Low intensity spectra were obtained through trypsin digestion and *m/z* could be

putatively identified and localised within the tissue. Spatial resolution with Synapt G2 is however limited to 50 µm, thus it was not possible to obtain spatial information on the different areas of the 3D model of invasion.

It was not possible to obtain MSI analysis with MALDI-MRT. This was probably due to the spraying technique employed for the deposition of the matrix. The matrix deposited on the tissue allows the extraction of peptides and a good balance of matrix deposition is essential to avoid ion suppression. Number of sprayed layers, velocity of the spraying flows are all features that need to be considered when optimising the spraying method (Huizing *et al*., 2019). This is essential to find the right balance of matrix requested to extract peptides. However, many spraying methods have been attempted, but none of them succeeded in covering the 3D model. This indicated that the combination of FFPE processing of the models and the condensed collagen matrix created a surface which was insensitive to the finer spraying of the HTX Sprayer™.

## 6.2.2 Comparison of levels of collagens in plasma and in lung 3D model

### *6.2.2.1 Introduction and aim*

The main aim in the continuous development of *in vitro* 3D models is to obtain biologically relevant representations of *in vivo* diseases and events. Levels of collagen expression in plasma can indicate the grade of matrix degradation in the tissues and ECM remodelling (Kehlet *et al*., 2016; Lipton *et al*., 2018). Comparing levels of analytes present in the blood to the levels released by 3D culture can offer a validation of the established *in vitro* settings. Here, the levels of collagen found in the supernatant of the lung 3D models after the treatment with SW480 and SW620 EVs were compared to plasma levels found in CRC patients.

### *6.2.2.2 Methods*

Plasma from CRC patients and HC from Section 5.3.8 was analysed for collagen III, VI, XI. The dot blot method is described in Section 3.2.7.

### *6.2.2.3 Results*

No significant differences were identified in the collagen levels in the plasma between the different patient groups. A small decrease was observed in the late-stage patients for collagen III and VI (Figure 6.2 Bii, Cii).

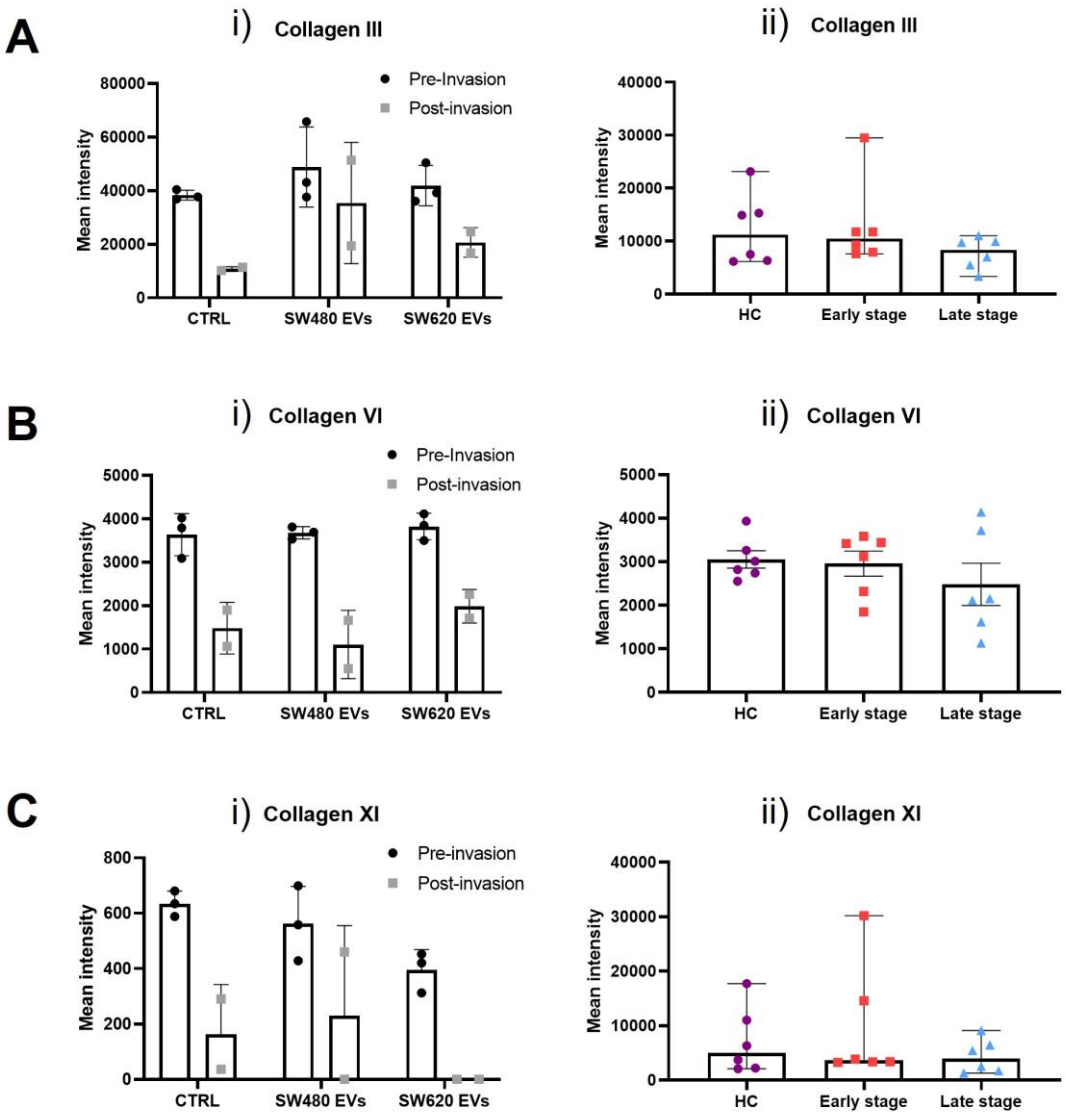


**Figure 6.2. Comparison of collagen levels in lung 3D model and patient plasma.** (A) Collagen type III expression; (i) in lung 3D. Mean ± SEM (n ≥ 2), (ii) in plasma. Median ± 95% CI (n=6); Kruskal-Wallis. (B) Collagen type VI expression; (i) in lung 3D. Mean ± SEM (n ≥ 2), (ii) in plasma. Mean ± SEM (n=6); ANOVA. (C) Collagen type XI expression; (i) in lung 3D. Mean ± SEM (n ≥ 2), (ii) in plasma. Median ± 95% CI (n=6); Kruskal-Wallis.

#### *6.2.2.4 Discussion*

Collagen levels in the supernatant deriving from the lung 3D model treated with CRC EVs (Section 3.4.3) were aligned to the expression in the plasma deriving from CRC patients, to evaluate whether similar patterns could be observed. Collagen type III is the most abundantly found in blood from cancer patients and it has been previously associated to fibrotic events in solid tumours (Willumsen *et al*., 2022). Similarly, collagen VI fragments were observed increased in serum from CRC patients compared to HC (Qiao *et al*., 2015). Although collagen XI is

being considered a potential novel cancer biomarker, blood levels have yet to be fully evaluated.

In general, no significant differences were observed in the serum deriving from patients and HCs apart from a small decrease was observed in late-stage patients for both collagen III and VI compared to HC. Whether the decrease found in the 3D models after SW620 invasion and the decrease found in the plasma can be consequences of the same mechanisms is unclear, since increased collagen levels in plasma is generally associated to higher ECM turnover and degradation in cancer tissues. Overall, increasing the number of patients might help to clarify the involvement of EVs in ECM remodelling and in determining whether the changes of collagens in the 3D model can be reflected in the blood levels of CRC patients.

## 6.3 Concluding remarks

*In vitro* models have the potential to uncover the underlying processes of cancer development and metastasis, as well as aiding in the discovery of novel biomarkers. In this project, the organotypic models developed for the evaluation of EV bioactivities in the TME crosstalk provided novel biological information on cancer progression and metastasis. The 3D model of cancer invasion provided a semi-quantifiable system to investigate patterns of CRC invasion and demonstrated that CRC EVs increase cancer cell invasion in a stage-dependent manner. The 3D model of lung metastasis confirmed the role of CRC EVs in activation of TME cells, including CAFs and endothelial cells. Further optimisation to improve the stability of the 3D models could be implemented to explore long-term EV-driven alterations of the TME. Furthermore, preliminary proteomic analysis suggested the feasibility of high-throughput screening methods, such as unlabelled mass spectrometry, to investigate the proteomics of the organotypic models. Finally, the information on EV alterations provided by the development of the 3D models was leveraged to establish a preliminary screening platform based on cell responses to EVs. Taken together, these results provide a new perspective in the investigation of EVs as cancer biomarkers and in the development of screening technologies to support cancer diagnosis and prognosis.

# 7 Appendix

## 7.1 Supplementary data

### 7.1.1 Cytokine array on SW480

| | CTRL | | SW620 | | Fold change | |
|---|---|---|---|---|---|---|
| | R1 | R2 | R1 | R2 | R1 | R2 |
| Adiposin | 0.02235 | 0.01255 | 0.029452 | 0.009858 | 1.3177 | 0.7854 |
| BCAM | 0.0359 | 0.01465 | 0.048402 | 0.015765 | 1.3482 | 1.0760 |
| CD30 | 0.01625 | 0.00818 | 0.025596 | 0.006166 | 1.5751 | 0.7537 |
| CD40 | 0.01105 | 0.00688 | 0.018229 | 0.005707 | 1.6493 | 0.8288 |
| Fcr RIIB/C | 0.0121 | 0.00607 | 0.017958 | 0.006119 | 1.4841 | 1.0072 |
| Ferritin | 0.06415 | 0.0769 | 0.064236 | 0.051543 | 1.0013 | 0.6702 |
| FLRG | 0.02005 | 0.01325 | 0.02092 | 0.008877 | 1.0433 | 0.6699 |
| Follistatin | 0.03315 | 0.0225 | 0.042249 | 0.017082 | 1.2744 | 0.7592 |
| Furin | 0.02215 | 0.00942 | 0.012626 | 0.009391 | 0.5700 | 0.9963 |
| Galectin-7 | 0.00626 | 0.00367 | 0.00594 | 0.003255 | 0.9480 | 0.8869 |
| GDF-15 | 0.226 | 0.13 | 0.559494 | 0.222234 | 2.475 | 1.7094 |
| Growth Hormone | 0.0195 | 0.01004 | 0.026826 | 0.010241 | 1.3756 | 1.0194 |
| IL-10 R α | 0.0289 | 0.01405 | 0.042332 | 0.014787 | 1.4647 | 1.0524 |
| IL-22 | 0.0187 | 0.00929 | 0.025924 | 0.009688 | 1.3863 | 1.0428 |
| IL-28A | 0.00946 | 0.00522 | 0.020264 | 0.005099 | 2.1420 | 0.9758 |
| IL-29 | 0.0277 | 0.0133 | 0.049715 | 0.015042 | 1.7947 | 1.1309 |
| IL-31 | 0.01305 | 0.00827 | 0.020756 | 0.007491 | 1.5904 | 0.9058 |
| Insulin | 0.0086 | 0.00440 | 0.014061 | 0.004967 | 1.635 | 1.1276 |
| Luteinizing Hormone | 0.0194 | 0.01012 | 0.02133 | 0.011261 | 1.0994 | 1.1126 |
| LIMPII | 0.00671 | 0.00338 | 0.006465 | 0.009255 | 0.9634 | 2.7381 |
| LYVE-1 | 0.0158 | 0.00859 | 0.007786 | 0.00583 | 0.4927 | 0.6786 |
| Maraspin | 0.0106 | 0.00589 | 0.013077 | 0.004742 | 1.2336 | 0.8050 |
| MICA | 0.03185 | 0.017 | 0.037983 | 0.018144 | 1.1925 | 1.0673 |
| MICB | 0 | 0 | 0.000281 | 0 | 0 | 0 |
| MMP-2 | 0.0155 | 0.00774 | 0.025842 | 0.008923 | 1.6672 | 1.1528 |
| MMP-7 | 0.014 | 0.00711 | 0.033389 | 0.007377 | 2.3849 | 1.0368 |
| MMP-8 | 0.0123 | 0.00565 | 0.023299 | 0.00546 | 1.8942 | 0.9664 |
| MMP-10 | 0.0268 | 0.01265 | 0.050864 | 0.013258 | 1.8978 | 1.0480 |
| NCAM-1 | 0.046 | 0.01735 | 0.0781 | 0.024178 | 1.6978 | 1.3935 |
| Nidogen-1 | 0.1495 | 0.0815 | 0.379012 | 0.10878 | 2.5351 | 1.3347 |
| NrCAM | 0.0305 | 0.01535 | 0.038065 | 0.013555 | 1.2480 | 0.8830 |

| | | | | | | |
|---|---|---|---|---|---|---|
| NRG1-β1 | 0.02385 | 0.01525 | 0.02699 | 0.013725 | 1.1316 | 0.9 |
| Osteopontin | 0.01625 | 0.00947 | 0.007679 | 0.007173 | 0.4725 | 0.7570 |
| PAI-I | 0.232 | 0.1485 | 0.255136 | 0.161895 | 1.0997 | 1.0901 |
| Platelet Factor 4 | 0.01785 | 0.00811 | 0.02658 | 0.007678 | 1.4890 | 0.9461 |
| PSA-total | 0.01245 | 0.00645 | 0.017966 | 0.004547 | 1.4430 | 0.7049 |
| RAGE | 0.01115 | 0.00530 | 0.014972 | 0.004781 | 1.3427 | 0.9011 |
| RANK | 0.00649 | 0.00270 | 0.009664 | 0.003837 | 1.4879 | 1.4184 |
| Resistin | 0.00062 | 0 | 0 | 0.000134 | 0 | 1.5845 |
| SAA | 0.01875 | 0.00856 | 0.029288 | 0.007292 | 1.562 | 0.8513 |
| Siglec-9 | 0.019 | 0.00936 | 0.037491 | 0.006777 | 1.9732 | 0.7237 |
| TACE | 0.0241 | 0.01185 | 0.035194 | 0.011218 | 1.4603 | 0.9466 |
| TIM-1 | 0.01155 | 0.00595 | 0.014767 | 0.006646 | 1.2785 | 1.1160 |
| TRAIL R2 | 0.0182 | 0.00985 | 0.023135 | 0.010071 | 1.2711 | 1.0223 |
| Trappin-2 | 0.0106 | 0.00915 | 0.00617 | 0.006697 | 0.5820 | 0.7314 |
| TREM-1 | 0.0145 | 0.00906 | 0.02174 | 0.008108 | 1.49931 | 0.8948 |
| TSH | 0.02905 | 0.01455 | 0.041921 | 0.017167 | 1.44306 | 1.1798 |
| TSLP | 0.0123 | 0.00695 | 0.012199 | 0.006913 | 0.9917 | 0.9940 |
| VCAM-1 | 0.01255 | 0.00717 | 0.011239 | 0.006183 | 0.89553 | 0.8622 |
| VEGF-C | 0.01465 | 0.00931 | 0.012167 | 0.007513 | 0.8304 | 0.8069 |
| XEADR | 0.02665 | 0.01415 | 0.023299 | 0.01092 | 0.8742 | 0.7717 |

### 7.1.2 Cytokine array on MRC5

| | CTRL | | SW620 | | Fold change | |
|---|---|---|---|---|---|---|
| | R1 | R2 | R1 | R2 | R1 | R2 |
| ENA-78 | 0.101 | 0.0182 | 0.110055 | 0.029407 | 1.0896 | 1.6158 |
| GCSF | 0.0107 | 0.00169 | 0.007956 | 0.006023 | 0.7435 | 3.5639 |
| GM-CSF | 0.0065 | 0 | 0.005828 | 0 | 0.8857 | 0 |
| GRO | 0.109 | 0.0114 | 0.088177 | 0.013741 | 0.8100 | 1.2053 |
| GRO-α | 0.0573 | 0.0143 | 0.050785 | 0.010222 | 0.8863 | 0.7148 |
| I-309 | 0.0318 | 0.00645 | 0.022674 | 0.006254 | 0.7130 | 0.9696 |
| IL-1α | 0.0383 | 0.00203 | 0.030166 | 0.00967 | 0.7876 | 4.7635 |
| IL-1β | 0.0727 | 0.00755 | 0.0661 | 0.022216 | 0.9092 | 2.9425 |
| IL-2 | 0.0161 | 0.00127 | 0.012928 | 0.009066 | 0.8029 | 7.1385 |
| IL-3 | 0.0677 | 0.00488 | 0.088177 | 0.031462 | 1.3024 | 6.4471 |
| IL-4 | 0.0266 | 0.00301 | 0.025923 | 0.007949 | 0.9745 | 2.6408 |
| IL-5 | 0.0229 | 0 | 0.019558 | 0.003942 | 0.8540 | 0 |
| IL-6 | 0.957 | 0.0198 | 1.200002 | 0.030435 | 1.2539 | 1.5371 |
| IL-7 | 0.00391 | 0 | 0.002446 | 0.001913 | 0 | 0 |

| | | | | | | |
|---|---|---|---|---|---|---|
| IL-8 | 0.568 | 0.0925 | 0.5642 | 0.25298 | 0.9933 | 2.7349 |
| IL-10 | 0.0571 | 0.00944 | 0.0541 | 0.004867 | 0.9474 | 0.5155 |
| IL-12 | 0.0617 | 0.0278 | 0.059403 | 0.014254 | 0.9627 | 0.5127 |
| IL-13 | 0.0478 | 0 | 0.047536 | 0.000119 | 0.9944 | 0 |
| IL-15 | 0.0426 | 0.00787 | 0.050387 | 0.018749 | 1.1827 | 2.3823 |
| IFN-γ | 0.0666 | 0.011 | 0.078895 | 0.027738 | 1.1846 | 2.5216 |
| MCP-1 | 1.22 | 0.213 | 1.538124 | 0.602272 | 1.2607 | 2.8275 |
| MCP-2 | 0.0258 | 0.00504 | 0.030961 | 0.011069 | 1.2000 | 2.1962 |
| MCP-3 | 0.0324 | 0.00613 | 0.041304 | 0.006883 | 1.2748 | 1.1228 |
| MCSF | 0.0955 | 0.0164 | 0.104752 | 0.03159 | 1.0968 | 1.9262 |
| MDC | 0.0583 | 0.00999 | 0.069613 | 0.020161 | 1.1940 | 2.0181 |
| MIG | 0.0811 | 0.00461 | 0.052243 | 0.023115 | 0.6441 | 5.0140 |
| MIP-1b | 0.141 | 0.0353 | 0.131934 | 0.015282 | 0.9357 | 0.4329 |
| MIP-1δ | 0.046 | 0.00665 | 0.033083 | 0.010196 | 0.7191 | 1.5332 |
| RANTES | 0.104 | 0.0115 | 0.096133 | 0.023243 | 0.9243 | 2.0211 |
| SCF | 0.0534 | 0.00811 | 0.043624 | 0.018492 | 0.8169 | 2.2801 |
| SDF-1 | 0.0574 | 0.0115 | 0.045216 | 0.068317 | 0.7877 | 5.9406 |
| TARC | 0.0491 | 0.00593 | 0.067624 | 0.015667 | 1.3772 | 2.6419 |
| TGF-β1 | 0.0115 | 0.00074 | 0.017768 | 0.013741 | 1.5450 | 18.4690 |
| TNF-α | 0.0585 | 0.00862 | 0.053635 | 0.017978 | 0.9168 | 2.0856 |
| TNF-β | 0.0401 | 0.00673 | 0.033348 | 0.014254 | 0.8316 | 2.1179 |
| EGF | 0.0888 | 0.015 | 0.092155 | 0.029407 | 1.0377 | 1.9604 |
| IGF-1 | 0.218 | 0.0278 | 0.129945 | 0.060356 | 0.5960 | 2.1710 |
| Angiogenin | 0.438 | 0.0596 | 0.424973 | 0.053036 | 0.9702 | 0.8898 |
| Oncostatin M | 0.143 | 0.0216 | 0.116685 | 0.037112 | 0.8159 | 1.7181 |
| Thrombopoietin | 0.0578 | 0.0087 | 0.034608 | 0.014254 | 0.5987 | 1.6383 |
| VEGF | 0.0827 | 0.0128 | 0.066961 | 0.024784 | 0.8096 | 1.9362 |
| PDGF-BB | 0.0451 | 0.00753 | 0.040972 | 0.014254 | 0.9084 | 1.8929 |
| Leptin | 0.0824 | 0.0074 | 0.076243 | 0.017721 | 0.9252 | 2.3947 |
| BDNF | 0.507 | 0.0526 | 0.716023 | 0.086553 | 1.4122 | 1.6454 |
| BLC | 0.0456 | 0.0078 | 0.03368 | 0.018364 | 0.7385 | 2.3543 |
| Ck β 8-1 | 0.0822 | 0.0129 | 0.074254 | 0.024528 | 0.9033 | 1.9013 |
| Eotaxin | 0.0552 | 0.0185 | 0.065039 | 0.022344 | 1.1782 | 1.2077 |
| Eotaxin-2 | 0.0641 | 0.0341 | 0.048066 | 0.017336 | 0.7498 | 0.5083 |
| Eotaxin-3 | 0.0385 | 0.0117 | 0.033348 | 0.010338 | 0.8661 | 0.8835 |
| FGF-4 | 0.0543 | 0.0115 | 0.042961 | 0.018235 | 0.7911 | 1.5856 |
| FGF-6 | 0.0849 | 0.0179 | 0.057547 | 0.023243 | 0.6778 | 1.2984 |
| FGF-7 | 0.0631 | 0.00335 | 0.043492 | 0.009451 | 0.6892 | 2.8211 |
| FGF-9 | 0.102 | 0.0208 | 0.086851 | 0.037112 | 0.8514 | 1.7842 |
| Flt-3 Ligand | 0.0585 | 0.0106 | 0.044221 | 0.011776 | 0.7559 | 1.1109 |

| | | | | | | |
|---|---|---|---|---|---|---|
| Fractalkine | 0.0476 | 0.0105 | 0.046541 | 0.022601 | 0.9777 | 2.1524 |
| GCP-2 | 0.0573 | 0.0127 | 0.050718 | 0.019391 | 0.8851 | 1.5268 |
| GDNF | 0.0928 | 0.0149 | 0.093481 | 0.025812 | 1.0073 | 1.7323 |
| HGF | 1.95 | 0.401 | 1.809947 | 0.395522 | 0.9281 | 0.9863 |
| IGFBP-1 | 0.0752 | 0.0105 | 0.055823 | 0.015153 | 0.7423 | 1.4431 |
| IGFBP-2 | 0.131 | 0.0261 | 0.082873 | 0.029022 | 0.6326 | 1.1119 |
| IGFBP-3 | 0.0745 | 0.0109 | 0.066961 | 0.012649 | 0.8988 | 1.1604 |
| IGFBP-4 | 0.0843 | 0.0109 | 0.071602 | 0.009015 | 0.8493 | 0.8270 |
| IL-16 | 0.0964 | 0.0155 | 0.071602 | 0.01618 | 0.7427 | 1.0438 |
| IP-10 | 0.118 | 0.0244 | 0.099448 | 0.01862 | 0.8427 | 0.7631 |
| LIF | 0.143 | 0.02 | 0.099448 | 0.017336 | 0.6954 | 0.8668 |
| LIGHT | 0.0773 | 0.0216 | 0.065702 | 0.020547 | 0.8499 | 0.9512 |
| MCP-4 | 0.0404 | 0.00806 | 0.036995 | 0.007641 | 0.9157 | 0.9480 |
| MIF | 0.0714 | 0.0139 | 0.055293 | 0.013355 | 0.7744 | 0.9607 |
| MIP-3α | 0.0612 | 0.0119 | 0.019558 | 0.010736 | 0.3195 | 0.9021 |
| NAP-2 | 0.192 | 0.014 | 0.081547 | 0.011994 | 0.4247 | 0.8567 |
| NT-3 | 0.156 | 0.0135 | 0.07558 | 0.013741 | 0.4844 | 1.0178 |
| NT-4 | 0.0849 | 0.00972 | 0.066298 | 0.008578 | 0.7808 | 0.8825 |
| Osteopontin | 0.132 | 0.0168 | 0.08884 | 0.007243 | 0.6730 | 0.4311 |
| Osteoprotegerin | 2.74 | 0.593 | 2.333705 | 0.410932 | 0.8517 | 0.6929 |
| PARC | 0.0929 | 0.0112 | 0.06358 | 0.005252 | 0.6843 | 0.4689 |
| PIGF | 0.075 | 0.00888 | 0.051514 | 0.006151 | 0.6868 | 0.6926 |
| TGF-β2 | 0.0448 | 0.00112 | 0.028044 | 0.001926 | 0.6259 | 1.7196 |
| TGF-β3 | 0.0856 | 0.0108 | 0.056884 | 0.006036 | 0.6645 | 0.5588 |
| TIMP-1 | 1.69 | 0.559 | 1.206631 | 0.308199 | 0.7139 | 0.5513 |
| TIMP-2 | 2.5 | 0.00737 | 1.770168 | 0.007975 | 0.7080 | 1.0820 |

## 7.2 Publications and presentations

### 7.2.1 Published papers

Tempest, R., **Guarnerio, S.**, Maani, R., Cooper, J., & Peake, N. (2021). The Biological and Biomechanical Role of Transglutaminase-2 in the Tumour Microenvironment. Cancers, 13(11), 2788. https://doi.org/10.3390/cancers13112788

### 7.2.2 Oral presentations

Responses to EVs as screening biomarkers for CRC. *UKEV, Edinburgh, Scotland, UK (2022)*. **Awarded 2nd best talk**.

MALDI-MS Imaging to analyse 3D models of bowel cancer invasion and metastasis. *Workshop of the Liver Regenerative Medicine Network, Online (2020)*.

### 7.2.3 Poster presentations

Extracellular vesicles: small packages with a big role in bowel cancer metastasis. *Winter Poster, Sheffield Hallam University (2019).* **Awarded Best Poster by the public vote**.

Characterisation of a 3D model of invasive colorectal cancer. Winter Poster, *Sheffield Hallam University, Sheffield, UK (2020)*.

Development of 3D model of lung for the analysis and imaging of colorectal cancer invasiveness and stromal alterations. *BioMedENG, The University of Sheffield, Sheffield, UK (2021)*.

Development of 3D model of lung for the analysis and imaging of colorectal cancer invasiveness and stromal alterations. *Winter Poster, Sheffield Hallam University, Sheffield, UK (2021)*.

Colorectal cancer derived EVs drive invasion and tumour microenvironment remodelling in a 3D organotypic culture model. *ISEV 2022, Lyon, France (2022)*.

Responses to EVs as biomarkers for colorectal cancer. *Winter Poster, Sheffield Hallam University, Sheffield, UK (2022)*. **Awarded 3rd Best Poster**.

## 7.3 Ethics approval letter

Ymchwil Iechyd a Gofal Cymru
Health and Care Research Wales

NHS
Health Research Authority

Dr Nick Peake
Senior Lecturer
Sheffield Hallam University
Biomolecular Research Centre
Faculty of Health & Wellbeing
Howard Street, Sheffield
S1 1WB

Email: approvals@hra.nhs.uk
HCRW.approvals@wales.nhs.uk

20 May 2020

Dear Dr Peake

**HRA and Health and Care Research Wales (HCRW) Approval Letter**

| | |
|---|---|
| **Study title:** | **Extracellular vesicles - key mediators and potential biomarkers in colorectal cancer patients.** |
| **IRAS project ID:** | **244453** |
| **REC reference:** | **19/NI/0221** |
| **Sponsor** | **Sheffield Teaching Hospitals NHS FT** |

I am pleased to confirm that HRA and Health and Care Research Wales (HCRW) Approval has been given for the above referenced study, on the basis described in the application form, protocol, supporting documentation and any clarifications received. You should not expect to receive anything further relating to this application.

Please now work with participating NHS organisations to confirm capacity and capability, in line with the instructions provided in the "Information to support study set up" section towards the end of this letter.

**How should I work with participating NHS/HSC organisations in Northern Ireland and Scotland?**
HRA and HCRW Approval does not apply to NHS/HSC organisations within Northern Ireland and Scotland.

If you indicated in your IRAS form that you do have participating organisations in either of these devolved administrations, the final document set and the study wide governance report (including this letter) have been sent to the coordinating centre of each participating nation. The relevant national coordinating function/s will contact you as appropriate.

Please see IRAS Help for information on working with NHS/HSC organisations in Northern Ireland and Scotland.

**How should I work with participating non-NHS organisations?**
HRA and HCRW Approval does not apply to non-NHS organisations. You should work with your non-NHS organisations to obtain local agreement in accordance with their procedures.

**What are my notification responsibilities during the study?**

The standard conditions document "*After Ethical Review – guidance for sponsors and investigators*", issued with your REC favourable opinion, gives detailed guidance on reporting expectations for studies, including:

- Registration of research
- Notifying amendments
- Notifying the end of the study

The HRA website also provides guidance on these topics, and is updated in the light of changes in reporting expectations or procedures.

**Who should I contact for further information?**
Please do not hesitate to contact me for assistance with this application. My contact details are below.

Your IRAS project ID is **244453**. Please quote this on all correspondence.

Yours sincerely,

Helen Poole
Approvals Specialist

Email: approvals@hra.nhs.uk

*Copy to:* *Dr Modhumita Harris, Sheffield Teaching Hospitals NHS FT*

# 8 References


Abdouh, M., Floris, M., Gao, Z.-H., Arena, V., Arena, M., & Arena, G. O. (2019). Colorectal cancer-derived extracellular vesicles induce transformation of fibroblasts into colon carcinoma cells. *Journal of Experimental & Clinical Cancer Research*, *38*(1), 257. https://doi.org/10.1186/s13046-019-1248-2

Affo, S., Yu, L.-X., & Schwabe, R. F. (2017). The Role of Cancer-Associated Fibroblasts and Fibrosis in Liver Cancer. *Annual Review of Pathology: Mechanisms of Disease*, *12*(1), 153–186. https://doi.org/10.1146/annurev-pathol-052016-100322

Aizawa, T., Karasawa, H., Funayama, R., Shirota, M., Suzuki, T., Maeda, S., Suzuki, H., Yamamura, A., Naitoh, T., Nakayama, K., & Unno, M. (2019). Cancer-associated fibroblasts secrete Wnt2 to promote cancer progression in colorectal cancer. *Cancer Medicine*, *8*(14), 6370–6382. https://doi.org/10.1002/cam4.2523

Akagi, K., Ikeda, Y., Miyazaki, M., Abe, T., Kinoshita, J., Maehara, Y., & Sugimachi, K. (2000). Vascular endothelial growth factor-C (VEGF-C) expression in human colorectal cancer tissues. *British Journal of Cancer*, *83*(7), 887–891. https://doi.org/10.1054/bjoc.2000.1396

Akao, Y., Khoo, F., Kumazaki, M., Shinohara, H., Miki, K., & Yamada, N. (2014). Extracellular Disposal of Tumor-Suppressor miRs-145 and -34a via Microvesicles and 5-FU Resistance of Human Colon Cancer Cells. *International Journal of Molecular Sciences*, *15*(1), 1392–1401. https://doi.org/10.3390/ijms15011392

Akbar, A., Malekian, F., Baghban, N., Kodam, S. P., & Ullah, M. (2022). Methodologies to Isolate and Purify Clinical Grade Extracellular Vesicles for Medical Applications. *Cells*, *11*(2), 186. https://doi.org/10.3390/cells11020186

Akhtar, M., Haider, A., Rashid, S., & Al-Nabet, A. D. M. H. (2019). Paget's "Seed and Soil" Theory of Cancer Metastasis: An Idea Whose Time has Come. *Advances in Anatomic Pathology*, *26*(1), 69–74. https://doi.org/10.1097/PAP.0000000000000219

Al Halawani, A., Mithieux, S. M., Yeo, G. C., Hosseini-Beheshti, E., & Weiss, A. S. (2022). Extracellular Vesicles: Interplay with the Extracellular Matrix and Modulated Cell Responses. *International Journal of Molecular Sciences*, *23*(6), 3389. https://doi.org/10.3390/ijms23063389

Alečković, M., Wei, Y., LeRoy, G., Sidoli, S., Liu, D. D., Garcia, B. A., & Kang, Y. (2017). Identification of Nidogen 1 as a lung metastasis protein through secretome analysis. *Genes & Development*, *31*(14), 1439–1455. https://doi.org/10.1101/gad.301937.117

Al-Nedawi, K., Meehan, B., Micallef, J., Lhotak, V., May, L., Guha, A., & Rak, J. (2008). Intercellular transfer of the oncogenic receptor EGFRvIII by microvesicles derived from tumour cells. *Nature Cell Biology*, *10*(5), 619–624. https://doi.org/10.1038/ncb1725

Al-Ostoot, F. H., Salah, S., Khamees, H. A., & Khanum, S. A. (2021). Tumor angiogenesis: Current challenges and therapeutic opportunities. *Cancer Treatment and Research Communications*, *28*, 100422. https://doi.org/10.1016/j.ctarc.2021.100422

Angel, P. M., Schwamborn, K., Comte-Walters, S., Clift, C. L., Ball, L. E., Mehta, A. S., & Drake, R. R. (2019). Extracellular Matrix Imaging of Breast Tissue Pathologies by MALDI–Imaging Mass Spectrometry. *PROTEOMICS – Clinical Applications*, *13*(1), 1700152. https://doi.org/10.1002/prca.201700152

Antonyak, M. A., Li, B., Boroughs, L. K., Johnson, J. L., Druso, J. E., Bryant, K. L., Holowka, D. A., & Cerione, R. A. (2011). Cancer cell-derived microvesicles induce transformation by transferring tissue transglutaminase and fibronectin to recipient cells. *Proceedings of the National Academy of Sciences*, *108*(12), 4852–4857. https://doi.org/10.1073/pnas.1017667108

Artuyants, A., Chang, V., Reshef, G., Blenkiron, C., Chamley, L. W., Leung, E., & Hisey, C. L. (2021). *Production of Extracellular Vesicles Using a CELLine Adherent Bioreactor Flask* (pp. 183–192). https://doi.org/10.1007/7651_2021_413

Asano, T., Tada, M., Cheng, S., Takemoto, N., Kuramae, T., Abe, M., Takahashi, O., Miyamoto, M., Hamada, J.-I., Moriuchi, T., & Kondo, S. (2008).

Prognostic Values of Matrix Metalloproteinase Family Expression in Human Colorectal Carcinoma. *Journal of Surgical Research*, *146*(1), 32–42. https://doi.org/10.1016/j.jss.2007.02.011

Atkin-Smith, G. K., Miles, M. A., Tixeira, R., Lay, F. T., Duan, M., Hawkins, C. J., Phan, T. K., Paone, S., Mathivanan, S., Hulett, M. D., Chen, W., & Poon, I. K. H. (2019). Plexin B2 Is a Regulator of Monocyte Apoptotic Cell Disassembly. *Cell Reports*, *29*(7), 1821-1831.e3. https://doi.org/10.1016/j.celrep.2019.10.014

Aung, T., Chapuy, B., Vogel, D., Wenzel, D., Oppermann, M., Lahmann, M., Weinhage, T., Menck, K., Hupfeld, T., Koch, R., Trümper, L., & Wulf, G. G. (2011). Exosomal evasion of humoral immunotherapy in aggressive B-cell lymphoma modulated by ATP-binding cassette transporter A3. *Proceedings of the National Academy of Sciences*, *108*(37), 15336–15341. https://doi.org/10.1073/pnas.1102855108

Axelrad, J. E., & Shah, S. C. (2020). Diagnosis and management of inflammatory bowel disease-associated neoplasia: considerations in the modern era. *Therapeutic Advances in Gastroenterology*, *13*, 175628482092077. https://doi.org/10.1177/1756284820920779

Azubuike, U. F., & Tanner, K. (2023). Biophysical determinants of cancer organotropism. *Trends in Cancer*, *9*(3), 188–197. https://doi.org/10.1016/j.trecan.2022.11.002

Baker, A.-M., Cox, T. R., Bird, D., Lang, G., Murray, G. I., Sun, X.-F., Southall, S. M., Wilson, J. R., & Erler, J. T. (2011). The Role of Lysyl Oxidase in SRC-Dependent Proliferation and Metastasis of Colorectal Cancer. *JNCI: Journal of the National Cancer Institute*, *103*(5), 407–424. https://doi.org/10.1093/jnci/djq569

Baker, L., Robinson, N., Wilson, D., Tabaqchali, M., & Leaper, D. (2019). Vascular endothelial growth factor in colorectal cancer pathology, survival and treatment. *Annals of Oncology*, *30*, v12. https://doi.org/10.1093/annonc/mdz238.039

Balkwill, F. R., Capasso, M., & Hagemann, T. (2012). The tumor microenvironment at a glance. *Journal of Cell Science*, *125*(23), 5591–5596. https://doi.org/10.1242/jcs.116392

Baruffaldi, D., Palmara, G., Pirri, C., & Frascella, F. (2021). 3D Cell Culture: Recent Development in Materials with Tunable Stiffness. *ACS Applied Bio Materials*, *4*(3), 2233–2250. https://doi.org/10.1021/acsabm.0c01472

Batlle, E., & Clevers, H. (2017). Cancer stem cells revisited. *Nature Medicine*, *23*(10), 1124–1134. https://doi.org/10.1038/nm.4409

Bauleth-Ramos, T., Feijão, T., Gonçalves, A., Shahbazi, M.-A., Liu, Z., Barrias, C., Oliveira, M. J., Granja, P., Santos, H. A., & Sarmento, B. (2020). Colorectal cancer triple co-culture spheroid model to assess the biocompatibility and anticancer properties of polymeric nanoparticles. *Journal of Controlled Release*, *323*, 398–411. https://doi.org/10.1016/j.jconrel.2020.04.025

Beninati, S., Piacentini, M., & Bergamini, C. M. (2017). Transglutaminase 2, a double face enzyme. *Amino Acids*, *49*(3), 415–423. https://doi.org/10.1007/s00726-017-2394-5

Bhatia, S. N., & Ingber, D. E. (2014). Microfluidic organs-on-chips. *Nature Biotechnology*, *32*(8), 760–772. https://doi.org/10.1038/nbt.2989

Bhave, M. S., Hassanbhai, A. M., Anand, P., Luo, K. Q., & Teoh, S. H. (2015). Effect of Heat-Inactivated Clostridium sporogenes and Its Conditioned Media on 3-Dimensional Colorectal Cancer Cell Models. *Scientific Reports*, *5*(1), 15681. https://doi.org/10.1038/srep15681

Bhedi, C. D., Nasirova, S., Toksoz, D., Warburton, R. R., Morine, K. J., Kapur, N. K., Galper, J. B., Preston, I. R., Hill, N. S., Fanburg, B. L., & Penumatsa, K. C. (2020). Glycolysis regulated transglutaminase 2 activation in cardiopulmonary fibrogenic remodeling. *The FASEB Journal*, *34*(1), 930–944. https://doi.org/10.1096/fj.201902155R

Bhome, R., Emaduddin, M., James, V., House, L. M., Thirdborough, S. M., Mellone, M., Tulkens, J., Primrose, J. N., Thomas, G. J., De Wever, O., Mirnezami, A. H., & Sayan, A. E. (2022). Epithelial to mesenchymal transition influences fibroblast phenotype in colorectal cancer by altering miR-200

levels in extracellular vesicles. *Journal of Extracellular Vesicles*, *11*(5). https://doi.org/10.1002/jev2.12226

Bonnet, D., & Dick, J. E. (1997). Human acute myeloid leukemia is organized as a hierarchy that originates from a primitive hematopoietic cell. *Nature Medicine*, *3*(7), 730–737. https://doi.org/10.1038/nm0797-730

Botta, G. P., Reginato, M. J., Reichert, M., Rustgi, A. K., & Lelkes, P. I. (2012). Constitutive *K - Ras* G12D Activation of ERK2 Specifically Regulates 3D Invasion of Human Pancreatic Cancer Cells via MMP-1. *Molecular Cancer Research*, *10*(2), 183–196. https://doi.org/10.1158/1541-7786.MCR-11-0399

Boyle, S. T., Johan, M. Z., & Samuel, M. S. (2020). Tumour-directed microenvironment remodelling at a glance. *Journal of Cell Science*, *133*(24). https://doi.org/10.1242/jcs.247783

Brauchle, E., Kasper, J., Daum, R., Schierbaum, N., Falch, C., Kirschniak, A., Schäffer, T. E., & Schenke-Layland, K. (2018). Biomechanical and biomolecular characterization of extracellular matrix structures in human colon carcinomas. *Matrix Biology*, *68–69*, 180–193. https://doi.org/10.1016/j.matbio.2018.03.016

Brennan, K., Martin, K., FitzGerald, S. P., O'Sullivan, J., Wu, Y., Blanco, A., Richardson, C., & Mc Gee, M. M. (2020). A comparison of methods for the isolation and separation of extracellular vesicles from protein and lipid particles in human serum. *Scientific Reports*, *10*(1), 1039. https://doi.org/10.1038/s41598-020-57497-7

Breslin, S., & O'Driscoll, L. (2016). The relevance of using 3D cell cultures, in addition to 2D monolayer cultures, when evaluating breast cancer drug sensitivity and resistance. *Oncotarget*, *7*(29), 45745–45756. https://doi.org/10.18632/oncotarget.9935

Bretthauer, M., Løberg, M., Wieszczy, P., Kalager, M., Emilsson, L., Garborg, K., Rupinski, M., Dekker, E., Spaander, M., Bugajski, M., Holme, Ø., Zauber, A. G., Pilonis, N. D., Mroz, A., Kuipers, E. J., Shi, J., Hernán, M. A., Adami, H.-O., Regula, J., … Kaminski, M. F. (2022). Effect of Colonoscopy Screening

on Risks of Colorectal Cancer and Related Death. *New England Journal of Medicine*, *387*(17), 1547–1556. https://doi.org/10.1056/NEJMoa2208375

Brisson, B. K., Mauldin, E. A., Lei, W., Vogel, L. K., Power, A. M., Lo, A., Dopkin, D., Khanna, C., Wells, R. G., Puré, E., & Volk, S. W. (2015). Type III Collagen Directs Stromal Organization and Limits Metastasis in a Murine Model of Breast Cancer. *The American Journal of Pathology*, *185*(5), 1471–1486. https://doi.org/10.1016/j.ajpath.2015.01.029

Bruner, H. C., & Derksen, P. W. B. (2018). Loss of E-Cadherin-Dependent Cell–Cell Adhesion and the Development and Progression of Cancer. *Cold Spring Harbor Perspectives in Biology*, *10*(3), a029330. https://doi.org/10.1101/cshperspect.a029330

Buchberger, A. R., DeLaney, K., Johnson, J., & Li, L. (2018). Mass Spectrometry Imaging: A Review of Emerging Advancements and Future Insights. *Analytical Chemistry*, *90*(1), 240–265. https://doi.org/10.1021/acs.analchem.7b04733

Buntsma, N. C., Gąsecka, A., Roos, Y. B. W. E. M., van Leeuwen, T. G., van der Pol, E., & Nieuwland, R. (2022). EDTA stabilizes the concentration of platelet-derived extracellular vesicles during blood collection and handling. *Platelets*, *33*(5), 764–771. https://doi.org/10.1080/09537104.2021.1991569

Calon, A., Tauriello, D. V. F., & Batlle, E. (2014). TGF-beta in CAF-mediated tumor growth and metastasis. *Seminars in Cancer Biology*, *25*, 15–22. https://doi.org/10.1016/j.semcancer.2013.12.008

Cannon, A., Thompson, C., Hall, B. R., Jain, M., Kumar, S., & Batra, S. K. (2018). Desmoplasia in pancreatic ductal adenocarcinoma: insight into pathological function and therapeutic potential. *Genes & Cancer*, *9*(3–4), 78–86. https://doi.org/10.18632/genesandcancer.171

Cao, M., Ning, J., Hernandez-Lara, C. I., Belzile, O., Wang, Q., Dutcher, S. K., Liu, Y., & Snell, W. J. (2015). Uni-directional ciliary membrane protein trafficking by a cytoplasmic retrograde IFT motor and ciliary ectosome shedding. *ELife*, *4*. https://doi.org/10.7554/eLife.05242

Cao, Z.-Q., Wang, Z., & Leng, P. (2019). Aberrant N-cadherin expression in cancer. *Biomedicine & Pharmacotherapy*, *118*, 109320. https://doi.org/10.1016/j.biopha.2019.109320

Carpino, G., Morini, S., Ginannicorradini, S., Franchitto, A., Merli, M., Siciliano, M., Gentili, F., Onettimuda, A., Berloco, P., & Rossi, M. (2005). Alpha-SMA expression in hepatic stellate cells and quantitative analysis of hepatic fibrosis in cirrhosis and in recurrent chronic hepatitis after liver transplantation. *Digestive and Liver Disease*, *37*(5), 349–356. https://doi.org/10.1016/j.dld.2004.11.009

Casasanta, M. A., Yoo, C. C., Udayasuryan, B., Sanders, B. E., Umaña, A., Zhang, Y., Peng, H., Duncan, A. J., Wang, Y., Li, L., Verbridge, S. S., & Slade, D. J. (2020). *Fusobacterium nucleatum* host-cell binding and invasion induces IL-8 and CXCL1 secretion that drives colorectal cancer cell migration. *Science Signaling*, *13*(641). https://doi.org/10.1126/scisignal.aba9157

Cattin, S., Ramont, L., & Rüegg, C. (2018). Characterization and In Vivo Validation of a Three-Dimensional Multi-Cellular Culture Model to Study Heterotypic Interactions in Colorectal Cancer Cell Growth, Invasion and Metastasis. *Frontiers in Bioengineering and Biotechnology*, *6*. https://doi.org/10.3389/fbioe.2018.00097

Caviglia, G. P., Garrone, A., Bertolino, C., Vanni, R., Bretto, E., Poshnjari, A., Tribocco, E., Frara, S., Armandi, A., Astegiano, M., Saracco, G. M., Bertolusso, L., & Ribaldone, D. G. (2023). Epidemiology of Inflammatory Bowel Diseases: A Population Study in a Healthcare District of North-West Italy. *Journal of Clinical Medicine*, *12*(2), 641. https://doi.org/10.3390/jcm12020641

Cavnar, M. J., Turcotte, S., Katz, S. C., Kuk, D., Gönen, M., Shia, J., Allen, P. J., Balachandran, V. P., D'Angelica, M. I., Kingham, T. P., Jarnagin, W. R., & DeMatteo, R. P. (2017). Tumor-Associated Macrophage Infiltration in Colorectal Cancer Liver Metastases is Associated With Better Outcome. *Annals of Surgical Oncology*, *24*(7), 1835–1842. https://doi.org/10.1245/s10434-017-5812-8

Cekanova, M., & Rathore, K. (2014). Animal models and therapeutic molecular targets of cancer: utility and limitations. *Drug Design, Development and Therapy*, 1911. https://doi.org/10.2147/DDDT.S49584

Cellura, D., Pickard, K., Quaratino, S., Parker, H., Strefford, J. C., Thomas, G. J., Mitter, R., Mirnezami, A. H., & Peake, N. J. (2015). miR-19–Mediated Inhibition of Transglutaminase-2 Leads to Enhanced Invasion and Metastasis in Colorectal Cancer. *Molecular Cancer Research*, *13*(7), 1095–1105. https://doi.org/10.1158/1541-7786.MCR-14-0466

Chaicharoenaudomrung, N., Kunhorm, P., & Noisa, P. (2019). Three-dimensional cell culture systems as an *in vitro* platform for cancer and stem cell modeling. *World Journal of Stem Cells*, *11*(12), 1065–1083. https://doi.org/10.4252/wjsc.v11.i12.1065

Chandrasekera, P., Perfetto, M., Lu, C., Zhuo, M., Bahudhanapati, H., Li, J., Chen, W.-C., Kulkarni, P., Christian, L., Liu, J., Yien, Y. Y., Yu, C., & Wei, S. (2022). Metalloprotease ADAM9 cleaves ephrin-B ligands and differentially regulates Wnt and mTOR signaling downstream of Akt kinase in colorectal cancer cells. *Journal of Biological Chemistry*, *298*(8), 102225. https://doi.org/10.1016/j.jbc.2022.102225

Chang, L.-C., Chiu, H.-M., Wu, M.-S., & Shen, T.-L. (2022). The Role of Small Extracellular Vesicles in the Progression of Colorectal Cancer and Its Clinical Applications. *International Journal of Molecular Sciences*, *23*(3), 1379. https://doi.org/10.3390/ijms23031379

Chang, W.-H., Cerione, R. A., & Antonyak, M. A. (2021). *Extracellular Vesicles and Their Roles in Cancer Progression* (pp. 143–170). https://doi.org/10.1007/978-1-0716-0759-6_10

Chen, J., Luo, Y., Zhou, Y., Qin, S., Qiu, Y., Cui, R., Yu, M., Qin, J., & Zhong, M. (2018). Promotion of Tumor Growth by ADAMTS4 in Colorectal Cancer: Focused on Macrophages. *Cellular Physiology and Biochemistry*, *46*(4), 1693–1703. https://doi.org/10.1159/000489245

Chen, M., Xu, R., Rai, A., Suwakulsiri, W., Izumikawa, K., Ishikawa, H., Greening, D. W., Takahashi, N., & Simpson, R. J. (2019). Distinct shed microvesicle and exosome microRNA signatures reveal diagnostic markers for colorectal

cancer. *PLOS ONE*, *14*(1), e0210003. https://doi.org/10.1371/journal.pone.0210003

Chen, S., Su, T., Zhang, Y., Lee, A., He, J., Ge, Q., Wang, L., Si, J., Zhuo, W., & Wang, L. (2020). *Fusobacterium nucleatum* promotes colorectal cancer metastasis by modulating *KRT7-AS* /KRT7. *Gut Microbes*, *11*(3), 511–525. https://doi.org/10.1080/19490976.2019.1695494

Chen, W., Hoffmann, A. D., Liu, H., & Liu, X. (2018). Organotropism: new insights into molecular mechanisms of breast cancer metastasis. *Npj Precision Oncology*, *2*(1), 4. https://doi.org/10.1038/s41698-018-0047-0

Chen, W., & Miao, C. (2022). KRT15 promotes colorectal cancer cell migration and invasion through β-catenin/MMP-7 signaling pathway. *Medical Oncology*, *39*(6), 68. https://doi.org/10.1007/s12032-021-01619-2

Chen, Y., Zhu, S., Liu, T., Zhang, S., Lu, J., Fan, W., Lin, L., Xiang, T., Yang, J., Zhao, X., Xi, Y., Ma, Y., Cheng, G., Lin, D., & Wu, C. (2023). Epithelial cells activate fibroblasts to promote esophageal cancer development. *Cancer Cell*, *41*(5), 903-918.e8. https://doi.org/10.1016/j.ccell.2023.03.001

Cheng, D., Jin, L., Chen, Y., Xi, X., & Guo, Y. (2020). YAP promotes epithelial mesenchymal transition by upregulating Slug expression in human colorectal cancer cells. *International Journal of Clinical and Experimental Pathology*, *13*(4), 701–710.

Cheteh, E. H., Sarne, V., Ceder, S., Bianchi, J., Augsten, M., Rundqvist, H., Egevad, L., Östman, A., & Wiman, K. G. (2020). Interleukin-6 derived from cancer-associated fibroblasts attenuates the p53 response to doxorubicin in prostate cancer cells. *Cell Death Discovery*, *6*(1), 42. https://doi.org/10.1038/s41420-020-0272-5

Chistiakov, D. A., Killingsworth, M. C., Myasoedova, V. A., Orekhov, A. N., & Bobryshev, Y. V. (2017). CD68/macrosialin: not just a histochemical marker. *Laboratory Investigation*, *97*(1), 4–13. https://doi.org/10.1038/labinvest.2016.116

Christianson, H. C., Svensson, K. J., van Kuppevelt, T. H., Li, J.-P., & Belting, M. (2013). Cancer cell exosomes depend on cell-surface heparan sulfate proteoglycans for their internalization and functional activity. *Proceedings of*

*the National Academy of Sciences*, *110*(43), 17380–17385. https://doi.org/10.1073/pnas.1304266110

Clift, C. L., Drake, R. R., Mehta, A., & Angel, P. M. (2021). Multiplexed imaging mass spectrometry of the extracellular matrix using serial enzyme digests from formalin-fixed paraffin-embedded tissue sections. *Analytical and Bioanalytical Chemistry*, *413*(10), 2709–2719. https://doi.org/10.1007/s00216-020-03047-z

Condello, S., Sima, L., Ivan, C., Cardenas, H., Schiltz, G., Mishra, R. K., & Matei, D. (2018). Tissue Tranglutaminase Regulates Interactions between Ovarian Cancer Stem Cells and the Tumor Niche. *Cancer Research*, *78*(11), 2990–3001. https://doi.org/10.1158/0008-5472.CAN-17-2319

Crapo, J. D., Barry, B. E., Gehr, P., Bachofen, M., & Weibel, E. R. (1982). Cell number and cell characteristics of the normal human lung. *The American Review of Respiratory Disease*, *126*(2), 332–337. https://doi.org/10.1164/arrd.1982.126.2.332

Cui, Y.-L., Li, H.-K., Zhou, H.-Y., Zhang, T., & Li, Q. (2013). Correlations of Tumor-associated Macrophage Subtypes with Liver Metastases of Colorectal Cancer. *Asian Pacific Journal of Cancer Prevention*, *14*(2), 1003–1007. https://doi.org/10.7314/APJCP.2013.14.2.1003

Das, S., & Johnson, D. B. (2019). Immune-related adverse events and anti-tumor efficacy of immune checkpoint inhibitors. *Journal for ImmunoTherapy of Cancer*, *7*(1), 306. https://doi.org/10.1186/s40425-019-0805-8

De Palma, F., D'Argenio, V., Pol, J., Kroemer, G., Maiuri, M., & Salvatore, F. (2019). The Molecular Hallmarks of the Serrated Pathway in Colorectal Cancer. *Cancers*, *11*(7), 1017. https://doi.org/10.3390/cancers11071017

de Ridder, J., de Wilt, J. H. W., Simmer, F., Overbeek, L., Lemmens, V., & Nagtegaal, I. (2016). Incidence and origin of histologically confirmed liver metastases: an explorative case-study of 23,154 patients. *Oncotarget*, *7*(34), 55368–55376. https://doi.org/10.18632/oncotarget.10552

De Smedt, L., Palmans, S., & Sagaert, X. (2016). Tumour budding in colorectal cancer: what do we know and what can we do? *Virchows Archiv*, *468*(4), 397–408. https://doi.org/10.1007/s00428-015-1886-5

Deep, G., Jain, A., Kumar, A., Agarwal, C., Kim, S., Leevy, W. M., & Agarwal, R. (2020). Exosomes secreted by prostate cancer cells under hypoxia promote matrix metalloproteinases activity at pre-metastatic niches. *Molecular Carcinogenesis*, *59*(3), 323–332. https://doi.org/10.1002/mc.23157

Dekker, E., Tanis, P. J., Vleugels, J. L. A., Kasi, P. M., & Wallace, M. B. (2019). Colorectal cancer. *The Lancet*, *394*(10207), 1467–1480. https://doi.org/10.1016/S0140-6736(19)32319-0

Delaine-Smith, R., Wright, N., Hanley, C., Hanwell, R., Bhome, R., Bullock, M., Drifka, C., Eliceiri, K., Thomas, G., Knight, M., Mirnezami, A., & Peake, N. (2019). Transglutaminase-2 Mediates the Biomechanical Properties of the Colorectal Cancer Tissue Microenvironment that Contribute to Disease Progression. *Cancers*, *11*(5), 701. https://doi.org/10.3390/cancers11050701

Deng, L., Jiang, N., Zeng, J., Wang, Y., & Cui, H. (2021). The Versatile Roles of Cancer-Associated Fibroblasts in Colorectal Cancer and Therapeutic Implications. *Frontiers in Cell and Developmental Biology*, *9*. https://doi.org/10.3389/fcell.2021.733270

Depciuch, J., Klębowski, B., Stec, M., Szatanek, R., Węglarczyk, K., Baj-Krzyworzeka, M., Parlińska-Wojtan, M., & Baran, J. (2020). Similarities in the General Chemical Composition of Colon Cancer Cells and Their Microvesicles Investigated by Spectroscopic Methods-Potential Clinical Relevance. *International Journal of Molecular Sciences*, *21*(5), 1826. https://doi.org/10.3390/ijms21051826

Deschepper, F. M., Zoppi, R., Pirro, M., Hensbergen, P. J., Dall'Olio, F., Kotsias, M., Gardner, R. A., Spencer, D. I. R., & Videira, P. A. (2020). L1CAM as an E-selectin Ligand in Colon Cancer. *International Journal of Molecular Sciences*, *21*(21), 8286. https://doi.org/10.3390/ijms21218286

De-Souza, A. S. C., & Costa-Casagrande, T. A. (2018). Animal Models for Colorectal Cancer. *ABCD. Arquivos Brasileiros de Cirurgia Digestiva (São Paulo)*, *31*(2). https://doi.org/10.1590/0102-672020180001e1369

Dhami, S. P. S., Patmore, S., Comerford, C., Byrne, C. M., Cavanagh, B., Castle, J., Kirwan, C. C., Kenny, M., Schoen, I., O'Donnell, J. S., & O'Sullivan, J. M. (2022). Breast cancer cells mediate endothelial cell activation, promoting von

Willebrand factor release, tumor adhesion, and transendothelial migration. *Journal of Thrombosis and Haemostasis*, *20*(10), 2350–2365. https://doi.org/10.1111/jth.15794

Di Martino, J. S., Nobre, A. R., Mondal, C., Taha, I., Farias, E. F., Fertig, E. J., Naba, A., Aguirre-Ghiso, J. A., & Bravo-Cordero, J. J. (2021). A tumor-derived type III collagen-rich ECM niche regulates tumor cell dormancy. *Nature Cancer*, *3*(1), 90–107. https://doi.org/10.1038/s43018-021-00291-9

Diaz-Hidalgo, L., Altuntas, S., Rossin, F., D'Eletto, M., Marsella, C., Farrace, M. G., Falasca, L., Antonioli, M., Fimia, G. M., & Piacentini, M. (2016). Transglutaminase type 2-dependent selective recruitment of proteins into exosomes under stressful cellular conditions. *Biochimica et Biophysica Acta (BBA) - Molecular Cell Research*, *1863*(8), 2084–2092. https://doi.org/10.1016/j.bbamcr.2016.05.005

Ding, C., Yu, Z., Li, X., Zhu, J., Dai, M., & He, Q. (2023). Collagen type VII α1 chain: A promising prognostic and immune infiltration biomarker of pancreatic cancer. *Oncology Letters*, *25*(2), 77. https://doi.org/10.3892/ol.2023.13663

Dmitrieva, N. I., & Burg, M. B. (2014). Secretion of von Willebrand factor by endothelial cells links sodium to hypercoagulability and thrombosis. *Proceedings of the National Academy of Sciences*, *111*(17), 6485–6490. https://doi.org/10.1073/pnas.1404809111

Doglioni, G., Parik, S., & Fendt, S.-M. (2019). Interactions in the (Pre)metastatic Niche Support Metastasis Formation. *Frontiers in Oncology*, *9*. https://doi.org/10.3389/fonc.2019.00219

Dong, G., Chen, P., Xu, Y., Liu, T., & Yin, R. (2023). Cancer-associated fibroblasts: Key criminals of tumor pre-metastatic niche. *Cancer Letters*, *566*, 216234. https://doi.org/10.1016/j.canlet.2023.216234

Dong, L., Zieren, R. C., Horie, K., Kim, C., Mallick, E., Jing, Y., Feng, M., Kuczler, M. D., Green, J., Amend, S. R., Witwer, K. W., de Reijke, T. M., Cho, Y., Pienta, K. J., & Xue, W. (2020). Comprehensive evaluation of methods for small extracellular vesicles separation from human plasma, urine and cell

culture medium. *Journal of Extracellular Vesicles*, *10*(2). https://doi.org/10.1002/jev2.12044

Dong, Q., Liu, X., Cheng, K., Sheng, J., Kong, J., & Liu, T. (2021). Pre-metastatic Niche Formation in Different Organs Induced by Tumor Extracellular Vesicles. *Frontiers in Cell and Developmental Biology*, *9*. https://doi.org/10.3389/fcell.2021.733627

Doolin, M. T., Smith, I. M., & Stroka, K. M. (2021). Fibroblast to myofibroblast transition is enhanced by increased cell density. *Molecular Biology of the Cell*, *32*(22). https://doi.org/10.1091/mbc.E20-08-0536

Dou, R., Liu, K., Yang, C., Zheng, J., Shi, D., Lin, X., Wei, C., Zhang, C., Fang, Y., Huang, S., Song, J., Wang, S., & Xiong, B. (2021). EMT-cancer cells-derived exosomal miR-27b-3p promotes circulating tumour cells-mediated metastasis by modulating vascular permeability in colorectal cancer. *Clinical and Translational Medicine*, *11*(12). https://doi.org/10.1002/ctm2.595

Doubeni, C. A., Corley, D. A., Quinn, V. P., Jensen, C. D., Zauber, A. G., Goodman, M., Johnson, J. R., Mehta, S. J., Becerra, T. A., Zhao, W. K., Schottinger, J., Doria-Rose, V. P., Levin, T. R., Weiss, N. S., & Fletcher, R. H. (2018). Effectiveness of screening colonoscopy in reducing the risk of death from right and left colon cancer: a large community-based study. *Gut*, *67*(2), 291–298. https://doi.org/10.1136/gutjnl-2016-312712

Dugina, V., Alexandrova, A., Chaponnier, C., Vasiliev, J., & Gabbiani, G. (1998). Rat Fibroblasts Cultured from Various Organs Exhibit Differences in α-Smooth Muscle Actin Expression, Cytoskeletal Pattern, and Adhesive Structure Organization. *Experimental Cell Research*, *238*(2), 481–490. https://doi.org/10.1006/excr.1997.3868

Duval, K., Grover, H., Han, L.-H., Mou, Y., Pegoraro, A. F., Fredberg, J., & Chen, Z. (2017). Modeling Physiological Events in 2D vs. 3D Cell Culture. *Physiology*, *32*(4), 266–277. https://doi.org/10.1152/physiol.00036.2016

Eckert, R. L. (2019). Transglutaminase 2 takes center stage as a cancer cell survival factor and therapy target. *Molecular Carcinogenesis*, *58*(6), 837–853. https://doi.org/10.1002/mc.22986

Elwakeel, E., & Weigert, A. (2021). Breast Cancer CAFs: Spectrum of Phenotypes and Promising Targeting Avenues. *International Journal of Molecular Sciences*, *22*(21), 11636. https://doi.org/10.3390/ijms222111636

Endzelins, E., Ābols, A., Buss, A., Zandberga, E., Palviaien, M., Siljander, P., & Line, A. (2018). Extracellular Vesicles Derived from Hypoxic Colorectal Cancer Cells Confer Metastatic Phenotype to Non-metastatic Cancer Cells. *Anticancer Research*, *38*(9), 5139–5147. https://doi.org/10.21873/anticanres.12836

Engen, P. A., Green, S. J., Voigt, R. M., Forsyth, C. B., & Keshavarzian, A. (2015). The Gastrointestinal Microbiome: Alcohol Effects on the Composition of Intestinal Microbiota. *Alcohol Research : Current Reviews*, *37*(2), 223–236.

Escalona, R. M., Bilandzic, M., Western, P., Kadife, E., Kannourakis, G., Findlay, J. K., & Ahmed, N. (2020). TIMP-2 regulates proliferation, invasion and STAT3-mediated cancer stem cell-dependent chemoresistance in ovarian cancer cells. *BMC Cancer*, *20*(1), 960. https://doi.org/10.1186/s12885-020-07274-6

Fares, J., Fares, M. Y., Khachfe, H. H., Salhab, H. A., & Fares, Y. (2020). Molecular principles of metastasis: a hallmark of cancer revisited. *Signal Transduction and Targeted Therapy*, *5*(1), 28. https://doi.org/10.1038/s41392-020-0134-x

Feagins, L. A., Souza, R. F., & Spechler, S. J. (2009). Carcinogenesis in IBD: potential targets for the prevention of colorectal cancer. *Nature Reviews Gastroenterology & Hepatology*, *6*(5), 297–305. https://doi.org/10.1038/nrgastro.2009.44

Fesus, L., & Piacentini, M. (2002). Transglutaminase 2: an enigmatic enzyme with diverse functions. *Trends in Biochemical Sciences*, *27*(10), 534–539. https://doi.org/10.1016/S0968-0004(02)02182-5

Field, K. (2007). Metastatic colorectal cancer-past, progress and future. *World Journal of Gastroenterology*, *13*(28), 3806. https://doi.org/10.3748/wjg.v13.i28.3806

Filipiak-Duliban, A., Brodaczewska, K., Kajdasz, A., & Kieda, C. (2022). Spheroid Culture Differentially Affects Cancer Cell Sensitivity to Drugs in Melanoma

and RCC Models. *International Journal of Molecular Sciences*, *23*(3), 1166. https://doi.org/10.3390/ijms23031166

Fingleton, B. (2008). MMPs as therapeutic targets—Still a viable option? *Seminars in Cell & Developmental Biology*, *19*(1), 61–68. https://doi.org/10.1016/j.semcdb.2007.06.006

Flint, L. E., Hamm, G., Ready, J. D., Ling, S., Duckett, C. J., Cross, N. A., Cole, L. M., Smith, D. P., Goodwin, R. J. A., & Clench, M. R. (2020). Characterization of an Aggregated Three-Dimensional Cell Culture Model by Multimodal Mass Spectrometry Imaging. *Analytical Chemistry*, *92*(18), 12538–12547. https://doi.org/10.1021/acs.analchem.0c02389

Foster, D. S., Januszyk, M., Delitto, D., Yost, K. E., Griffin, M., Guo, J., Guardino, N., Delitto, A. E., Chinta, M., Burcham, A. R., Nguyen, A. T., Bauer-Rowe, K. E., Titan, A. L., Salhotra, A., Jones, R. E., da Silva, O., Lindsay, H. G., Berry, C. E., Chen, K., … Longaker, M. T. (2022). Multiomic analysis reveals conservation of cancer-associated fibroblast phenotypes across species and tissue of origin. *Cancer Cell*, *40*(11), 1392-1406.e7. https://doi.org/10.1016/j.ccell.2022.09.015

Franchi-Mendes, T., Lopes, N., & Brito, C. (2021). Heterotypic Tumor Spheroids in Agitation-Based Cultures: A Scaffold-Free Cell Model That Sustains Long-Term Survival of Endothelial Cells. *Frontiers in Bioengineering and Biotechnology*, *9*. https://doi.org/10.3389/fbioe.2021.649949

Francia, G., Cruz-Munoz, W., Man, S., Xu, P., & Kerbel, R. S. (2011). Mouse models of advanced spontaneous metastasis for experimental therapeutics. *Nature Reviews Cancer*, *11*(2), 135–141. https://doi.org/10.1038/nrc3001

Franzen, C. A., Blackwell, R. H., Todorovic, V., Greco, K. A., Foreman, K. E., Flanigan, R. C., Kuo, P. C., & Gupta, G. N. (2015). Urothelial cells undergo epithelial-to-mesenchymal transition after exposure to muscle invasive bladder cancer exosomes. *Oncogenesis*, *4*(8), e163–e163. https://doi.org/10.1038/oncsis.2015.21

Freeman, K., Ryan, R., Parsons, N., Taylor-Phillips, S., Willis, B. H., & Clarke, A. (2021). The incidence and prevalence of inflammatory bowel disease in UK primary care: a retrospective cohort study of the IQVIA Medical Research

Database. *BMC Gastroenterology*, *21*(1), 139. https://doi.org/10.1186/s12876-021-01716-6

Friberg, S., & Nystrom, A. (2015). Cancer Metastases: Early Dissemination and Late Recurrences. *Cancer Growth and Metastasis*, *8*, CGM.S31244. https://doi.org/10.4137/CGM.S31244

Friedl, P. (2004). Prespecification and plasticity: shifting mechanisms of cell migration. *Current Opinion in Cell Biology*, *16*(1), 14–23. https://doi.org/10.1016/j.ceb.2003.11.001

Friedl, P., Locker, J., Sahai, E., & Segall, J. E. (2012). Classifying collective cancer cell invasion. *Nature Cell Biology*, *14*(8), 777–783. https://doi.org/10.1038/ncb2548

Froeling, F. E. M., Mirza, T. A., Feakins, R. M., Seedhar, A., Elia, G., Hart, I. R., & Kocher, H. M. (2009). Organotypic Culture Model of Pancreatic Cancer Demonstrates that Stromal Cells Modulate E-Cadherin, β-Catenin, and Ezrin Expression in Tumor Cells. *The American Journal of Pathology*, *175*(2), 636–648. https://doi.org/10.2353/ajpath.2009.090131

Fujiyoshi, K., Väyrynen, J. P., Borowsky, J., Papke, D. J., Arima, K., Haruki, K., Kishikawa, J., Akimoto, N., Ugai, T., Lau, M. C., Gu, S., Shi, S., Zhao, M., Da Silva, A. F. L., Twombly, T. S., Nan, H., Meyerhardt, J. A., Song, M., Zhang, X., … Ogino, S. (2020). Tumour budding, poorly differentiated clusters, and T-cell response in colorectal cancer. *EBioMedicine*, *57*, 102860. https://doi.org/10.1016/j.ebiom.2020.102860

Furini, G., Burhan, I., Huang, L., Savoca, M. P., Atobatele, A., Johnson, T., & Verderio, E. A. M. (2020). Insights into the heparan sulphate-dependent externalisation of transglutaminase-2 (TG2) in glucose-stimulated proximal-like tubular epithelial cells. *Analytical Biochemistry*, *603*, 113628. https://doi.org/10.1016/j.ab.2020.113628

Gaggioli, C., Hooper, S., Hidalgo-Carcedo, C., Grosse, R., Marshall, J. F., Harrington, K., & Sahai, E. (2007). Fibroblast-led collective invasion of carcinoma cells with differing roles for RhoGTPases in leading and following cells. *Nature Cell Biology*, *9*(12), 1392–1400. https://doi.org/10.1038/ncb1658

Ganesh, K., Stadler, Z. K., Cercek, A., Mendelsohn, R. B., Shia, J., Segal, N. H., & Diaz, L. A. (2019). Immunotherapy in colorectal cancer: rationale, challenges and potential. *Nature Reviews Gastroenterology & Hepatology*, *16*(6), 361–375. https://doi.org/10.1038/s41575-019-0126-x

Garam, N., Maláti, É., Sinkovits, G., Gombos, T., Szederjesi, A., Barabás, L., Gráf, L., Kocsis, J., & Prohászka, Z. (2018). Platelet Count, ADAMTS13 Activity, von Willebrand Factor Level and Survival in Patients with Colorectal Cancer: 5-Year Follow-up Study. *Thrombosis and Haemostasis*, *118*(01), 123–131. https://doi.org/10.1160/TH17-07-0548

Garcia-Hernandez, A., Reyes-Uribe, E., Arce-Salinas, C., de la Cruz-Lopez, K.-G., Manzo-Merino, J., Guzman-Ortiz, A.-L., Quezada, H., Cortes-Reynosa, P., Breton-Mora, F., Elizalde-Acosta, I., Thompson-Bonilla, R., & Salazar, E. P. (2022). Extracellular vesicles from blood of breast cancer women induce angiogenic processes in HUVECs. *Tissue and Cell*, *76*, 101814. https://doi.org/10.1016/j.tice.2022.101814

Giusti, I., Di Francesco, M., Poppa, G., Esposito, L., D'Ascenzo, S., & Dolo, V. (2022). Tumor-Derived Extracellular Vesicles Activate Normal Human Fibroblasts to a Cancer-Associated Fibroblast-Like Phenotype, Sustaining a Pro-Tumorigenic Microenvironment. *Frontiers in Oncology*, *12*. https://doi.org/10.3389/fonc.2022.839880

Glimelius, B., Norling, B., Nederman, T., & Carlsson, J. (1988). Extracellular matrices in multicellular spheroids of human glioma origin: Increased incorporation of proteoglycans and flbronectin as compared to monolayer cultures. *APMIS*, *96*(1–6), 433–444. https://doi.org/10.1111/j.1699-0463.1988.tb05327.x

Goliwas, K. F., Ashraf, H. M., Wood, A. M., Wang, Y., Hough, K. P., Bodduluri, S., Athar, M., Berry, J. L., Ponnazhagan, S., Thannickal, V. J., & Deshane, J. S. (2021). Extracellular Vesicle Mediated Tumor-Stromal Crosstalk Within an Engineered Lung Cancer Model. *Frontiers in Oncology*, *11*. https://doi.org/10.3389/fonc.2021.654922

Golshani, G., & Zhang, Y. (2020). Advances in immunotherapy for colorectal cancer: a review. *Therapeutic Advances in Gastroenterology*, *13*, 175628482091752. https://doi.org/10.1177/1756284820917527

Gong, Y., Scott, E., Lu, R., Xu, Y., Oh, W. K., & Yu, Q. (2013). TIMP-1 Promotes Accumulation of Cancer Associated Fibroblasts and Cancer Progression. *PLoS ONE*, *8*(10), e77366. https://doi.org/10.1371/journal.pone.0077366

Gordon-Weeks, A., Lim, S. Y., Yuzhalin, A., Lucotti, S., Vermeer, J. A. F., Jones, K., Chen, J., & Muschel, R. J. (2019). Tumour-Derived Laminin α5 (LAMA5) Promotes Colorectal Liver Metastasis Growth, Branching Angiogenesis and Notch Pathway Inhibition. *Cancers*, *11*(5), 630. https://doi.org/10.3390/cancers11050630

Goulet, C. R., Champagne, A., Bernard, G., Vandal, D., Chabaud, S., Pouliot, F., & Bolduc, S. (2019). Cancer-associated fibroblasts induce epithelial–mesenchymal transition of bladder cancer cells through paracrine IL-6 signalling. *BMC Cancer*, *19*(1), 137. https://doi.org/10.1186/s12885-019-5353-6

Greening, D. W., Gopal, S. K., Mathias, R. A., Liu, L., Sheng, J., Zhu, H.-J., & Simpson, R. J. (2015). Emerging roles of exosomes during epithelial–mesenchymal transition and cancer progression. *Seminars in Cell & Developmental Biology*, *40*, 60–71. https://doi.org/10.1016/j.semcdb.2015.02.008

Grenard, P., Bresson-Hadni, S., El Alaoui, S., Chevallier, M., Vuitton, D. A., & Ricard-Blum, S. (2001). Transglutaminase-mediated cross-linking is involved in the stabilization of extracellular matrix in human liver fibrosis. *Journal of Hepatology*, *35*(3), 367–375. https://doi.org/10.1016/S0168-8278(01)00135-0

Groseclose, M. R., Massion, P. P., Chaurand, P., & Caprioli, R. M. (2008). High-throughput proteomic analysis of formalin-fixed paraffin-embedded tissue microarrays using MALDI imaging mass spectrometry. *PROTEOMICS*, *8*(18), 3715–3724. https://doi.org/10.1002/pmic.200800495

Gui, X., Yang, Z., & Li, M. D. (2021). Effect of Cigarette Smoke on Gut Microbiota: State of Knowledge. *Frontiers in Physiology*, *12*. https://doi.org/10.3389/fphys.2021.673341

Gunaydin, G. (2021). CAFs Interacting With TAMs in Tumor Microenvironment to Enhance Tumorigenesis and Immune Evasion. *Frontiers in Oncology*, *11*. https://doi.org/10.3389/fonc.2021.668349

Gupta, S. (2022). Screening for Colorectal Cancer. *Hematology/Oncology Clinics of North America*, *36*(3), 393–414. https://doi.org/10.1016/j.hoc.2022.02.001

Hadjipanayi, E., Mudera, V., & Brown, R. A. (2009). Guiding cell migration in 3D: A collagen matrix with graded directional stiffness. *Cell Motility and the Cytoskeleton*, *66*(3), 121–128. https://doi.org/10.1002/cm.20331

Han, S. J., Kwon, S., & Kim, K. S. (2021). Challenges of applying multicellular tumor spheroids in preclinical phase. *Cancer Cell International*, *21*(1), 152. https://doi.org/10.1186/s12935-021-01853-8

Han, W., Chen, S., Yuan, W., Fan, Q., Tian, J., Wang, X., Chen, L., Zhang, X., Wei, W., Liu, R., Qu, J., Jiao, Y., Austin, R. H., & Liu, L. (2016). Oriented collagen fibers direct tumor cell intravasation. *Proceedings of the National Academy of Sciences*, *113*(40), 11208–11213. https://doi.org/10.1073/pnas.1610347113

Hanahan, D. (2022). Hallmarks of Cancer: New Dimensions. *Cancer Discovery*, *12*(1), 31–46. https://doi.org/10.1158/2159-8290.CD-21-1059

Hanahan, D., & Weinberg, R. A. (2011). Hallmarks of Cancer: The Next Generation. *Cell*, *144*(5), 646–674. https://doi.org/10.1016/j.cell.2011.02.013

Harding, C., Heuser, J., & Stahl, P. (1983). Receptor-mediated endocytosis of transferrin and recycling of the transferrin receptor in rat reticulocytes. *The Journal of Cell Biology*, *97*(2), 329–339. https://doi.org/10.1083/jcb.97.2.329

Harryvan, T. J., Visser, M., de Bruin, L., Plug, L., Griffioen, L., Mulder, A., van Veelen, P. A., van der Heden van Noort, G. J., Jongsma, M. L., Meeuwsen, M. H., Wiertz, E. J., Santegoets, S. J., Hardwick, J. C., Van Hall, T., Neefjes, J., Van der Burg, S. H., Hawinkels, L. J., & Verdegaal, E. M. (2022).

Enhanced antigen cross-presentation in human colorectal cancer-associated fibroblasts through upregulation of the lysosomal protease cathepsin S. *Journal for ImmunoTherapy of Cancer*, *10*(3), e003591. https://doi.org/10.1136/jitc-2021-003591

Hawinkels, L. J. A. C., Paauwe, M., Verspaget, H. W., Wiercinska, E., van der Zon, J. M., van der Ploeg, K., Koelink, P. J., Lindeman, J. H. N., Mesker, W., ten Dijke, P., & Sier, C. F. M. (2014). Interaction with colon cancer cells hyperactivates TGF-β signaling in cancer-associated fibroblasts. *Oncogene*, *33*(1), 97–107. https://doi.org/10.1038/onc.2012.536

Hayden, P. J., & Harbell, J. W. (2021). Special review series on 3D organotypic culture models: Introduction and historical perspective. *In Vitro Cellular & Developmental Biology - Animal*, *57*(2), 95–103. https://doi.org/10.1007/s11626-020-00500-2

Hennessey, J. V. (2017). The emergence of levothyroxine as a treatment for hypothyroidism. *Endocrine*, *55*(1), 6–18. https://doi.org/10.1007/s12020-016-1199-8

Henriksson, M. L., Edin, S., Dahlin, A. M., Oldenborg, P.-A., Öberg, Å., Van Guelpen, B., Rutegård, J., Stenling, R., & Palmqvist, R. (2011). Colorectal Cancer Cells Activate Adjacent Fibroblasts Resulting in FGF1/FGFR3 Signaling and Increased Invasion. *The American Journal of Pathology*, *178*(3), 1387–1394. https://doi.org/10.1016/j.ajpath.2010.12.008

Hervieu, C., Christou, N., Battu, S., & Mathonnet, M. (2021). The Role of Cancer Stem Cells in Colorectal Cancer: From the Basics to Novel Clinical Trials. *Cancers*, *13*(5), 1092. https://doi.org/10.3390/cancers13051092

Hinman, S. S., Wang, Y., Kim, R., & Allbritton, N. L. (2021). In vitro generation of self-renewing human intestinal epithelia over planar and shaped collagen hydrogels. *Nature Protocols*, *16*(1), 352–382. https://doi.org/10.1038/s41596-020-00419-8

Hinz, B. (2016). The role of myofibroblasts in wound healing. *Current Research in Translational Medicine*, *64*(4), 171–177. https://doi.org/10.1016/j.retram.2016.09.003

Holch, J. W., Ricard, I., Stintzing, S., Modest, D. P., & Heinemann, V. (2017). The relevance of primary tumour location in patients with metastatic colorectal cancer: A meta-analysis of first-line clinical trials. *European Journal of Cancer*, *70*, 87–98. https://doi.org/10.1016/j.ejca.2016.10.007

Hoshiba, T. (2019). Decellularized Extracellular Matrix for Cancer Research. *Materials*, *12*(8), 1311. https://doi.org/10.3390/ma12081311

Hoshino, A., Costa-Silva, B., Shen, T.-L., Rodrigues, G., Hashimoto, A., Tesic Mark, M., Molina, H., Kohsaka, S., Di Giannatale, A., Ceder, S., Singh, S., Williams, C., Soplop, N., Uryu, K., Pharmer, L., King, T., Bojmar, L., Davies, A. E., Ararso, Y., … Lyden, D. (2015). Tumour exosome integrins determine organotropic metastasis. *Nature*, *527*(7578), 329–335. https://doi.org/10.1038/nature15756

Hrncir, T. (2022). Gut Microbiota Dysbiosis: Triggers, Consequences, Diagnostic and Therapeutic Options. *Microorganisms*, *10*(3), 578. https://doi.org/10.3390/microorganisms10030578

Hu, X., Marietta, A., Dai, W., Li, Y., Ma, X., Zhang, L., Cai, S., & Peng, J. (2020). Prediction of hepatic metastasis and relapse in colorectal cancers based on concordance analyses with liver fibrosis scores. *Clinical and Translational Medicine*, *9*(1). https://doi.org/10.1186/s40169-020-0264-3

Huang, W.-H., Zhou, M.-W., Zhu, Y.-F., Xiang, J.-B., Li, Z.-Y., Wang, Z.-H., Zhou, Y.-M., Yang, Y., Chen, Z.-Y., & Gu, X.-D. (2019). The Role Of Hepatic Stellate Cells In Promoting Liver Metastasis Of Colorectal Carcinoma. *OncoTargets and Therapy*, *Volume 12*, 7573–7580. https://doi.org/10.2147/OTT.S214409

Huels, D. J., & Sansom, O. J. (2015). Stem vs non-stem cell origin of colorectal cancer. *British Journal of Cancer*, *113*(1), 1–5. https://doi.org/10.1038/bjc.2015.214

Huizing, L. R. S., Ellis, S. R., Beulen, B. W. A. M. M., Barré, F. P. Y., Kwant, P. B., Vreeken, R. J., & Heeren, R. M. A. (2019). Development and evaluation of matrix application techniques for high throughput mass spectrometry imaging of tissues in the clinic. *Clinical Mass Spectrometry*, *12*, 7–15. https://doi.org/10.1016/j.clinms.2019.01.004

Ihara, T., Yamamoto, T., Sugamata, M., Okumura, H., & Ueno, Y. (1998). The process of ultrastructural changes from nuclei to apoptotic body. *Virchows Archiv*, *433*(5), 443–447. https://doi.org/10.1007/s004280050272

Ilina, O., Gritsenko, P. G., Syga, S., Lippoldt, J., La Porta, C. A. M., Chepizhko, O., Grosser, S., Vullings, M., Bakker, G.-J., Starruß, J., Bult, P., Zapperi, S., Käs, J. A., Deutsch, A., & Friedl, P. (2020). Cell-cell adhesion and 3D matrix confinement determine jamming transitions in breast cancer invasion. *Nature Cell Biology*, *22*(9), 1103–1115. https://doi.org/10.1038/s41556-020-0552-6

Ishihara, S., & Haga, H. (2022). Matrix Stiffness Contributes to Cancer Progression by Regulating Transcription Factors. *Cancers*, *14*(4), 1049. https://doi.org/10.3390/cancers14041049

Ishimoto, T., Miyake, K., Nandi, T., Yashiro, M., Onishi, N., Huang, K. K., Lin, S. J., Kalpana, R., Tay, S. T., Suzuki, Y., Cho, B. C., Kuroda, D., Arima, K., Izumi, D., Iwatsuki, M., Baba, Y., Oki, E., Watanabe, M., Saya, H., … Tan, P. (2017). Activation of Transforming Growth Factor Beta 1 Signaling in Gastric Cancer-associated Fibroblasts Increases Their Motility, via Expression of Rhomboid 5 Homolog 2, and Ability to Induce Invasiveness of Gastric Cancer Cells. *Gastroenterology*, *153*(1), 191-204.e16. https://doi.org/10.1053/j.gastro.2017.03.046

Izutsu, R., Osaki, M., Jehung, J. P., Seong, H. K., & Okada, F. (2022). Liver Metastasis Formation Is Defined by AMIGO2 Expression via Adhesion to Hepatic Endothelial Cells in Human Gastric and Colorectal Cancer Cells. *Pathology - Research and Practice*, *237*, 154015. https://doi.org/10.1016/j.prp.2022.154015

Jayaram, A., Barr, N., Plummer, R., Yao, M., Chen, L., & Yoo, J. (2019). Combined endo-laparoscopic surgery (CELS) for benign colon polyps: a single institution cost analysis. *Surgical Endoscopy*, *33*(10), 3238–3242. https://doi.org/10.1007/s00464-018-06610-z

Jayasingam, S. D., Citartan, M., Thang, T. H., Mat Zin, A. A., Ang, K. C., & Ch'ng, E. S. (2020). Evaluating the Polarization of Tumor-Associated Macrophages Into M1 and M2 Phenotypes in Human Cancer Tissue: Technicalities and

Challenges in Routine Clinical Practice. *Frontiers in Oncology*, *9*. https://doi.org/10.3389/fonc.2019.01512

Ji, H., Greening, D. W., Barnes, T. W., Lim, J. W., Tauro, B. J., Rai, A., Xu, R., Adda, C., Mathivanan, S., Zhao, W., Xue, Y., Xu, T., Zhu, H.-J., & Simpson, R. J. (2013). Proteome profiling of exosomes derived from human primary and metastatic colorectal cancer cells reveal differential expression of key metastatic factors and signal transduction components. *PROTEOMICS*, *13*(10–11), 1672–1686. https://doi.org/10.1002/pmic.201200562

Ji, Q., Zhou, L., Sui, H., Yang, L., Wu, X., Song, Q., Jia, R., Li, R., Sun, J., Wang, Z., Liu, N., Feng, Y., Sun, X., Cai, G., Feng, Y., Cai, J., Cao, Y., Cai, G., Wang, Y., & Li, Q. (2020). Primary tumors release ITGBL1-rich extracellular vesicles to promote distal metastatic tumor growth through fibroblast-niche formation. *Nature Communications*, *11*(1), 1211. https://doi.org/10.1038/s41467-020-14869-x

Jia, C., Wang, G., Wang, T., Fu, B., Zhang, Y., Huang, L., Deng, Y., Chen, G., Wu, X., Chen, J., Pan, Y., Tai, Y., Liang, J., Li, X., Hu, K., Xie, B., Li, S., Yang, Y., Chen, G., … Liu, W. (2020). Cancer-associated Fibroblasts induce epithelial-mesenchymal transition *via* the Transglutaminase 2-dependent IL-6/IL6R/STAT3 axis in Hepatocellular Carcinoma. *International Journal of Biological Sciences*, *16*(14), 2542–2558. https://doi.org/10.7150/ijbs.45446

Jobin, G., Rodriguez-Suarez, R., & Betito, K. (2017). Association Between Natural Killer Cell Activity and Colorectal Cancer in High-Risk Subjects Undergoing Colonoscopy. *Gastroenterology*, *153*(4), 980–987. https://doi.org/10.1053/j.gastro.2017.06.009

Kalluri, R. (2016). The biology and function of fibroblasts in cancer. *Nature Reviews Cancer*, *16*(9), 582–598. https://doi.org/10.1038/nrc.2016.73

Kamel, F., Eltarhoni, K., Nisar, P., & Soloviev, M. (2022). Colorectal Cancer Diagnosis: The Obstacles We Face in Determining a Non-Invasive Test and Current Advances in Biomarker Detection. *Cancers*, *14*(8), 1889. https://doi.org/10.3390/cancers14081889

Kamp, J. C., Neubert, L., Stark, H., Hinrichs, J. B., Boekhoff, C., Seidel, A. D., Ius, F., Haverich, A., Gottlieb, J., Welte, T., Braubach, P., Laenger, F.,

Hoeper, M. M., Kuehnel, M. P., & Jonigk, D. D. (2022). Comparative Analysis of Gene Expression in Fibroblastic Foci in Patients with Idiopathic Pulmonary Fibrosis and Pulmonary Sarcoidosis. *Cells*, *11*(4), 664. https://doi.org/10.3390/cells11040664

Kanth, P., & Inadomi, J. M. (2021). Screening and prevention of colorectal cancer. *BMJ*, n1855. https://doi.org/10.1136/bmj.n1855

Kapałczyńska, M., Kolenda, T., Przybyła, W., Zajączkowska, M., Teresiak, A., Filas, V., Ibbs, M., Bliźniak, R., Łuczewski, Ł., & Lamperska, K. (2016). 2D and 3D cell cultures – a comparison of different types of cancer cell cultures. *Archives of Medical Science*. https://doi.org/10.5114/aoms.2016.63743

Kasi, A., Handa, S., Bhatti, S., Umar, S., Bansal, A., & Sun, W. (2020). Molecular Pathogenesis and Classification of Colorectal Carcinoma. *Current Colorectal Cancer Reports*, *16*(5), 97–106. https://doi.org/10.1007/s11888-020-00458-z

Kasper, S. H., Morell-Perez, C., Wyche, T. P., Sana, T. R., Lieberman, L. A., & Hett, E. C. (2020). Colorectal cancer-associated anaerobic bacteria proliferate in tumor spheroids and alter the microenvironment. *Scientific Reports*, *10*(1), 5321. https://doi.org/10.1038/s41598-020-62139-z

Kato, T., Jenkins, R. P., Derzsi, S., Tozluoglu, M., Rullan, A., Hooper, S., Chaleil, R. A., Joyce, H., Fu, X., Thavaraj, S., Bates, P. A., & Sahai, E. (2023). Interplay of adherens junctions and matrix proteolysis determines the invasive pattern and growth of squamous cell carcinoma. *ELife*, *12*. https://doi.org/10.7554/eLife.76520

Katt, M. E., Placone, A. L., Wong, A. D., Xu, Z. S., & Searson, P. C. (2016). In Vitro Tumor Models: Advantages, Disadvantages, Variables, and Selecting the Right Platform. *Frontiers in Bioengineering and Biotechnology*, *4*. https://doi.org/10.3389/fbioe.2016.00012

Kazazi-Hyseni, F., Beijnen, J. H., & Schellens, J. H. M. (2010). Bevacizumab. *The Oncologist*, *15*(8), 819–825. https://doi.org/10.1634/theoncologist.2009-0317

Keane, M. G., & Johnson, G. J. (2012). Early diagnosis improves survival in colorectal cancer. *The Practitioner*, *256*(1753), 15–18, 2.

Kehlet, S. N., Sanz-Pamplona, R., Brix, S., Leeming, D. J., Karsdal, M. A., & Moreno, V. (2016). Excessive collagen turnover products are released during colorectal cancer progression and elevated in serum from metastatic colorectal cancer patients. *Scientific Reports*, *6*(1), 30599. https://doi.org/10.1038/srep30599

Khalaf, K., Hana, D., Chou, J. T.-T., Singh, C., Mackiewicz, A., & Kaczmarek, M. (2021). Aspects of the Tumor Microenvironment Involved in Immune Resistance and Drug Resistance. *Frontiers in Immunology*, *12*. https://doi.org/10.3389/fimmu.2021.656364

Kim, H.-R., Mun, Y., Lee, K.-S., Park, Y.-J., Park, J.-S., Park, J.-H., Jeon, B.-N., Kim, C.-H., Jun, Y., Hyun, Y.-M., Kim, M., Lee, S.-M., Park, C.-S., Im, S.-H., & Jun, C.-D. (2018). T cell microvilli constitute immunological synaptosomes that carry messages to antigen-presenting cells. *Nature Communications*, *9*(1), 3630. https://doi.org/10.1038/s41467-018-06090-8

Kim, J., Lee, C., Kim, I., Ro, J., Kim, J., Min, Y., Park, J., Sunkara, V., Park, Y.-S., Michael, I., Kim, Y.-A., Lee, H. J., & Cho, Y.-K. (2020). Three-Dimensional Human Liver-Chip Emulating Premetastatic Niche Formation by Breast Cancer-Derived Extracellular Vesicles. *ACS Nano*, *14*(11), 14971–14988. https://doi.org/10.1021/acsnano.0c04778

Knops, A. M., South, A., Rodeck, U., Martinez-Outschoorn, U., Harshyne, L. A., Johnson, J., Luginbuhl, A. J., & Curry, J. M. (2020). Cancer-Associated Fibroblast Density, Prognostic Characteristics, and Recurrence in Head and Neck Squamous Cell Carcinoma: A Meta-Analysis. *Frontiers in Oncology*, *10*. https://doi.org/10.3389/fonc.2020.565306

Ko, S. Y., & Naora, H. (2020). Extracellular Vesicle Membrane-Associated Proteins: Emerging Roles in Tumor Angiogenesis and Anti-Angiogenesis Therapy Resistance. *International Journal of Molecular Sciences*, *21*(15), 5418. https://doi.org/10.3390/ijms21155418

Kobayashi, K., Yoshioka, T., Miyauchi, J., Nakazawa, A., Kiyokawa, N., Maihara, T., & Usami, I. (2018). Role of monocyte chemoattractant protein-1 in liver fibrosis with transient myeloproliferative disorder in down syndrome.

*Hepatology Communications*, *2*(3), 230–236. https://doi.org/10.1002/hep4.1150

Koelzer, V. H., Canonica, K., Dawson, H., Sokol, L., Karamitopoulou-Diamantis, E., Lugli, A., & Zlobec, I. (2016). Phenotyping of tumor-associated macrophages in colorectal cancer: Impact on single cell invasion (tumor budding) and clinicopathological outcome. *OncoImmunology*, *5*(4), e1106677. https://doi.org/10.1080/2162402X.2015.1106677

Kogure, A., Yoshioka, Y., & Ochiya, T. (2020). Extracellular Vesicles in Cancer Metastasis: Potential as Therapeutic Targets and Materials. *International Journal of Molecular Sciences*, *21*(12), 4463. https://doi.org/10.3390/ijms21124463

Koido, S., Hara, E., Homma, S., Torii, A., Toyama, Y., Kawahara, H., Watanabe, M., Yanaga, K., Fujise, K., Tajiri, H., Gong, J., & Toda, G. (2005). Dendritic Cells Fused with Allogeneic Colorectal Cancer Cell Line Present Multiple Colorectal Cancer–Specific Antigens and Induce Antitumor Immunity against Autologous Tumor Cells. *Clinical Cancer Research*, *11*(21), 7891–7900. https://doi.org/10.1158/1078-0432.CCR-05-1330

Kondo, T., Okabayashi, K., Hasegawa, H., Tsuruta, M., Shigeta, K., & Kitagawa, Y. (2016). The impact of hepatic fibrosis on the incidence of liver metastasis from colorectal cancer. *British Journal of Cancer*, *115*(1), 34–39. https://doi.org/10.1038/bjc.2016.155

Kotelevets, L., & Chastre, E. (2023). Extracellular Vesicles in Colorectal Cancer: From Tumor Growth and Metastasis to Biomarkers and Nanomedications. *Cancers*, *15*(4), 1107. https://doi.org/10.3390/cancers15041107

Kourtidis, A., Ngok, S. P., & Anastasiadis, P. Z. (2013). *p120 Catenin: an essential regulator of cadherin stability, adhesion-induced signaling, and cancer progression* (pp. 409–432). https://doi.org/10.1016/B978-0-12-394311-8.00018-2

Kuipers, E. J., Grady, W. M., Lieberman, D., Seufferlein, T., Sung, J. J., Boelens, P. G., van de Velde, C. J. H., & Watanabe, T. (2015). Colorectal cancer. *Nature Reviews Disease Primers*, *1*(1), 15065. https://doi.org/10.1038/nrdp.2015.65

Lai, T., Liu, Y., Li, W., & Greenberg, C. S. (2007). Identification of two GTP-independent alternatively spliced forms of tissue transglutaminase in human leukocytes, vascular smooth muscle, and endothelial cells. *The FASEB Journal*, *21*(14), 4131–4143. https://doi.org/10.1096/fj.06-7598com

Lamberti, M. J., Rettel, M., Krijgsveld, J., Rivarola, V. A., & Rumie Vittar, N. B. (2019). Secretome profiling of heterotypic spheroids suggests a role of fibroblasts in HIF-1 pathway modulation and colorectal cancer photodynamic resistance. *Cellular Oncology*, *42*(2), 173–196. https://doi.org/10.1007/s13402-018-00418-8

Lattmann, E., Deng, T., & Hajnal, A. (2021). To Divide or Invade: A Look Behind the Scenes of the Proliferation-Invasion Interplay in the Caenorhabditis elegans Anchor Cell. *Frontiers in Cell and Developmental Biology*, *8*. https://doi.org/10.3389/fcell.2020.616051

LeBleu, V. S., & Kalluri, R. (2018). A peek into cancer-associated fibroblasts: origins, functions and translational impact. *Disease Models & Mechanisms*, *11*(4). https://doi.org/10.1242/dmm.029447

Lee, J., Condello, S., Yakubov, B., Emerson, R., Caperell-Grant, A., Hitomi, K., Xie, J., & Matei, D. (2015). Tissue Transglutaminase Mediated Tumor–Stroma Interaction Promotes Pancreatic Cancer Progression. *Clinical Cancer Research*, *21*(19), 4482–4493. https://doi.org/10.1158/1078-0432.CCR-15-0226

Lee, L. C., Liong, C.-Y., & Jemain, A. A. (2018). Partial least squares-discriminant analysis (PLS-DA) for classification of high-dimensional (HD) data: a review of contemporary practice strategies and knowledge gaps. *The Analyst*, *143*(15), 3526–3539. https://doi.org/10.1039/C8AN00599K

Lee, U. E., & Friedman, S. L. (2011). Mechanisms of hepatic fibrogenesis. *Best Practice & Research Clinical Gastroenterology*, *25*(2), 195–206. https://doi.org/10.1016/j.bpg.2011.02.005

Lees, R., Tempest, R., Law, A., Aubert, D., Davies, O. G., Williams, S., Peake, N., & Peacock, B. (2022). Single Extracellular Vesicle Transmembrane Protein Characterization by Nano-Flow Cytometry. *Journal of Visualized Experiments*, *185*. https://doi.org/10.3791/64020

Lehrich, B. M., Liang, Y., & Fiandaca, M. S. (2021). Foetal bovine serum influence on in vitro extracellular vesicle analyses. *Journal of Extracellular Vesicles*, *10*(3). https://doi.org/10.1002/jev2.12061

Leibovitz, A., Stinson, J. C., McCombs, W. B., McCoy, C. E., Mazur, K. C., & Mabry, N. D. (1976). Classification of human colorectal adenocarcinoma cell lines. *Cancer Research*, *36*(12), 4562–4569.

Lenzini, S., Bargi, R., Chung, G., & Shin, J.-W. (2020). Matrix mechanics and water permeation regulate extracellular vesicle transport. *Nature Nanotechnology*, *15*(3), 217–223. https://doi.org/10.1038/s41565-020-0636-2

Lerman, M. J., Lembong, J., Gillen, G., & Fisher, J. P. (2018). 3D printing in cell culture systems and medical applications. *Applied Physics Reviews*, *5*(4), 041109. https://doi.org/10.1063/1.5046087

Levental, K. R., Yu, H., Kass, L., Lakins, J. N., Egeblad, M., Erler, J. T., Fong, S. F. T., Csiszar, K., Giaccia, A., Weninger, W., Yamauchi, M., Gasser, D. L., & Weaver, V. M. (2009). Matrix Crosslinking Forces Tumor Progression by Enhancing Integrin Signaling. *Cell*, *139*(5), 891–906. https://doi.org/10.1016/j.cell.2009.10.027

Lewis, M. P., Lygoe, K. A., Nystrom, M. L., Anderson, W. P., Speight, P. M., Marshall, J. F., & Thomas, G. J. (2004). Tumour-derived TGF-β1 modulates myofibroblast differentiation and promotes HGF/SF-dependent invasion of squamous carcinoma cells. *British Journal of Cancer*, *90*(4), 822–832. https://doi.org/10.1038/sj.bjc.6601611

Li, C., Wang, J., Kong, J., Tang, J., Wu, Y., Xu, E., Zhang, H., & Lai, M. (2016). GDF15 promotes EMT and metastasis in colorectal cancer. *Oncotarget*, *7*(1), 860–872. https://doi.org/10.18632/oncotarget.6205

Li, C., Zhou, T., Chen, J., Li, R., Chen, H., Luo, S., Chen, D., Cai, C., & Li, W. (2022). The role of Exosomal miRNAs in cancer. *Journal of Translational Medicine*, *20*(1), 6. https://doi.org/10.1186/s12967-021-03215-4

Li, H., Courtois, E. T., Sengupta, D., Tan, Y., Chen, K. H., Goh, J. J. L., Kong, S. L., Chua, C., Hon, L. K., Tan, W. S., Wong, M., Choi, P. J., Wee, L. J. K., Hillmer, A. M., Tan, I. B., Robson, P., & Prabhakar, S. (2017). Reference

component analysis of single-cell transcriptomes elucidates cellular heterogeneity in human colorectal tumors. *Nature Genetics*, *49*(5), 708–718. https://doi.org/10.1038/ng.3818

Li, J., Li, L., Li, Y., Long, Y., Zhao, Q., Ouyang, Y., Bao, W., & Gong, K. (2020). Tumor-associated macrophage infiltration and prognosis in colorectal cancer: systematic review and meta-analysis. *International Journal of Colorectal Disease*, *35*(7), 1203–1210. https://doi.org/10.1007/s00384-020-03593-z

Li, J., Ma, X., Chakravarti, D., Shalapour, S., & DePinho, R. A. (2021). Genetic and biological hallmarks of colorectal cancer. *Genes & Development*, *35*(11–12), 787–820. https://doi.org/10.1101/gad.348226.120

Li, J., Xu, X., Jiang, Y., Hansbro, N. G., Hansbro, P. M., Xu, J., & Liu, G. (2020). Elastin is a key factor of tumor development in colorectal cancer. *BMC Cancer*, *20*(1), 217. https://doi.org/10.1186/s12885-020-6686-x

Li, L., Yuan, S., Zhao, X., & Luo, T. (2020). ADAMTS8 is frequently down-regulated in colorectal cancer and functions as a tumor suppressor. *Biochemical and Biophysical Research Communications*, *524*(3), 663–671. https://doi.org/10.1016/j.bbrc.2020.01.020

Li, R., Zhou, R., Wang, H., Li, W., Pan, M., Yao, X., Zhan, W., Yang, S., Xu, L., Ding, Y., & Zhao, L. (2019). Gut microbiota-stimulated cathepsin K secretion mediates TLR4-dependent M2 macrophage polarization and promotes tumor metastasis in colorectal cancer. *Cell Death & Differentiation*, *26*(11), 2447–2463. https://doi.org/10.1038/s41418-019-0312-y

Li, S., Ma, Y.-M., Zheng, P.-S., & Zhang, P. (2018). GDF15 promotes the proliferation of cervical cancer cells by phosphorylating AKT1 and Erk1/2 through the receptor ErbB2. *Journal of Experimental & Clinical Cancer Research*, *37*(1), 80. https://doi.org/10.1186/s13046-018-0744-0

Li, S., Man, Q., Gao, X., Lin, H., Wang, J., Su, F., Wang, H., Bu, L., Liu, B., & Chen, G. (2021). Tissue-derived extracellular vesicles in cancers and non-cancer diseases: Present and future. *Journal of Extracellular Vesicles*, *10*(14). https://doi.org/10.1002/jev2.12175

Li, X., Li, Z., Gu, S., & Zhao, X. (2022). A pan-cancer analysis of collagen VI family on prognosis, tumor microenvironment, and its potential therapeutic effect. *BMC Bioinformatics*, *23*(1), 390. https://doi.org/10.1186/s12859-022-04951-0

Li, Z.-Y., Xiao, L., Lin, G., Tang, J., Chen, Y., Chen, L., Li, B., Wu, M., Liu, S., Huang, C., Ferrandon, D., & Li, Z. (2019). Contribution of tissue transglutaminase to the severity of hepatic fibrosis resulting from Schistosoma japonicum infection through the regulation of IL-33/ST2 expression. *Parasites & Vectors*, *12*(1), 302. https://doi.org/10.1186/s13071-019-3542-4

Lindgren, M., Rask, G., Jonsson, J., Berglund, A., Lundin, C., Jonsson, P., Ljuslinder, I., & Nyström, H. (2022). Type IV Collagen in Human Colorectal Liver Metastases—Cellular Origin and a Circulating Biomarker. *Cancers*, *14*(14), 3396. https://doi.org/10.3390/cancers14143396

Lipton, A., Leitzel, K., Ali, S. M., Polimera, H. V., Nagabhairu, V., Marks, E., Richardson, A. E., Krecko, L., Ali, A., Koestler, W., Esteva, F. J., Leeming, D. J., Karsdal, M. A., & Willumsen, N. (2018). High turnover of extracellular matrix reflected by specific protein fragments measured in serum is associated with poor outcomes in two metastatic breast cancer cohorts. *International Journal of Cancer*, *143*(11), 3027–3034. https://doi.org/10.1002/ijc.31627

Liu, C., Pei, H., & Tan, F. (2020). Matrix Stiffness and Colorectal Cancer. *OncoTargets and Therapy*, *Volume 13*, 2747–2755. https://doi.org/10.2147/OTT.S231010

Liu, C.-C., Lin, S.-P., Hsu, H.-S., Yang, S.-H., Lin, C.-H., Yang, M.-H., Hung, M.-C., & Hung, S.-C. (2016). Suspension survival mediated by PP2A-STAT3-Col XVII determines tumour initiation and metastasis in cancer stem cells. *Nature Communications*, *7*(1), 11798. https://doi.org/10.1038/ncomms11798

Liu, H., Lu, T., Kremers, G.-J., Seynhaeve, A. L. B., & ten Hagen, T. L. M. (2020). A microcarrier-based spheroid 3D invasion assay to monitor dynamic cell

movement in extracellular matrix. *Biological Procedures Online*, *22*(1), 3. https://doi.org/10.1186/s12575-019-0114-0

Liu, J., Chen, Y., Pei, F., Zeng, C., Yao, Y., Liao, W., & Zhao, Z. (2021). Extracellular Vesicles in Liquid Biopsies: Potential for Disease Diagnosis. *BioMed Research International*, *2021*, 1–17. https://doi.org/10.1155/2021/6611244

Liu, L., Stephens, B., Bergman, M., May, A., & Chiang, T. (2021). Role of Collagen in Airway Mechanics. *Bioengineering*, *8*(1), 13. https://doi.org/10.3390/bioengineering8010013

Liu, S., Liao, Y., Hosseinifard, H., Imani, S., & Wen, Q. (2021). Diagnostic Role of Extracellular Vesicles in Cancer: A Comprehensive Systematic Review and Meta-Analysis. *Frontiers in Cell and Developmental Biology*, *9*. https://doi.org/10.3389/fcell.2021.705791

Liu, T., Han, C., Wang, S., Fang, P., Ma, Z., Xu, L., & Yin, R. (2019). Cancer-associated fibroblasts: an emerging target of anti-cancer immunotherapy. *Journal of Hematology & Oncology*, *12*(1), 86. https://doi.org/10.1186/s13045-019-0770-1

Liu, W., & Meng, K. (2022). COL11A1 is Downregulated by miR-339-5p and Promotes Colon Carcinoma Progression. *Canadian Journal of Gastroenterology and Hepatology*, *2022*, 1–10. https://doi.org/10.1155/2022/8116990

Liu, X.-Y., Liu, R.-X., Hou, F., Cui, L.-J., Li, C.-Y., Chi, C., Yi, E., Wen, Y., & Yin, C.-H. (2016). Fibronectin expression is critical for liver fibrogenesis in vivo and in vitro. *Molecular Medicine Reports*, *14*(4), 3669–3675. https://doi.org/10.3892/mmr.2016.5673

Liu, Y., Wang, G., Liang, Z., Mei, Z., Wu, T., Cui, A., Liu, C., & Cui, L. (2018). Lysyl oxidase: A colorectal cancer biomarker of lung and hepatic metastasis. *Thoracic Cancer*, *9*(7), 785–793. https://doi.org/10.1111/1759-7714.12645

Liu, Z., Qi, L., Li, Y., Zhao, X., & Sun, B. (2017). VEGFR2 regulates endothelial differentiation of colon cancer cells. *BMC Cancer*, *17*(1), 593. https://doi.org/10.1186/s12885-017-3578-9

Lizárraga-Verdugo, E., Avendaño-Félix, M., Bermúdez, M., Ramos-Payán, R., Pérez-Plasencia, C., & Aguilar-Medina, M. (2020). Cancer Stem Cells and Its Role in Angiogenesis and Vasculogenic Mimicry in Gastrointestinal Cancers. *Frontiers in Oncology*, *10*. https://doi.org/10.3389/fonc.2020.00413

Loh, C.-Y., Chai, J., Tang, T., Wong, W., Sethi, G., Shanmugam, M., Chong, P., & Looi, C. (2019). The E-Cadherin and N-Cadherin Switch in Epithelial-to-Mesenchymal Transition: Signaling, Therapeutic Implications, and Challenges. *Cells*, *8*(10), 1118. https://doi.org/10.3390/cells8101118

Lone, S. N., Nisar, S., Masoodi, T., Singh, M., Rizwan, A., Hashem, S., El-Rifai, W., Bedognetti, D., Batra, S. K., Haris, M., Bhat, A. A., & Macha, M. A. (2022). Liquid biopsy: a step closer to transform diagnosis, prognosis and future of cancer treatments. *Molecular Cancer*, *21*(1), 79. https://doi.org/10.1186/s12943-022-01543-7

Lugini, L., Valtieri, M., Federici, C., Cecchetti, S., Meschini, S., Condello, M., Signore, M., & Fais, S. (2016). Exosomes from human colorectal cancer induce a tumor-like behavior in colonic mesenchymal stromal cells. *Oncotarget*, *7*(31), 50086–50098. https://doi.org/10.18632/oncotarget.10574

Lusby, R., Dunne, P., & Tiwari, V. K. (2022). Tumour invasion and dissemination. *Biochemical Society Transactions*, *50*(3), 1245–1257. https://doi.org/10.1042/BST20220452

Ma, L., Li, Y., Peng, J., Wu, D., Zhao, X., Cui, Y., Chen, L., Yan, X., Du, Y., & Yu, L. (2015). Discovery of the migrasome, an organelle mediating release of cytoplasmic contents during cell migration. *Cell Research*, *25*(1), 24–38. https://doi.org/10.1038/cr.2014.135

Mah, A. T., Yan, K. S., & Kuo, C. J. (2016). Wnt pathway regulation of intestinal stem cells. *The Journal of Physiology*, *594*(17), 4837–4847. https://doi.org/10.1113/JP271754

Mahipal, A., & Grothey, A. (2016). Role of Biologics in First-Line Treatment of Colorectal Cancer. *Journal of Oncology Practice*, *12*(12), 1219–1228. https://doi.org/10.1200/JOP.2016.018382

Majidpoor, J., & Mortezaee, K. (2021). Steps in metastasis: an updated review. *Medical Oncology*, *38*(1), 3. https://doi.org/10.1007/s12032-020-01447-w

Makaremi, S., Asadzadeh, Z., Hemmat, N., Baghbanzadeh, A., Sgambato, A., Ghorbaninezhad, F., Safarpour, H., Argentiero, A., Brunetti, O., Bernardini, R., Silvestris, N., & Baradaran, B. (2021). Immune Checkpoint Inhibitors in Colorectal Cancer: Challenges and Future Prospects. *Biomedicines*, *9*(9), 1075. https://doi.org/10.3390/biomedicines9091075

Malawista, S. E., & Van Blaricom, G. (1987). Cytoplasts made from human blood polymorphonuclear leukocytes with or without heat: preservation of both motile function and respiratory burst oxidase activity. *Proceedings of the National Academy of Sciences*, *84*(2), 454–458. https://doi.org/10.1073/pnas.84.2.454

Malki, A., ElRuz, R. A., Gupta, I., Allouch, A., Vranic, S., & Al Moustafa, A.-E. (2020). Molecular Mechanisms of Colon Cancer Progression and Metastasis: Recent Insights and Advancements. *International Journal of Molecular Sciences*, *22*(1), 130. https://doi.org/10.3390/ijms22010130

Mangala, L. S., Fok, J. Y., Zorrilla-Calancha, I. R., Verma, A., & Mehta, K. (2007). Tissue transglutaminase expression promotes cell attachment, invasion and survival in breast cancer cells. *Oncogene*, *26*(17), 2459–2470. https://doi.org/10.1038/sj.onc.1210035

Mao, X., Tey, S. K., Yeung, C. L. S., Kwong, E. M. L., Fung, Y. M. E., Chung, C. Y. S., Mak, L., Wong, D. K. H., Yuen, M., Ho, J. C. M., Pang, H., Wong, M. P., Leung, C. O., Lee, T. K. W., Ma, V., Cho, W. C., Cao, P., Xu, X., Gao, Y., & Yam, J. W. P. (2020). Nidogen 1-Enriched Extracellular Vesicles Facilitate Extrahepatic Metastasis of Liver Cancer by Activating Pulmonary Fibroblasts to Secrete Tumor Necrosis Factor Receptor 1. *Advanced Science*, *7*(21), 2002157. https://doi.org/10.1002/advs.202002157

Marki, A., Buscher, K., Lorenzini, C., Meyer, M., Saigusa, R., Fan, Z., Yeh, Y.-T., Hartmann, N., Dan, J. M., Kiosses, W. B., Golden, G. J., Ganesan, R., Winkels, H., Orecchioni, M., McArdle, S., Mikulski, Z., Altman, Y., Bui, J., Kronenberg, M., … Ley, K. (2021). Elongated neutrophil-derived structures are blood-borne microparticles formed by rolling neutrophils during sepsis. *Journal of Experimental Medicine*, *218*(3). https://doi.org/10.1084/jem.20200551

Martin, T. A., & Jiang, W. G. (2009). Loss of tight junction barrier function and its role in cancer metastasis. *Biochimica et Biophysica Acta (BBA) - Biomembranes*, *1788*(4), 872–891. https://doi.org/10.1016/j.bbamem.2008.11.005

Martini, G., Troiani, T., Cardone, C., Vitiello, P., Sforza, V., Ciardiello, D., Napolitano, S., Della Corte, C. M., Morgillo, F., Raucci, A., Cuomo, A., Selvaggi, F., Ciardiello, F., & Martinelli, E. (2017). Present and future of metastatic colorectal cancer treatment: A review of new candidate targets. *World Journal of Gastroenterology*, *23*(26), 4675. https://doi.org/10.3748/wjg.v23.i26.4675

Matsushima, S., Aoshima, Y., Akamatsu, T., Enomoto, Y., Meguro, S., Kosugi, I., Kawasaki, H., Fujisawa, T., Enomoto, N., Nakamura, Y., Inui, N., Funai, K., Suda, T., & Iwashita, T. (2020). CD248 and integrin alpha-8 are candidate markers for differentiating lung fibroblast subtypes. *BMC Pulmonary Medicine*, *20*(1), 21. https://doi.org/10.1186/s12890-020-1054-9

McDonald, B., Spicer, J., Giannais, B., Fallavollita, L., Brodt, P., & Ferri, L. E. (2009). Systemic inflammation increases cancer cell adhesion to hepatic sinusoids by neutrophil mediated mechanisms. *International Journal of Cancer*, *125*(6), 1298–1305. https://doi.org/10.1002/ijc.24409

Mehla, K., & Singh, P. K. (2019). Metabolic Regulation of Macrophage Polarization in Cancer. *Trends in Cancer*, *5*(12), 822–834. https://doi.org/10.1016/j.trecan.2019.10.007

Melentijevic, I., Toth, M. L., Arnold, M. L., Guasp, R. J., Harinath, G., Nguyen, K. C., Taub, D., Parker, J. A., Neri, C., Gabel, C. V., Hall, D. H., & Driscoll, M. (2017). C. elegans neurons jettison protein aggregates and mitochondria under neurotoxic stress. *Nature*, *542*(7641), 367–371. https://doi.org/10.1038/nature21362

Melincovici, C. S., Boşca, A. B., Şuşman, S., Mărginean, M., Mihu, C., Istrate, M., Moldovan, I. M., Roman, A. L., & Mihu, C. M. (2018). Vascular endothelial growth factor (VEGF) - key factor in normal and pathological angiogenesis. *Romanian Journal of Morphology and Embryology = Revue Roumaine de Morphologie et Embryologie*, *59*(2), 455–467.

Meng, X.-M., Wang, S., Huang, X.-R., Yang, C., Xiao, J., Zhang, Y., To, K.-F., Nikolic-Paterson, D. J., & Lan, H.-Y. (2016). Inflammatory macrophages can transdifferentiate into myofibroblasts during renal fibrosis. *Cell Death & Disease*, *7*(12), e2495–e2495. https://doi.org/10.1038/cddis.2016.402

Merlos Rodrigo, M. A., Zitka, O., Krizkova, S., Moulick, A., Adam, V., & Kizek, R. (2014). MALDI-TOF MS as evolving cancer diagnostic tool: A review. *Journal of Pharmaceutical and Biomedical Analysis*, *95*, 245–255. https://doi.org/10.1016/j.jpba.2014.03.007

Mizenko, R. R., Brostoff, T., Rojalin, T., Koster, H. J., Swindell, H. S., Leiserowitz, G. S., Wang, A., & Carney, R. P. (2021). Tetraspanins are unevenly distributed across single extracellular vesicles and bias sensitivity to multiplexed cancer biomarkers. *Journal of Nanobiotechnology*, *19*(1), 250. https://doi.org/10.1186/s12951-021-00987-1

Mondello, C., & Scovassi, A. I. (2010). *Apoptosis: A Way to Maintain Healthy Individuals* (pp. 307–323). https://doi.org/10.1007/978-90-481-3471-7_16

Morgan, R., Mortensson, E., & Williams, A. (2018). Targeting LGR5 in Colorectal Cancer: therapeutic gold or too plastic? *British Journal of Cancer*, *118*(11), 1410–1418. https://doi.org/10.1038/s41416-018-0118-6

Morris, V. K., Kennedy, E. B., Baxter, N. N., Benson, A. B., Cercek, A., Cho, M., Ciombor, K. K., Cremolini, C., Davis, A., Deming, D. A., Fakih, M. G., Gholami, S., Hong, T. S., Jaiyesimi, I., Klute, K., Lieu, C., Sanoff, H., Strickler, J. H., White, S., … Eng, C. (2023). Treatment of Metastatic Colorectal Cancer: ASCO Guideline. *Journal of Clinical Oncology*, *41*(3), 678–700. https://doi.org/10.1200/JCO.22.01690

Murdocca, M., Capuano, R., Pucci, S., Cicconi, R., Polidoro, C., Catini, A., Martinelli, E., Paolesse, R., Orlandi, A., Mango, R., Novelli, G., Di Natale, C., & Sangiuolo, F. (2019). Targeting LOX-1 Inhibits Colorectal Cancer Metastasis in an Animal Model. *Frontiers in Oncology*, *9*. https://doi.org/10.3389/fonc.2019.00927

Na, T.-Y., Schecterson, L., Mendonsa, A. M., & Gumbiner, B. M. (2020). The functional activity of E-cadherin controls tumor cell metastasis at multiple

steps. *Proceedings of the National Academy of Sciences*, *117*(11), 5931–5937. https://doi.org/10.1073/pnas.1918167117

Naba, A., Clauser, K. R., Hoersch, S., Liu, H., Carr, S. A., & Hynes, R. O. (2012). The Matrisome: In Silico Definition and In Vivo Characterization by Proteomics of Normal and Tumor Extracellular Matrices. *Molecular & Cellular Proteomics*, *11*(4), M111.014647. https://doi.org/10.1074/mcp.M111.014647

Naito, Y., Yoshioka, Y., & Ochiya, T. (2022). Intercellular crosstalk between cancer cells and cancer-associated fibroblasts via extracellular vesicles. *Cancer Cell International*, *22*(1), 367. https://doi.org/10.1186/s12935-022-02784-8

Nakhaei-Nejad, M., Farhan, M., Mojiri, A., Jabbari, H., Murray, A. G., & Jahroudi, N. (2019). Regulation of von Willebrand Factor Gene in Endothelial Cells That Are Programmed to Pluripotency and Differentiated Back to Endothelial Cells. *Stem Cells*, *37*(4), 542–554. https://doi.org/10.1002/stem.2978

Nakurte, I., Jekabsons, K., Rembergs, R., Zandberga, E., Abols, A., Line, A., & Muceniece, R. (2018). Colorectal Cancer Cell Line SW480 and SW620 Released Extravascular Vesicles: Focus on Hypoxia-induced Surface Proteome Changes. *Anticancer Research*, *38*(11), 6133–6138. https://doi.org/10.21873/anticanres.12965

Novo, D., Heath, N., Mitchell, L., Caligiuri, G., MacFarlane, A., Reijmer, D., Charlton, L., Knight, J., Calka, M., McGhee, E., Dornier, E., Sumpton, D., Mason, S., Echard, A., Klinkert, K., Secklehner, J., Kruiswijk, F., Vousden, K., Macpherson, I. R., … Norman, J. C. (2018). Mutant p53s generate pro-invasive niches by influencing exosome podocalyxin levels. *Nature Communications*, *9*(1), 5069. https://doi.org/10.1038/s41467-018-07339-y

Nowacka, M., Sterzynska, K., Andrzejewska, M., Nowicki, M., & Januchowski, R. (2021). Drug resistance evaluation in novel 3D in vitro model. *Biomedicine & Pharmacotherapy*, *138*, 111536. https://doi.org/10.1016/j.biopha.2021.111536

Nunes, I., Gleizes, P.-E., Metz, C. N., & Rifkin, D. B. (1997). Latent Transforming Growth Factor-β Binding Protein Domains Involved in Activation and

Transglutaminase-dependent Cross-Linking of Latent Transforming Growth Factor-β. *Journal of Cell Biology*, *136*(5), 1151–1163. https://doi.org/10.1083/jcb.136.5.1151

Nurminskaya, M. V., & Belkin, A. M. (2012). *Cellular Functions of Tissue Transglutaminase* (pp. 1–97). https://doi.org/10.1016/B978-0-12-394305-7.00001-X

Nyström, H. (2021). Extracellular matrix proteins in metastases to the liver – Composition, function and potential applications. *Seminars in Cancer Biology*, *71*, 134–142. https://doi.org/10.1016/j.semcancer.2020.06.004

Nyström, M., Thomas, G., Stone, M., Mackenzie, I., Hart, I., & Marshall, J. (2005). Development of a quantitative method to analyse tumour cell invasion in organotypic culture. *The Journal of Pathology*, *205*(4), 468–475. https://doi.org/10.1002/path.1716

Ogata-Kawata, H., Izumiya, M., Kurioka, D., Honma, Y., Yamada, Y., Furuta, K., Gunji, T., Ohta, H., Okamoto, H., Sonoda, H., Watanabe, M., Nakagama, H., Yokota, J., Kohno, T., & Tsuchiya, N. (2014). Circulating Exosomal microRNAs as Biomarkers of Colon Cancer. *PLoS ONE*, *9*(4), e92921. https://doi.org/10.1371/journal.pone.0092921

Okawa, M., Tanabe, A., Ohta, S., Nagatoishi, S., Tsumoto, K., & Ito, T. (2022). Extracellular matrix-inspired hydrogel of hyaluronan and gelatin crosslinked via a Link module with a transglutaminase reactive sequence. *Communications Materials*, *3*(1), 81. https://doi.org/10.1038/s43246-022-00309-4

Onaciu, A., Munteanu, R., Munteanu, V. C., Gulei, D., Raduly, L., Feder, R.-I., Pirlog, R., Atanasov, A. G., Korban, S. S., Irimie, A., & Berindan-Neagoe, I. (2020). Spontaneous and Induced Animal Models for Cancer Research. *Diagnostics*, *10*(9), 660. https://doi.org/10.3390/diagnostics10090660

Ostrowska-Podhorodecka, Z., Ali, A., Norouzi, M., Ding, I., Abbasi, S., Arora, P. D., Wong, T. H. F., Magalhaes, M., & McCulloch, C. A. (2023). Vimentin-mediated myosin 10 aggregation at tips of cell extensions drives <scp>MT1-MMP</scp> -dependent collagen degradation in colorectal cancer. *The FASEB Journal*, *37*(8). https://doi.org/10.1096/fj.202300672R

Paget, S. (1889). The Distribution of Secondary Growths in Cancer of the Breast. *The Lancet*, *133*(3421), 571–573. https://doi.org/10.1016/S0140-6736(00)49915-0

Paget, S. (1989). The distribution of secondary growths in cancer of the breast. 1889. *Cancer Metastasis Reviews*, *8*(2), 98–101.

Palmieri, V., Lucchetti, D., Maiorana, A., Papi, M., Maulucci, G., Calapà, F., Ciasca, G., Giordano, R., Sgambato, A., & De Spirito, M. (2015). Mechanical and structural comparison between primary tumor and lymph node metastasis cells in colorectal cancer. *Soft Matter*, *11*(28), 5719–5726. https://doi.org/10.1039/C5SM01089F

Palmulli, R., Bresteau, E., Raposo, G., Montagnac, G., & van Niel, G. (2023). In Vitro Interaction of Melanoma-Derived Extracellular Vesicles with Collagen. *International Journal of Molecular Sciences*, *24*(4), 3703. https://doi.org/10.3390/ijms24043703

Pandya, P., Orgaz, J. L., & Sanz-Moreno, V. (2017). Modes of invasion during tumour dissemination. *Molecular Oncology*, *11*(1), 5–27. https://doi.org/10.1002/1878-0261.12019

Pang, H., Liu, L., Sun, X., Xi, W., Bao, Y., Wu, L., Shan, J., Wang, Z., Guo, Y., & Zhao, C. (2021). Exosomes derived from colon cancer cells and plasma of colon cancer patients promote migration of SW480 cells through Akt/mTOR pathway. *Pathology - Research and Practice*, *222*, 153454. https://doi.org/10.1016/j.prp.2021.153454

Paňková, K., Rösel, D., Novotný, M., & Brábek, J. (2010). The molecular mechanisms of transition between mesenchymal and amoeboid invasiveness in tumor cells. *Cellular and Molecular Life Sciences*, *67*(1), 63–71. https://doi.org/10.1007/s00018-009-0132-1

Paolillo, & Schinelli. (2019). Extracellular Matrix Alterations in Metastatic Processes. *International Journal of Molecular Sciences*, *20*(19), 4947. https://doi.org/10.3390/ijms20194947

Parvatikar, P. P., Patil, S., Hoskeri, J., Swargam, S., Kulkarni, R. V., & Das, K. K. (2022). Screening and Development of Transglutaminase-2 Inhibitors and their Derivative as Anti-lung Cancer Agent by in silico and in vitro

Approaches. *Current Computer-Aided Drug Design*, *18*(1), 41–51. https://doi.org/10.2174/1573409917666210322120350

Patmore, S., Dhami, S. P. S., & O'Sullivan, J. M. (2020). Von Willebrand factor and cancer; metastasis and coagulopathies. *Journal of Thrombosis and Haemostasis*, *18*(10), 2444–2456. https://doi.org/10.1111/jth.14976

Patras, L., Shaashua, L., Matei, I., & Lyden, D. (2023). Immune determinants of the pre-metastatic niche. *Cancer Cell*, *41*(3), 546–572. https://doi.org/10.1016/j.ccell.2023.02.018

Payton, C., Pang, L. Y., Gray, M., & Argyle, D. J. (2021). Exosomes Derived from Radioresistant Breast Cancer Cells Promote Therapeutic Resistance in Naïve Recipient Cells. *Journal of Personalized Medicine*, *11*(12), 1310. https://doi.org/10.3390/jpm11121310

Pearson, G. W. (2019). Control of Invasion by Epithelial-to-Mesenchymal Transition Programs during Metastasis. *Journal of Clinical Medicine*, *8*(5), 646. https://doi.org/10.3390/jcm8050646

Peeney, D., Jensen, S. M., Castro, N. P., Kumar, S., Noonan, S., Handler, C., Kuznetsov, A., Shih, J., Tran, A. D., Salomon, D. S., & Stetler-Stevenson, W. G. (2020). TIMP-2 suppresses tumor growth and metastasis in murine model of triple-negative breast cancer. *Carcinogenesis*, *41*(3), 313–325. https://doi.org/10.1093/carcin/bgz172

Peinado, H., Zhang, H., Matei, I. R., Costa-Silva, B., Hoshino, A., Rodrigues, G., Psaila, B., Kaplan, R. N., Bromberg, J. F., Kang, Y., Bissell, M. J., Cox, T. R., Giaccia, A. J., Erler, J. T., Hiratsuka, S., Ghajar, C. M., & Lyden, D. (2017). Pre-metastatic niches: organ-specific homes for metastases. *Nature Reviews Cancer*, *17*(5), 302–317. https://doi.org/10.1038/nrc.2017.6

Pinto, M. L., Rios, E., Silva, A. C., Neves, S. C., Caires, H. R., Pinto, A. T., Durães, C., Carvalho, F. A., Cardoso, A. P., Santos, N. C., Barrias, C. C., Nascimento, D. S., Pinto-do-Ó, P., Barbosa, M. A., Carneiro, F., & Oliveira, M. J. (2017). Decellularized human colorectal cancer matrices polarize macrophages towards an anti-inflammatory phenotype promoting cancer cell invasion via CCL18. *Biomaterials*, *124*, 211–224. https://doi.org/10.1016/j.biomaterials.2017.02.004

Popēna, I., Ābols, A., Saulīte, L., Pleiko, K., Zandberga, E., Jēkabsons, K., Endzeliņš, E., Llorente, A., Linē, A., & Riekstiņa, U. (2018). Effect of colorectal cancer-derived extracellular vesicles on the immunophenotype and cytokine secretion profile of monocytes and macrophages. *Cell Communication and Signaling*, *16*(1), 17. https://doi.org/10.1186/s12964-018-0229-y

Popov, Y., Sverdlov, D. Y., Sharma, A. K., Bhaskar, K. R., Li, S., Freitag, T. L., Lee, J., Dieterich, W., Melino, G., & Schuppan, D. (2011). Tissue Transglutaminase Does Not Affect Fibrotic Matrix Stability or Regression of Liver Fibrosis in Mice. *Gastroenterology*, *140*(5), 1642–1652. https://doi.org/10.1053/j.gastro.2011.01.040

Prasanna, T., Karapetis, C. S., Roder, D., Tie, J., Padbury, R., Price, T., Wong, R., Shapiro, J., Nott, L., Lee, M., Chua, Y. J., Craft, P., Piantadosi, C., Sorich, M., Gibbs, P., & Yip, D. (2018). The survival outcome of patients with metastatic colorectal cancer based on the site of metastases and the impact of molecular markers and site of primary cancer on metastatic pattern. *Acta Oncologica*, *57*(11), 1438–1444. https://doi.org/10.1080/0284186X.2018.1487581

Pugsley, M. K., & Tabrizchi, R. (2000). The vascular system. *Journal of Pharmacological and Toxicological Methods*, *44*(2), 333–340. https://doi.org/10.1016/S1056-8719(00)00125-8

Qiao, J., Fang, C.-Y., Chen, S.-X., Wang, X.-Q., Cui, S.-J., Liu, X.-H., Jiang, Y.-H., Wang, J., Zhang, Y., Yang, P.-Y., & Liu, F. (2015). Stroma derived COL6A3 is a potential prognosis marker of colorectal carcinoma revealed by quantitative proteomics. *Oncotarget*, *6*(30), 29929–29946. https://doi.org/10.18632/oncotarget.4966

Rabie, E. M., Zhang, S. X., Kourouklis, A. P., Kilinc, A. N., Simi, A. K., Radisky, D. C., Tien, J., & Nelson, C. M. (2021). Matrix degradation and cell proliferation are coupled to promote invasion and escape from an engineered human breast microtumor. *Integrative Biology*, *13*(1), 17–29. https://doi.org/10.1093/intbio/zyaa026

Rai, A., Greening, D. W., Chen, M., Xu, R., Ji, H., & Simpson, R. J. (2019). Exosomes Derived from Human Primary and Metastatic Colorectal Cancer Cells Contribute to Functional Heterogeneity of Activated Fibroblasts by Reprogramming Their Proteome. *PROTEOMICS*, *19*(8), 1800148. https://doi.org/10.1002/pmic.201800148

Rai, A., Greening, D. W., Xu, R., Chen, M., Suwakulsiri, W., & Simpson, R. J. (2021). Secreted midbody remnants are a class of extracellular vesicles molecularly distinct from exosomes and microparticles. *Communications Biology*, *4*(1), 400. https://doi.org/10.1038/s42003-021-01882-z

Ramamoorthy, P., Thomas, S. M., Kaushik, G., Subramaniam, D., Chastain, K. M., Dhar, A., Tawfik, O., Kasi, A., Sun, W., Ramalingam, S., Gunewardena, S., Umar, S., Mammen, J. M., Padhye, S. B., Weir, S. J., Jensen, R. A., Sittampalam, G. S., & Anant, S. (2019). Metastatic Tumor-in-a-Dish, a Novel Multicellular Organoid to Study Lung Colonization and Predict Therapeutic Response. *Cancer Research*, *79*(7), 1681–1695. https://doi.org/10.1158/0008-5472.CAN-18-2602

Ramos, S., Ferreira, S., Fernandes, A. S., & Saraiva, N. (2022). Lysyl Oxidases Expression and Breast Cancer Progression: A Bioinformatic Analysis. *Frontiers in Pharmacology*, *13*. https://doi.org/10.3389/fphar.2022.883998

Rao, V. S., Gu, Q., Tzschentke, S., Lin, K., Ganig, N., Thepkaysone, M.-L., Wong, F. C., Polster, H., Seifert, L., Seifert, A. M., Buck, N., Riediger, C., Weiße, J., Gutschner, T., Michen, S., Temme, A., Schneider, M., Baenke, F., Weitz, J., & Kahlert, C. (2022). Extravesicular TIMP-1 is a non-invasive independent prognostic marker and potential therapeutic target in colorectal liver metastases. *Oncogene*, *41*(12), 1809–1820. https://doi.org/10.1038/s41388-022-02218-9

Ray, A., Slama, Z. M., Morford, R. K., Madden, S. A., & Provenzano, P. P. (2017). Enhanced Directional Migration of Cancer Stem Cells in 3D Aligned Collagen Matrices. *Biophysical Journal*, *112*(5), 1023–1036. https://doi.org/10.1016/j.bpj.2017.01.007

Reggiani Bonetti, L., Barresi, V., Bettelli, S., Domati, F., & Palmiere, C. (2016). Poorly differentiated clusters (PDC) in colorectal cancer: what is and ought

to be known. *Diagnostic Pathology*, *11*(1), 31. https://doi.org/10.1186/s13000-016-0481-7

Reis, S. T. dos, Viana, N. I., Iscaife, A., Pontes Junior, J., Dip, N., Antunes, A. A., Guimarães, V. R., Santana, I., Nahas, W. C., Srougi, M., & Leite, K. R. M. (2015). Loss of TIMP-1 immune expression and tumor recurrence in localized prostate cancer. *International Braz j Urol*, *41*(6), 1088–1095. https://doi.org/10.1590/S1677-5538.IBJU.2014.0451

Ren, R., Sun, H., Ma, C., Liu, J., & Wang, H. (2019). Colon cancer cells secrete exosomes to promote self-proliferation by shortening mitosis duration and activation of STAT3 in a hypoxic environment. *Cell & Bioscience*, *9*(1), 62. https://doi.org/10.1186/s13578-019-0325-8

Ribatti, D., Tamma, R., & Annese, T. (2020). Epithelial-Mesenchymal Transition in Cancer: A Historical Overview. *Translational Oncology*, *13*(6), 100773. https://doi.org/10.1016/j.tranon.2020.100773

Riedl, A., Schlederer, M., Pudelko, K., Stadler, M., Walter, S., Unterleuthner, D., Unger, C., Kramer, N., Hengstschläger, M., Kenner, L., Pfeiffer, D., Krupitza, G., & Dolznig, H. (2016). Comparison of cancer cells cultured in 2D vs 3D reveals differences in AKT/mTOR/S6-kinase signaling and drug response. *Journal of Cell Science*. https://doi.org/10.1242/jcs.188102

Riihimäki, M., Thomsen, H., Sundquist, K., Sundquist, J., & Hemminki, K. (2018). Clinical landscape of cancer metastases. *Cancer Medicine*, *7*(11), 5534–5542. https://doi.org/10.1002/cam4.1697

Rubinstein, M. R., Baik, J. E., Lagana, S. M., Han, R. P., Raab, W. J., Sahoo, D., Dalerba, P., Wang, T. C., & Han, Y. W. (2019). *Fusobacterium nucleatum* promotes colorectal cancer by inducing Wnt/β-catenin modulator Annexin A1. *EMBO Reports*, *20*(4). https://doi.org/10.15252/embr.201847638

Russo, C., Lewis, E. E. L., Flint, L., & Clench, M. R. (2018). Mass Spectrometry Imaging of 3D Tissue Models. *PROTEOMICS*, *18*(14), 1700462. https://doi.org/10.1002/pmic.201700462

Sahai, E., Garcia-Medina, R., Pouysségur, J., & Vial, E. (2007). Smurf1 regulates tumor cell plasticity and motility through degradation of RhoA leading to

localized inhibition of contractility. *Journal of Cell Biology*, *176*(1), 35–42. https://doi.org/10.1083/jcb.200605135

Saitoh, M. (2018). Involvement of partial EMT in cancer progression. *The Journal of Biochemistry*, *164*(4), 257–264. https://doi.org/10.1093/jb/mvy047

Sant, S., & Johnston, P. A. (2017). The production of 3D tumor spheroids for cancer drug discovery. *Drug Discovery Today: Technologies*, *23*, 27–36. https://doi.org/10.1016/j.ddtec.2017.03.002

Sanz-Ros, J., Mas-Bargues, C., Romero-García, N., Huete-Acevedo, J., Dromant, M., & Borrás, C. (2023). Extracellular Vesicles as Therapeutic Resources in the Clinical Environment. *International Journal of Molecular Sciences*, *24*(3), 2344. https://doi.org/10.3390/ijms24032344

Sato, T., Vries, R. G., Snippert, H. J., van de Wetering, M., Barker, N., Stange, D. E., van Es, J. H., Abo, A., Kujala, P., Peters, P. J., & Clevers, H. (2009). Single Lgr5 stem cells build crypt-villus structures in vitro without a mesenchymal niche. *Nature*, *459*(7244), 262–265. https://doi.org/10.1038/nature07935

Savina, A., Furlán, M., Vidal, M., & Colombo, M. I. (2003). Exosome Release Is Regulated by a Calcium-dependent Mechanism in K562 Cells. *Journal of Biological Chemistry*, *278*(22), 20083–20090. https://doi.org/10.1074/jbc.M301642200

Scavo, M. P., Rizzi, F., Depalo, N., Fanizza, E., Ingrosso, C., Curri, M. L., & Giannelli, G. (2020). A Possible Role of FZD10 Delivering Exosomes Derived from Colon Cancers Cell Lines in Inducing Activation of Epithelial–Mesenchymal Transition in Normal Colon Epithelial Cell Line. *International Journal of Molecular Sciences*, *21*(18), 6705. https://doi.org/10.3390/ijms21186705

Schillaci, O., Fontana, S., Monteleone, F., Taverna, S., Di Bella, M. A., Di Vizio, D., & Alessandro, R. (2017). Exosomes from metastatic cancer cells transfer amoeboid phenotype to non-metastatic cells and increase endothelial permeability: their emerging role in tumor heterogeneity. *Scientific Reports*, *7*(1), 4711. https://doi.org/10.1038/s41598-017-05002-y

Schmidt-Arras, D., & Rose-John, S. (2016). IL-6 pathway in the liver: From physiopathology to therapy. *Journal of Hepatology*, *64*(6), 1403–1415. https://doi.org/10.1016/j.jhep.2016.02.004

Schneikert, J., & Behrens, J. (2007). The canonical Wnt signalling pathway and its APC partner in colon cancer development. *Gut*, *56*(3), 417–425. https://doi.org/10.1136/gut.2006.093310

Schwager, S. C., Young, K. M., Hapach, L. A., Carlson, C. M., Mosier, J. A., McArdle, T. J., Wang, W., Schunk, C., Jayathilake, A. L., Bates, M. E., Bordeleau, F., Antonyak, M. A., Cerione, R. A., & Reinhart-King, C. A. (2022). Weakly migratory metastatic breast cancer cells activate fibroblasts via microvesicle-Tg2 to facilitate dissemination and metastasis. *ELife*, *11*. https://doi.org/10.7554/eLife.74433

Segeritz, C.-P., & Vallier, L. (2017). Cell Culture. In *Basic Science Methods for Clinical Researchers* (pp. 151–172). Elsevier. https://doi.org/10.1016/B978-0-12-803077-6.00009-6

Sepulveda, A. R., Hamilton, S. R., Allegra, C. J., Grody, W., Cushman-Vokoun, A. M., Funkhouser, W. K., Kopetz, S. E., Lieu, C., Lindor, N. M., Minsky, B. D., Monzon, F. A., Sargent, D. J., Singh, V. M., Willis, J., Clark, J., Colasacco, C., Rumble, R. B., Temple-Smolkin, R., Ventura, C. B., & Nowak, J. A. (2017). Molecular Biomarkers for the Evaluation of Colorectal Cancer: Guideline From the American Society for Clinical Pathology, College of American Pathologists, Association for Molecular Pathology, and the American Society of Clinical Oncology. *Journal of Clinical Oncology*, *35*(13), 1453–1486. https://doi.org/10.1200/JCO.2016.71.9807

Shangguan, W., Fan, C., Chen, X., Lu, R., Liu, Y., Li, Y., Shang, Y., Yin, D., Zhang, S., Huang, Q., Li, X., Meng, W., Xu, H., Zhou, Z., Hu, J., & Mo, X. (2017). Endothelium originated from colorectal cancer stem cells constitute cancer blood vessels. *Cancer Science*, *108*(7), 1357–1367. https://doi.org/10.1111/cas.13262

Shapouri-Moghaddam, A., Mohammadian, S., Vazini, H., Taghadosi, M., Esmaeili, S., Mardani, F., Seifi, B., Mohammadi, A., Afshari, J. T., & Sahebkar, A. (2018). Macrophage plasticity, polarization, and function in

health and disease. *Journal of Cellular Physiology*, *233*(9), 6425–6440. https://doi.org/10.1002/jcp.26429

Shi, H., Xu, J. M., Hu, N. Z., Wang, X. L., Mei, Q., & Song, Y. L. (2006). Transfection of mouse macrophage metalloelastase gene into murine CT-26 colon cancer cells suppresses orthotopic tumor growth, angiogenesis and vascular endothelial growth factor expression. *Cancer Letters*, *233*(1), 139–150. https://doi.org/10.1016/j.canlet.2005.03.010

Shiga, K., Hara, M., Nagasaki, T., Sato, T., Takahashi, H., & Takeyama, H. (2015). Cancer-Associated Fibroblasts: Their Characteristics and Their Roles in Tumor Growth. *Cancers*, *7*(4), 2443–2458. https://doi.org/10.3390/cancers7040902

Shimoda, M. (2019). *Extracellular vesicle-associated MMPs: A modulator of the tissue microenvironment* (pp. 35–66). https://doi.org/10.1016/bs.acc.2018.10.006

Shinde, A., Kulkoyluoglu Cotul, E., Chen, H., Smith, A., Libring, S., Solorio, L., & Wendt, M. K. (2022). Transglutaminase-2 mediates acquisition of neratinib resistance in metastatic breast cancer. *Molecular Biomedicine*, *3*(1), 19. https://doi.org/10.1186/s43556-022-00079-y

Shinde, A., Paez, J. S., Libring, S., Hopkins, K., Solorio, L., & Wendt, M. K. (2020). Transglutaminase-2 facilitates extracellular vesicle-mediated establishment of the metastatic niche. *Oncogenesis*, *9*(2), 16. https://doi.org/10.1038/s41389-020-0204-5

Shinohara, H., Kuranaga, Y., Kumazaki, M., Sugito, N., Yoshikawa, Y., Takai, T., Taniguchi, K., Ito, Y., & Akao, Y. (2017). Regulated Polarization of Tumor-Associated Macrophages by miR-145 via Colorectal Cancer–Derived Extracellular Vesicles. *The Journal of Immunology*, *199*(4), 1505–1515. https://doi.org/10.4049/jimmunol.1700167

Shiromizu, T., Kume, H., Ishida, M., Adachi, J., Kano, M., Matsubara, H., & Tomonaga, T. (2017). Quantitation of putative colorectal cancer biomarker candidates in serum extracellular vesicles by targeted proteomics. *Scientific Reports*, *7*(1), 12782. https://doi.org/10.1038/s41598-017-13092-x

Shivji, S., Cyr, D. P., Pun, C., Duan, K., Sari, A., Tomin, R., Ng, D., Brar, A., Zerhouni, S., Kennedy, E., Brar, M., Swallow, C. J., Conner, J., & Kirsch, R. (2022). A Novel Combined Tumor Budding-Poorly Differentiated Clusters Grading System Predicts Recurrence and Survival in Stage I-III Colorectal Cancer. *American Journal of Surgical Pathology*, *46*(10), 1340–1351. https://doi.org/10.1097/PAS.0000000000001920

Shweke, N., Boulos, N., Jouanneau, C., Vandermeersch, S., Melino, G., Dussaule, J.-C., Chatziantoniou, C., Ronco, P., & Boffa, J.-J. (2008). Tissue Transglutaminase Contributes to Interstitial Renal Fibrosis by Favoring Accumulation of Fibrillar Collagen through TGF-β Activation and Cell Infiltration. *The American Journal of Pathology*, *173*(3), 631–642. https://doi.org/10.2353/ajpath.2008.080025

Siddiqui, J. A., Pothuraju, R., Khan, P., Sharma, G., Muniyan, S., Seshacharyulu, P., Jain, M., Nasser, M. W., & Batra, S. K. (2022). Pathophysiological role of growth differentiation factor 15 (GDF15) in obesity, cancer, and cachexia. *Cytokine & Growth Factor Reviews*, *64*, 71–83. https://doi.org/10.1016/j.cytogfr.2021.11.002

Siegel, R. L., Miller, K. D., Wagle, N. S., & Jemal, A. (2023). Cancer statistics, 2023. *CA: A Cancer Journal for Clinicians*, *73*(1), 17–48. https://doi.org/10.3322/caac.21763

Singh, R. K., Chang, H.-W., Yan, D., Lee, K. M., Ucmak, D., Wong, K., Abrouk, M., Farahnik, B., Nakamura, M., Zhu, T. H., Bhutani, T., & Liao, W. (2017). Influence of diet on the gut microbiome and implications for human health. *Journal of Translational Medicine*, *15*(1), 73. https://doi.org/10.1186/s12967-017-1175-y

Slater, C., de La Mare, J., & Edkins, A. (2018). In vitro analysis of putative cancer stem cell populations and chemosensitivity in the SW480 and SW620 colon cancer metastasis model. *Oncology Letters*. https://doi.org/10.3892/ol.2018.8431

Sökeland, G., & Schumacher, U. (2019). The functional role of integrins during intra- and extravasation within the metastatic cascade. *Molecular Cancer*, *18*(1), 12. https://doi.org/10.1186/s12943-018-0937-3

Song, G., Xu, S., Zhang, H., Wang, Y., Xiao, C., Jiang, T., Wu, L., Zhang, T., Sun, X., Zhong, L., Zhou, C., Wang, Z., Peng, Z., Chen, J., & Wang, X. (2016). TIMP1 is a prognostic marker for the progression and metastasis of colon cancer through FAK-PI3K/AKT and MAPK pathway. *Journal of Experimental & Clinical Cancer Research*, *35*(1), 148. https://doi.org/10.1186/s13046-016-0427-7

Spence, J. R., Mayhew, C. N., Rankin, S. A., Kuhar, M. F., Vallance, J. E., Tolle, K., Hoskins, E. E., Kalinichenko, V. V., Wells, S. I., Zorn, A. M., Shroyer, N. F., & Wells, J. M. (2011). Directed differentiation of human pluripotent stem cells into intestinal tissue in vitro. *Nature*, *470*(7332), 105–109. https://doi.org/10.1038/nature09691

Sprenger, H., Kaufmann, A., Garn, H., Lahme, B., Gemsa, D., & Gressner, A. M. (1999). Differential expression of monocyte chemotactic protein-1 (MCP-1) in transforming rat hepatic stellate cells. *Journal of Hepatology*, *30*(1), 88–94. https://doi.org/10.1016/S0168-8278(99)80011-7

Stamnaes, J., Cardoso, I., Iversen, R., & Sollid, L. M. (2016). Transglutaminase 2 strongly binds to an extracellular matrix component other than fibronectin via its second C-terminal beta-barrel domain. *The FEBS Journal*, *283*(21), 3994–4010. https://doi.org/10.1111/febs.13907

Stella, G. M., Kolling, S., Benvenuti, S., & Bortolotto, C. (2019). Lung-Seeking Metastases. *Cancers*, *11*(7), 1010. https://doi.org/10.3390/cancers11071010

Stewart, C. L., Warner, S., Ito, K., Raoof, M., Wu, G. X., Kessler, J., Kim, J. Y., & Fong, Y. (2018). Cytoreduction for colorectal metastases: liver, lung, peritoneum, lymph nodes, bone, brain. When does it palliate, prolong survival, and potentially cure? *Current Problems in Surgery*, *55*(9), 330–379. https://doi.org/10.1067/j.cpsurg.2018.08.004

Stock, K., Estrada, M. F., Vidic, S., Gjerde, K., Rudisch, A., Santo, V. E., Barbier, M., Blom, S., Arundkar, S. C., Selvam, I., Osswald, A., Stein, Y., Gruenewald, S., Brito, C., van Weerden, W., Rotter, V., Boghaert, E., Oren, M., Sommergruber, W., … Graeser, R. (2016). Capturing tumor complexity

in vitro: Comparative analysis of 2D and 3D tumor models for drug discovery. *Scientific Reports*, *6*(1), 28951. https://doi.org/10.1038/srep28951

Sun, Y., Liu, S., Qiao, Z., Shang, Z., Xia, Z., Niu, X., Qian, L., Zhang, Y., Fan, L., Cao, C.-X., & Xiao, H. (2017). Systematic comparison of exosomal proteomes from human saliva and serum for the detection of lung cancer. *Analytica Chimica Acta*, *982*, 84–95. https://doi.org/10.1016/j.aca.2017.06.005

Suwakulsiri, W., Rai, A., Xu, R., Chen, M., Greening, D. W., & Simpson, R. J. (2019). Proteomic profiling reveals key cancer progression modulators in shed microvesicles released from isogenic human primary and metastatic colorectal cancer cell lines. *Biochimica et Biophysica Acta (BBA) - Proteins and Proteomics*, *1867*(12), 140171. https://doi.org/10.1016/j.bbapap.2018.11.008

Suwakulsiri, W., Xu, R., Rai, A., Shafiq, A., Chen, M., Greening, D. W., & Simpson, R. J. (2023). Comparative proteomic analysis of three major extracellular vesicle classes secreted from human primary and metastatic colorectal cancer cells: Exosomes, microparticles, and shed midbody remnants. *PROTEOMICS*. https://doi.org/10.1002/pmic.202300057

Szvicsek, Z., Oszvald, Á., Szabó, L., Sándor, G. O., Kelemen, A., Soós, A. Á., Pálóczi, K., Harsányi, L., Tölgyes, T., Dede, K., Bursics, A., Buzás, E. I., Zeöld, A., & Wiener, Z. (2019). Extracellular vesicle release from intestinal organoids is modulated by Apc mutation and other colorectal cancer progression factors. *Cellular and Molecular Life Sciences*, *76*(12), 2463–2476. https://doi.org/10.1007/s00018-019-03052-1

Tachibana, T., Onodera, H., Tsuruyama, T., Mori, A., Nagayama, S., Hiai, H., & Imamura, M. (2005). Increased Intratumor Vα24-Positive Natural Killer T Cells: A Prognostic Factor for Primary Colorectal Carcinomas. *Clinical Cancer Research*, *11*(20), 7322–7327. https://doi.org/10.1158/1078-0432.CCR-05-0877

Tang, M. K. S., Yue, P. Y. K., Ip, P. P., Huang, R.-L., Lai, H.-C., Cheung, A. N. Y., Tse, K. Y., Ngan, H. Y. S., & Wong, A. S. T. (2018). Soluble E-cadherin

promotes tumor angiogenesis and localizes to exosome surface. *Nature Communications*, *9*(1), 2270. https://doi.org/10.1038/s41467-018-04695-7

Tarin, D., Price, J. E., Kettlewell, M. G., Souter, R. G., Vass, A. C., & Crossley, B. (1984). Mechanisms of human tumor metastasis studied in patients with peritoneovenous shunts. *Cancer Research*, *44*(8), 3584–3592.

Tatsukawa, H., Takeuchi, T., Shinoda, Y., & Hitomi, K. (2020). Identification and characterization of substrates crosslinked by transglutaminases in liver and kidney fibrosis. *Analytical Biochemistry*, *604*, 113629. https://doi.org/10.1016/j.ab.2020.113629

Tempest, R., Guarnerio, S., Maani, R., Cooper, J., & Peake, N. (2021). The Biological and Biomechanical Role of Transglutaminase-2 in the Tumour Microenvironment. *Cancers*, *13*(11), 2788. https://doi.org/10.3390/cancers13112788

Teng, F., & Fussenegger, M. (2021). Shedding Light on Extracellular Vesicle Biogenesis and Bioengineering. *Advanced Science*, *8*(1), 2003505. https://doi.org/10.1002/advs.202003505

Theocharis, A. D., Skandalis, S. S., Gialeli, C., & Karamanos, N. K. (2016). Extracellular matrix structure. *Advanced Drug Delivery Reviews*, *97*, 4–27. https://doi.org/10.1016/j.addr.2015.11.001

Théry, C., Witwer, K. W., Aikawa, E., Alcaraz, M. J., Anderson, J. D., Andriantsitohaina, R., Antoniou, A., Arab, T., Archer, F., Atkin-Smith, G. K., Ayre, D. C., Bach, J.-M., Bachurski, D., Baharvand, H., Balaj, L., Baldacchino, S., Bauer, N. N., Baxter, A. A., Bebawy, M., … Zuba-Surma, E. K. (2018). Minimal information for studies of extracellular vesicles 2018 (MISEV2018): a position statement of the International Society for Extracellular Vesicles and update of the MISEV2014 guidelines. *Journal of Extracellular Vesicles*, *7*(1), 1535750. https://doi.org/10.1080/20013078.2018.1535750

Thiery, J. P., Acloque, H., Huang, R. Y. J., & Nieto, M. A. (2009). Epithelial-Mesenchymal Transitions in Development and Disease. *Cell*, *139*(5), 871–890. https://doi.org/10.1016/j.cell.2009.11.007

Thippabhotla, S., Zhong, C., & He, M. (2019). 3D cell culture stimulates the secretion of in vivo like extracellular vesicles. *Scientific Reports*, *9*(1), 13012. https://doi.org/10.1038/s41598-019-49671-3

Thongchot, S., Jamjuntra, P., Therasakvichya, S., Warnnissorn, M., Ferraresi, A., Thuwajit, P., Isidoro, C., & Thuwajit, C. (2021). Interleukin-8 released by cancer-associated fibroblasts attenuates the autophagy and promotes the migration of ovarian cancer cells. *International Journal of Oncology*, *58*(5), 14. https://doi.org/10.3892/ijo.2021.5194

Thursby, E., & Juge, N. (2017). Introduction to the human gut microbiota. *Biochemical Journal*, *474*(11), 1823–1836. https://doi.org/10.1042/BCJ20160510

Torres, S., Garcia-Palmero, I., Herrera, M., Bartolomé, R. A., Peña, C., Fernandez-Aceñero, M. J., Padilla, G., Peláez-García, A., Lopez-Lucendo, M., Rodriguez-Merlo, R., de Herreros, A. G., Bonilla, F., & Casal, J. I. (2015). LOXL2 Is Highly Expressed in Cancer-Associated Fibroblasts and Associates to Poor Colon Cancer Survival. *Clinical Cancer Research*, *21*(21), 4892–4902. https://doi.org/10.1158/1078-0432.CCR-14-3096

Travaglini, K. J., Nabhan, A. N., Penland, L., Sinha, R., Gillich, A., Sit, R. V., Chang, S., Conley, S. D., Mori, Y., Seita, J., Berry, G. J., Shrager, J. B., Metzger, R. J., Kuo, C. S., Neff, N., Weissman, I. L., Quake, S. R., & Krasnow, M. A. (2020). A molecular cell atlas of the human lung from single-cell RNA sequencing. *Nature*, *587*(7835), 619–625. https://doi.org/10.1038/s41586-020-2922-4

Unnikrishnan, K., Thomas, L. V., & Ram Kumar, R. M. (2021). Advancement of Scaffold-Based 3D Cellular Models in Cancer Tissue Engineering: An Update. *Frontiers in Oncology*, *11*. https://doi.org/10.3389/fonc.2021.733652

Valcz, G., Buzás, E. I., Kittel, Á., Krenács, T., Visnovitz, T., Spisák, S., Török, G., Homolya, L., Zsigrai, S., Kiszler, G., Antalffy, G., Pálóczi, K., Szállási, Z., Szabó, V., Sebestyén, A., Solymosi, N., Kalmár, A., Dede, K., Lőrincz, P., … Molnár, B. (2019). En bloc release of MVB-like small extracellular vesicle clusters by colorectal carcinoma cells. *Journal of Extracellular Vesicles*, *8*(1), 1596668. https://doi.org/10.1080/20013078.2019.1596668

Van Norman, G. A. (2019). Limitations of Animal Studies for Predicting Toxicity in Clinical Trials. *JACC: Basic to Translational Science*, *4*(7), 845–854. https://doi.org/10.1016/j.jacbts.2019.10.008

Vasudevan, J., Jiang, K., Fernandez, Javier. G., & Teck, L. C. (2022). Extracellular Matrix Mechanobiology in Cancer Cell Migration. *Acta Biomaterialia*. https://doi.org/10.1016/j.actbio.2022.10.016

Vuik, F. E., Nieuwenburg, S. A., Bardou, M., Lansdorp-Vogelaar, I., Dinis-Ribeiro, M., Bento, M. J., Zadnik, V., Pellisé, M., Esteban, L., Kaminski, M. F., Suchanek, S., Ngo, O., Májek, O., Leja, M., Kuipers, E. J., & Spaander, M. C. (2019). Increasing incidence of colorectal cancer in young adults in Europe over the last 25 years. *Gut*, *68*(10), 1820–1826. https://doi.org/10.1136/gutjnl-2018-317592

Wang, K., Zheng, J., Yu, J., Wu, Y., Guo, J., Xu, Z., & Sun, X. (2020). Knockdown of MMP-1 inhibits the progression of colorectal cancer by suppressing the PI3K/Akt/c-myc signaling pathway and EMT. *Oncology Reports*. https://doi.org/10.3892/or.2020.7490

Wang, P.-W., Wu, T.-H., Lin, T.-Y., Chen, M.-H., Yeh, C.-T., & Pan, T.-L. (2019). Characterization of the Roles of Vimentin in Regulating the Proliferation and Migration of HSCs during Hepatic Fibrogenesis. *Cells*, *8*(10), 1184. https://doi.org/10.3390/cells8101184

Wang, W., Li, D., Xiang, L., Lv, M., Tao, L., Ni, T., Deng, J., Gu, X., Masatara, S., Liu, Y., & Zhou, Y. (2019). TIMP-2 inhibits metastasis and predicts prognosis of colorectal cancer via regulating MMP-9. *Cell Adhesion & Migration*, *13*(1), 272–283. https://doi.org/10.1080/19336918.2019.1639303

Webber, J., Steadman, R., Mason, M. D., Tabi, Z., & Clayton, A. (2010). Cancer Exosomes Trigger Fibroblast to Myofibroblast Differentiation. *Cancer Research*, *70*(23), 9621–9630. https://doi.org/10.1158/0008-5472.CAN-10-1722

Wei, B., Zhou, X., Liang, C., Zheng, X., Lei, P., Fang, J., Han, X., Wang, L., Qi, C., & Wei, H. (2017). Human colorectal cancer progression correlates with LOX-induced ECM stiffening. *International Journal of Biological Sciences*, *13*(11), 1450–1457. https://doi.org/10.7150/ijbs.21230

Wei, C., Yang, C., Wang, S., Shi, D., Zhang, C., Lin, X., Liu, Q., Dou, R., & Xiong, B. (2019). Crosstalk between cancer cells and tumor associated macrophages is required for mesenchymal circulating tumor cell-mediated colorectal cancer metastasis. *Molecular Cancer*, *18*(1), 64. https://doi.org/10.1186/s12943-019-0976-4

Wei, Q., Qian, Y., Yu, J., & Wong, C. C. (2020). Metabolic rewiring in the promotion of cancer metastasis: mechanisms and therapeutic implications. *Oncogene*, *39*(39), 6139–6156. https://doi.org/10.1038/s41388-020-01432-7

Wells, R. G. (2013). Tissue mechanics and fibrosis. *Biochimica et Biophysica Acta (BBA) - Molecular Basis of Disease*, *1832*(7), 884–890. https://doi.org/10.1016/j.bbadis.2013.02.007

Weydert, Z., Lal-Nag, M., Mathews-Greiner, L., Thiel, C., Cordes, H., Küpfer, L., Guye, P., Kelm, J. M., & Ferrer, M. (2020). A 3D Heterotypic Multicellular Tumor Spheroid Assay Platform to Discriminate Drug Effects on Stroma versus Cancer Cells. *SLAS Discovery*, *25*(3), 265–276. https://doi.org/10.1177/2472555219880194

Willumsen, N., Jensen, C., Green, G., Nissen, N. I., Neely, J., Nelson, D. M., Pedersen, R. S., Frederiksen, P., Chen, I. M., Boisen, M. K., Johansen, A. Z., Madsen, D. H., Svane, I. M., Lipton, A., Leitzel, K., Ali, S. M., Erler, J. T., Hurkmans, D. P., Mathijssen, R. H. J., … Karsdal, M. A. (2022). Fibrotic activity quantified in serum by measurements of type III collagen pro-peptides can be used for prognosis across different solid tumor types. *Cellular and Molecular Life Sciences*, *79*(4), 204. https://doi.org/10.1007/s00018-022-04226-0

Winkler, J., Abisoye-Ogunniyan, A., Metcalf, K. J., & Werb, Z. (2020). Concepts of extracellular matrix remodelling in tumour progression and metastasis. *Nature Communications*, *11*(1), 5120. https://doi.org/10.1038/s41467-020-18794-x

Witwer, K. W., Goberdhan, D. C., O'Driscoll, L., Théry, C., Welsh, J. A., Blenkiron, C., Buzás, E. I., Di Vizio, D., Erdbrügger, U., Falcón-Pérez, J. M., Fu, Q., Hill, A. F., Lenassi, M., Lötvall, J., Nieuwland, R., Ochiya, T., Rome, S., Sahoo,

S., & Zheng, L. (2021). Updating MISEV: Evolving the minimal requirements for studies of extracellular vesicles. *Journal of Extracellular Vesicles*, *10*(14). https://doi.org/10.1002/jev2.12182

Wolf, P. (1967). The Nature and Significance of Platelet Products in Human Plasma. *British Journal of Haematology*, *13*(3), 269–288. https://doi.org/10.1111/j.1365-2141.1967.tb08741.x

Wu, X., Cai, J., Zuo, Z., & Li, J. (2019). Collagen facilitates the colorectal cancer stemness and metastasis through an integrin/PI3K/AKT/Snail signaling pathway. *Biomedicine & Pharmacotherapy*, *114*, 108708. https://doi.org/10.1016/j.biopha.2019.108708

Wu, X., Tao, P., Zhou, Q., Li, J., Yu, Z., Wang, X., Li, J., Li, C., Yan, M., Zhu, Z., Liu, B., & Su, L. (2017). IL-6 secreted by cancer-associated fibroblasts promotes epithelial-mesenchymal transition and metastasis of gastric cancer via JAK2/STAT3 signaling pathway. *Oncotarget*, *8*(13), 20741–20750. https://doi.org/10.18632/oncotarget.15119

Wu, Y., & Xu, Y. (2020). Integrated bioinformatics analysis of expression and gene regulation network of COL12A1 in colorectal cancer. *Cancer Medicine*, *9*(13), 4743–4755. https://doi.org/10.1002/cam4.2899

Wu, Y.-H., & Chou, C.-Y. (2022). Collagen XI Alpha 1 Chain, a Novel Therapeutic Target for Cancer Treatment. *Frontiers in Oncology*, *12*. https://doi.org/10.3389/fonc.2022.925165

Xi, S., Zheng, X., Li, X., Jiang, Y., Wu, Y., Gong, J., Jie, Y., Li, Z., Cao, J., Sha, L., Zhang, M., & Chong, Y. (2021). Activated Hepatic Stellate Cells Induce Infiltration and Formation of CD163+ Macrophages via CCL2/CCR2 Pathway. *Frontiers in Medicine*, *8*. https://doi.org/10.3389/fmed.2021.627927

Xiang, D.-M., Sun, W., Ning, B.-F., Zhou, T.-F., Li, X.-F., Zhong, W., Cheng, Z., Xia, M.-Y., Wang, X., Deng, X., Wang, W., Li, H.-Y., Cui, X.-L., Li, S.-C., Wu, B., Xie, W.-F., Wang, H.-Y., & Ding, J. (2018). The HLF/IL-6/STAT3 feedforward circuit drives hepatic stellate cell activation to promote liver fibrosis. *Gut*, *67*(9), 1704–1715. https://doi.org/10.1136/gutjnl-2016-313392

Xie, D., Jia, S., Ping, D., Wang, D., & Cao, L. (2022). Scaffold-based three-dimensional cell model of pancreatic cancer is more suitable than scaffold-free three-dimensional cell model of pancreatic cancer for drug discovery. *Cytotechnology*, *74*(6), 657–667. https://doi.org/10.1007/s10616-022-00553-z

Xu, L., Lin, W., Wen, L., & Li, G. (2019). Lgr5 in cancer biology: functional identification of Lgr5 in cancer progression and potential opportunities for novel therapy. *Stem Cell Research & Therapy*, *10*(1), 219. https://doi.org/10.1186/s13287-019-1288-8

Xu, M., Zhang, T., Xia, R., Wei, Y., & Wei, X. (2022). Targeting the tumor stroma for cancer therapy. *Molecular Cancer*, *21*(1), 208. https://doi.org/10.1186/s12943-022-01670-1

Xu, R., Zhou, X., Wang, S., & Trinkle, C. (2021). Tumor organoid models in precision medicine and investigating cancer-stromal interactions. *Pharmacology & Therapeutics*, *218*, 107668. https://doi.org/10.1016/j.pharmthera.2020.107668

Xuefeng, X., Hou, M.-X., Yang, Z.-W., Agudamu, A., Wang, F., Su, X.-L., Li, X., Shi, L., Terigele, T., Bao, L.-L., & Wu, X.-L. (2020). Epithelial–mesenchymal transition and metastasis of colon cancer cells induced by the FAK pathway in cancer-associated fibroblasts. *Journal of International Medical Research*, *48*(6), 030006052093124. https://doi.org/10.1177/0300060520931242

Yamada, K. M., & Sixt, M. (2019). Mechanisms of 3D cell migration. *Nature Reviews Molecular Cell Biology*, *20*(12), 738–752. https://doi.org/10.1038/s41580-019-0172-9

Yamada, Y., Yoshida, C., Hamada, K., Kikkawa, Y., & Nomizu, M. (2020). Development of Three-Dimensional Cell Culture Scaffolds Using Laminin Peptide-Conjugated Agarose Microgels. *Biomacromolecules*, *21*(9), 3765–3771. https://doi.org/10.1021/acs.biomac.0c00871

Yamagishi, H., Kuroda, H., Imai, Y., & Hiraishi, H. (2016). Molecular pathogenesis of sporadic colorectal cancers. *Chinese Journal of Cancer*, *35*(1), 4. https://doi.org/10.1186/s40880-015-0066-y

Yáñez-Mó, M., Siljander, P. R.-M., Andreu, Z., Bedina Zavec, A., Borràs, F. E., Buzas, E. I., Buzas, K., Casal, E., Cappello, F., Carvalho, J., Colás, E., Cordeiro-da Silva, A., Fais, S., Falcon-Perez, J. M., Ghobrial, I. M., Giebel, B., Gimona, M., Graner, M., Gursel, I., … De Wever, O. (2015). Biological properties of extracellular vesicles and their physiological functions. *Journal of Extracellular Vesicles*, *4*(1), 27066. https://doi.org/10.3402/jev.v4.27066

Yang, A., Wang, M., Wang, Y., Cai, W., Li, Q., Zhao, T., Zhang, L., Houck, K., Chen, X., Jin, Y., Mu, J., Dong, J., & Li, M. (2018). Cancer cell-derived von Willebrand factor enhanced metastasis of gastric adenocarcinoma. *Oncogenesis*, *7*(1), 12. https://doi.org/10.1038/s41389-017-0023-5

Yang, L., Gong, S., Qiao, P., Zhao, R., Huang, S., Zhou, J., & Hu, A. (2023). CAFs-derived rho-associated kinase1 mediated EMT to promote laryngeal squamous cell carcinoma metastasis. *Cancer Cell International*, *23*(1), 70. https://doi.org/10.1186/s12935-023-02911-z

Yang, Q., Xu, J., Gu, J., Shi, H., Zhang, J., Zhang, J., Chen, Z., Fang, X., Zhu, T., & Zhang, X. (2022). Extracellular Vesicles in Cancer Drug Resistance: Roles, Mechanisms, and Implications. *Advanced Science*, *9*(34), 2201609. https://doi.org/10.1002/advs.202201609

Yang, W., Arii, S., Gorrin-Rivas, M. J., Mori, A., Onodera, H., & Imamura, M. (2001). Human macrophage metalloelastase gene expression in colorectal carcinoma and its clinicopathologic significance. *Cancer*, *91*(7), 1277–1283.

Yang, Y., & Cao, Y. (2022). The impact of VEGF on cancer metastasis and systemic disease. *Seminars in Cancer Biology*, *86*, 251–261. https://doi.org/10.1016/j.semcancer.2022.03.011

Yao, C., Weng, J., Feng, L., Zhang, W., Xu, Y., Zhang, P., Tanaka, Y., & Su, L. (2022). SIPA1 Enhances Aerobic Glycolysis Through HIF-2α Pathway to Promote Breast Cancer Metastasis. *Frontiers in Cell and Developmental Biology*, *9*. https://doi.org/10.3389/fcell.2021.779169

Yin, Y., Liu, B., Cao, Y., Yao, S., Liu, Y., Jin, G., Qin, Y., Chen, Y., Cui, K., Zhou, L., Bian, Z., Fei, B., Huang, S., & Huang, Z. (2022). Colorectal Cancer-Derived Small Extracellular Vesicles Promote Tumor Immune Evasion by

Upregulating PD-L1 Expression in Tumor-Associated Macrophages. *Advanced Science*, *9*(9), 2102620. https://doi.org/10.1002/advs.202102620

Yin, Y., Yao, S., Hu, Y., Feng, Y., Li, M., Bian, Z., Zhang, J., Qin, Y., Qi, X., Zhou, L., Fei, B., Zou, J., Hua, D., & Huang, Z. (2017). The Immune-microenvironment Confers Chemoresistance of Colorectal Cancer through Macrophage-Derived IL6. *Clinical Cancer Research*, *23*(23), 7375–7387. https://doi.org/10.1158/1078-0432.CCR-17-1283

Yoshimura, T. (2018). The chemokine MCP-1 (CCL2) in the host interaction with cancer: a foe or ally? *Cellular & Molecular Immunology*, *15*(4), 335–345. https://doi.org/10.1038/cmi.2017.135

Yuan, Q., Chu, Y., Li, X., Shi, Y., Chen, Y., Zhao, J., Lu, J., Liu, K., & Guo, Y. (2023). CAFrgDB: a database for cancer-associated fibroblasts related genes and their functions in cancer. *Cancer Gene Therapy*. https://doi.org/10.1038/s41417-023-00603-4

Yuzhalin, A. E., Lim, S. Y., Kutikhin, A. G., & Gordon-Weeks, A. N. (2018). Dynamic matrisome: ECM remodeling factors licensing cancer progression and metastasis. *Biochimica et Biophysica Acta (BBA) - Reviews on Cancer*, *1870*(2), 207–228. https://doi.org/10.1016/j.bbcan.2018.09.002

Zeltz, C., Primac, I., Erusappan, P., Alam, J., Noel, A., & Gullberg, D. (2020). Cancer-associated fibroblasts in desmoplastic tumors: emerging role of integrins. *Seminars in Cancer Biology*, *62*, 166–181. https://doi.org/10.1016/j.semcancer.2019.08.004

Zeng, Z., Li, Y., Pan, Y., Lan, X., Song, F., Sun, J., Zhou, K., Liu, X., Ren, X., Wang, F., Hu, J., Zhu, X., Yang, W., Liao, W., Li, G., Ding, Y., & Liang, L. (2018). Cancer-derived exosomal miR-25-3p promotes pre-metastatic niche formation by inducing vascular permeability and angiogenesis. *Nature Communications*, *9*(1), 5395. https://doi.org/10.1038/s41467-018-07810-w

Zeng, Z.-S., Cohen, A. M., & Guillem, J. G. (1999). Loss of basement membrane type IV collagen is associated with increased expression of metalloproteinases 2 and 9 (MMP-2 and MMP-9) during human colorectal tumorigenesis. *Carcinogenesis*, *20*(5), 749–755. https://doi.org/10.1093/carcin/20.5.749

Zhai, J., Shen, J., Xie, G., Wu, J., He, M., Gao, L., Zhang, Y., Yao, X., & Shen, L. (2019). Cancer-associated fibroblasts-derived IL-8 mediates resistance to cisplatin in human gastric cancer. *Cancer Letters*, *454*, 37–43. https://doi.org/10.1016/j.canlet.2019.04.002

Zhang, C., Fei, Y., Wang, H., Hu, S., Liu, C., Hu, R., & Du, Q. (2023). CAFs orchestrates tumor immune microenvironment—A new target in cancer therapy? *Frontiers in Pharmacology*, *14*. https://doi.org/10.3389/fphar.2023.1113378

Zhang, C., Wang, X.-Y., Zhang, P., He, T.-C., Han, J.-H., Zhang, R., Lin, J., Fan, J., Lu, L., Zhu, W.-W., Jia, H.-L., Zhang, J.-B., & Chen, J.-H. (2022). Cancer-derived exosomal HSPC111 promotes colorectal cancer liver metastasis by reprogramming lipid metabolism in cancer-associated fibroblasts. *Cell Death & Disease*, *13*(1), 57. https://doi.org/10.1038/s41419-022-04506-4

Zhang, J., Gu, C., Song, Q., Zhu, M., Xu, Y., Xiao, M., & Zheng, W. (2020). Identifying cancer-associated fibroblasts as emerging targets for hepatocellular carcinoma. *Cell & Bioscience*, *10*(1), 127. https://doi.org/10.1186/s13578-020-00488-y

Zhang, R., Qi, F., Zhao, F., Li, G., Shao, S., Zhang, X., Yuan, L., & Feng, Y. (2019). Cancer-associated fibroblasts enhance tumor-associated macrophages enrichment and suppress NK cells function in colorectal cancer. *Cell Death & Disease*, *10*(4), 273. https://doi.org/10.1038/s41419-019-1435-2

Zhang, S., Yao, H.-F., Li, H., Su, T., Jiang, S.-H., Wang, H., Zhang, Z.-G., Dong, F.-Y., Yang, Q., & Yang, X.-M. (2023). Transglutaminases are oncogenic biomarkers in human cancers and therapeutic targeting of TGM2 blocks chemoresistance and macrophage infiltration in pancreatic cancer. *Cellular Oncology*. https://doi.org/10.1007/s13402-023-00824-7

Zhang, X., Quan, F., Xu, J., Xiao, Y., Li, X., & Li, Y. (2020). Combination of multiple tumor-infiltrating immune cells predicts clinical outcome in colon cancer. *Clinical Immunology*, *215*, 108412. https://doi.org/10.1016/j.clim.2020.108412

Zhang, X., Zhang, Y., Qiu, X., Cai, J., Yang, Z., & Song, F. (2022). Extracellular Vesicles Derived from Lung Cancer Cells Induce Transformation of Normal Fibroblasts into Lung Cancer-Associated Fibroblasts and Promote Metastasis of Lung Cancer by Delivering lncRNA HOTAIR. *Stem Cells International*, *2022*, 1–13. https://doi.org/10.1155/2022/3805013

Zhang, Y., Zhang, L., Zheng, S., Li, M., Xu, C., Jia, D., Qi, Y., Hou, T., Wang, L., Wang, B., Li, A., Chen, S., Si, J., & Zhuo, W. (2022). *Fusobacterium nucleatum* promotes colorectal cancer cells adhesion to endothelial cells and facilitates extravasation and metastasis by inducing ALPK1/NF-κB/ICAM1 axis. *Gut Microbes*, *14*(1). https://doi.org/10.1080/19490976.2022.2038852

Zhang, Z., & Castelló, A. (2017). Principal components analysis in clinical studies. *Annals of Translational Medicine*, *5*(17), 351–351. https://doi.org/10.21037/atm.2017.07.12

Zhao, H., Ming, T., Tang, S., Ren, S., Yang, H., Liu, M., Tao, Q., & Xu, H. (2022). Wnt signaling in colorectal cancer: pathogenic role and therapeutic target. *Molecular Cancer*, *21*(1), 144. https://doi.org/10.1186/s12943-022-01616-7

Zhao, Z., Chen, X., Dowbaj, A. M., Sljukic, A., Bratlie, K., Lin, L., Fong, E. L. S., Balachander, G. M., Chen, Z., Soragni, A., Huch, M., Zeng, Y. A., Wang, Q., & Yu, H. (2022). Organoids. *Nature Reviews Methods Primers*, *2*(1), 94. https://doi.org/10.1038/s43586-022-00174-y

Zheng, X., Xu, K., Zhou, B., Chen, T., Huang, Y., Li, Q., Wen, F., Ge, W., Wang, J., Yu, S., Sun, L., Zhu, L., Liu, W., Gao, H., Yue, L., Cai, X., Zhang, Q., Ruan, G., Zhu, T., … Zheng, S. (2020). A circulating extracellular vesicles-based novel screening tool for colorectal cancer revealed by shotgun and data-independent acquisition mass spectrometry. *Journal of Extracellular Vesicles*, *9*(1), 1750202. https://doi.org/10.1080/20013078.2020.1750202

Zhong, B., Cheng, B., Huang, X., Xiao, Q., Niu, Z., Chen, Y., Yu, Q., Wang, W., & Wu, X.-J. (2021). Colorectal cancer-associated fibroblasts promote metastasis by up-regulating LRG1 through stromal IL-6/STAT3 signaling. *Cell Death & Disease*, *13*(1), 16. https://doi.org/10.1038/s41419-021-04461-6

Zhou, B., Huang, Y., Feng, Q., Zhu, H., Xu, Z., Chen, L., Peng, X., Yang, W., Xu, D., & Qiu, Y. (2022). TRIM16 promotes aerobic glycolysis and pancreatic cancer metastasis by modulating the NIK-SIX1 axis in a ligase-independent manner. *American Journal of Cancer Research*, *12*(11), 5205–5225.

Zhuyan, J., Chen, M., Zhu, T., Bao, X., Zhen, T., Xing, K., Wang, Q., & Zhu, S. (2020). Critical steps to tumor metastasis: alterations of tumor microenvironment and extracellular matrix in the formation of pre-metastatic and metastatic niche. *Cell & Bioscience*, *10*(1), 89. https://doi.org/10.1186/s13578-020-00453-9

Zoetemelk, M., Rausch, M., Colin, D. J., Dormond, O., & Nowak-Sliwinska, P. (2019). Short-term 3D culture systems of various complexity for treatment optimization of colorectal carcinoma. *Scientific Reports*, *9*(1), 7103. https://doi.org/10.1038/s41598-019-42836-0

Zygulska, A. L., & Pierzchalski, P. (2022). Novel Diagnostic Biomarkers in Colorectal Cancer. *International Journal of Molecular Sciences*, *23*(2), 852. https://doi.org/10.3390/ijms23020852


. . . AFTER A FEW YEARS
WE DID IT
DR. VESICLES
THE END.